AD-A203 460

REPORT DOCUMENTATION PAGE

1a. REPORT SECURITY CLASSIFICATION: Unclassified	1b. RESTRICTIVE MARKINGS
2a. SECURITY CLASSIFICATION AUTHORITY	3. DISTRIBUTION/AVAILABILITY OF REPORT: Approved for public release; distribution unlimited.
2b. DECLASSIFICATION/DOWNGRADING SCHEDULE	
4. PERFORMING ORGANIZATION REPORT NUMBER(S)	5. MONITORING ORGANIZATION REPORT NUMBER(S): ARO 25796.1-EL-CF
6a. NAME OF PERFORMING ORGANIZATION: Palisades Institute for Research Services, Inc / 6b. OFFICE SYMBOL (If applicable)	7a. NAME OF MONITORING ORGANIZATION: U. S. Army Research Office
6c. ADDRESS (City, State, and ZIP Code): New York, NY 10014-4899	7b. ADDRESS (City, State, and ZIP Code): P. O. Box 12211, Research Triangle Park, NC 27709-2211
8a. NAME OF FUNDING/SPONSORING ORGANIZATION: U. S. Army Research Office / 8b. OFFICE SYMBOL (If applicable)	9. PROCUREMENT INSTRUMENT IDENTIFICATION NUMBER: DAAL03-88-G-0041
8c. ADDRESS (City, State, and ZIP Code): P. O. Box 12211, Research Triangle Park, NC 27709-2211	10. SOURCE OF FUNDING NUMBERS: PROGRAM ELEMENT NO. / PROJECT NO. / TASK NO. / WORK UNIT ACCESSION NO.

11. TITLE (Include Security Classification): Workshop on Physics and Chemistry of Mercury Cadmium Telluride

12. PERSONAL AUTHOR(S): Jan Schetzina and Joe Schmit (Co-Chairmen)

13a. TYPE OF REPORT	13b. TIME COVERED	14. DATE OF REPORT (Year, Month, Day)	15. PAGE COUNT
Final	FROM 7/25/88 TO 7/24/89	December 1988	

16. SUPPLEMENTARY NOTATION: The view, opinions and/or findings contained in this report are those of the author(s) and should not be construed as an official Department of the Army position, policy, or decision, unless so designated by other documentation.

17. COSATI CODES		
FIELD	GROUP	SUB-GROUP

18. SUBJECT TERMS (Continue on reverse if necessary and identify by block number): Mercury Cadmium Telluride, Heterostructures, Superlattices, Substrates, Interfaces.

19. ABSTRACT (Continue on reverse if necessary and identify by block number)

The workshop was held as scheduled. Sessions included 1. Growth and Propteries I: HgCdTe and related properties, 2. Novel Heterostructures and measurements, 3. Superlattices and electronic Properties, 4. Growth and properties II: mostly substrates, 5, Surfaces and interfaces, and 6. Defects.

20. DISTRIBUTION/AVAILABILITY OF ABSTRACT: ☐ UNCLASSIFIED/UNLIMITED ☐ SAME AS RPT. ☐ DTIC USERS	21. ABSTRACT SECURITY CLASSIFICATION: Unclassified
22a. NAME OF RESPONSIBLE INDIVIDUAL	22b. TELEPHONE (Include Area Code) / 22c. OFFICE SYMBOL

DD FORM 1473, 84 MAR — 83 APR edition may be used until exhausted. All other editions are obsolete.

SECURITY CLASSIFICATION OF THIS PAGE: UNCLASSIFIED

ARO 25796.1-EL-CF

EXTENDED ABSTRACTS

THE 1988
U.S. WORKSHOP on the
PHYSICS and CHEMISTRY of
MERCURY CADMIUM TELLURIDE

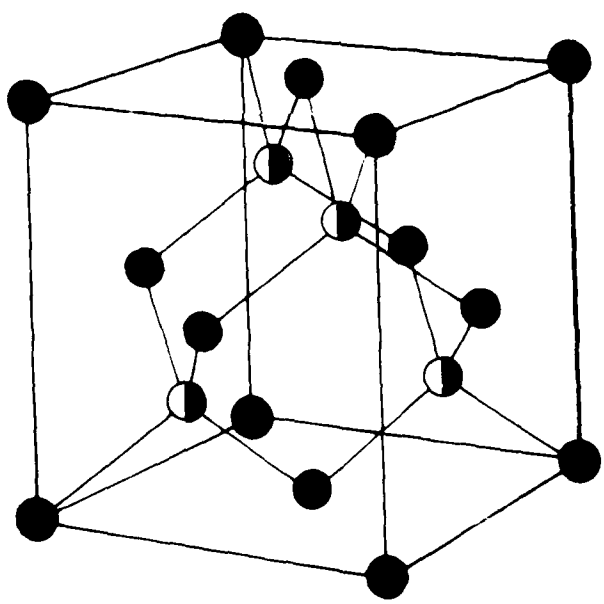

Sponsored by

Army Research Office
...rch Projects Agency
...ific Research
...Division

...13, 1988

"The views, opinions, and/or findings contained in this report are those of the author(s) and should not be construed as an official Department of the Army position, policy, or decision, unless so designated by *other documentation.*"

ACKNOWLEDGEMENTS

The Workshop Committee would like to acknowledge the special contributions, pertinent to the sucess of the Workshop, which were made by the following institutions:

HONEYWELL

NORTH CAROLINA STATE UNIVERSITY

ROCKWELL INTERNATIONAL

SANTA BARBARA RESEARCH CENTER

TEXAS INSTRUMENTS

CO-CHAIRMEN

Jan Schetzina
North Carolina State University
Joe Schmit
Honeywell

PROGRAM COMMITTEE

Jack Furdyna
Notre Dame University
Colin Jones
Santa Barbara Research Center
Ed Gertner
Rockwell International
Mike Kinch
Texas Instruments
Tom McGill
California Institute of Technology
Paul Raccah
University of Illinois at Chicago
Herb Schaake, Proceedings Editor
Texas Instruments
Dave Seiler
North Texas State University
Bill Spicer
Stanford University
Peter Wolff
Massachusetts Institute of Technology

GOVERNMENT ADVISORS

Charles Freeman
Army NV&EO Center
Gordon Griffith
AFWAL
Jim Murphy
DARPA
Dick Reynolds
DARPA
Bob Wagner
NRL
Horst Wittmann
AFOSR

WORKSHOP COORDINATORS

Jay Morreale
Mark Goldfarb
Palisades Institute for Research Services, Inc.

WORKSHOP SPONSORS

Army Research Office
Defense Advanced Research Projects Agency
Air Force Office of Scientific Research
American Vacuum Society

PROGRAM

MONDAY, OCTOBER 10, 1988

7:00-10:00 pm	Pre-Workshop Check-In

TUESDAY, OCTOBER 11, 1988

7:00- 8:00 am	Workshop Check-In
8:00- 8:10 am	Opening Remarks
8:10-10:00 am	I. Growth and Properties I: HgCdTe and Related Materials
10:00-10:20 am	BREAK
10:20-12:00 pm	I. Continued
12:00- 1:30 pm	LUNCH
1:30- 3:20 pm	II. Novel Heterostructures and Measurements
3:20- 3:50 pm	BREAK
3:50- 5:30 pm	II. Continued
5:30- 6:30 pm	Wine and Cheese Break

WEDNESDAY, OCTOBER 12, 1988

7:00- 8:00 am	Workshop Check-In
8:00- 9:50 am	III. Superlattices and Electronic Properties
9:50-10:20 am	BREAK
10:20-12:00 pm	III. Continued
12:00- 1:30 pm	LUNCH
1:30- 3:20 pm	IV. Growth and Properties II: Mostly Substrates
3:20- 3:50 pm	BREAK
3:50- 5:30 pm	IV. Continued
5:30- 6:30 pm	Wine and Cheese Break / Panel Discussion

THURSDAY, OCTOBER 13, 1988

7:00- 8:00 am	Workshop Check-In
8:00- 9:50 am	V. Surfaces and Interfaces
9:50-10:20 am	BREAK
10:20-12:00 pm	V. Continued
12:00- 1:30 pm	LUNCH
1:30- 3:20 pm	VI. Defects
3:20- 3:50 pm	BREAK
3:50- 5:30 pm	VI. Continued

TABLE OF CONTENTS

STANDARD RELATIONSHIPS IN THE PROPERTIES OF HgCdTe

William M. Higgins, Honeywell Electro-Optics Division

and

Joseph L. Schmit, Honeywell Sensors and Signal Processing Laboratories

Since its discovery in the late 1950's as an infrared detector material, there have been significant variations in the reported properties of the HgCdTe family of materials prepared at different laboratories [1-8]. Such variations can be a result of the growth processes, the measurement techniques and the standard relationships used. The objective of this paper is to present standard relationships that can be used to interrelate HgCdTe material and device properties. The specific relationships that will be discussed are: E_g vs. x and T, n_i vs. x and T, lattice constant vs. x, density vs. x, interdiffusion coefficient, mercury vapor pressure over melts and alloys, coefficient of thermal expansion, electron mobility vs. x, electron concentration vs. x and resistivity vs. x. The following are several examples of standard relationships that will be expanded on in the paper.

E_g vs. x and T (ref. 1):

$$E_g = -0.302 + 1.93x + 5.35 \times 10^{-4} T (1 - 2X) - 0.810x^2 + 0.832x^3 \quad (1)$$

n_i vs. x and T (ref. 2):

$$n_i = (5.585 - 3.820x + 1.753 \times 10^{-3} T - 1.364 \times 10^{-3} \times T) \times 10^{14} E_g^{3/4} T^{3/2} \exp(-E_g/2kT) \quad (2)$$

Interdiffusion coefficient (ref. 7):

$$D = 1.33 \times \exp(-4.218x - 18568/T) \quad (3)$$

Electron mobility vs. x (ref. 8):

$$\text{Mobility (RT)} = ((8.754 \times 10^{-4} \times - 1.044 \times 10^{-4})^{-1}) \quad (4)$$

Valid for $0.18 < x < 0.25$

Electron concentration vs. x (ref. 8):

$$x = ((18.6289 - \log (N)) / 10.6026) \quad (5)$$

Valid for $0.18 < X < 0.25$ and room temperature electron concentration

Electrical resistivity vs. x (ref. 8):

$$x = ((4.9042 - \log (R)) \times 15.2201) \quad (6)$$

Valid for $0.18 < x < 0.25$ and room temperature electrical resistivity

It is the authors' hope that the central forum of the U.S. Workshop on the Physics and Chemistry of HgCdTe will encourage the critical evaluation, reporting and general widespread usage of accepted standard HgCdTe relationships and the eventual development and usage of standard reference materials for the HgCdTe community which will minimize or eliminate data confusion and allow comparison and acceptance of results from different HgCdTe laboratories.

References

[1]G. L. Hansen, J. L. Schmit and T. N. Casselmann, "E_g vs. x and T", J. Appl. Phys. 53, 1982, p. 7099.

[2]G. L. Hansen and J. L. Schmit, "N_i in HgCdTe", J. Appl Phys. 53, 1983, p. 1639.

[3]R. A. Wood, J. L. Schmit, H K. Chung, T. J. Magee and G. R. Woolhouse, "Summary Abstract: Liquid-Phase Epitaxial Growth of (HgCd)Te on Cd(TeSe) Substrates", J. Vac. Sci. Technol. A3 (1), Jan/Feb 1985 p. 93-94.

[4]J. Steininger, "Hg-Cd-Te Phase Diagram Determination by High Pressure Reflux", J. Elec. Mat., Vol. 5, No. 3, 1976, p. 299-320.

[5]J. P. Schwartz, T. Tung and R. F. Brebrick, "Partial Pressures over HgTe-CdTe Solid Solutions, I. Calibration Experiments and Results for 41.6 Mole Percent CdTe and II". Results for 10, 20, and 58 Mole Percent CdTe", J. Electrochem, Soc., Feb. 1981, Vol. 128, No. 2, p. 438-456.

[6]O. Caporaletti and G. M. Graham, "The Low-Temperature Thermal Expansion Of Hg_{1-x} Cd_x Te Alloys", Appl. Phys. Lett. 39(4), 15 August 1981, p. 338-339.

[7]M. Grimbergen and A. Szilagyi, "Micro-Reflection Spectroscopy Profiling of Interdiffusion in Epitaxial HgCdTe", Mat. Res. Soc. Proc., Vol. 69, 1986, p. 257-263.

[8]D. A. Nelson, W. M. Higgins, R. A. Lancaster, R. P. Murosako, and R. G. Roy, "A New Bulk Crystal Growth Process for HgCdTe", 1984 National IRIS Meeting, April 1984.

Ultraviolet spectra of II-VI organometallic compounds and their application to in-situ measurement of the photolysis in a MOCVD reactor

Y. Fujita, S. Fujii and T. Iuchi
R&D Laboratories-I, Nippon Steel Corporation,
1618 Ida, Nakahara-ku, Kawasaki 211, Japan

Introduction

Low temperature growth by photo-assisted Metal Organic Chemical Vapor Deposition (PMOCVD) is supposed to be the most attractive approach to fabricate the semiconductor alloys such as $Hg_{1-x}Cd_xTe$(MCT), and their passivants.

The photo-absorption cross sections of the organometallic compounds which are used for the growth of $Hg_{1-x}Cd_xTe$ have been measured by Chen et al.[1] and Irvine et al.[2] However, our knowledge about photo-absorption of organometallic compounds and the mechanism of photolysis is still limited.

In order to improve positively this sort of technique, we have carried out the investigation of organometallic compounds which are the sources of $Hg_{1-x}Cd_xTe$, $Hg_{1-x}Zn_xTe$ and ZnS, ZnSe as their passivants, respectively.

Experimental Procedures

We present the following experiments in this paper.

(1) The measurements of ultraviolet photo-absorption cross sections of dimethyles and diethyles of Cd, Te, Zn, S and Se at the wavelength between 190 and 400 nm.

(2) The in-situ measurements of the photolysis of these organometallic compounds by monitoring of ultraviolet photo-absorption spectra in MOCVD.

Results and Discussion

The measured spectra of the above alkyls show the intense absorption bands from 190 to 250 nm. For example, the peak values of cross sections of dimethyltelluride

and diethyltelluride are about $5x10^{-17}cm^2molec.^{-1}$ as shown in Figure 1. The absorption cross sections of the above alkyls at the wavelengths corresponding to several excimer lasers are experimentally obtained as shown in Table 1.

The densities of these organometallic compounds in the reactor of MOCVD have been directly measured by in-situ monitoring of ultraviolet absorption spectra, which has a significant advantage compared with a conventional estimation from the data of vapor pressure to control MOCVD. The pyrolysis and the photolysis by the laser irradiation have been measured by the same approach. Figure 2 shows the in-situ absorption spectra of diethyltelluride. These in-situ spectra show that the photolysis of these organometallic compounds can be quantitatively controlled by laser power .

We have successfully achieved the photo-assisted MOCVD of CdTe at the temperature range of 100~150°C using a KrF excimer laser[3] as one of the applications of these results. We believe that these studies are promissing to create the new epitaxial growth technique for MCT and its passivant.

References

1 C. J. Chen and R. M. Osgood : J. Chem. Phys. 81, 327 (1984)

2 S. J. C. Irvine et al. : J. Electrochem. Soc. 132, 968 (1985)

3 S. Fujii et al. : 4th International Conf. on MOVPE, p6-8, May (1988)

Table 1 Absorption cross sections ($\times 10^{-17}$cm^{2}molecule^{-1}) of II-VI organometallic compounds at wavelengths of excimer lasers

	ArF (193nm)	KrCl (222nm)	KrF (248nm)	XeCl (308nm)	XeF (350nm)
$Cd(CH_3)_2$	0.9	3.0	0.4	0	0
$Te(CH_3)_2$	2.8	0.3	3.6	0.05	<0.03
$Te(C_2H_5)_2$	4.8	1.2	3.6	0.05	<0.03
$Zn(CH_3)_2$	1.8	0.9	0	0	0
$S(CH_3)_2$	0.6	0.17	<0.01	0	0
$S(C_2H_5)_2$	1.7	1.7	<0.03	0	0
$Se(CH_3)_2$	1.9	1.3	0.2	0.06	0
$Se(C_2H_5)_2$	1.1	0.9	0.1	0	0

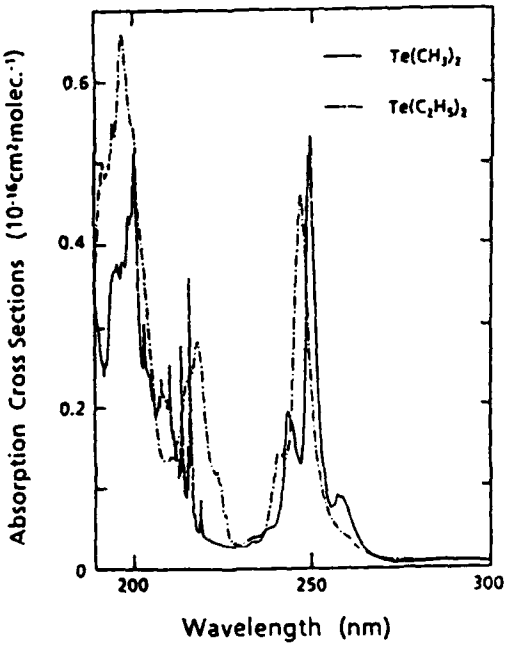

Fig. 1 Absorption cross sections of dimethyltelluride and diethyltelluride

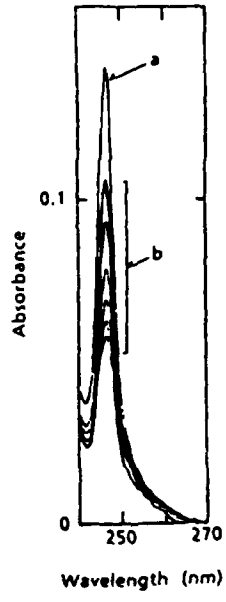

Fig. 2 In-situ absorption spectra of diethyltelluride
a: without laser irradiation
b: with KrF excimer laser irradiation (10 mJ/pulse, 100, 200, 400, 600, 800, 1000 Hz from upper spectrum, respectively)

THE ORGANOMETALLIC EPITAXY OF EXTRINSIC p-DOPED HgCdTe

N.R. TASKAR, B. BHAT, K.K. PARAT, D. TERRY, AND S.K. GHANDHI
ELECTRICAL, COMPUTER, AND SYSTEMS ENGINEERING DEPARTMENT
RENSSELAER POLYTECHNIC INSTITUTE
TROY, NEW YORK 12180

Mercury cadmium telluride (MCT or $Hg_{1-x}Cd_xTe$) layers, grown by organometallic vapor phase epitaxy (OMVPE), have the uniformity in composition and thickness that are required for present day device structures (1). The as-grown material is generally p-type due to the presence of native defects such as mercury vacancies. In order to obtain layers with stable and controllable doping, either n- or p-type, it is necessary to introduce external impurities. However, acceptor doping of MCT by group V elements such as Sb, As and P has not been very successful by many methods such as liquid phase epitaxy from Te-rich solutions or by MBE (2, 3). Here, we report on the p-doping of HgCdTe, grown by OMVPE, using arsine gas as the dopant source. We have shown earlier (4) that this dopant can be used successfully to obtain p- type doping of CdTe epilayers.

MCT layers were grown in an atmospheric pressure, horizontal reactor using diisopropyltelluride, dimethylcadmium and elemental mercury. The alloy growth method was used in which Cd, Te and Hg sources are introduced simultaneously into the reactor. Substrates were 2° misoriented (100), semi- insulating GaAs, on which a 2 μm thick undoped CdTe buffer layer was first grown at 350°C. A 0.5 μm thick CdTe cap was grown on the MCT as a passivant layer. The thickness of all the MCT layers in this study was 7 μm, and the composition x was in the range 0.27 to 0.31. Hall mobility and resistivity measurements were made in cloverleaf-patterned samples with a magnetic field strength of 2.1 kG, and over the temperature range from 20 to 300K. Only layers which showed negligible surface inversion at low temperatures were used in our study.

All the layers grown in this reactor, without any intentional doping, were weakly n-type (in the low 10^{15} cm^{-3} range) due to the presence of residual impurities in the chemicals. The Hall coefficient and Hall mobility for an MCT layer ($x = 0.3$) with no intentional doping is shown in Fig. 1. The curve shows typical n-type behavior with a carrier concentration of $3.5 \times 10^{15} cm^{-3}$. The Hall mobility at 40K was $2.3 \times 10^4 cm^2/V\text{-}s$, which is typical for layers of this composition and doping concentration. This result shows that the net Hg vacancy concentration in the layers is low, assuming low compensation. The n-type doping levels generally observed were in the range 2 to $4 \times 10^{15} cm^{-3}$, for layers of 20-30% cadmium composition.

Arsenic-doped layers were grown with p-doping levels from 3.5×10^{15} to 3.7×10^{16} cm^{-3}. No evidence of surface inversion was observed in these doped layers, except for lower doped samples, and at temperatures below 30K. Table I shows the carrier concentration and mobility at room temperature and at 40K for layers grown with $x = 0.3$, with various

arsine flow. There is a monotonic increase in the acceptor concentrations as the arsine flow is increased, indicating that the doping is extrinsic and not due to Hg vacancies. All the layers show high mobility (400-600 cm^2/Vs) at low temperature. Also, shown in the table is the ionization energy of arsenic obtained by fitting the low temperature Hall coefficient curve to the theoretical model assuming a fully ionized donor N_d and a single acceptor N_a at E_a above the valence band. The ionization E_a decreased with increasing doping concentration as expected, due to the increased interaction between neighboring impurity atoms (5). The ionization energy for the mercury acceptor is generally found to be a factor of 2 higher than that for the arsenic values listed here.

Isothermal annealing was carried out in order to annihilate the excess mercury vacancies, and reduce their contribution to the measured acceptor concentration. The annealing was performed for 15 hours at 205°C, in a sealed quartz ampoule in which a small amount of Hg was placed to maintain a mercury-rich ambient. For these experiments, uncapped, doped MCT layers were grown side-by-side, in the same run. CdTe substrates were used in order to eliminate the possibility of any influence from the GaAs substrate during the annealing step. The as-grown layer had a p-type carrier concentration of 3.7×10^{16} cm^{-3}. The second layer, annealed in a Hg-rich ambient as described above, had a measured carrier concentration of 4.3×10^{16} cm^{-3}. The small increase observed here was most probably due to the non-uniformity in the doping of the adjacent layers. The Hall constant curves for the as grown and annealed samples are shown in Fig. 2.

In conclusion, we have shown that As can be incorporated in MCT, grown by OMVPE, using arsine in hydrogen as the dopant gas. Layers were grown with carrier concentration in the range 3.5×10^{15} to 3.7×10^{16} cm^{-3}. All the layers studied showed freezeout at low temperature, and the ionization energy was calculated from the theoretical fit to the Hall coefficient curve as a function of temperature. Isothermal annealing of doped layers in Hg, at 205°C for 15 hours, did not decrease the acceptor doping concentration, confirming that the doping observed is due to arsenic, and not to an excess of Hg vacancies.

ACKNOWLEDGEMENT

The authors would like to thank J. Barthel for technical assistance on this program and P. Magilligan for manuscript preparation. This work was sponsored by the Defense Advanced Research Projects Agency (contract No. N-00014-85-K- 0151), administered through the Office of Naval Research, Arlington, VA. This support is greatly appreciated.

REFERENCES

1. S.K. Ghandhi, I.B. Bhat and H. Fardi, Appl. Phys. Lett., 52, 392 (1988).
2. H.R. Vydyanath, J.A. Ellsworth and C.M. Devaney, J. Electron. Mat., 16, 13 (1987).
3. P.S. Wijewarnasuriya, I.K. Sou, Y.J. Kim, K.K. Mahavadi, S. Sivananthan, M. Bourkerche and J.P. Faurie, Appl. Phys. Lett., 51, 2025 (1987).
4. N.R. Taskar, V. Natarajan, I.B. Bhat and S.K. Ghandhi, J. Crys. Growth, 86, 228 (1988).

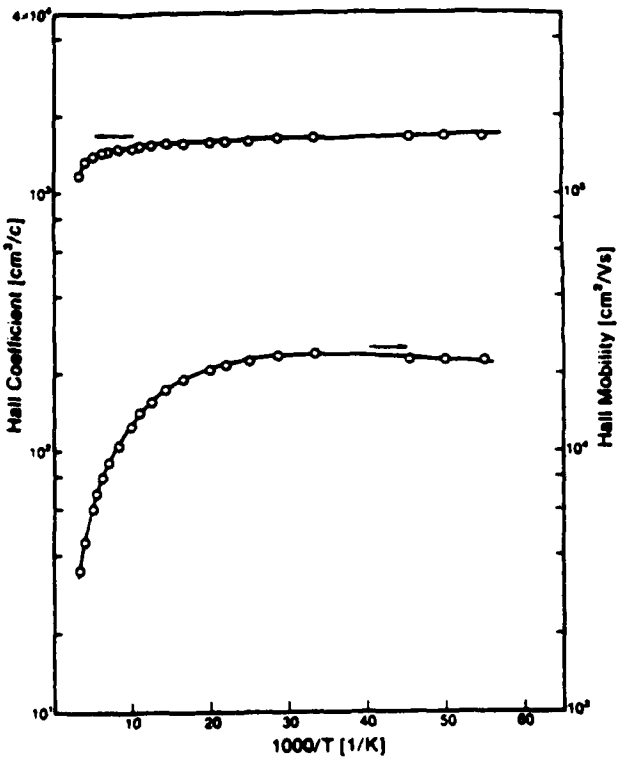

Fig. 1 Hall Mobility and Hall Coeff. of undoped MCT layer.

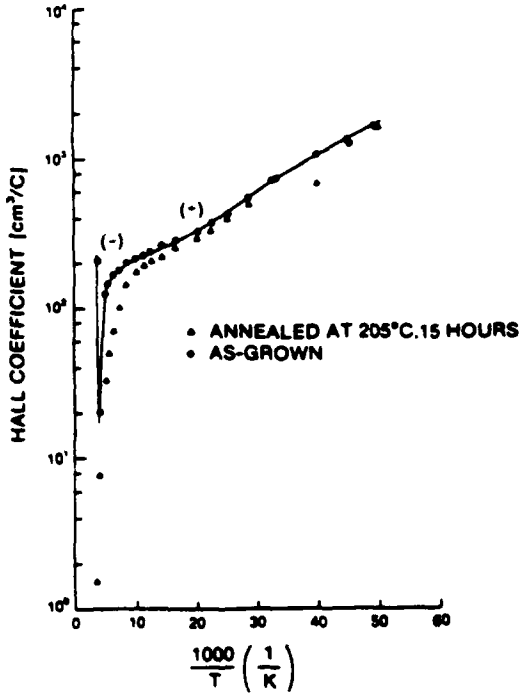

Fig. 2. Hall Coeff. of as grown and annealed arsenic doped MCT layer

Table I Electrical Properties of As Doped MCT Layers

Run No.	Arsine Flow (c.c/min)	Compo-sition (x)	type n or p	Na-Nd (cm^{-3})	u_{40k} (cm^2/Vs)	Ea (meV)
334	0	0.3	n	-3.5×10^{15}	2.4×10^4	-
352	50	0.3	p	3.5×10^{15}	570	11
354	150	0.3	p	5.5×10^{15}	420	10.5
355	350	0.3	p	1.15×10^{15}	520	8.5

A STUDY OF THE STRUCTURE AND ELECTRICAL PROPERTIES OF CMT GROWN BY MOVPE (IMP)

S J C Irvine, J S Gough, J Giess, A Royle, G T Brown A M Keir and J B Mullin

Royal Signals and Radar Establishment, St Andrews Road,
Malvern, Worcs WR14 3PS. UK

Introduction

Metal Organic Vapour Phase Epitaxy (MOVPE) has emerged as one of the more promising techniques for preparing epitaxial films of $Cd_xHg_{1-x}Te$ (CMT) for large area focal plane arrays[1]. Diode performance, yield and uniformity over an array of detectors demands a very high quality of epitaxy in terms of both the electrical properties and structural characteristics. The structural characteristics include both crystalline perfection and surface quality. In our own laboratory a variant of the MOVPE process, that of the interdiffused multilayer process (IMP) is used in order to grow alloys of superior compositional uniformity than can be prepared by conventional direct alloy growth[1,2]. The process of growing alternate layers of HgTe and CdTe raises the question of whether the dislocation structure generated by the 0.3% lattice mismatch will result in epitaxial layers of inferior epitaxial quality as has been suggested elsewhere[3]. This paper will describe some recent results on IMP grown CMT at 350°C and on their properties which are relevant to the fabrication of high performance diodes. A comparison will be made between the properties of layers grown onto CdTe (100) and GaAs (100) substrates.

Electrical Results

It has been shown previously that under the thermodynamic conditions of growth (substrate temperature 350°C, Hg pressure 0.01 atm) that the expected Hg vacancy concentration and hence hole concentration would be ~ 7×10^{16} cm^{-3}. Conversion of epitaxial layers can occur during the cooling phase at the end of growth due to in-diffusion of Hg. Fig 1 shows a plot of the cooling curve for a typical layer, giving the relationship between Hg pressure and the inverse of the substrate temperature. This curve is superimposed on the equilibrium phase diagram showing the transition from n-φ, assuming $1 \times 10^{15}cm^{-3}$ impurity donors. When the cooling curve crosses this line, conversion to n-type will start to occur from the surface due to in-diffusion of Hg. Fig 2 shows a series of Hall coefficient (R_H) curves versus 1000/T for a CMT layer

(x = 0.21) on a CdTe substrate. By etching off 2μm progressively from the CMT surface between measurements, the approximate location of this junction can be found. For the unetched layer, 16.5μm of CMT, the Hall voltage was n-type over the whole range of temperatures with carrier concentration of $1.3 \times 10^{15} cm^{-3}$ and mobility of $3.6 \times 10^{5} cm^{2}/V-s$ at 10K. Curves a, b, c in Fig 2 show the Hall coefficients for 8.5μm, 4.5μm and 2.5μm of CMT, respectively. A single n→p conversion can be seen for 2.5μm of CMT with 20K carrier concentration of $4.4 \times 10^{16} cm^{-3}$ and mobility of $400 cm^{2}/V-s$. The junction appears to be located around 4.5μm from the CMT/CdTe interface. Ways of controlling this junction and of growing uniform p-type layers will be discussed.

X-ray Diffraction

Maps of the 400 peak widths were obtained at typically 2mm intervals over each wafer in order to establish their distribution. For CMT layers on GaAs substrates buffered with 3-4μm CdTe, a variety of different post growth annealing conditions were used. The post growth anneal is used to allow the last few IMP layers (i.e. near the surface) to completely interdiffuse. This is normally carried out at the growth temperature and for growth at 350°C would typically be in the range 10 to 30 minutes. Table 1 shows the annealing conditions and the mean and standard deviations of the rocking curve widths over a $1 cm^{2}$ area for a number of CMT layers. All the longer anneals, except for layer 352 show a much narrower spread of values with mean rocking curve widths of 75 and 80 arc seconds for layers 334 and 348 respectively. Both were annealed for one hour but at different temperatures. The narrowest peak width is 58 arc seconds which is one of the best results reported for hetero-epitaxial CMT on GaAs.

The one layer that does not appear to show an improvement in uniformity with an increase in anneal time is layer 352. This layer differed from the others in having a substantially enhanced surface defect density. The density of 'pyramids' over a typical surface is $10/cm^{2}$ whereas layer 352 had regions of high density, greater than $10^{4}/cm^{2}$ which gave peak widths of greater than 1000 arc seconds.

CMT layers grown onto CdTe substrates tend to give broader peak widths compared with layers on CdTe buffered GaAs. The peak widths measured on the substrates were in the range 20 to 30 arc seconds but the CMT layer peak widths are always broader. This

cannot be explained by alloy broadening. For example, a typical 12μm thick CMT layer with x of 0.21 gave measured peak widths in the region of 96 to 174 arc seconds. A thicker layer, 22μm of x = 0.22 gave narrower peak widths of 67 to 135 arc seconds. However, the best peak widths reported here are narrower than those in the literature grown onto similar quality CdTe substrates, as can be seen in table 2.

Conclusion

A detailed study using Hall measurements and x-ray diffraction have shown that MOVPE-IMP can be used to prepare very high quality CMT epitaxial layers on CdTe or GaAs substrates. The control of Hg vacancy concentration and of crystalline quality will be discussed for epitaxy on both CdTe and GaAs substrates.

Table 1

Mean and standard deviation of x-ray 400 reflection full width half maximum (fwhm) for CMT on CdTe buffered GaAs

Layer no	x	Anneal temperature °C	Anneal time minutes	Mean arc seconds	Standard deviation arc seconds
332	0.225	350	10	192	76
353	0.25	350	10	168	38
334	0.235	270	60	75	11
352	0.215	350	30	349	164
348	0.235	350	60	80	11

Table 2

Epitaxial CMT Layer Crystallographic Quality

Layer Structure	Growth Technique	X-ray fwhm in arc secs	Reference
CMT (x=0.3)/CdTe/Al_2O_3	Conventional	72-150	3
CMT (x=0.3)/CdTe/Al_2O_3	IMP	150-210	3
CMT (x=0.3)/CdTe/Al_2O_3	LPE	78-108	3
CMT (x=0.22)/CdTe	IMP	67-135 9 x 7.5mm	
CMT (x=0.235)/CdTe/GaAs	IMP	<84 8 x 8mm	
CMT (x=0.18)/CdTe	Conventional	151 ± 15	4
CMT (x=0.2)/CdTe/GaAs	Conventional	110	5
CMT (x=0.182)/ $CdSe_{0.04}Te_{0.96}$	Conventional	47-51	4

References

1. S.J.C. Irvine, J.B. Mullin, J. Giess, J.S. Gough, A. Royle and G. Crimes, J. Crystal Growth (in press).

2. J. Tunnicliffe, S.J.C. Irvine, O.D. Dosser and J.B. Mullin, J. Crystal Growth, 68 (1984) 245.

3. D.D. Edwall, E.R. Gertner and L.O. Bubulac, J. Crystal Growth 86 (1988) 240.

4. S.K. Ghandhi, I.B. Bhat and H. Fardi, Appl. Phys. Lett. 52 (1988) 392.

5. I.B. Bhat, N.R. Taskar, K. Patel, J.E. Ayers, S.K. Ghandhi, J. Petruzzello and D. Olego, SPIE 796 (1987) 194.

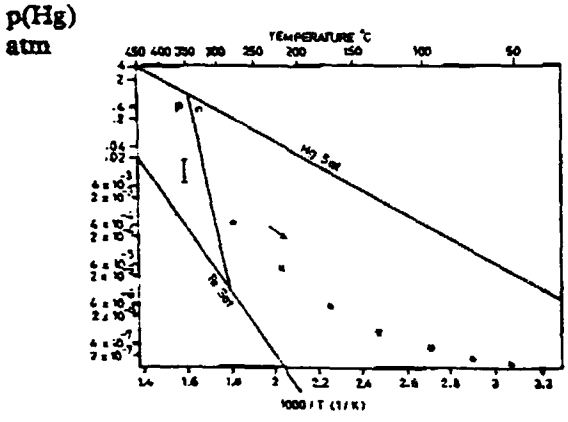

Fig 1 Typical cooling conditions for CMT grown at 350°C from dimethylcadmium and diisopropyltelluride. The Hg rich and Cd rich phase boundaries are shown with the transition from p to n type as determined by ionised Hg vacancies.

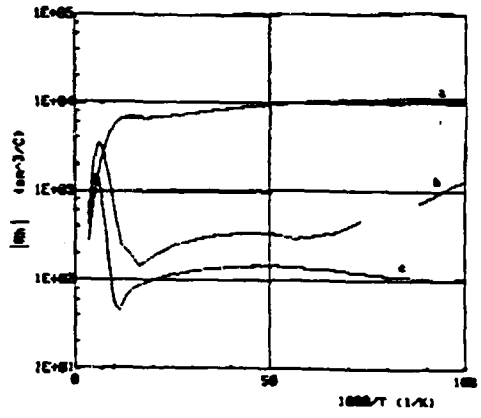

Fig 2 Hall coefficient curves after sequential etching of a CMT ($x = 0.21$) layer grown onto a CdTe substrate (original thickness 16.5μm), (a) 8.5μm, (b) 4.5μm and (c) 2.5μm remaining.

DISLOCATIONS IN $Hg_{1-x}Cd_xTe/Al_2O_3$ (SAPPHIRE) GROWN BY MOCVD

Kenji Maruyama and Koji Shinohara
Fujitsu Laboratories Ltd., Atsugi 243-01, Japan

Introduction

HgCdTe grown on Al_2O_3 (sapphire) substrates is desirable because of its optical characteristics and the availability of large diameter wafers[1,2]. We estimated the dislocations in $Hg_{0.83}Cd_{0.17}Te$ layers on (0001) sapphire substrates grown by MOCVD. We compared the dislocation distribution of MOCVD-grown HgCdTe with that of LPE-grown HgCdTe and investigated the difference between non-equilibrium growth and equilibrium growth mechanisms.

Experiment

The HgCdTe layers were grown continuously after growing CdTe buffer layers in a horizontal MOCVD reactor at atmospheric pressure. (0001)-oriented sapphire substrates with an offset angle of 3° were used to avoid the formation of twinned domains[3]. Dimethylcadmium (DMCd), diethyltelluride (DETe), and elemental mercury (Hg) were the source materials. The growth temperature was maintained at 400-420°C for the 100-200 min growth time.

Results and Discussion

We investigated dislocation etch pit densities on the (111)B $Hg_{0.83}Cd_{0.17}Te$ surface after step and pit etching. Figure 1 shows etch pits in a $Hg_{0.83}Cd_{0.17}Te$ layer; in the surface and near the HgCdTe/CdTe interface. The dislocation density of the HgCdTe layer was $5.6\times10^6\ cm^{-2}$ at a location 2.5 μm from the HgCdTe/CdTe interface, and was $2.1\times10^7\ cm^{-2}$ at a location 1 μm from the interface. A dislocation density of more than $10^8\ cm^{-2}$ was observed near the interface. As

another examination of the crystallinity, the FWHM of the double crystal X-ray rocking curve was 250 arc sec at the 3 μm-thick HgCdTe layer.

Figure 2 compares the dislocation etch pit densities of two wafers grown at different conditions. The dislocation etch pit density gradually decreases from the HgCdTe/CdTe interface to the surface.

We compared the distribution of dislocation etch pit density with the composition profile in HgCdTe layer (Fig. 3). The composition profiles were measured using XMA (X-ray microprobe analysis). The 10-90% transition width of the composition profile is about 2 μm in an MOCVD-grown layer at 415°C for 100 min. The compositionally graded regions correspond to the regions of decreased dislocation etch pit density (Fig. 2). This transition width is similar to that of the 2 μm width in our LPE-grown HgCdTe/CdTe at 430-426°C for 60 min. These results suggest that the high dislocation densities near the HgCdTe/CdTe interface are due to the lattice mismatch induced by the interdiffusion between HgCdTe and CdTe during growth[4]. On the surface of the thicker layer, dislocation etch pit density is similar to that of CdTe buffer layers, 4×10^{6} cm^{-2}. This implies that residual dislocations penetrate the HgCdTe layers and the 0.2% lattice mismatch between $Hg_{0.83}Cd_{0.17}Te$ and CdTe is completely accommodated by the misfit dislocations.

We can conclude that the dislocation density distributions are caused by interdiffusion, for both MOCVD and LPE. The crystallinity of buffer layers should be improved to decrease the dislocations of MOCVD-grown HgCdTe layers on alternative substrates.

References

[1]W. E. Hoke, R. Traczewski, V. G. Kreismanis, R. Korenstein and P. J. Lemonias, Appl. Phys. Lett. 47, 276 (1985).

[2]D. D. Edwall, E. R. Gertner and L. O. Bubulac, J. Crystal Growth 86, 240 (1988).

[3]K. Maruyama, M. Yoshikawa and H. Takigawa, J. Crystal Growth, to be published.

[4]M. Yoshikawa, J. Appl. Phys. 63, 1533 (1988).

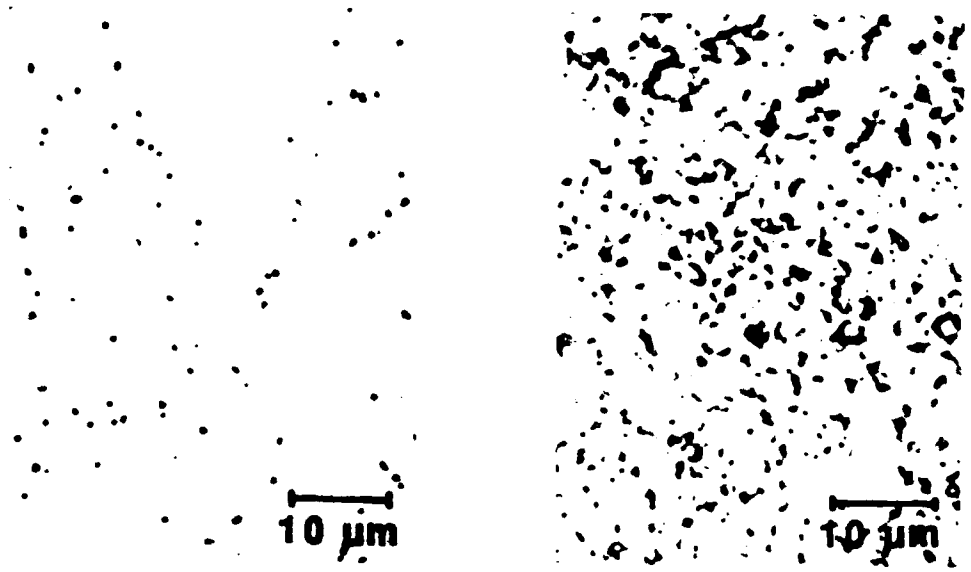

Fig. 1. Etch pits in a $Hg_{0.83}Cd_{0.17}Te$ layer (a) at the surface and (b) near the HgCdTe/CdTe interface.

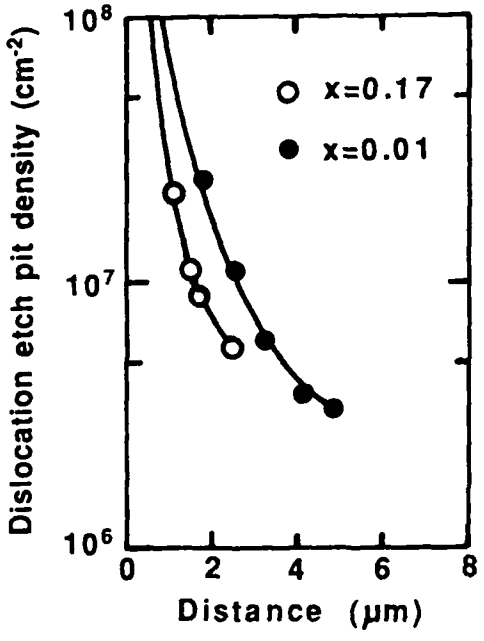

Fig. 2. Dislocation etch pit densities as a function of distance in the growth direction from the HgCdTe/CdTe interface.

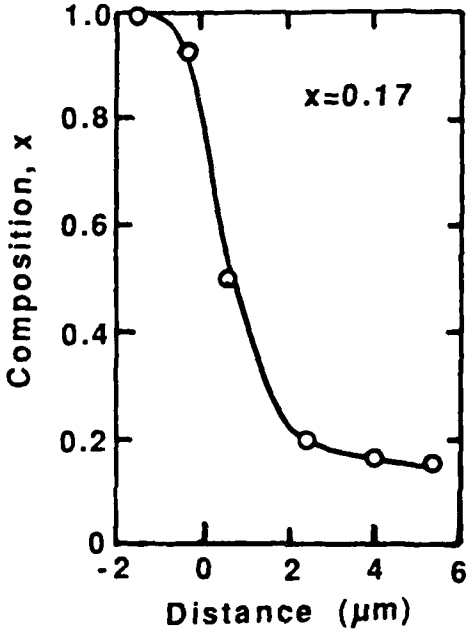

Fig. 3. Composition profiles in $Hg_{0.83}Cd_{0.17}Te$/CdTe layer measured by XMA.

A NEW FAST-RESPONSE Hg-VAPOR SOURCE FOR HgCdTe MBE GROWTH

B. K. Wagner, R. Benz II, and C. J. Summers
Microelectronics Research Center
Georgia Tech Research Institute
Atlanta, Georgia 30332

We report a new technique for producing a highly stable, fast-response Hg-vapor source for HgCdTe growth. The design principles for the Hg-vapor source are based on the viscous flow of gas through an orifice. When the pressure on the upstream side of an orifice is greater than twice the pressure on the downstream side, the flow is choked and the gas flow rate is dependent only on the upstream pressure. Thus, the Hg-flux is controlled only by the regulation of the Hg vapor pressure on the upstream side of an orifice and perturbations of the downstream pressure will not affect the flux as long as choked flow conditions are maintained. The equations governing viscous choked flow through an orifice are reviewed by Santeler.[1]

The Hg-vapor source operates as follows. Hg-vapor is generated in a heated stainless steel reservoir. The vapor flows into a randomizing plenum where the pressure is maintained by a capacitance manometer/control valve feedback loop to ±0.002 torr. The Hg-vapor then exits the plenum through a small orifice into a nozzle where the flux is directed onto the substrate. To shutter the beam and prevent flux transients, a vent/run valve system is placed just after the orifice. In the vent mode, the Hg-flow is directed along an alternate path to prevent a pressure increase in the plenum, thus improving the time response of the Hg-vapor source. Hg-condensation is prevented by maintaining all components downstream of the heated Hg reservoir at 10°C to 15°C above the Hg reservoir temperature. Nickel plating of all

stainless steel surfaces was originally attempted to prevent Hg contamination from the heated stainless steel. Unfortunately, the use of nickel plating solutions did not provide good adherence to the stainless steel and was also found to contain volatile impurities such as phosphorus, chlorine and alkali metals,[2] which could become entrained in the Hg flux and dope the HgCdTe layers. Thus, this procedure has been discontinued at present.

Figure 1 shows the dependence of the Hg-flux as measured by an ion gauge in the substrate position for stepped increases and decreases in the plenum pressure set points. Figure 2 shows that the Hg-flux accurately follows an externally supplied set point and indicates that the response time of the Hg-vapor source can be smaller than 10 seconds. Similar measurements show that this system has a dynamic range from 10^{-3} torr to 10^{-6} torr and a long term stability that exceeds our ability to measure with a conventional ion gauge. Additional measurements show that this system can maintain a constant Hg-flux for Hg reservoir temperature changes of 25°C, and possesses a set point repeatability of ±0.002 torr.

Preliminary results on the growth of HgCdTe and HgTe on GaAs substrates have been obtained. Growth was performed in a Varian GEN II molecular beam epitaxy system using elemental Hg and Te sources and a binary CdTe source. Both the HgTe and HgCdTe layers were grown on (001) CdTe buffer layers deposited on the (001)-oriented GaAs substrates. Growth of the CdTe layers was carried out at a substrate temperature of 300°C with thicknesses of 0.1 um to 2 um, while both the HgTe and HgCdTe layers were deposited at a substrate temperature of 185°C with thicknesses

ranging from 0.1 to 3.7 um. After growth of the HgTe or HgCdTe, a thin CdTe capping layer was deposited. Both the HgTe and HgCdTe layers exhibited specular surfaces.

The HgTe layers had Hall mobilities ranging from 24,000 $cm^2/V.s$ at room temperature to 54,000 $cm^2/V.s$ at 80 K. A 3.7 um thick HgCdTe layer with x = 0.17, as determined by Fourier transform infrared spectroscopy, exhibited room temperature, 80 K, and 12 K mobility values of 29,000, 117,000 and 198,000 $cm^2/V.s$, respectively. The temperature dependence of the carrier concentration and mobility for this layer is shown in Figure 3.

As demonstrated, this source concept provides greater ease in setpoint changes, improved flux stability and reproducibly, and fast response times. In addition, the flux parameters can be computer controlled and changed rapidly. The fast response characteristics and the vent/run system make it possible to grow very abrupt CdTe/HgCdTe interfaces, ternary heterojunctions, and graded bandgap structures with great accuracy and repeatability. Additionally, small changes in Hg-flux can be used to minimize stoichiometric doping.

We thank J. Reekstin for useful discussions and acknowledge Aerojet ElectroSystems Company and the Solar Energy Research Institute for their support of this work.

[1]D. J. Santeler, J. Vac. Sci. Technol. A 4, 348 (1986).
[2]J. Henry, Metal Finishing Guidebook and Directory 84, 374 (1986).

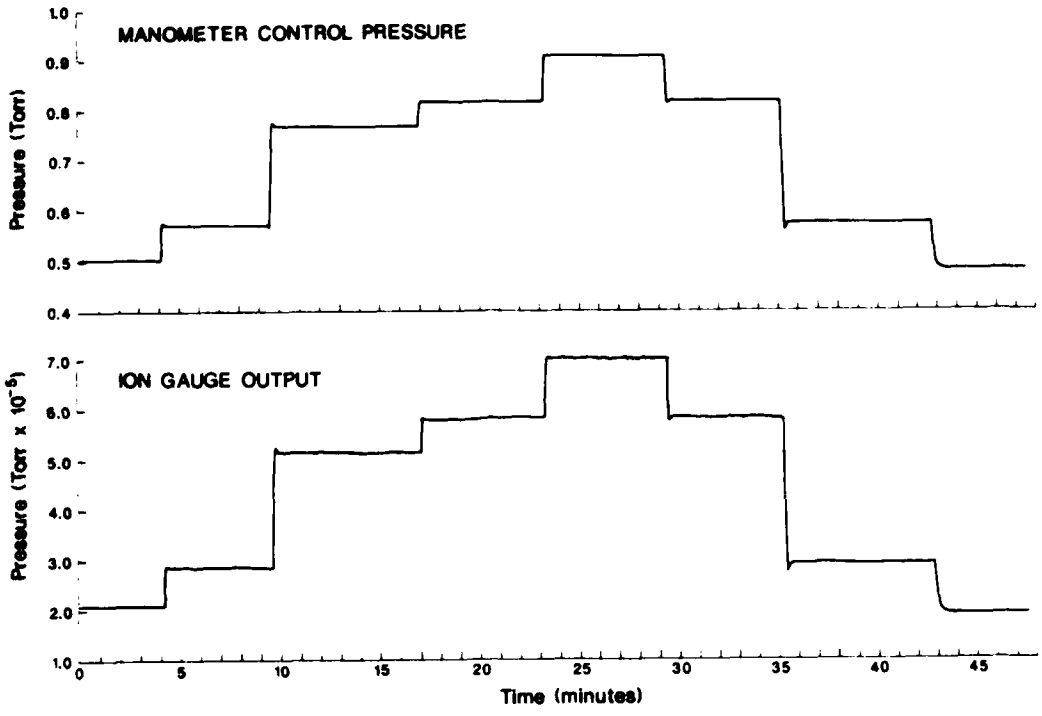

Fig. 1. Hg flux response to sudden set point changes.

Fig. 2. Demonstration of response characteristics to saw-tooth waveform regulating Hg source set point.

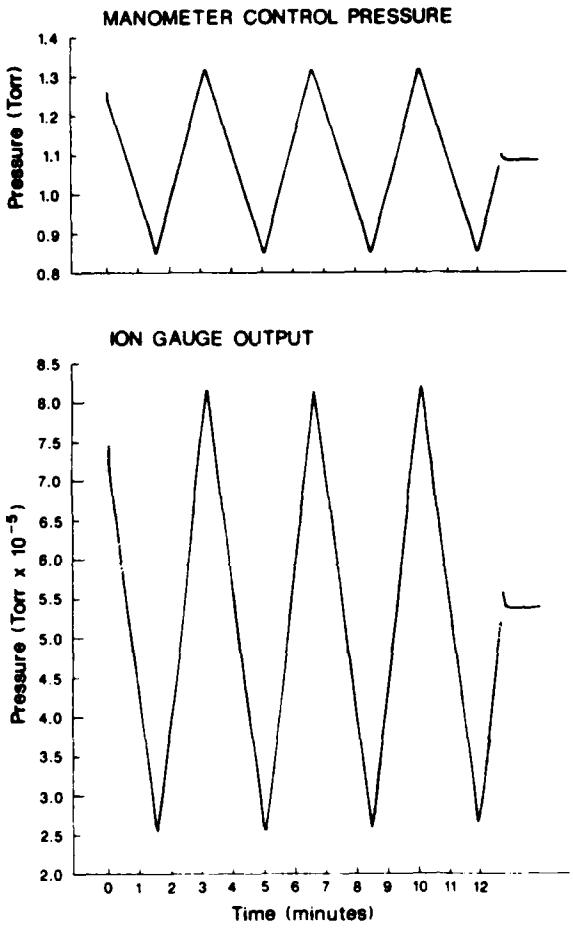

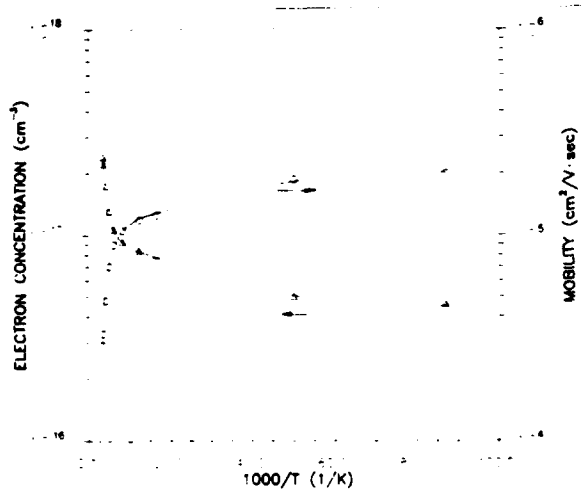

Fig. 3. Temperature dependence of carrier concentration and mobility for a 3.7 um thick HgCdTe (x = 0.17) layer.

Properties of HgCdTe Films and Hg-Based Quantum Well Structures Grown by Photoassisted Molecular Beam Epitaxy

T.H. Myers, R.W. Yanka and K.A. Harris
Electronics Laboratory, General Electric Company
Syracuse, NY 13221

J. Han, S. Hwang, J.W. Cook, Jr. and J.F. Schetzina
Department of Physics, North Carolina State University
Raleigh, NC 27695

R.W. Green
Corporate Research and Development Center, General Electric Company
Schenectady, NY 12301

S. McDevitt
II-VI, Incorporated, Saxonburg, PA 16056

Growth of HgCdTe by molecular beam epitaxy (MBE) has been plagued by problems arising from the rapid and incongruent decomposition of HgCdTe at high temperatures and the high over-pressure of Hg needed during film growth. This has resulted in layers that generally have relatively high dislocation densities. In addition, controlled doping of HgCdTe and other Hg-based layered structures through the introduction of substitutional impurities during MBE growth has been found to be a complex problem, particularly with respect to p-type doping.

In an attempt to address and circumvent the above problems we have employed a new deposition technique, photoassisted MBE [1], in which the substrate is illuminated during the entire film growth process. In the present work, an argon ion laser with broad band blue-green optics was used as an illumination source. Film growth experiments were completed both at GE (Syracuse) and NCSU using custom MBE systems designed specifically for Hg-based film growth, which were modified for photoassisted MBE.

At GE, HgCdTe epilayers were grown on (100), (111)B, and (211)B lattice-matched CdZnTe substrates obtained from II-VI Incorporated. Several of the (211)B substrates were specially selected to be free of Te precipitates and have low dislocation density. At NCSU, (100) and (111)B lattice-matched CdZnTe provided by II-VI Incorporated and Fermionics were used to grow HgCdTe films and Hg-based double heterostructures. The substrates underwent standard chemical etching and heat treatment immediately prior to film growth. Epilayers were grown at temperatures ranging from 170 to 190 °C. Laser illumination intensities from 50 to 250 mW/cm^2 were investigated.

Our initial results indicate that illumination during epilayer growth has a pronounced effect on growth kinetics. The most obvious indication of this change is an increase in the growth rate of up to 40% under certain illumination conditions. A decrease in x-value of up to 10-15% is generally observed to accompany this increase in growth rate. This suggests that more Te, and possibly some Cd, is being incorporated into the illuminated epilayers. An important corollary is that Te has a non-unity sticking coefficient for typical MBE growth conditions.

The most important development, however, is the growth of HgCdTe epilayers of extremely high structural perfection under illumination. At both GE and NCSU, we have determined condtions which result in epilayers with large areas exhibiting x-ray double crystal rocking curves (DCRC) as narrow as 13 arc sec (FWHM). Fig. 1 shows a (333) DCRC measurement taken on a (111)B film grown and measured at NCSU. Fig. 2 shows a DCRC map consisting of FWHMs measured for nine 3 mm x 3 mm spots taken across a 1 cm x 1 cm (211)B HgCdTe epilayer grown and measured at GE. Note that the average FWHM over this area is only 22 arc sec, comparable in sharpness to rocking curve FWHMs obtained for high quality GaAs.

The electrical properties of the HgCdTe layers grown by photoassisted MBE are also outstanding. Mobilities of as-grown n-type HgCdTe films prepared at GE are comparable to the best reported for HgCdTe of a given x-value, as shown in Fig. 3. P-type as-grown epilayers can also be obtained by photoassisted MBE. The mobility and carrier concentration versus temperature for one such layer grown at NCSU is shown in Fig. 4.

The microstructure of the HgCdTe layers also reveals high quality material. Defect etches have been used to investigate the microstructure of epilayers grown at GE. While twinning is apparent on some of the (111)B films, we have also grown epilayers that are essentially free of twins. EPD counts as low as 3×10^4 cm^{-2} have been observed in isolated regions in some of the better samples. Typical EPD counts are in the mid-to-upper 10^5 cm^{-3}. This is comparable to the best results obtained for other growth techniques.

Recently, at NCSU, Hg-based multilayers have also been grown by photoassisted MBE. Fig. 5 show a schematic of one of these structures--a double heterojunction (DH) in which the wide band gap layers are CdTe and the active region is a HgCdTe superlattice. This structure was fabricated as a potential IR light source. Fig. 6 shows the photoluminescence spectrum measured at GE that one of the DH samples exhibited when optically pumped with a 200 mW YAG laser. The main luminescence peak is very bright -- 50% brighter than the PL from state-of-the-art InSb epilayers prepared at GE by LPE -- and luminescence was observed up to ~140 K. This initial result is extremely encouraging since it suggests that in the near-to-mid IR spectral region structures of this type may be useful as radiation sources. It might be pointed out that, with the CdTe cladding layers doped n-type and p-type, respectively, (which can be routinely achieved by photoassisted MBE) the DH shown in Fig. 5 corresponds to that required for the fabrication of an injection laser. Additional multilayers of this type are presently being grown at NCSU. New results will be reported at the MCT workshop.

To summarize, at this point we have grown high quality HgCdTe films and double heterostructures by means of photoassisted MBE. The HgCdTe films exhibit outstanding electrical and structural properties. The HgCdTe multilayers exhibit bright IR luminescence. In the next several months, substitutional doping studies of HgCdTe films and multilayers grown by photoassisted MBE will be completed, both at GE and NCSU. Results of these doping studies will also be reported at the MCT workshop.

Work at GE was supported by ABG IR&D funding. Work at NCSU was supported by DARPA contract DAAL03-86-K-0039.

Reference

[1] R.N. Bicknell, N.C. Giles, and J.F. Schetzina, Appl. Phys. Lett. 49, 1095 (1986).

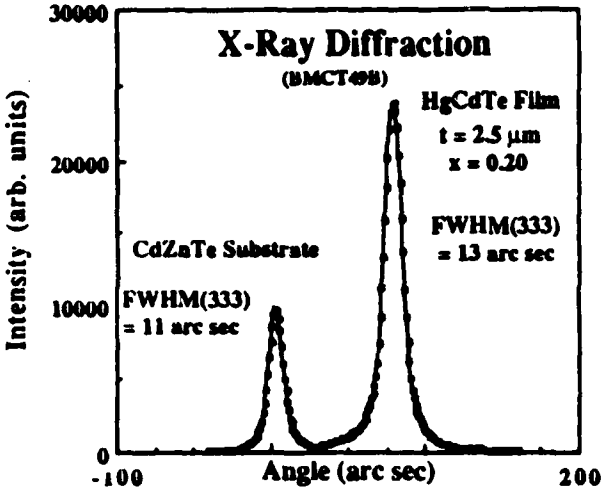

Figure 1

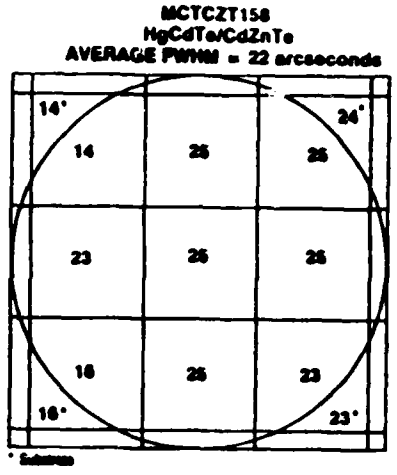

Figure 2

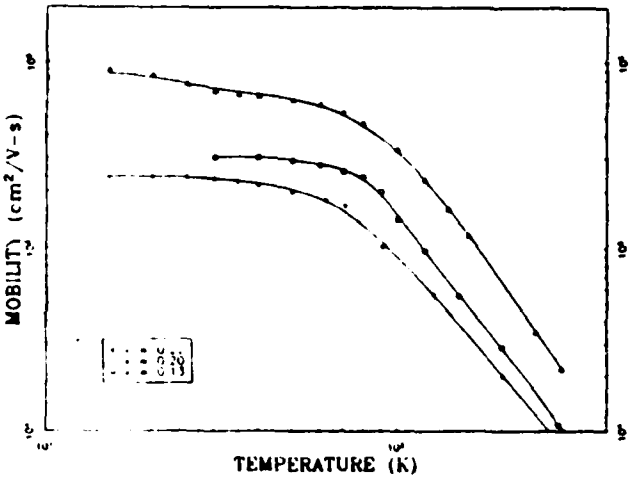

Figure 3

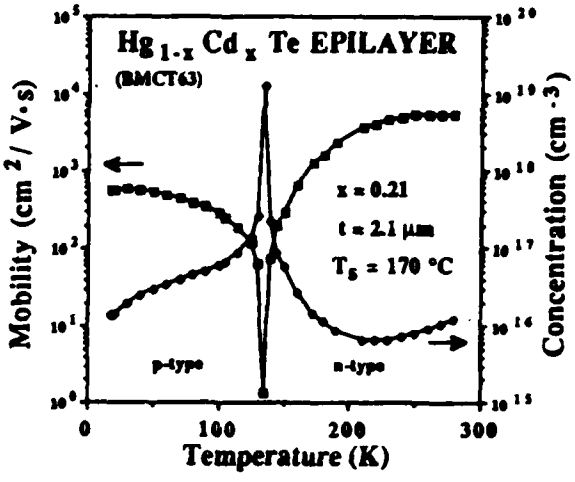

Figure 4

HgCdTe DOUBLE HETEROJUNCTION

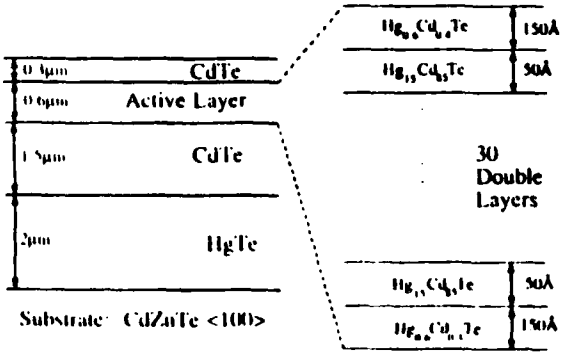

Figure 5

PHOTOLUMINESCENCE OF
HgCdTe DOUBLE HETEROJUNCTION
(x ≈ 0.4)

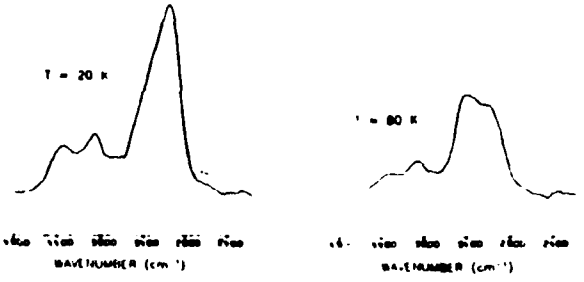

• Photoluminescence observed up to T=140 K

Figure 6

Modulation-Doped HgCdTe

Jeong W. Han, S. Hwang, Y. Lansari, R.L. Harper, Z. Yang, N.C. Giles, J.W. Cook, Jr., and J.F. Schetzina
North Carolina State University, Raleigh, NC 27695-8202

S. Sen
Santa Barbara Research Center, Goleta, CA 93117

At North Carolina State University (NCSU), we have recently employed photoassisted molecular beam epitaxy (MBE) [1] to successfully prepare p-type modulation-doped HgCdTe. The modulation-doped HgCdTe samples were grown on lattice-matched CdZnTe substrates cut from boules grown at Santa Barbara Research Center (SBRC). In this paper, we report details of the MBE growth experiments and describe the various physical properties (optical, structural, electrical, etc.) that this new infrared material possesses. A framework, which includes n-type and p-type modulation-doping as two of its elements, is used to illustrate various device configurations of this new quantum alloy of HgCdTe.

Modulation doping involves the transfer of carriers (electrons or holes) from a substitutionally doped layer (modifier layer) to an adjacent matrix material having a smaller band gap. In 1969, in their pioneering work on superlattices, Esaki and Tsu [2] proposed a selectively-doped heterojunction structure for enhanced carrier transport parallel to the interface. Independently in 1978, Dingle *et al.* [3], using n-type AlGaAs-GaAs heterostructures, first demonstrated that such enhanced carrier transport does, indeed, occur and first evoked the name "modulation doping". Since then, modulation-doped structures composed of III-V semiconductor layers have been studied in detail, and the properties that these novel structures possess have subsequently been exploited in many planar device applications [4]. In 1987, n-type modulation-doped CdMnTe:In-CdTe quantum well structures were successfully prepared for the first time by photoassisted MBE at NCSU [5]. We have also recently demonstrated at NCSU that highly conducting p-type CdTe:As layers ($p_0 \sim 10^{19}$ holes/cm^3) can also be prepared using the new doping technology based on photoassisted MBE [6].

In the present work [7], p-type modulation-doped HgCdTe samples were obtained by using thin CdTe layers that were heavily doped with arsenic and located periodically in the HgCdTe matrix as shown schematically in Figure 1. It should be pointed out that these modifier layers were grown with the Hg MBE source shutter open, so that they are actually composed of $Hg_{0.15}Cd_{0.85}Te$:As rather than pure CdTe:As. The thickness of the modifier layers was $L_b \sim 50$ Å

in each of the samples, with the As dopant uniformly distributed (no setback). For the small band gap matrix layers, we have used $Hg_{1-x}Cd_xTe$ of thickness $L_z \sim 1000$ - 1,100 Å and x-value = 0.18 - 0.26 in the various growth experiments. The total thickness of the modulation-doped HgCdTe samples ranged from 1.9 - 2.5 μm. Details of the photoassisted MBE systems located at NCSU along with the growth techniques employed are described in earlier publications [1,5].

By means of modulation doping, we have successfully prepared p-type $Hg_{1-x}Cd_xTe$ samples for which x = 0.18 - 0.26. All of the p-type samples were grown on SBRC (100) $Cd_{1-x}Zn_xTe$ substrates ($x \sim 0.04$). Figures 2, 3, and 4 show plots of Hall mobility and carrier concentration versus temperature for three representative modulation-doped samples. Figure 2 shows data for a sample having an x-value of 0.19. In this case, the Hall coefficient changes sign at $T \sim 55$ K. Below about 40 K, the hole mobility ($\mu_p \sim 280$ cm^2/V-s) and hole concentration ($p_0 \sim 1.7 \times 10^{17}$ holes/cm^3) are independent of temperature. In Figure 3, corresponding data for a modulation-doped $Hg_{1-x}Cd_xTe$ sample having an x-value of 0.21 is shown. Note that the Hall coefficient changes sign at $T \sim 195$ K. Below about T ~120 K, both the hole mobility ($\mu_p \sim 325$ cm^2/V-s) and concentration ($p_0 \sim 5 \times 10^{16}$ holes/cm^3) are constant. Figure 4 shows similar data for a heavily-doped sample for which x = 0.24. In this case, the Hall coefficient is positive at room temperature. Below $T \sim 230$ K, the hole mobility $\mu_p \sim 200$ cm^2/V-s is constant. Note that the hole concentration $p_0 \sim 10^{18}$ holes/cm^3 is a factor of five larger than the maximum soluability of Hg-vacancies in HgCdTe for this x-value. This provides direct evidence that the holes are not due to Hg-vacancies. Rather, the holes come from the As ions in the modifier layers and are transferred to the HgCdTe matrix by means of the modulation doping mechanism. Note also in Figures 2-4, that there is no evidence of hole freeze-out at low temperatures. Hole freeze-out does not occur in modulation-doped structures because, unlike conventionally doped semiconductors, there are no acceptor ions present in the small-band-gap HgCdTe material.

It should be pointed out that because modulation doping occurs in the structures described above implies there is an appreciable valence band offset at the HgTe/CdTe interface (VBO ≥ 97 meV at all temperatures in the range T = 20 - 300 K), otherwise holes would not transfer from the As acceptors in the modifier layers (where the acceptor ionization energy is $E_{As} \sim 57$ meV) to the HgCdTe matrix ($0.18 \leq x \leq 0.26$).

All of the p-type modulation-doped samples exhibit appreciable photoluminescence (PL) in the infrared spectral region. This is illustrated in Figure 5 where a PL spectrum taken at 77 K for a representative sample is shown. Note that the principal feature is a sharp peak at 8.6 μm having a FWHM = 37 meV. Based on theoretical calculations, we have reason to believe that this feature is a composite of two peaks corresponding to transitions from the n = 1 electron subband to the heavy hole and light hole ground states (1H and 1L transitions) of this 2D quantum structure. The

small diffuse peak at ~ 5 μm (~2000 wavenumbers) is due to 2H,2L, and 3H excited-state transitions.

The periodic nature of the modulation-doped HgCdTe samples is clearly manifested by the x-ray diffraction spectrum which they exhibit. This is shown in Figure 6 for sample B15B which consists of modifier layers separated by ~1130 Å thick HgCdTe matrix layers (x = 0.26). With the modifier layers placed periodically, the sample is thus a superlattice. This is reflected by the occurrence of x-ray satellite peaks. Seven orders of satellites are shown in Figure 6, attesting to the excellent structural quality that has been achieved. Note that the spectrum was obtained using a double-crystal diffractometer with the detector full open (rocking curve configuration) and that the FWHM of the main superlattice peak and each of the satellites is ~ 30 arc sec. This spectrum is comparable in quality to similar x-ray spectra obtained for the best AlGaAs-GaAs superlattices.

Work at NCSU was supported by DARPA contract DAAL03-86-K-0146. Substrate development at SBRC was supported by NRL contract N00014-87-C-2501.

References

1. R.N. Bicknell, N.C. Giles, and J.F. Schetzina, Appl. Phys. Lett. **49**, 1095, (1986).
2. L. Esaki and R. Tsu, IBM Research Note RC-2418 (1969).
3. R. Dingle, H.L. Stormer, A.C. Gossard, and W. Wiegmann, *Appl. Phys. Lett.* **37**, 805 (1978).
4. "The Technology and Physics of Molecular Beam Epitaxy", edited by E.H.C. Parker, (Plenum Press, New York, 1985).
5. R.N. Bicknell, N.C. Giles, and J.F. Schetzina, Appl. Phys. Lett. **50**, 691 (1987).
6. To be published.
7. J.F. Schetzina, NATO Conference on "The Future of Small Band Gap II-VI Materials", Liege, Belgium, September 5 - 9 (1988).

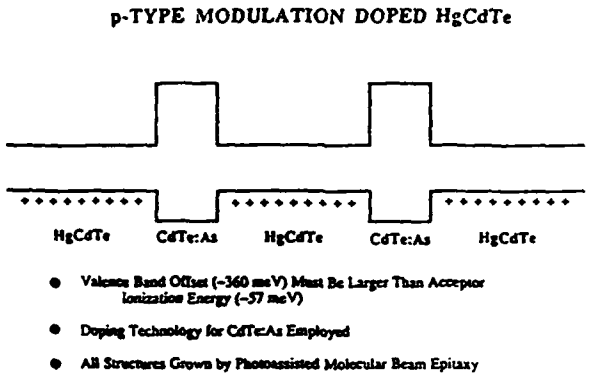

Figure 1

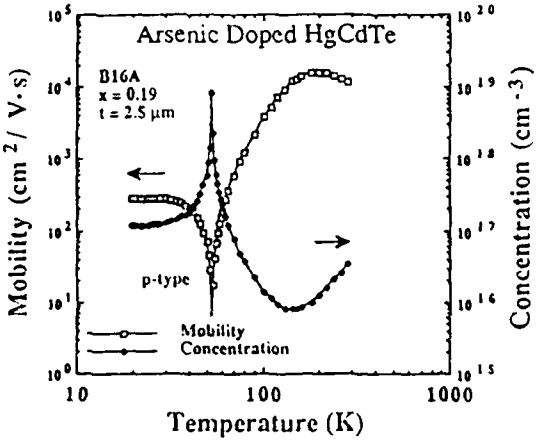

Figure 2

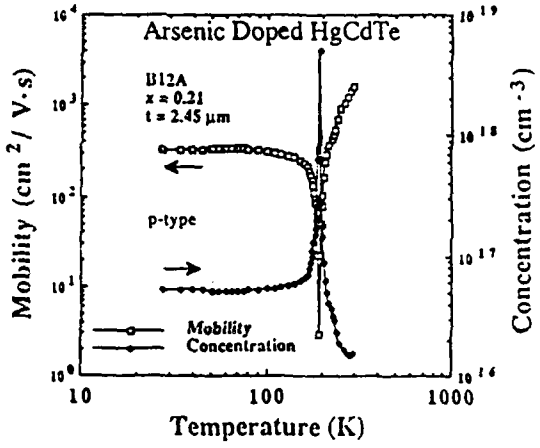

Figure 3

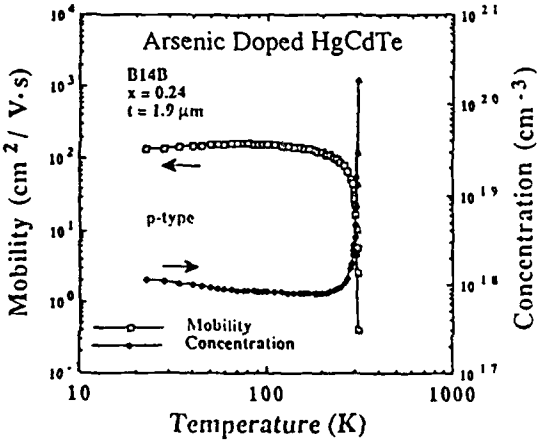

Figure 4

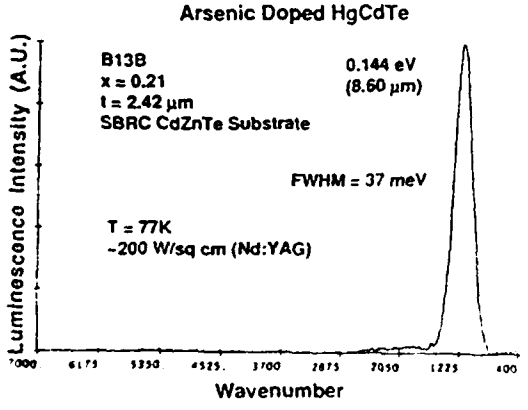

Figure 5

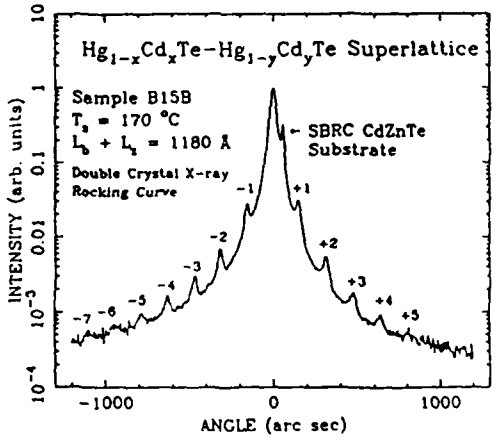

Figure 6

Minority-carrier Lifetime in p-Type $Cd_xHg_{1-x}Te$ Layers Grown by Molecular Beam Epitaxy

M.E. DeSouza, M. Boukerche and J.P. Faurie
University of Illinois at Chicago, Dept. of Physics

The lifetime of excess photogenerated carriers is of great importance for understanding the limiting mechanisms in $Hg_{1-x}Cd_xTe$ material. Lifetime measurements were carried out on unintentionally doped p-type epilayers grown by molecular beam epitaxy in the composition range $.219 < x < .304$. The samples were grrown on CdTe, CdZnTe, CdTeSe and GaAs substrates in the (111)B direction. All samples had a thin layer of CdTe (~300A) on top for protection. We used the photoconductive decay technique with a GaAlAs laser beam illuminating the samples. The photocurrents generated were acquired with a low noise cryogenic preamplifier. The light intensity on each sample was kept low to satisfy the low injection condition and the exponential decay of the generated photocurrent versus time.

The temperature dependence of the lifetime shows that the recombination is dominated by the Shockley-Read process below 200K. The Auger process is influent only at high temperatures.

We carried out a fitting of the Hall data of these samples to determine the concentrations of acceptors and donors, N_a and N_d respectively, and the Fermi level versus temperature, F(T). With the values of F(T), and using the lifetime expression for Shockley-Read recombination for low injection and a small trap density, we were able to determine the electron trap energies E_t considering a single dominant level. The trap energies found show a level at mid-gap which has also been reported by many other researchers that used samples grown by other techniques. This fact shows that this level is a very fundamental one. Contrary to what some researchers have found, E_t/E_g showed no dependence with x.

From the lifetime data we have τ_{no}, the shortest time constant for electron capture. Taking for the electron capture cross section a value of 10^{-16} cm^2 we found a density of traps in the range 10^{15}-10^{16} cm^{-3} which is one order of magnitude smaller than N_a.

IMPROVEMENTS IN THE DOPING OF MERCURY CADMIUM TELLURIDE FILMS GROWN BY MOLECULAR BEAM EPITAXY

M. Boukerche*, S. Sivananthan, M. Lange, P.S. Wijewarnasuriya, I.K. Sou and J.P. Faurie
University of Illinois at Chicago, Dept. of Physics

Mercury cadmium telluride (MCT) material as grown is not suitable for infrared device applications when it is grown by conventional techniques. Like for other II-VI materials, the residual doping by native defects (intrinsic doping) is unavoidable due to the large stoichiometry deviation range ($\Delta y \leq 10^{-5}$). The necessary electronic properties are usually achieved through post growth annealing procedures. However, high quality as grown MCT has been obtained by using the molecular beam epitaxy technique (MBE). Several hundred samples were grown in our laboratory since the electrical results on MBE MCT layers were presented at this conference in 1985.[1] A systematic fitting of the low field Hall measurements in the whole temperature range was made for the intrinsic p-type layers. The cadmium composition deduced is very reliable and close to the one determined optically. The electron to hole mobility ratio at room temperature is in the range 35-40 for X=0.2-0.3. Most of the samples can be fitted very well assuming only one shallow level. The best samples have a compensation close to 5e16 cm^{-3}. This is a factor of 6 better than was previously reported.[1] Some samples could not be fitted with any certainty because of inhomogeneity in the doping along the growth axis. This fact is in good agreement with the latest study of extrinsic indium doping. Thanks to the progress made in the stoichiometry control, carrier concentrations in the low $10^{16}cm^{-3}$ range can be obtained now routinely for indium doped $Hg_{1-x}Cd_xTe$ (x=0.2-0.3). This represents a major improvement compared to what has been reported before.[2] The apparent electrical efficiency of indium doping is now close to 100% even in the $10^{17}cm^{-3}$ range. The memory effect linked to this material[3] has also been greatly reduced since p-type material can now be grown after indium doped layers. The extrinsic doping by arsenic and antimony has also been studied. It was found to be n-type and very inefficient, remaining in the $10^{15}cm^{-3}$ range. Activation by an Nd-Yag green laser pulsed at 10Khz only slightly increased the n-type character of As doping. We should also mention that a low photon power density tends to favor the intrinsic p-type character of the layers being grown without extrinsic dopants. We will also show that the cadmium composition of the samples is increased when the laser power increases.

1. M. Boukerche, P.S. Wijewarnasuriya, J. Reno, I.K. Sou and J.P. Faurie, J. Vac. Sci. Technol. A4, 2072 (1986).
2. M. Boukerche, J. Reno, I.K. Sou, C. Hsu and J.P. Faurie, Appl. Phys. Lett. 48, 1733 (1986).
3. M. Boukerche, P.S. Wijewarnasuriya, S. Sivananthan, I.K. Sou, Y.J. Kim, K.K. Mahavadi and J.P. Faurie, J. Vac. Sci. Technol. (in press).

ABSTRACT FOR INVITED TALK
The 1988 Workshop on the Physics and Chemistry of MCT

TUNNEL DEVICES BASED ON HgTe/CdTe HETEROJUNCTIONS†

by
D. H. Chow and T. C. McGill
T. J. Watson, Sr., Laboratory of Applied Physics
California Institute of Technology
Pasadena, California 91125

ABSTRACT

In recent years two novel, two-terminal negative differential resistance devices have been fabricated from HgTe/CdTe heterojunctions. Following on the developments in III-V heterostructures, negative resistance devices have been predicted[1] and observed[2] in double barrier HgTe-CdTe-HgTe-CdTe-HgTe heterostructures. In these microstructures, the CdTe layers act as barriers. The central HgTe layer produces a quantum well that is confined by the two CdTe barriers. Electrons are supplied and collected by the HgTe cladding layers on either side of the central barrier-well-barrier structure. Electrons tunnel through the resonance in the central well to produce negative resistance. Single barrier devices consisting of HgCdTe-CdTe-HgCdTe structures also show negative resistance.[3] Theoretical simulations indicate that these structures will only show negative resistance for small values of the valence band offset between the HgCdTe and CdTe. In this case, negative resistance is produced by having the tunneling electrons experience a higher value for the attenuation constant as a function of electron energy. The experimental observation of negative resistance in these structures at low temperatures[4] implies both a small value of the valence band offset and the applicability of the two-band model in accounting for the behavior of the tunneling wavefunctions.

1. J. N. Schulman, and C. L. Anderson , *Appl. Phys. Lett.* **48**, 1684 (1986).

2. M. A. Reed, R. J. Koestner, and M. W. Goodwin , *Appl. Phys. Lett.* **49**, 1293 (1986).

3. D. H. Chow and T. C. McGill , *Appl. Phys. Lett.* **48**, 1485 (1986).

4.. D. H. Chow, T. C. McGill, I. K. Sou, J. P. Faurie, and C. W. Nieh, *Appl. Phys. Lett.* **52**, 54 (1988).

†Work supported in part by the Air Force Office of Scientific Research Under Grant No. 86-0306.

NOVEL BAND-TUNING EFFECTS IN Hg-BASED QUANTUM STRUCTURES BY EXTERNAL ELECTRIC OR MAGNETIC FIELDS

Z. Yang, J. F. Schetzina
Department of Physics, North Carolina State University
and
J. K. Furdyna
Department of Physics, University of Notre Dame

In the $Hg_{1-x}Cd_xTe$ alloy, the cutoff wavelength is determined by the alloy x-value. However, precise control of the x-value has been a challenging crystal growth problem for many years, particularly with regards to alloys suitable for use in the far infrared regime. Schulman et al. [1] proposed the use of HgTe/CdTe superlattices to circumvent this problem. However, control of layer thicknesses to one-monolayer presicion in these structures is itself a non-trivial problem. In addition, the superlattice layer thicknesses are quantized (in monolayer units) which also prevents precise tuning of the superlattice band gap. In this paper we describe, based on a theoretical study, novel mechanisms for tuning the cutoff wavelength or band gap of Hg-based quantum structures by external electric or magnetic fields. In addition to band gap tuning of infrared detectors, the effects described herein can be used as the basis for new electro-optic and magneto-optic devices such as modulators, switches, non-linear optic devices, phase-shifters, and filters which can be designed to operate at selected wavelengths throughout the entire infrared spectral regime.

The theoretical model used to caculated these electro-optic and magnetic-optic effects is the **k.p** theory first introduced by Smith and Mailhiot [2]. In the present work, the theory was modified to include both the strain effects and a magnetic exchange interaction. For illustrative purpose, two specific Hg-based quantum structures will be discussed in detail. Sample-I is a quantum well structure composed of CdTe/HgTe(28Å)/$Hg_{0.78}Cd_{0.22}$Te(30Å)/HgTe(38Å)/CdTe, as shown in Fig. 1, in which the active layers are the two HgTe quantum wells and the HgCdTe

barrier. An electric field F is applied perpendicular to these layers as shown to give rise to the electro-optic effect. The valence band offset between HgTe and CdTe is taken to be 350 meV.

Sample-II consists of a $Hg_{0.915}Mn_{0.085}Te(54Å)/Hg_{0.89}Mn_{0.11}Te(54Å)$ diluted magnetic semiconductor (DMS) superlattice, as shown in Fig. 2. A magneitc field B is applied perpendicular to the plane of the SL layers. A zero valence band offset is assumed for this structure.

For sample-I, the calculated electro-optic effect at 300 K produces a substantial change in band gap vs applied electric field F, as shown in Fig. 3. For F = 0, the band gap of this quantum structure is 175 meV (7.1 μm). The band gap decreases with increasing applied electric field to 151 meV (8.2 μm) at F= 100 kV/cm. Although it may be unrealistic to apply steady-state electric field of this magnitude because of heating effects, pulsed fields of appropriate duration can certainly be sustained by this type of quantum structure represented by sample-I, as it is demonstrated on a similar quantum structure sample [3]. Or the electric field can be induced by a short-pulsed powerful laser beam. In deed, the electro-optic effect is expected to be very fast. As a consequence, the effect can be used as the basis for a ultra-fast non-linear optic device, or a fast infrared electro-optic modulator as shown in Fig. 4, its speed being limited only by the RC time constant of the device. The top curves in Fig. 4 show the optical absorption A for F=0 and F>0. The bottom curve shows the change in absorption vs wavelength. Note that the maximum modulation occurs in the vicinity of the absorption edge, since the absorption increases rapidly in this region. It should be pointed out that the modulator wavelength can be changed by simply changing the quantum well layer thicknesses. For strucutures having wider quantum wells, modulators operating in 9.6-10.6 μm region can be constructed, for example.

For sample-II at 77 K, the magnetic field also induces a substantial band gap change. In this case, the band gap increases with the applied magnetic field as shown in Fig. 5. The band gap changes from 49 meV (25.3 μm) at zero field to 65 meV(19.1 μm) for B=4T. Two points should be noted. First, a total change of 16 meV in band gap, or more than 6 μm in cut-off wavelength, is achieved within a magnetic field

range of 4T at 77K, a normal operating temperature for an infrared detector. Second, the applied magnetic field can be adjusted in a continuous fashion so that any band gap or cut-off wavelength in the difficult long wavelength region can be precisely obtained. In Fig. 6 we indicated how a high T_c superconductor wire or thin film loop might be integrated with a Hg-based DMS superlattice to make a tunable infrared detector.

We also studied a $Hg_{0.814}Cd_{0.186}Te(54Å)/Hg_{0.76}Cd_{0.24}Te(54Å)$ superlattice, as a comparison. At zero magnetic field, this superlattice has the same well and barrier band gaps as sample-II. The magnetic exchange interaction is, however, absent in this case. It is then found that the band gap of this non-DMS superlattice changes less than 3 meV as the magnetic field increases from zero to 4 T. It is therefore clear that the exchange interaction between the Mn^{++} ions and the conduction band electrons and valence band holes plays a major role in the magneto-band-gap-tuning.

Work at NCSU and Purdue was supported by DARPA/ONR contract N00014-K-86-0760.

[1] J. N. Schulman and T. C. McGill, Appl. Phys. Lett. 34, 663 (1979)

[2] D. L. Smith and C. Mailhiot, Phys. Rev. B33, 8345 (1986)

[3] M. A. Reed, R. J. Koestner and M. W. Goodwin, Appl. Phys. Lett., 49, 1293 (1986)

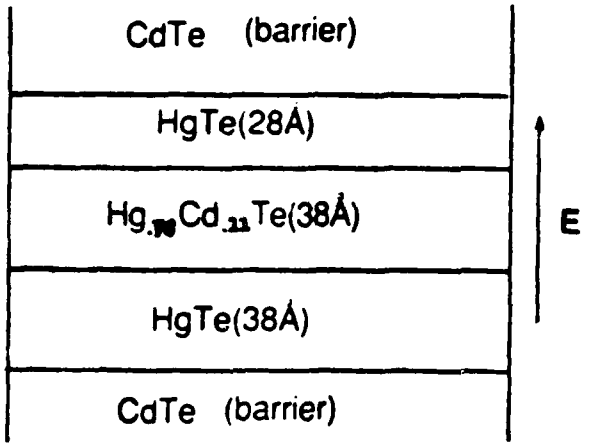

Fig. 1

SL Configuration:

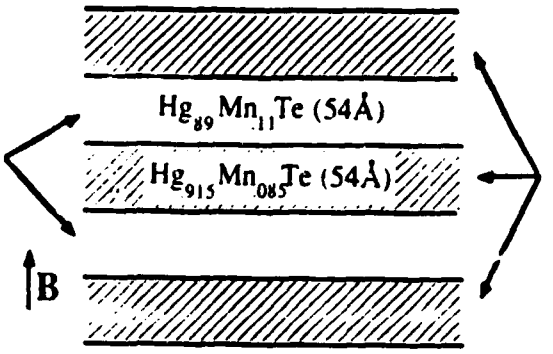

Fig. 2

ELECTRO-OPTIC EFFECT

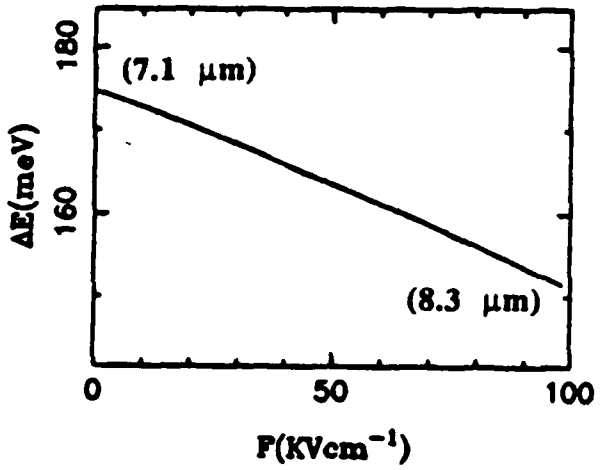

Fig. 3

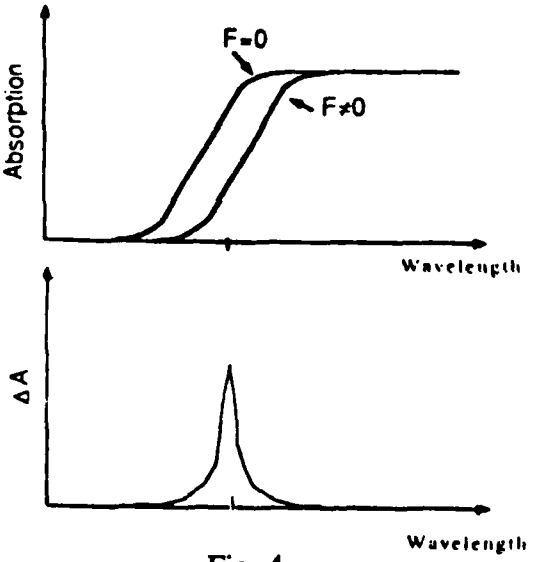

Fig. 4

MAGNETO-OPTIC EFFECT

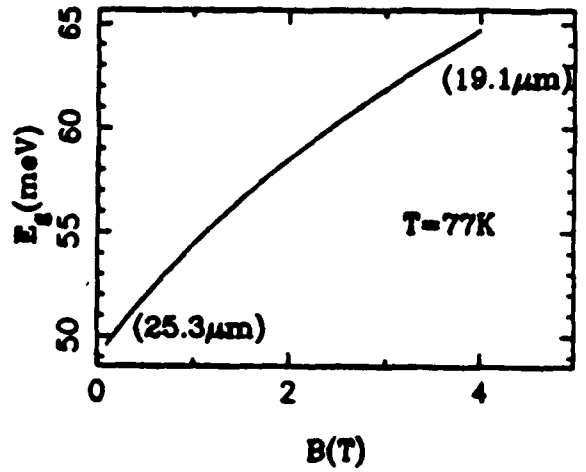

Fig. 5

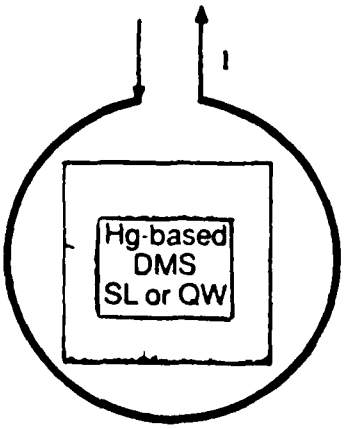

High T_C Superconductor Wire or Thin Film

Fig. 6

Nonlinear Optical Coefficients of Hg-Based Superlattices

E. R. Youngdale, C. A. Hoffman, J. R. Meyer, and F. J. Bartoli
Naval Research Laboratory, Washington, D. C. 20375

X. Chu and J. P. Faurie
Univeristy of Illinois at Chicago, Chicago, IL 60680

J. W. Han, J. W. Cook, Jr., and J. F. Schetzina
North Carolina State University, Raleigh, NC 27695

We discuss an experimental study of optical nonlinearities in Hg-based superlattices. A number of unique features in the theoretical band structures for these superlattices suggest that the system may be an attractive candidate for nonlinear optical applications. These include the predictions of very light electron and hole effective masses in the regime near zero bandgap as well as an extremely strong valence band nonparabolicity. Measurements have been performed on a series of well-characterized HgTe/CdTe and $Hg_{1-x}Zn_xTe$/CdTe superlattice samples. Nonlinear optical coefficients have been determined by the non-degenerate four-wave mixing technique, using a pair of grating tuned, Q-switched CO_2 lasers. Down to the lowest accessible frequency difference ($\Delta\omega \approx 1.8$ cm^{-1}), the data tend to exhibit an inverse square dependence of $\chi^{(3)}$ on $\Delta\omega$ (see Fig. 1). This implies a lower bound of 3 ps for the nonlinear response time. No saturation of the nonlinearity was observed for laser intensities up to 600 kW/cm^2 (see Fig. 2). The dependence of $\chi^{(3)}$ on temperature and superlattice band gap will also be discussed. Even though the samples were grown without regard to optimizing the nonlinear optical properties, $\chi^{(3)}$ values at 300 K and $\Delta\omega = 1.8$ cm^{-1} of up to 2.4×10^{-4} esu were determined from the non-degenerate four-wave mixing measurements. The nonlinearity is attributed to effects of carrier density modulation on the free carrier susceptibility due to optical heating of the electron and hole gases. The optical nonlinearity is predicted to occur over an extended spectral range in the infrared region.

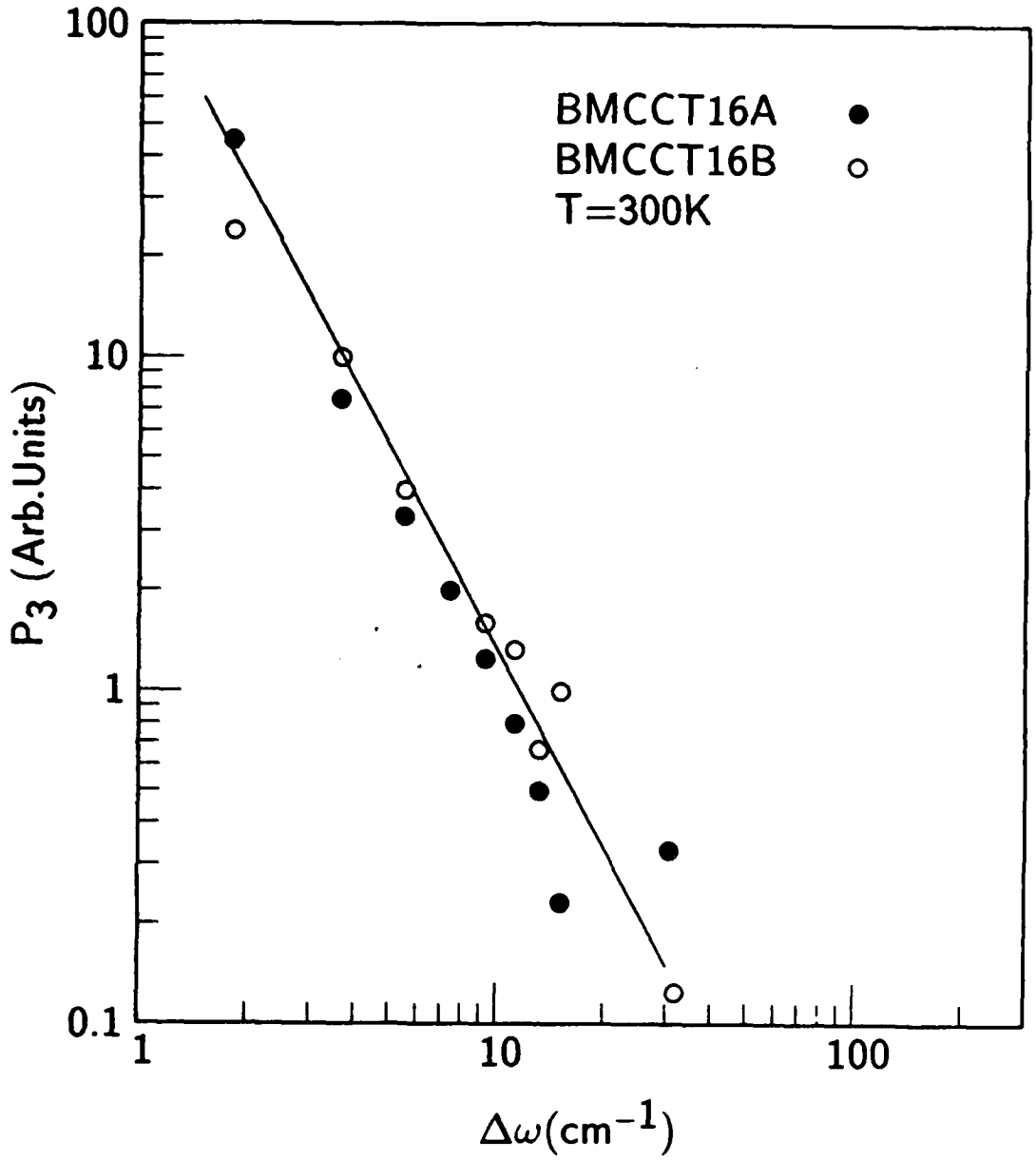

Figure 1:Four wave power as a function of the laser difference frequency, $\Delta\omega$. The points are experimental and the curve represents an inverse square dependence.

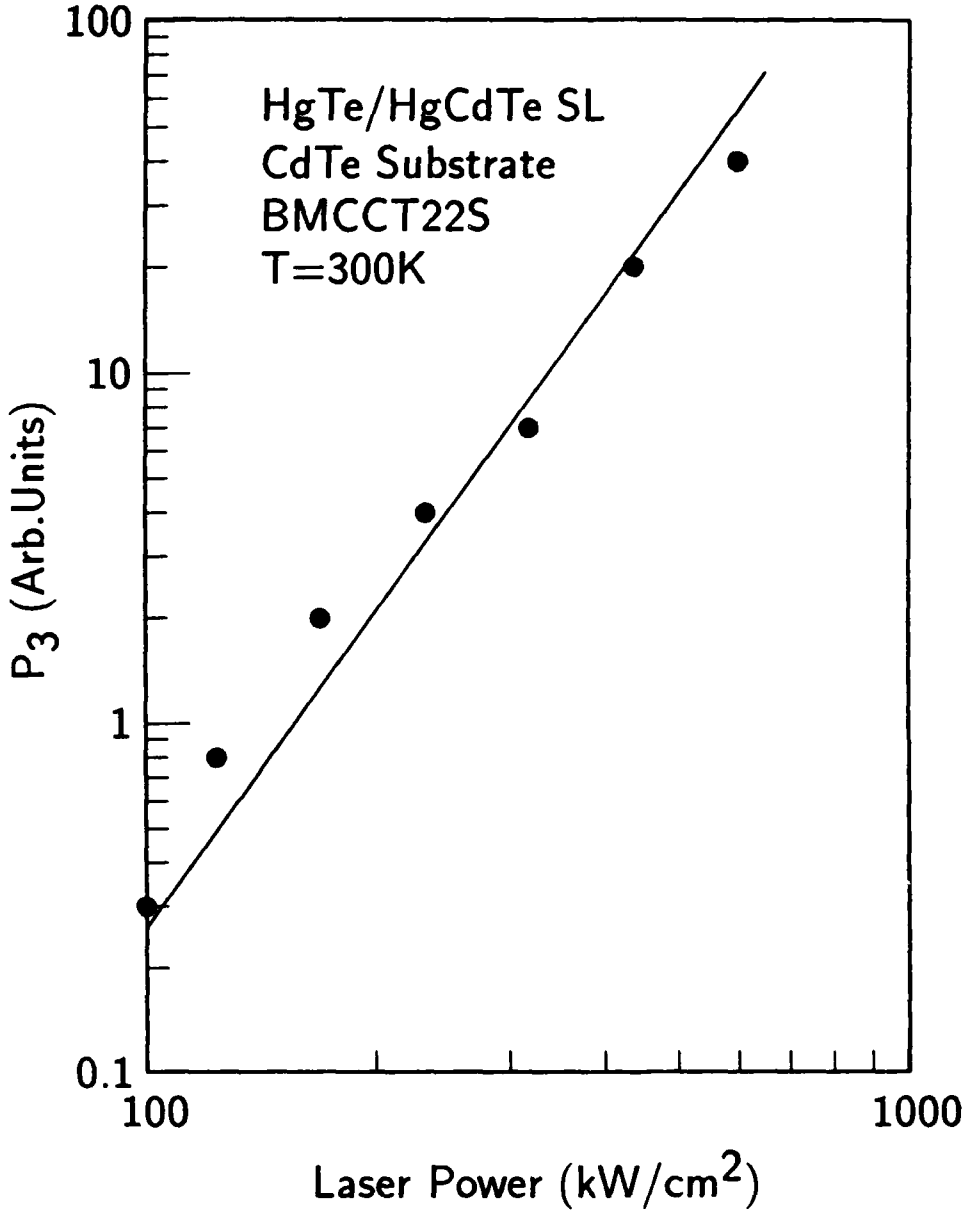

Figure 2: Four wave power as a function of incident laser intensity. The plotted power is $I_1 + I_2$, where the ratio of I_1/I_2 remains constant.

NONLINEAR MAGNETO-OPTICAL SPECTROSCOPY OF $Hg_{1-x}Cd_xTe$ BY TWO-PHOTON ABSORPTION TECHNIQUES*

D. G. Seiler, S. A. Milazzo, M. R. Loloee, A. J. Durkin
Center for Applied Quantum Electronics
Department of Physics
University of North Texas
Denton, Texas 76203

C. L. Littler
Central Research Laboratories
Texas Instruments
Dallas, Texas 75265

Introduction and Background

Nonlinear spectroscopy is an interesting and increasingly useful method for studying and characterizing semiconductors. In part, this is due to the additional information gained over linear spectroscopy and the ever increasing applications of nonlinear optical effects. Two-photon absorption (TPA is one of the numerous nonlinear optical effects arising from χ^3, the electric susceptibility tensor of the third order. Two-photon absorption in a magnetic field also allows the most accurate and detailed characterization of the energy band parameters of a semiconductor. In a previous study,[1,2] we have shown that two-photon absorption techniques can be used to determine TPA cut-off wavelengths and carrier lifetimes for samples of n-$Hg_{1-x}Cd_xTe$ with $x \simeq 0.32$. Here we present for the first time, resonant two-photon magneto-optical spectra for various n-type samples ($x = 0.24, 0.26, 0.28, 0.30$) and one p-type sample ($x = 0.29$).

Experimental Work

Bulk samples of n- and p-type $Hg_{1-x}Cd_xTe$ were polished and etched for these studies. Electrical contacts were made to the rectangular shaped samples with pure indium. All samples showed normal, expected behavior of the Hall coefficient and resistivity as a function of temperature.

Figure 1 shows a schematic diagram of the experimental apparatus used for these two-photon magneto-absorption (TPMA) studies. The grating tunable cw CO_2 laser pulses were obtained from a

mechanical chopper capable of producing 20 μsec wide pulses with a low duty cycle to prevent lattice heating effects. All data were taken in a constant current configuration under ohmic conditions. For this study, the photoconductive (PC) response of each sample was monitored by a boxcar averager. The laser beam propagated parallel to the magnetic field, while the samples were mounted in a transverse magnetoresistance geometry.

Some Experimental Results and Analysis

Figure 2 shows the PC response of an n-type sample with x = 0.236 for various CO_2 laser wavelengths. Some of the resonances in Fig. 2 have magnetic field positions which depend upon the photon energy (as shown by the arrow). We identify this structure as arising from two-photon absorption transitions that take an electron from an initial hole Landau level to a final conduction band Landau level. Other structure is wavelength independent, and is outside the main scope of this paper. We thus choose to concentrate on the two-photon structure.

A modified Pidgeon-Brown energy-band model is used to calculate the Landau level energies. The two-photon transition energies are then calculated by using $2\hbar\omega = E_C - E_V$, and spherical selection rules: σ_L ($\Delta n = +2$), σ_R ($\Delta n = -2$), and σ or π ($\Delta n = 0$). Here Δn is the change in Landau level number. Spin is conserved between the initial and final states. Excellent agreement is obtained between the theoretical and experimental variation of $2\hbar\omega$ versus B as seen in Fig. 3, using the set of band parameters given by Weiler:[3] E_p = 19.0 eV, Δ = 1.0 eV, γ_1 = 3.3, γ_2 = 0.1, γ_3 = 0.9, F = -0.8, q = 0, N_1 = 0, and κ = -0.8. The energy gap was adjusted to give a "best fit" using Eg = 121.0 ± 0.5 meV which corresponds to an x-value of 0.2363 ± 0.0003 using the Hansen, Schmit, Casselman relation.[4]

Other samples also show TPMA structure which can be studied and analyzed. For example, Fig. 4 shows the PC response of a sample which exhibits two major resonances of large amplitude and rather broad features. The peak resonances were analyzed to give Eg = 156.0 ± 0.5 meV or x = 0.2580 ± 0.0003. Using the positions of the half-maximum of the resonances, we can estimate that the inhomogeneity due to variations in x as $\Delta x = \pm 0.0025$. As a final example, we show the PC response for an n-type sample with x = 0.281 in Fig. 5. Again, two major resonances due to TPMA dominate. However, weaker, much broader resonances are seen to occur at higher fields.

Our calculations show that this structure can not be described by any two-photon transitions, but from electron transitions from midgap levels to the lowest conduction band.

Summary

Two-photon magneto absorption structure has been observed and studied in a wide variety of samples of both n- and p-type HgCdTe. Our studies demonstrate the uniqueness and importance of TPMA methods as tools to characterize HgCdTe. For example, we accurately determine the temperature dependence of the band gap and measure two-photon induced carrier lifetimes. Finally, impurity-to-conduction band transitions have been observed from midgap levels and shallow acceptor levels.

References

*Work supported in part by the U. S. Army Night Vision and Electro-Optics Center, Contract #DAAB07-87-C-FO94.

1. D. G. Seiler, S. W. McClure, R. J. Justice, M. R. Loloee, and D. A. Nelson, Appl. Phys. Lett. 48, 1159 (1986).
2. D. G. Seiler, S. W. McClure, R. J. Justice, M. R. Loloee, and D. A. Nelson, J. Vac. Sci. Technol. A4, 2034 (1986).
3. M. H. Weiler, Semiconductors & Semimetals, edited by R. K. Willardson and A. C. Beer (Academic Press, New York, 1981), Vol. 16, p. 119.
4. G. L. Hansen, J. L. Schmit, and T.N. Casselman, J. Appl. Phys. 53, 7099 (1982).

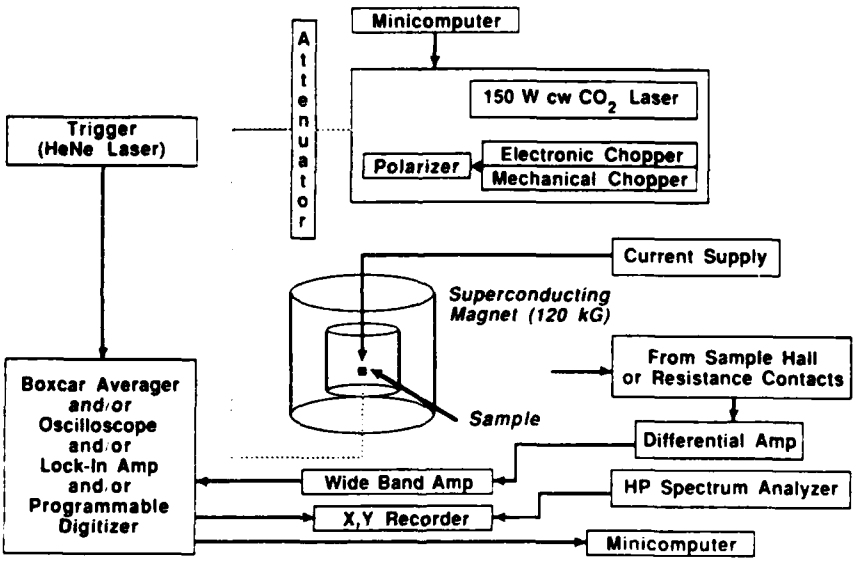

Figure 1. Experimental Set up

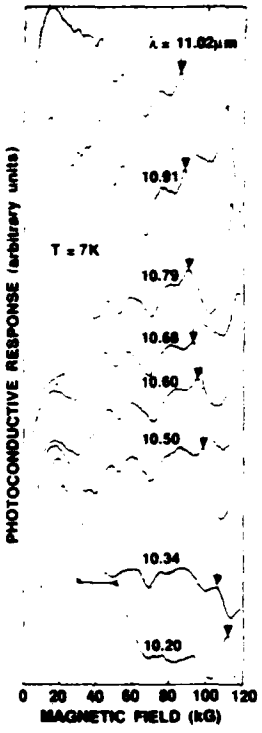

Figure 2. PC response for a sample with x = 0.236. The structure at high fields arises from TPA processes.

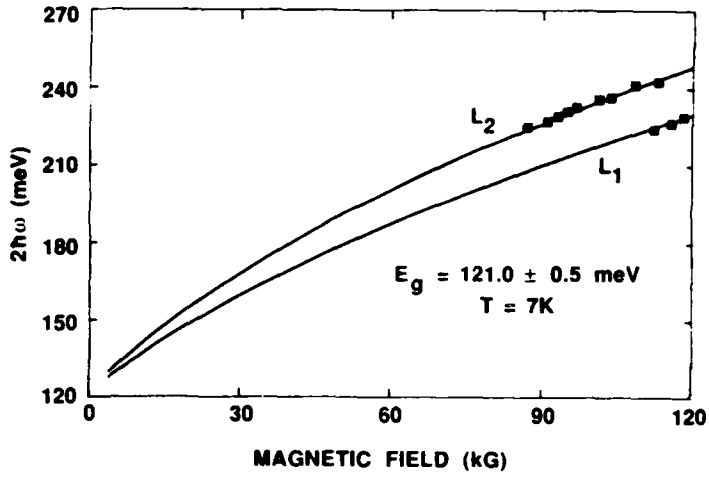

Figure 3. Experimental and calculated two-photon transition energies versus field. L_1 denotes an $a^+(-1)$ light hole level to a $a^c(1)$ conduction band level. L_2 denotes a $b^+(-1)$ to a $b^c(1)$ level.

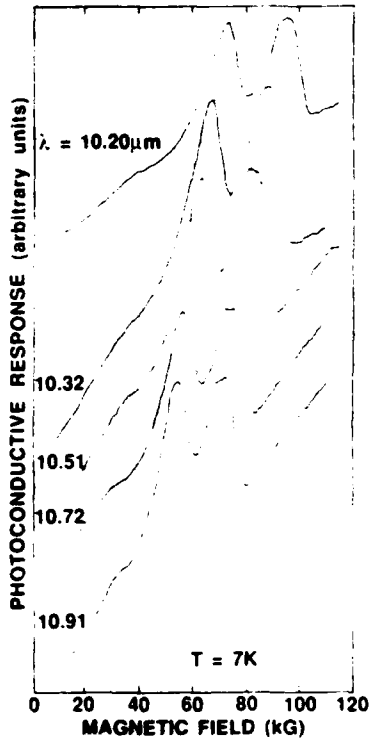

Figure 4. PC response showing TPA structure for a sample with x ≈ 0.26

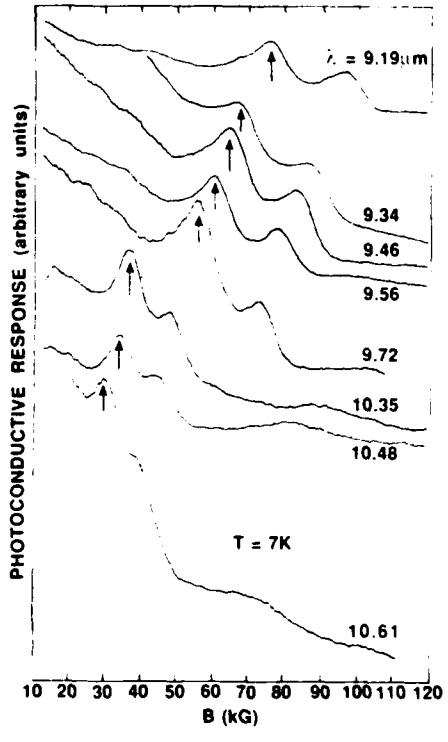

Figure 5. PC response showing TPA and impurity related structure for a sample with x ≈ 0.28

SPACE CHARGE LIMITED CURRENTS IN MBE GROWN CdTe

R. Graft, J. Dinan, U. Lee, T. Fischer,
J. Ramsey, T. Golding, and H. Wilson
US Army Center for Night Vision & Electro-Optics
Fort Belvoir, Virginia 22060

Introduction

CdTe is a technologically important material with applications in solar cells, nuclear particle detection, and infrared focal plane technology. The electrical properties of CdTe are dependent upon the growth method and chemical impurities. Nominally undoped material is generally insulating (resistivity > $1x10^7$ ohm cm) with electrical properties controlled by deep trap levels associated with native defects and/or defect-impurity complexes. When the mobile thermal charge is sufficiently small, charge injected from external contacts cannot be relaxed within the carrier transit time and the current density is proportional to the square of the applied potential. The current is limited by the injected charge density and commonly referred to as space charge limited (SCL). If there is a small but finite thermal charge, the current is initially ohmic ($j \propto V$), followed by a transition to a square law dependence. The filling of multiple trap levels is commonly observed as several square law regions in the IV curve. SCL current measurements in insulating CdTe have been reported by several authors[1-3] but we found no published measurements on MBE grown CdTe. We measured SCL currents in thin films of MBE CdTe grown on HgCdTe and InSb substrates; trapping effects are clearly

evident and classic SCL IV curves are obtained for both substrate materials.

Experiment

CdTe epitaxial layers were grown in a Varian 360 MBE system. The epitaxial layers were grown directly onto InSb substrates or on epitaxial layers of HgCdTe which had been previously grown in a separate reactor by the technique of Close-Spaced Vapor Phase Epitaxy. Typical growth temperatures and deposition rates were 200 C and 0.6 μm/hr respectively; additional details on the growth procedure are available from the literature[4,5]. The as-grown layers were cleaned with a light ion etch (Ar^+, 400V, 0.01 ma/cm^2) and sputtered Au contacts formed on the CdTe overlayer.

Results and Discussion

The data reported here were obtained on two samples with supporting data from several others. The characteristics of the principle samples, 112087B and 022988A, are summarized in Table 1. The measured IV data for 112087B are shown in Figures 1 and 2 for T = 300 K and 77 K respectively. An ohmic crossover region is clearly evident at 300 K and the presence of two or possibly three trap levels are indicated by the $I \propto V^2$ regions. An analysis of the data shows that the principle conduction path is normal to the epilayer plane and laterally along the growth interface. Some electrical characteristics of the CdTe layer can be estimated from the low voltage ohmic region of Figure 1. At 300 K we find: resistivity = 4×10^9 ohm cm, E_{Fermi} = 0.67 ev, thermal charge density = 2×10^7 holes/cm^3, and injected charge density at the ohmic - SCL crossover voltage = 1×10^{15} holes/cm^3.

From the latter two values the ratio of free to trapped holes is $2x10^{-8}$, indicating strong hole trapping in the CdTe layer. Analysis of the trap energy levels and densities apparent in Figure 2 is incomplete. Our best estimates are acceptor levels at 0.060, 0.055, and perhaps 0.04 ev above the valence band edge. A level at 0.06 ev is commonly seen in CdTe and attributed to either a Cadmium vacancy or Cadmium vacancy complex[6].

The current voltage data for Sample 022988A are shown in Figure 3. Two features of this data are of interest:

(1) The data were taken in two steps, the second measurement giving only the instrumentation dependent leakage current until the applied potential reaches the maximum potential applied in the first. Apparently, deep trap levels are filled during the initial measurement and not emptied prior to the second, this despite exposure to a laboratory environment for approximately two days between measurements.

(2) The current rises nearly 5 decades in a 0.2 volt increment near 10 volts with a complex voltage dependence beyond the rise.

Analysis of the 77 K ohmic crossover region gives: resistivity = $7x10^{11}$ ohm cm; free thermal charge = $6x10^{3}$ holes/cm^3; E_{Fermi} = 0.21 ev; and ratio of free to trapped charge = $1x10^{-12}$.

References

(1) S.S. Ou and O.M. Stafsudd, Thin Solid Films 112, 301(1984).
(2) A. Zoul and e. Klier, Czech. J. Phys. B 27, 789(1977).
(3) K. Mochizuki and K. Masumoto, Material Letters 4, 301(1986).
(4) J.H. Dinan and S.B. Qadri, Thin Solid Films 131, 267(1985).
(5) R.F.C. Farrow, G.R. Jones, G.M. Williams, and I.M. Young, Appl. Phys. Lett. 39, 954(1981).
(6) K. Zanio, Semiconductors and Semimetals, Vol. 13, Academic Press, New York, 1978.

Table 1. Sample Characteristics

Sample	Substrate	CdTe Thickness	Growth Temp
112067B	HgCdTe/CdZnTe (p-type, <100>)	2000 A	205 C
022968A	InSb (n-type, <100>	2000 A	220 C

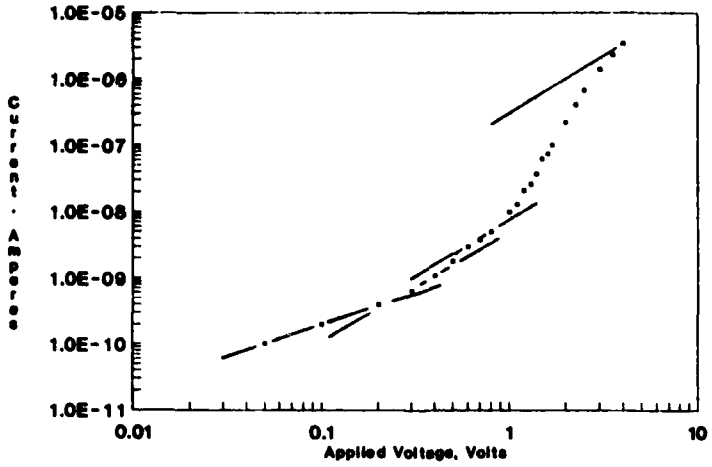

Figure 1. Sample 112067B, T=300K

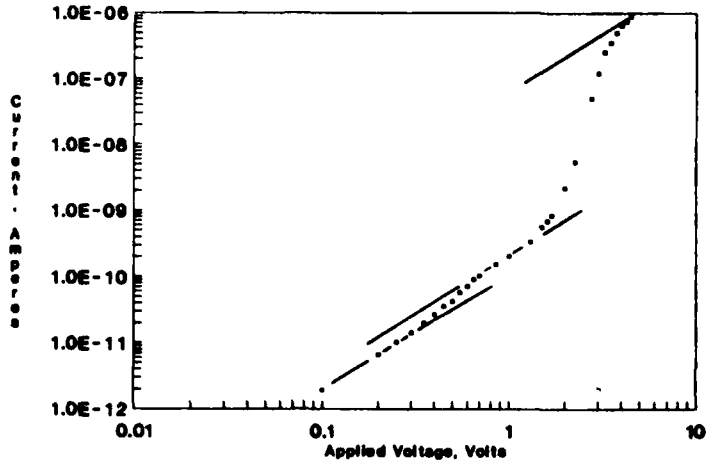

Figure 2. Sample 112067B, T=77K.

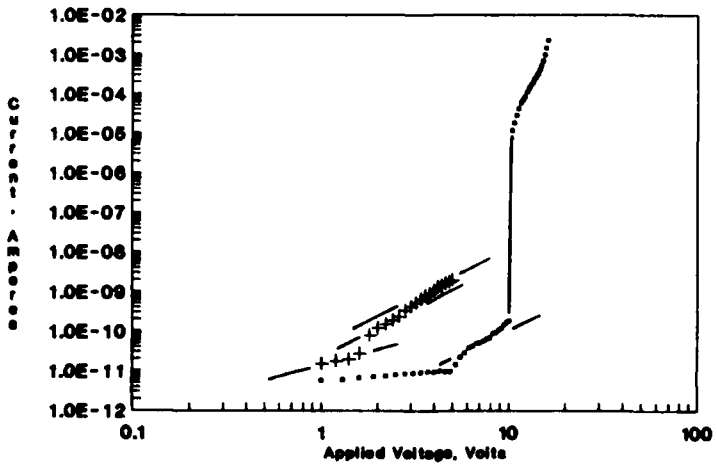

Figure 3. Sample 022968A, T=77K.

Characteristics of HgCdTe Single-Sided Gate Junction Field Effect Transistors

G.R. Chapman, E.A. Patten, P.R. Norton, T.N. Cassleman
Santa Barbara Research Center, 75 Coromar Drive, Goleta CA 93117

$Hg_{1-x}Cd_xTe$ Junction Field Effect Transistors (JFET) have been fabricated and characterized for transistor properties as well as noise. JFETs in general offer high input impedances and low noise simultaneously as opposed to MOSFETs which have high input impedances but suffer from high 1/f noise, whereas bipolar transistors have low 1/f noise but suffer from low input impedances.

The JFETs were fabricated from a 9μm thick layer of x=0.4 $Hg_{1-x}Cd_xTe$ grown by liquid phase epitaxy from the Te corner on a CdTe substrate. The undoped HgCdTe channel material used was n-type with an electron concentration of about $1x10^{14}/cm^3$. The devices have single-sided gates such that channel pinch-off occurs against the high resistance CdTe substrate. The average pinch-off voltage was determined to be about 4.5V.

Initial measurements at 77K for unoptimized n-channel JFETs show peak transconductances of about 250 μmho for a gate aspect ratio of 150μm/50μm. 1/f noise measured in a source-follower configuration is $5\mu v/\sqrt{Hz}$ at 1Hz.

For high drain currents the devices can be modeled by simple first-order theory. At low drain currents for which most of the channel is pinched off against the CdTe substrate, there is significant deviation from first-order theory.

Model calculations will be compared with I-V data, an example of which is shown in the figure. Detailed data consisting of noise spectra, transconductance as a function of bias point and gate diode characteristics will also be presented and compared with theory where applicable.

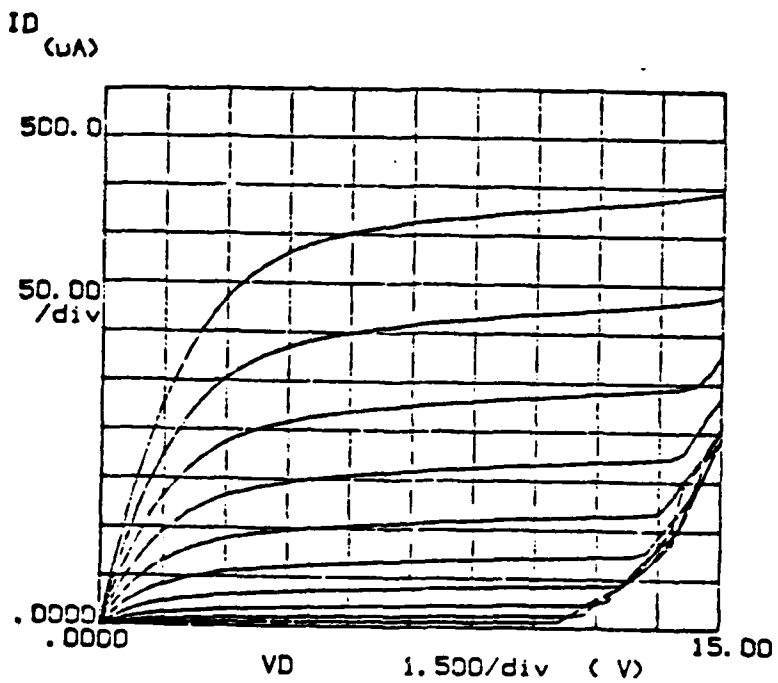

77 K Voltage-Current Data For a $Hg_{0.6}Cd_{0.4}Te$ Junction Field Effect Transistor. Gate Voltage Steps Are -.5V Starting at 0V(Top Curve)

Magnetic Field Effects on Trap-Assisted Tunneling in Hg(.78)Cd(.22)Te

J.R. Waterman, J.M. Perez, R.J. Wagner
Naval Research Laboratory, Washington, DC 20375

We have investigated trap assisted tunneling processes in p-type Hg(.78)Cd(.22)Te MIS capacitors using capacitance-voltage (C-V) and conductance-voltage (G-V) measurements in magnetic fields (B) up to 4.0 T.

At B=0 and 4.2K, oscillatory behavior in strong inversion C-V and G-V data indicates that the dominant minority carrier generation mechanism is the two step thermal generation/trap-assisted tunneling process into the two dimensional quantized electric subbands[1]. Four distinct subbands were observed as peaks in the "high frequency" G-V data for biases corresponding to the coincidence of the bulk Fermi level and an electric subband.

In a magnetic field, the electric subbands will split into Landau levels. To demonstrate the existence of the Landau levels, C-V data was taken with a guard ring biased to provide minority carriers, making the device analogous to a MOSFET. Here, spin degenerate Landau level series were observed for each subband.

One would expect the MIS G-V data to also reflect the Landau density of states. With B $\perp$ to the inversion layer, the positions of the G-V peaks were seen to increase linearly with B as expected for the n=0 Landau level (Figure 1). However, no indication of tunneling into higher order Landau levels was observed. The tunneling current also decreased by a factor of 7 for a field of 2.0 T. With B at 45° with respect to the inversion layer, tunneling was observed into the n=0 and higher order spin degenerate Landau levels in the G-V data (Figure 2), in agreement with the gate voltage positions observed in the "pseudo MOSFET" configuration C-V data. For B $\parallel$ to the interface, the G-V peak position shifted to larger gate voltages, reflecting the effect of B on the electric sub-band energies.[2] The tunneling current also decreased by a factor of 60 for B = 2.0 T.

A model will be presented to explain the "selection rules" governing the dependence of the tunneling current on the magnetic field direction as well as the dependence of the magnitude of the tunneling current on magnetic field.

---

[1] J.D. Beck, M.A. Kinch, E.J. Esposito, R.A. Chapman, J. Vac. Sci. Technol., 21(1), (1982).

[2] Stern, F., Phys. Rev. Lett. 21, 1687 (1968).

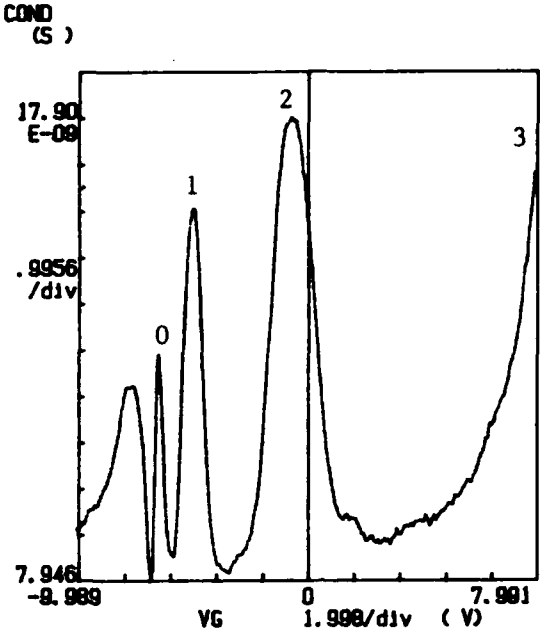

Figure 1. Conductance-voltage data with B=2.Ø T perpendicular to the inversion layer, showing tunneling into the i = Ø, 1, 2, and 3 electric sub-bands. Peak positions are in agreement with the n=Ø Landau levels observed in the pseudo MOSFET configuration C-V measurements.

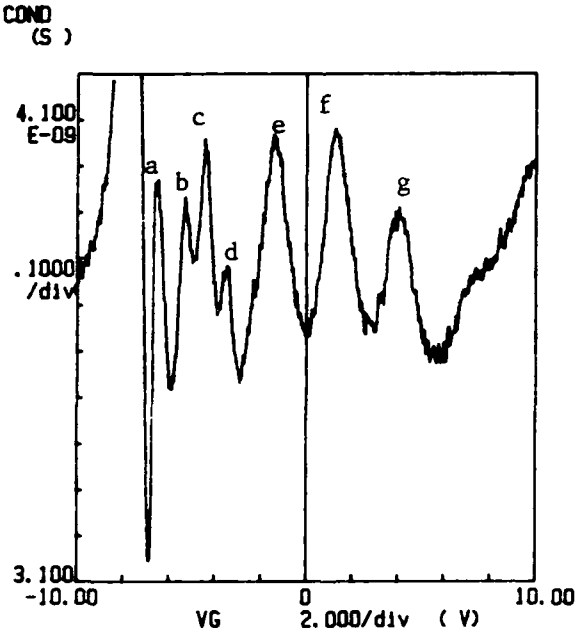

Figure 2. Conductance-voltage data with B=2.Ø T at 45° w.r.t. the inversion layer. Peaks labeled a, b, c, d, e, f, g, correspond to tunneling into the (Ø,Ø), (1,Ø), (1,1), (1,2), (2,Ø), (2,1), and (2,2) levels, with the first index representing the sub-band and the second the Landau level.

Magnetic Field Effect on the R_oA Product of HgCdTe Diodes

S.E. Schacham and E. Finkman

Microelectronics Research Center, Department of Electrical Engineering,
Technion - Israel Institute of Technology, Haifa 32000, Israel

Understanding the recombination mechanisms in $Hg_{1-x}Cd_xTe$ $p-n$ junctions is essential to improve device performance. These mechanisms affect directly the reverse saturation currents J_{on} and J_{op}, the form of the I-V characteristics, and the zero bias resistance area product (R_oA). The most common technique for implementing $Hg_{1-x}Cd_xTe$ diodes is by implanting an n^+ layer on top of a p-type substrate. It was generally argued that for such diodes J_o is governed by diffusion mechanism, that the contribution of generation-recombination in the space charge region is negligible, and that most contribution to the reverse saturation current is from the p-side of the junction ($J_{on} \gg J_{op}$) [1]. The analysis of the data was usually based on the depletion approximation, with two uniformly doped regions on each side of the space charge region. These assumptions are rather convenient to use, as they do not involve more complicated calculations in the implanted region, including gradients in material parameters like carrier concentration, lifetime etc. The arguments were based on the assumption that the Auger recombination rate, which is assumed to dominate the excess carrier lifetime in the n^+ side is greatly reduced in the heavily degenerate n-region thus minimizing its contribution. However, the arguments were mostly qualitative because there have been neither detailed theoretical calculations nor experimental study of the n-side diffusion current for such diodes [1]. Support for these assumptions came from an analysis of the temperature variation of R_oA which show, for a large temperature range, a characteristic dependence on n_i^2.

We started to question this picture after being unable to explain some contradictions that arose analyzing data of n^+-p $Hg_{1-x}Cd_xTe$ diodes. While the bulk excess carrier lifetime can be as high as several hundred nanosecond [2], and such is the case for analyzing the data of Shotky-barrier diodes [3], the effective lifetime in implanted n^+-p diode is only few nanoseconds, with an upper limit of 20-30 nsec. These effective lifetimes are found by analyzing the R_oA product or the reverse recovery time using the above mentioned assumptions. We then performed measurements of excess carrier lifetime as a function of depth in implanted $Hg_{1-x}Cd_xTe$ junctions with bulk lifetimes of 0.3-1 μsec. The results indicate that the lifetime recovers to its large bulk value close to the space charge region [4]. A long electron lifetime in the p-region, however, indicate a non-negligible contribution of the n^+ region to the diode current and to R_oA. This work is therefore concentrated on this aspect of the diode performance. Finally we would like to mention that we analyzed $p-n$ junctions for the case of a graded profile of electrons and lifetime in the n^+ region [5]. The results show that regardless of the actual recombination mechanism, J_o has approximately n_i^2 temperature dependence. Moreover, the drift term that arises from the concentration gradient also has the same dependence on temperature, and might be substantially high. Thus, the analysis based

on the simple assumptions is questionable.

The samples used were $Hg_{1-x}Cd_xTe\ B^+$ ion implanted p-n junctions with $x \approx 0.215$ (cut-off wavelength $\lambda_c \approx 11.5\ \mu m$, $R_oA = 1-2\ \Omega cm^2$ at 77 K). In order to separate the contribution of the n-side component to the R_oA product from that of the p-side, the diode was placed in a magnetic field perpendicular to the junction and the current-voltage characteristics were measured as a function of magnetic field for various temperatures in the range of 13 K to 160 K. Due to the high ratio between the electron and hole mobilities in HgCdTe, this method can be used to differentiate between the two components, with relatively modest magnetic fields. "The effective magnetic mobility, or diffusion coefficient", were defined by Zitter [6]. To a first approximation they vary with magnetic field as $1/(1+\mu_i^2 \cdot B^2)$, where μ_i is the mobility of the i-th carrier, B is the magnetic field. The effective diffusion length is reduced by a factor of $(1+\mu_i^2 \cdot B^2)^{-\frac{1}{4}}$. Since $Hg_{1-x}Cd_xTe$ is characterized by a very high electron mobility, and moderate hole mobility, only the effective parameters of the electrons will be reduced by the magnetic field. This effect is used to differentiate between the electron and hole components of the diode current. Recalling that J_{op} is the contribution of the n-side of the junction, and vice versa, only J_{on} is affected by the magnetic field.

The fit was carried out using a magnetic field dependence of $1/(1+\mu_e^2 \cdot B^2)^n$ for J_{on}. Where the electron mobility μ_e and the power n were the fitting parameters. The best fit for all temperatures gave $n=1.01 \mp 0.02$, verifying that the p-side of the diode can be considered as narrow [5]. Since the spacing between the diode electrodes is about 100 μm, the diffusion length is larger than that, which means that the effective lifetime in the p-side is quite long. Figure 1 shows an example of the parameter fit to the magnetic field dependence of J_o. There are three fitting parameters, J_{on}, J_{op}, and μ_e (assuming n=1). Figure 2 presents the results of the analysis of J_{on} and J_{op} at various temperatures. The ratio J_{on}/J_{op} is given in figure 2. Our results show that for temperatures above ~60 K, the ratio of the p-side current contribution to that of the n-side is about 3/1. This ratio decreases rapidly below ~60 K and approaches 1/2 at 13 K. This indicates that the contribution of the n-side current is of the same order of magnitude as that of the p-side, and therefore cannot be neglected at any temperature for this type of diodes.

References

[1] M.B. Reine, A.K. Sood and T.J. Tredwell in "Semiconductors and Semimetals", edited by R.K. Willardson and A.C. Beer (Academic, New York, 1981), Vol. 18, pp. 201-311.

[2] S.E. Schacham and E. Finkman, J. Appl. Phys. 57, 2001 (1985).

[3] D.L. Polla, S.P. Tobin, M.B. Reine, and A.K. Sood, J. Appl. Phys. 52, 5182 (1981).

[4] A. Fraenkel, S.E. Schacham, G. Bahir, and E. Finkman, J. Appl. Phys. 60, 3916 (1986).

[5] S.E. Schacham and E. Finkman, to be published.

[6] R.n. Zitter, Phys. Rev. 112, 852 (1958)

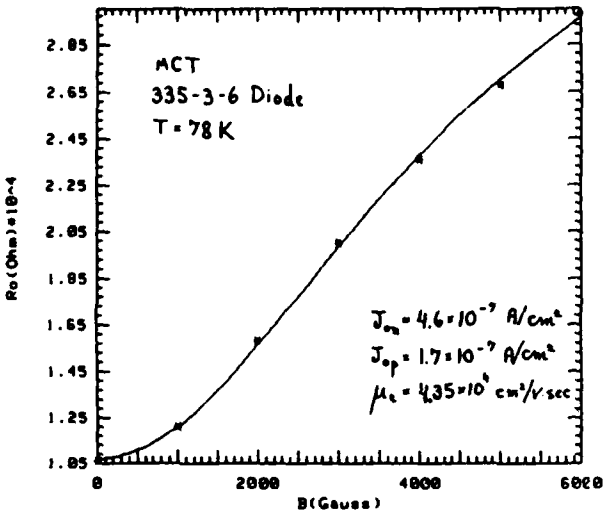

Fig. 1: Parameter fit for the magnetic field dependence of the reverse saturation current of an $Hg_{1-x}Cd_xTe$ n^+ on p diode.

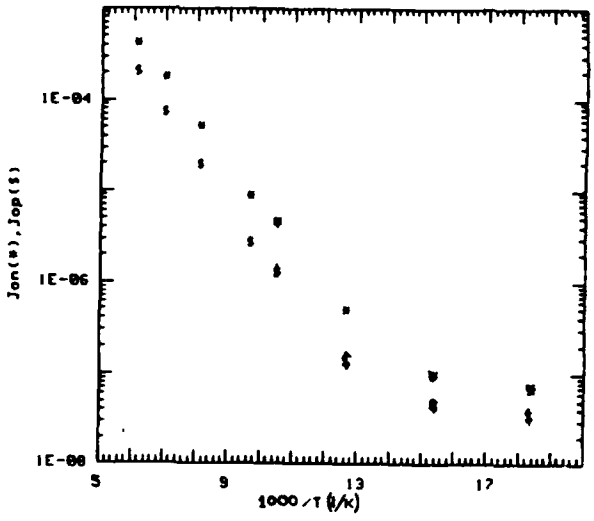

Fig. 2: The contributions of electrons and holes to the reverse saturation current in an $Hg_{1-x}Cd_xTe$ diode, as a function of temperature.

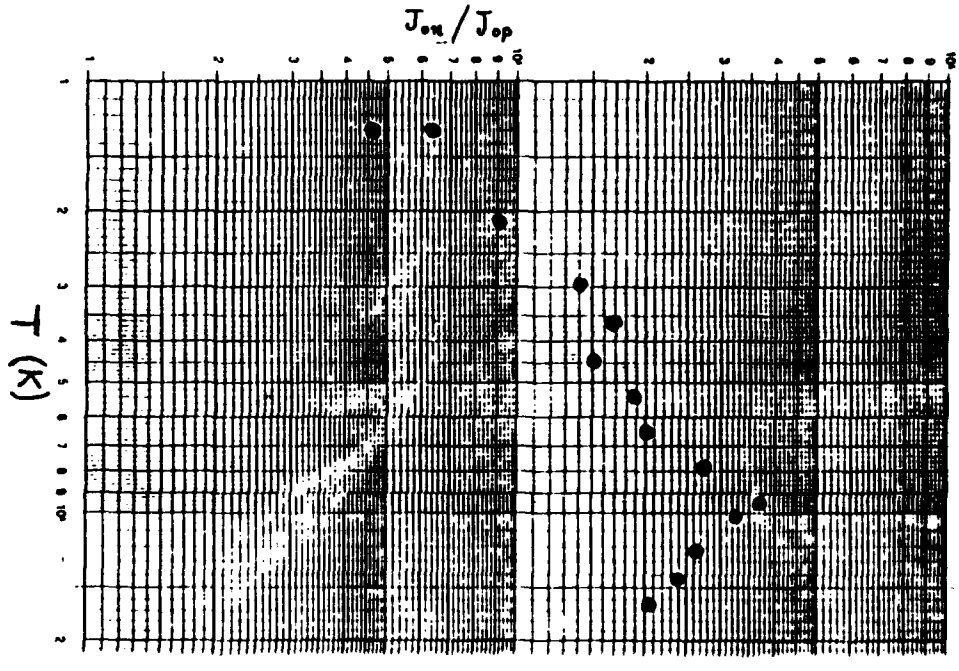

Fig. 3: The ratio J_{on}/J_{op} for the diode of figure 2, as a function of temperature.

STRAIN EFFECTS IN $Hg_{1-x}Cd_xTe$ (X~0.2) PHOTOVOLTAIC ARRAYS

Eliezer Weiss and Nili Mainzer
SCD - Semi-Conductor Devices
A Tadiran-Rafael Partnership,
Misgav Mobile Post, 20179,ISRAEL

The effect of strain and stress on the performance of $Hg_{1-x}Cd_xTe$ (x~0.2) n^+ on p photovoltaic arrays was studied, both in the dark and under illumination, by deliberately applying external strain to them under controlled conditions. It was found that external strain causes a shift in the current-voltage characteristic of the photodiode along the voltage axis, affecting its short current and R_0A product (Fig. 1a,b). The reverse current and breakdown voltage of the diode are also affected by external strain (Fig. 1b,c). The combined action of illumination and strain yields an anomalous response to light absorption in the device (Fig. 2).

A model was conceived wherein the photodiode and gaurd-ring are treated as a MISFET structure (Fig. 3). The strain caused by small apertures in the C common connection causes n-type damage, yielding a pseudo-Schottky diode. The open circuit voltage of this diode is treated as a strain and light induced voltage (V_C) in series with the photodiode. The change in the n-channel conductivity, caused by the strain, is expressed as a pseudo-voltage (V_{PG}) on an imaginary gate. The strain induced change in the n-channel conductivity is due either to the piezoelectric effect or to the formation of strain induced n-type damage.

Using V_C and V_{PG} the current-voltage characteristic of the diode subjected to stress, is calculated. Similarly, the effect of these parameters on the zero bias resistance, the reverse and short currents, and the open circuit voltage of the device is assessed.

Observed phenomena in $Hg_{1-x}Cd_xTe$ photovoltaic arrays are explained using this model and internal stresses. These elastic stresses originate from wafer deformation, probably induced during crystal growth. However, stress is also induced in the $Hg_{1-x}Cd_xTe$ substrate during the fabrication of the arrays, particularly in the vicinity of windows in the dielectric overlayer.

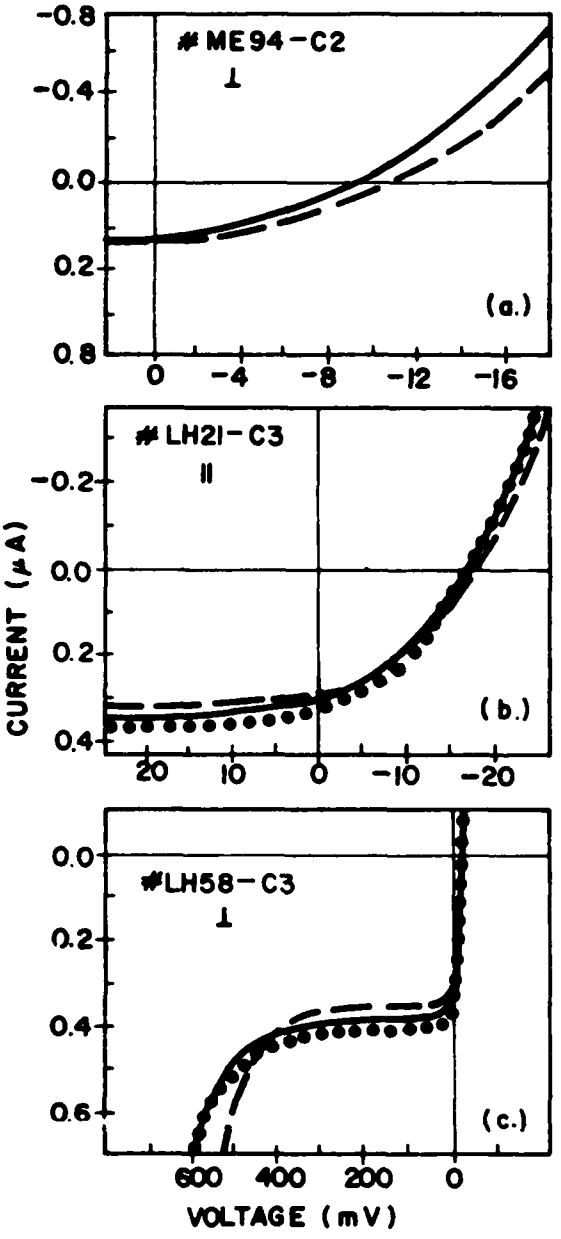

Fig. 1. I-V characteristic measurements of photodiodes under mechanical stress and illumination. The photodiodes are connected to common connections with small contact windows. Solid line - no external stress situation. Tensile stress - dashed. Compressive stress - dotted.

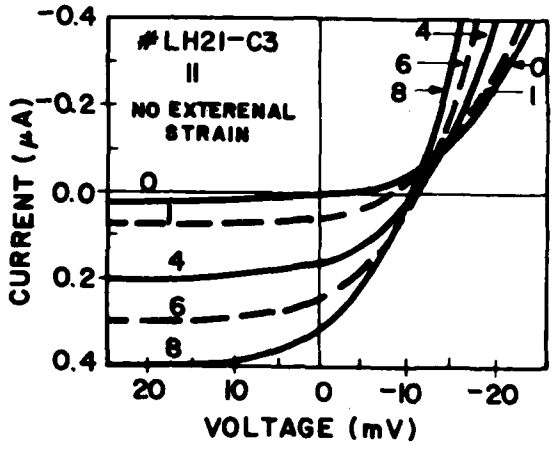

Fig. 2. I-V characteristic measurements of photodiodes under various photon fluxes (in arbitrary units). An unstressed photodiode is connected to the common connection with the small openings.

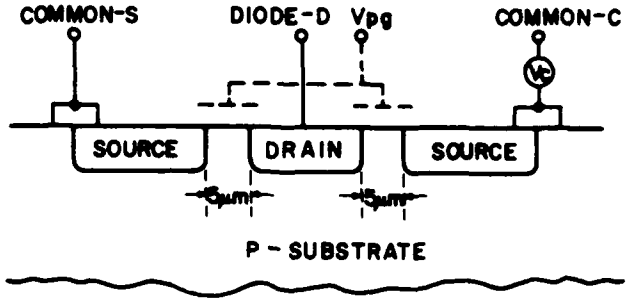

Fig. 3. Cross-section of the MISFET structure

THERMAL ANNEALING STUDIES ON BORON-IMPLANTED HgCdTe DIODES

by

Jing-Kai Syz[1], Jeff Beck[2], Tom Orent[2], and Herb Schaake[2]

[1]Department of Electrical Engineering and Computer Science,
Massachusetts Institute of Technology, Cambridge, MA 02139

[2]Central Research Laboratories, Texas Instruments Incorporated, Dallas, TX 75265

Although ion implantation is a useful technique in doping $Hg_{1-x}Cd_xTe$, precise control over dopant concentration, depth, and distribution has yet to be achieved. The present work involves an experimental study of annealing effects on the doping profile at the *np* junction and on electrical properties of ion-implanted $Hg_{1-x}Cd_xTe$ ($x = 0.22$-0.23). Junction profiling was performed by the reverse bias capacitance-voltage (C-V) technique. We could not directly apply Bubulac *et al.*'s model for ion-implanted, vacancy-doped material1 to our diodes which were formed on copper-doped material. We expand Bubulac *et al.*'s junction formation model to include the effects of the interstitial gettering mechanism operant in the presence of a highly mobile acceptor impurity such as copper.[2] During thermal anneal treatments, doping redistribution is observed.

The starting material was single-crystal solid state recrystallized (SSR) $Hg_{0.8}Cd_{0.2}Te$ that was homogeneously *p*-type due to copper contaminant introduced during high temperature steps in the SSR growth process[3]. *P*-type conductivity was dominated by the copper since the bulk material was post-annealed under Hg saturated conditions at 270°C for 4 weeks to produce a homogeneous metal vacancy concentration less than 10^{14} cm^{-3}.[4] Surface passivation was achieved using anodic sulfidization. The diodes were formed at room temperature by implanting 100 KeV B^+ ions at a fluence of 10^{13} cm^{-2}.

Implant distributions are determined via secondary ion mass spectroscopy (SIMS) and supplement the C-V doping profiles. These profiling methods are applied to four samples before and after various thermal anneals. Anneal times ranged from 30 seconds to 24 hours, and temperatures ranged from 100°C to 200°C. Diode reverse leakage behavior, R_0A, and reverse-recovery lifetimes were also measured to determine the full effects of thermal annealing.

As-implanted diodes can be sufficiently modelled by the abrupt junction approximation, consistent with our previous findings for anodic oxide passivated diodes[5]. An example of a linear fit representing the abrupt junction model to the C-V data is shown in Figure 1. Capacitance measurements were corrected for stray capacitance. The abrupt model yields the best fit over the widest range of data. Using the slope of the linear fit, we find that the reduced doping concentration, N_B, is 3.59 x 10^{14} cm^{-3}. This implies a net donor concentration, N_D, of 4.76 x 10^{14} cm^{-3} on the *n*-type side of the junction assuming the measured Hall net acceptor concentration, N_A, of 1.46 x 10^{15} cm^{-3} for the *p*-type side. Since the majority carrier concentrations on either side of the junction are within an order of magnitude of one another, we can ignore the finite tail penetrations into the space charge region in our calculations. We expect, however, the surface to be highly damaged[1,6] which explains the deviation for biases greater than 0.5 volts in Figure 1.

The unannealed junction apparently has an abrupt *n+/n-/p* characteristic. In contrast, Bubulac *et al.*'s model[1] for our case would predict a *n+/p* junction defined by the boundary between the highly damaged *n+ region and the impurity* doped *p*-type base. An interstitial gettering mechanism[2] in the presence of a highly mobile Group II site substitutional acceptor impurity (copper), together with the presence of a relatively immobile (and lower) background donor concentration, is proposed as the vehicle for type conversion in the vicinity of the electrical junction. Our model for junction formation in a material with a dominant, but mobile, acceptor, a lower concentration relatively immobile donor, and a much lower native defect acceptor is as follows: A vacancy concentration gradient created by the Hg interstitials causes the movement of the acceptor copper atoms, via an interstitial gettering mechanism, away from the lower vacancy concentration region leaving the background donor to dominate and form the *n-* region.

In general, we observed junction grading after thermal anneal cycles. Figure 2 illustrates the best fit we obtained for the diode in Figure 1 after an one hour, 150°C oven anneal. The doping redistribution yielded an excellent fit to a linearly graded junction model. Analysis of the general N_B versus total depletion width, W, results obtained from C-V data shows that doping near the junction is reduced. In fact, this and other anneal experiments, including a rapid thermal anneal sample, suggest that a near-junction donor source is thermally activated around 150°C. Post-anneal

junctions also exhibit the $n+/n-/p$ structure which can be explained by our interstitial gettering model.

SIMS profiles reveal no evidence of boron diffusion from the implant region after our anneal cycles. Furthermore, the location of the electrical junction was found to be much deeper than the implant. Thus, the primary junction formation mechanisms are related to implantation side effects. We model the observed post-anneal junction grading by assuming the in-diffusion of Hg interstitials generated by implantation. Further impurity and interstitial redistributions, leading to lower doping levels at the junction, occur during thermal anneal treatments.

Changes in the doping profiles correspond to observed changes in diode electrical properties. Dramatic improvement of tunnel-limited behavior is seen in Figure 3 after the 150°C, one hour anneal. The improvement at low temperatures after thermal annealing can be attributed to relatively lower electric fields in graded junctions. Lower doping concentration at the junction after thermal anneal also contributes to a lower electric field. Improvement of the reverse-recovery lifetime is seen and is attributed to thermal damage annealing.

Comparisons of before/after anneal diode and metal-insulator-semiconductor (MIS) capacitor data show only a reduction of fixed positive charge at the surface. No apparent improvement of the surface is seen, indicating that the primary effects of thermal treatments are electrically active species movement and bulk damage anneal. Our results indicate that thermal annealing is a promising method of improving diode electrical properties.

REFERENCES

1. L. O. Bubulac, W. E. Tennant, D. S. Lo, D. D. Edwall, J. C. Robinson, J. S. Chen, and G. Bostrup, J. Vac. Sci. Technol. A, 5 (5), 3166 (1987).

2. H. F. Schaake, J. H. Tregilgas, J. D. Beck, and M. A. Kinch, Solid State Communications, 50 (2), 133 (1984).

3. J. Tregilgas, J. Beck, and B. Gnade, J. Vac. Sci. Technol. A, 3 (1), 150 (1985).

4. H. F. Schaake, J. Electron. Materials, 14 (5), 513 (1985).

5. J. Syz, TI Internal Report, August 29, 1986.

6. A. Fraenkel, S. E. Schacham, G. Bahir, and E. Finkman, J. Appl. Phys., 60 (11), 3916 (1986).

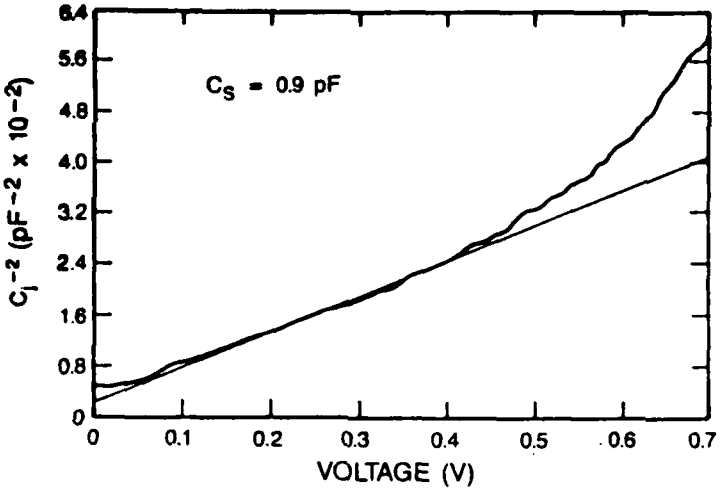

Figure 1. Linear fit of pre-anneal diode capacitance-voltage data to the abrupt junction model for $0 \leq V_R \leq 0.5$ V.

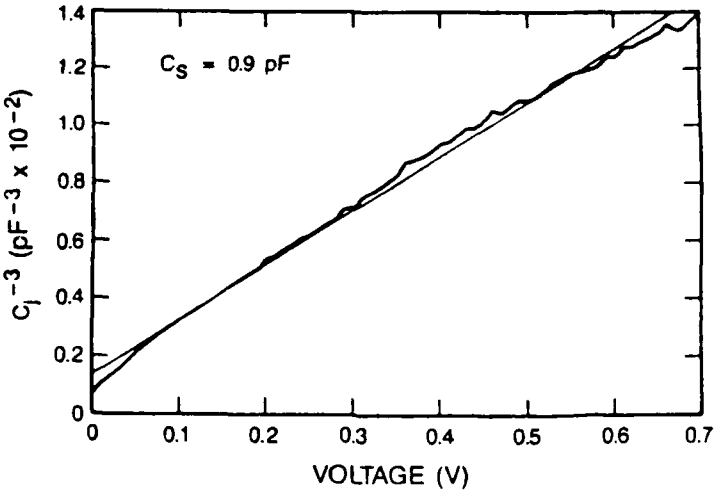

FROM 0 to 0.7 V,
R^2 = 0.99393
SLOPE = 1.868 x 10^{-2} pF^{-3} V^{-1}
Y-INTERCEPT = 1.352 x 10^{-3} pF^{-3}

Figure 2. Linear fit of diode capacitance-voltage data to the linearly graded model after an one hour, 150°C anneal for $0 \leq V_R \leq 0.7$ V.

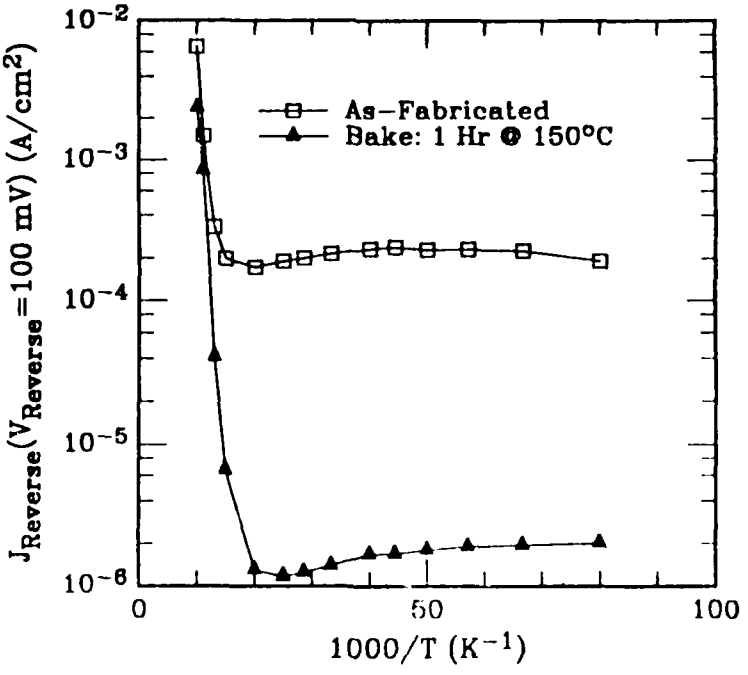

Figure 3. Reverse leakage current density at a bias of 100 mV versus 1000/T before and after an one hour, 150°C oven anneal.

BAND-EDGE PROPERTIES OF Hg-BASED SUPERLATTICES

J.R. Meyer, C.A. Hoffman, and F.J. Bartoli
Naval Research Laboratory
Washington, DC 20375

Recent magneto-transport and magneto-optical investigations of Hg-based superlattices will be reviewed, and their contribution to the understanding of superlattice band structure discussed. Hall and conductivity measurements as a function of magnetic field and temperature have been performed on a large number of HgTe-CdTe and $Hg_{1-x}Zn_xTe$-CdTe samples with a wide range of barrier and well spacings.[1,2] In narrow-gap samples ($0 < E_g < 100$ meV) for which intrinsic electrons could be observed over a broad temperature range, band gaps determined from $n_i(T)$ agree well with theoretical values obtained from a tight-binding band structure calculation[3] if one employs a large value for the valence-band offset (e.g., $\Delta = 350$ meV). Futhermore, the low-temperature mobilities for both electrons and holes are found to have a strong inverse dependences of E_g. In zero-gap samples, hole mobilities $> 10^5$ cm^2/V-sec are observed which are the highest ever reported for a II-VI semiconductor. It is also noteworthy that the ratio of electron-to-hole mobility at low temperatures is near unity in all p-type samples for which the determination could be made. All of these observations are consistent with the band structure calculations if one employs a valence band offset large enough to assure that the highest valence band is heavy-hole-like (HHL).[4] The theory then predicts nearly identical electron and hole masses in the plane, which become quite small ($<< 0.01m_0$) when the conduction and valence bands approach cross-over. Furthur experimentally observed features such as the presence of more than one hole species at low temperatures as well as an abrupt decrease in μ_p at temperatures above ~ 30 K are also qualitatively reproduced by the calculations, which predict a range of effective masses at the valence-band maximum and strong nonparabolicity of the highest valence band. However, the experimental findings are inconsistent with band structures calculated assuming $\Delta < 200$ meV, since strain then causes a light-hole-like valence band (LHL) to dominate, and the in-plane hole mass is much heavier than that of the electrons.[4]

A further test of the band structures is provided by recent magneto-optical measurements on a p-type HgTe-CdTe superlattice with band gap near zero.[5] Hole cyclotron resonance was observed for both magnetic field parallel to the growth direction (cyclotron orbits in the plane) and fields parallel to the plane (cyclotron orbits must tunnel through the barriers). The free hole effective mass at low temperatures is found to be ~ 280 times heavier in the growth direction than in the plane. While this is quite consistent with the assumption that HHL is the uppermost valence band, one obtains a mass ratio of ~ 0.1 if LHL dominates.[4] Both the cyclotron resonance and the free-carrier transport data therefore give convincing evidence that quantum confinement moves LH1 to a position somewhat below HH1, which, in turn, implies that the valence band offset must be greater than ~ 200 meV.

---

[1]J.R. Meyer, C.A. Hoffman, F.J. Bartoli, J.W. Han, J.W. Cook,Jr., J.F. Schetzina, X. Xhu, J.P. Faurie, and J.N. Schulman, Phys. Rev. B (Rapid Communications, in press).

[2]C.A. Hoffman, J.R. Meyer, F.J. Bartoli, J.W. Han, J.W. Cook, Jr., J.F. Schetzina, and J.N. Schulman (submitted for publication).

[3]J.N. Schulman and Y.-C. Chang, Phys. Rev. B 33, 2594 (1986).

[4]J.R. Meyer, F.J. Bartoli, C.A. Hoffman, and J.N. Schulman (to be submitted).

[5]J.M. Perex, R.J. Wagner, J.R. Meyer, J.W. Han, J.W. Cook, Jr., and J.F. Schetzina (submitted for publication).

Magneto-optical Properties of a Small Gap HgTe/CdTe Superlattice

R.J. Wagner, J.M. Perez[a] and J.R. Meyer
Naval Research Laboratory, Washington, D.C. 20375

and

Jeong W. Han, J.W. Cook, Jr., and J.F. Schetzina
North Carolina State University, Raleigh,N.C. 27695

Far infrared magneto-optical absorption spectroscopy nas been studied in a p-type HgTe/CdTe superlattice with a small effective band gap. Well-developed hole cyclotron resonance absorption lines were observed for magnetic field directions both parallel and perpendicular to the growth direction. These experiments were performed in a magnetic field regime where the semiclassical cyclotron orbit radius was large. In the parallel case, the orbit size was such that the holes traversed a number of superlattice periods of 127Å (78Å HgTe; 49Å CdTe). For orbital motion in the superlattice planes, a hole effective mass, m_x, of $0.0011m_e$ was deduced. For orbital motion through the superlattice planes, the data was analyzed assuming an ellipsoidal Fermi surface as in the case of a conduction band in Si or Ge. From this analysis, we find that the hole effective mass in the growth direction, m_z, is $0.30m_e$ and m_z/m_x is 280. Thus it appears that the most tightly bound hole subband is heavy hole-like in the growth direction. This is surprising in that it has been shown theoretically that the effect of biaxial tension (in the HgTe layers) should lift the light hole subband above the heavy hole subband if the valence band offset is small. [1,2] Thus we argue that strong quantum well confinement due to a large valence band offset must dominate over the stress-related light hole lifting effect.

We have also seen evidence of hole spin resonance ($g_x \approx 200$ and $g_z \approx 2$), light electron cyclotron and spin resonances which "mirror" the hole resonances and, finally, heavy electron-like cyclotron resonance at high magnetic fields (5-10 Tesla). This last result demonstrates that the band structure of our small gap superlattice is substantially modified by the effect of high magnetic fields.

a. NRC/NRL Resident Research Associate.

1. G.Y. Wu and T.C. McGill, Appl. Phys. Lett. 47, 634 (1985).
2. J.N. Schulman and Y.C. Chang, Phys. Rev. B33, 2594 (1986).

Determination of the HgTe-CdTe Valence Band Offset from Superlattice Intersubband Optical Transitions*

E. A. Patten, Santa Barbara Research Center, Goleta, CA 93117

J. N. Schulman and O. K. Wu, Hughes Research Laboratories, Malibu, CA 90265

Jeong W. Han, Y. Lansari, L. S. Kim, J. W. Cook, Jr., and J. F. Schetzina
Department of Physics, North Carolina State University, Raleigh, NC 27695

The heavy and light hole to conduction subband transitions have been identified in the optical absorption spectra of a series of HgTe-$Hg_{0.15}Cd_{0.85}Te$ superlattices. These data were used to determine, using a new approach, that the valence band offset of the HgTe-CdTe interface is large (≈ 350 meV). There has been considerable controversy in recent years about the order of magnitude of this offset, with one body of evidence pointing to a small offset (≈ 40 meV) and other data indicating a much larger offset value (≈ 300 meV). Much of the uncertainty in previous determinations of this valence band offset has been due to complications in the analysis of the data, whether obtained by photoemission, magneto-optical, absorption, or other methods. Here we use interband optical absorption to determine the valence band offset by direct observation of the superlattice subbands. The light hole to conduction band transition is the key to this determination, because the separation between the light (L1) and heavy (H1) hole energy levels is very sensitive to the valence band offset. The accuracy of the theoretically calculated values of these energy levels depends on the accuracy of the well and barrier layer thickness determinations. Special care was taken to determine these thicknesses by using several techniques including X-ray, TEM, and surface depth profiling so that the theoretical and experimental absorption spectra could be legitimately compared. Finally, an extremely important aspect of this work is that to confirm the validity of our determination of the offset, superlattice samples were both grown and characterized at two different laboratories.

Room temperature transmission/reflection measurements combined with computer models were used to experimentally determine the optical absorption coefficient spectra of several superlattices. These spectra exhibit the characteristic steplike features, related to the various superlattice intersubband transitions, which are expected for a 2-D quantum structure. Figure 1 shows the experimental absorption spectrum for a superlattice grown at Hughes Research Laboratories. The upward slopes in the data are the H1, L1 and H2 transitions. The dashed horizontal lines are the energy ranges of these first three intersubband transitions as calculated using a two-band tight-binding model and assuming an offset of 34 meV (85% of 40 meV). The solid lines represent these energy ranges using an offset of 298 meV (85% of 350 meV). We observe excellent agreement between the experimental spectra and the theoretical energy ranges of the transitions using the larger offset. Notice that using the smaller offset, the H1 and L1 transitions would overlap in energy which would imply no plateau in the absorption coefficient between these two transitions. The presence of a plateau is however clearly seen in our data thereby indicating a larger offset value. Figure 2 shows a similar curve for a superlattice grown at North Carolina State University. The theoretical values for the energy ranges for the first three transitions using the larger offset only are shown. Again, the agreement between theory and experiment is excellent. We conclude that the larger offset value (≈ 350 meV) of the HgTe-CdTe valence band offset is more accurate than the smaller value (≈ 40 meV). This work was partially supported by Contract No. N00014-86-C-2305 sponsored by SDIO/IST and managed by the Naval Research Laboratory.

* This is a revised version of abstract.

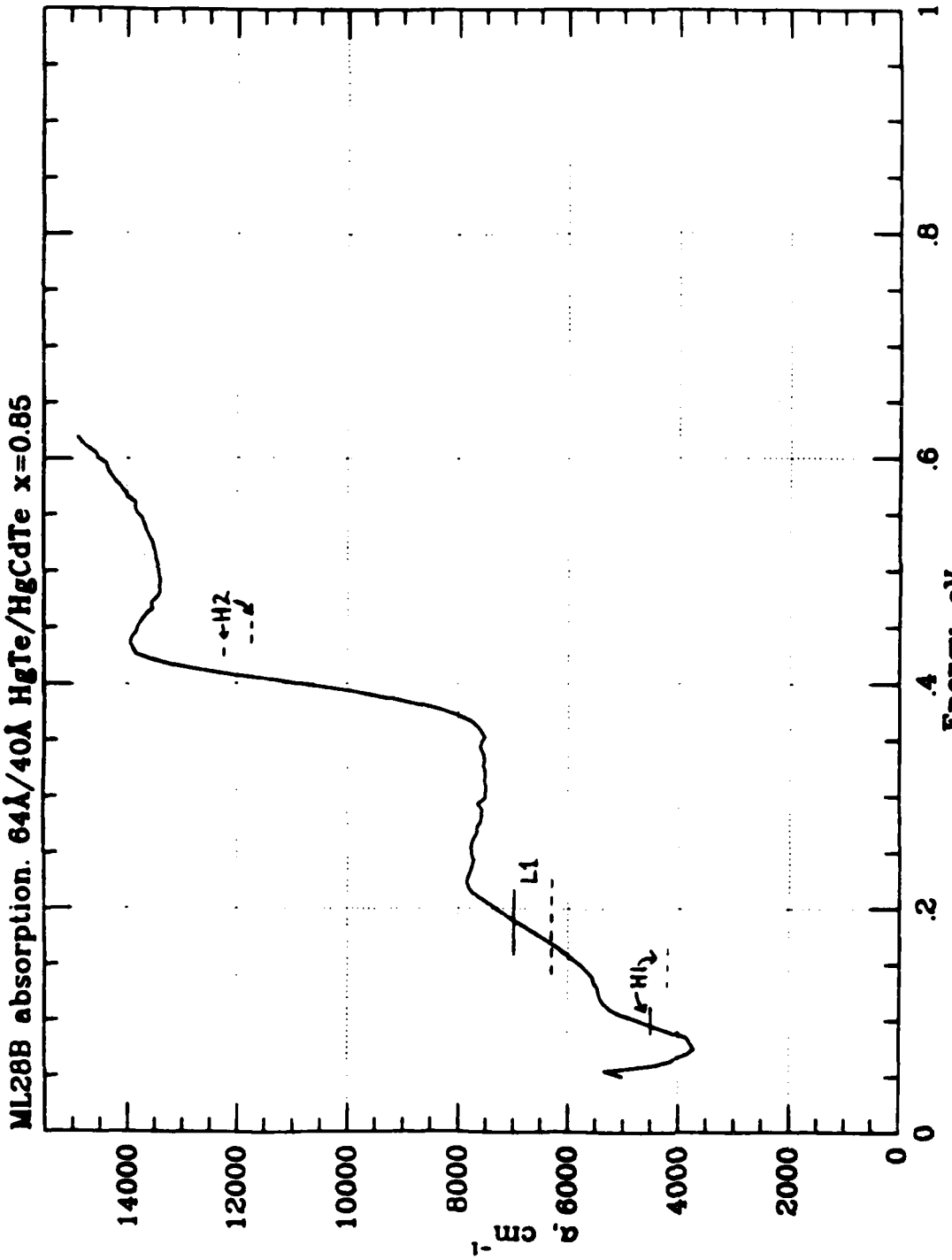

Figure 1. Room temperature absorption coefficient (solid curve) as a function of photon energy determined from experiment for a 64ÅHgTe/40ÅHgCdTe superlattice (grown at Hughes). The solid horizontal bars indicate the energy ranges of the lowest three intersubband optical transitions calculated using a 350 meV valence band offset for the HgTe-CdTe interface. The dashed lines correspond to these energy ranges using a 40 meV offset. Better agreement is obtained between theory and experiment using the larger offset since this predicts a plateau in the absorption coefficient between the first two transitions whereas the calculated ranges of these transitions overlap using the smaller offset.

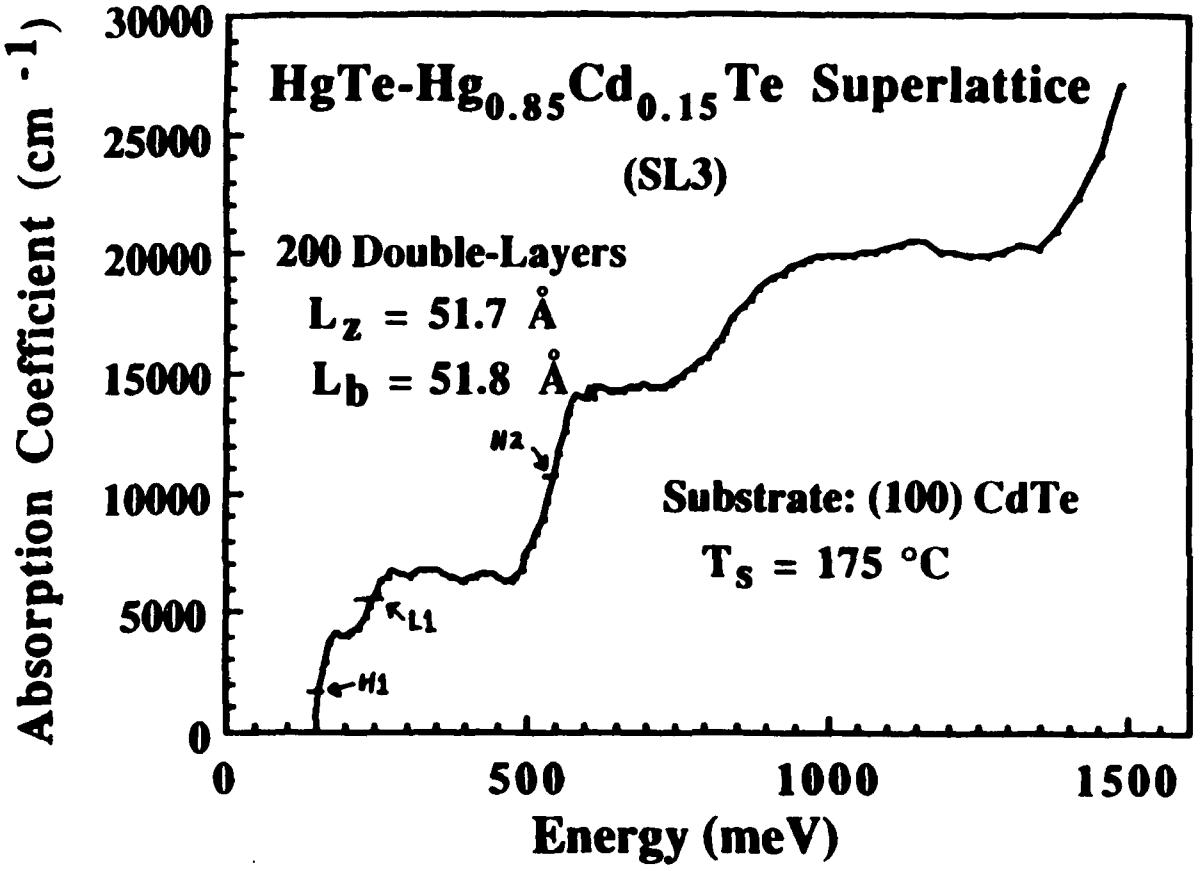

Figure 2. Room temperature absorption coefficient as a function of photon energy determined from experiment for a 52ÅHgTe/52ÅHgCdTe superlattice (grown at N. C. State University). The horizontal bars indicate the calculated energy ranges of the three lowest intersubband optical transitions using 350 meV for the HgTe-CdTe valence band offset and are in excellent agreement with the experimental curve features.

HgTe/CdTe SUPERLATTICE BAND CALCULATION WITH A TRANSFER MATRIX ALGORITHM*

K.H. Yoo and R.L. Aggarwal
Francis Bitter National Magnet Laboratory† and Department of Physics, MIT
Cambridge, MA 02139

and

L.R. Ram-Mohan
Department of Physics, Worcester Polytechnic Institute
Worcester, MA 01609

We have recently [1] developed a relatively compact (both conceptually and numerically) transfer matrix algorithm for the band calculation of superlattices (SL). This algorithm, using an 8x8 $\vec{k}\cdot\vec{p}$ Hamiltonian, has been applied to the HgTe/CdTe system with and without a magnetic field, using $\vec{k}\cdot\vec{p}$ parameters from Ref. 2, strain parameters from Ref. 1, and valence band offset V_p = 350 meV unless indicated otherwise. Using this algorithm, we find the following noteworthy features:

1) Energy at mid-zone of the bands is mostly determined by the HgTe well thickness d_{HgTe} and quickly converges to the energy of quantum well level with increasing CdTe layer thickness d_{CdTe}, as shown in Fig. 1(a). On the other hand, the bandwidth, especially for the conduction band, is mostly determined by d_{CdTe} as shown in Fig. 1(b). Hence dependence of energy gap E_g on layer thickness can be decomposed, to a first approximation, into mid-zone energy separation depending on d_{HgTe} and bandwidth depending on d_{CdTe}.

2) Figure 2 shows that the strain moves the band edges by amounts nearly constant with respect to V_p. The conduction band to heavy-hole band separation increases while the conduction band to light-hole band separation decreases. For smaller V_p ($\lesssim$50-150 meV depending on layer thicknesses) the uppermost valence band is light-hole band, but the quantum confinement effect [3], increasing with increasing V_p, makes the heavy-hole band the uppermost.

3) As in the case of bulk semiconductors, the selection rule for transitions between Landau levels is found to be $\Delta n = \pm 1$ for the $\sigma^{\pm}$ polarization, and $\Delta n = 0$ for the π polarization. Numerical calculations show, however, that half of the transitions allowed by $\Delta n = \pm 1$ selection rule are forbidden; this is analagous to the rule "within set a or within set b" in bulk materials, even though set a and set b get mixed in a superlattice. For example, Landau levels for a 60/30 A HgTe/CdTe SL, including strain, are shown in Fig. 3. For transitions between the Landau level in the superlattice, appreciable transition probability is found only for the transitions either within the primed set or within the unprimed set; in other words, the transition probability between the two sets is found to be negligible.

Our attempts to fit our [4] magnetoabsorption data to the transfer matrix algorithm calculations have not been completely successful. The main difficulty appears to be the uncertainty in the values of input parameters such as layer thicknesses, composition [5] of barrier layer, and the valence band offset. In addition, we need more reliable values for the $\vec{k}\cdot\vec{p}$ parameters and strain parameters.

*Work supported by SDI-ISTO (NRL, Agent) contract no N00014-86-C-2305.
†The Francis Bitter National Magnet Laboratory is supported by the National Science Foundation under cooperative agreement DMR-8511789.

1. L.R. Ram-Mohan, K.H. Yoo, and R.L. Aggarwal, Phys. Rev. B (in press).
2. J.M. Benoir, Y. Guldner, J.P. Vieren, M. Voos, and J.P. Faurie, Phys. Rev. B34, 891 (1986).
3. J.R. Meyer, F.J. Bartoli, C.A. Hoffman, and J.N. Schulman, submitted to Phys. Rev. B.
4. K.H. Yoo, R.L. Aggarwal, L.R. Ram-Mohan, J.F. Schetzina, and O. Wu, unpublished.
5. The barrier layer has been shown by O. Wu (private communication) to be $Hg_{0.15}Cd_{0.85}Te$ rather than pure CdTe due to the presence of residual Hg during MBE growth.

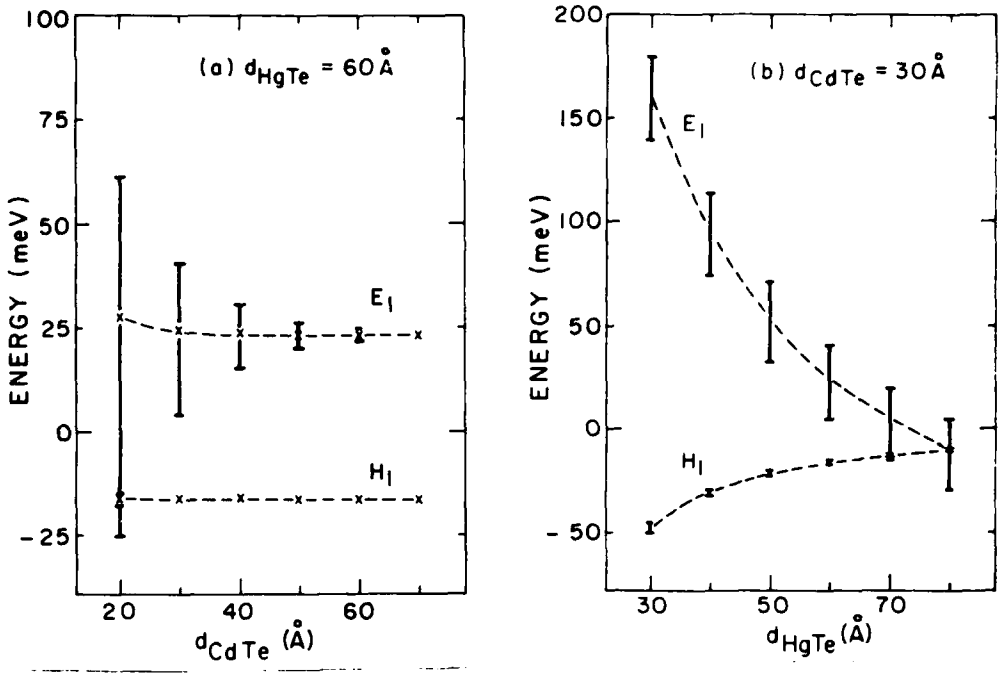

Fig. 1. Energy at mid-zone (crosses) and bandwidth (bars), (a) for fixed d_{HgTe}, and (b) for fixed d_{CdTe}. Dashed line is an eye-guide for the midzone energy.

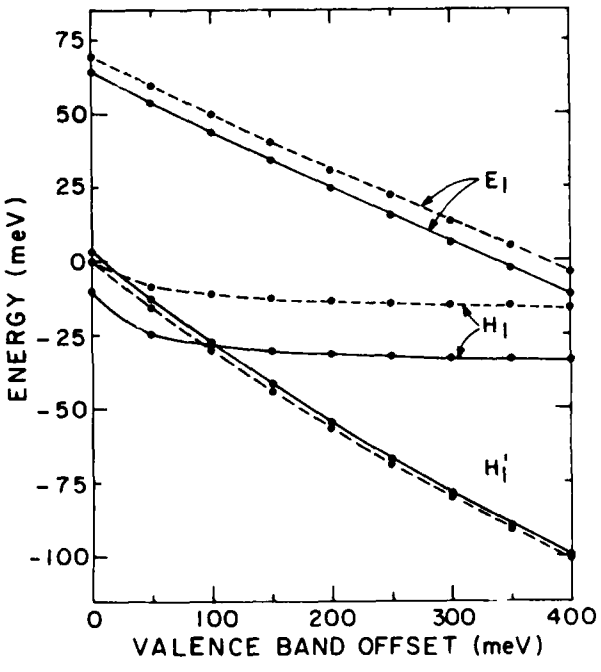

Fig. 2. Band energies as a function of valence band offset for a 60/30 A HgTe/CdTe superlattice. Solid and dashed lines are for strain and unstrained cases, respectively.

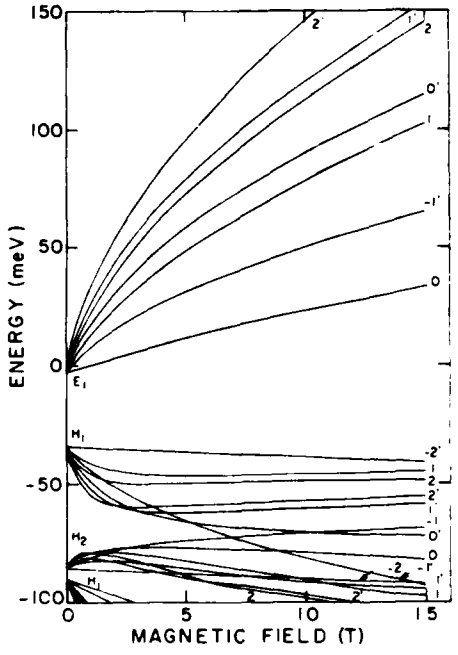

Fig. 3. Landau levels for a 60/30 A HgTe/CdTe strained superlattice.

The Effect of a Valence-Band Offset On Potential and Current Distributions in MCT Heterostructures

E. A. Kraut
Rockwell International Science Center
Thousand Oaks, CA 91360

Mercury Cadmium Telluride heterostructures are the subject of considerable technological interest and some controversy. Significant device performance claims have been made based on models of such structures. Most device modeling studies of MCT heterojunctions assume the validity of the common-anion rule. For an abrupt HgTe/CdTe heterojunction, the common-anion rule predicts that the valence-band offset ΔE_v should be small or zero, in agreement with some low temperature transport experiments. Recent ambient temperature photoemission measurements report ΔE_v values of about 0.35 eV. Results of a (77° K) numerical solution of Poisson's equation coupled to the drift-diffusion carrier transport equations, including Shockley-Read-Hall recombination are reported here for a $Cd_{.2}Hg_{.8}Te/Cd_{.4}Hg_{.6}Te$ pn-heterojunction (.05μ grading, ΔE_v = 0.07 eV). The space charge is $N_A = 5.0 \times 10^{15}$ cm^{-3} on the p-side and $N_D = 1.0 \times 10^{15}$ cm^{-3} on the n-side. The following figures show 1.) the band-shape at 77°K in the absence of doping and grading, 2.) the shape of the bands in the doped pn-junction at -0.3 volts reverse bias, and 3.) the I-V curve for this doping and grading.

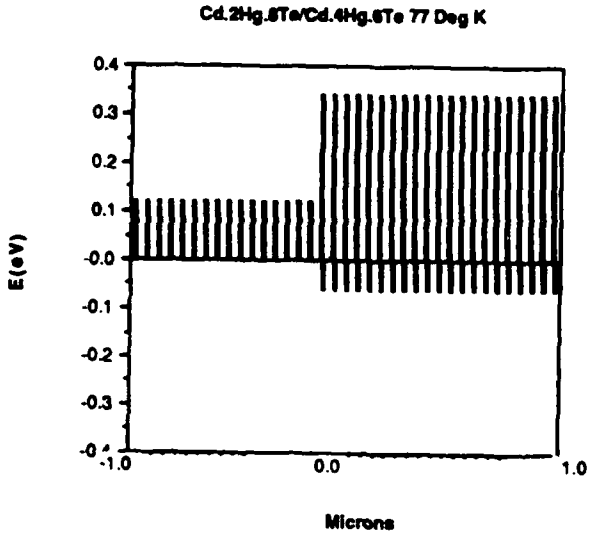
Cd.2Hg.8Te/Cd.4Hg.6Te 77 Deg K
E(eV)
0.4
0.3
0.2
0.1
-0.0
-0.1
-0.2
-0.3
-0.4
-1.0
0.0
1.0
Microns

FIG. 1.

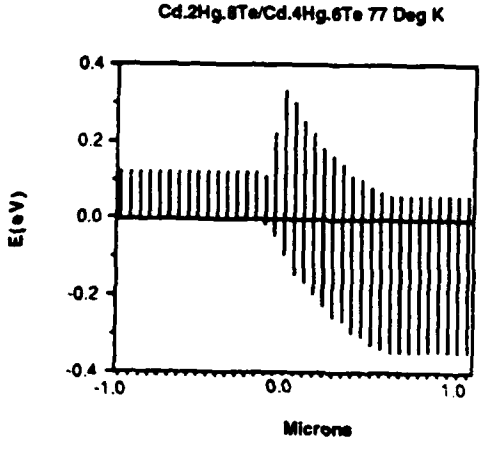
Cd.2Hg.8Te/Cd.4Hg.6Te 77 Deg K
E(eV)
0.4
0.2
0.0
-0.2
-0.4
-1.0
0.0
1.0
Microns

FIG. 2.

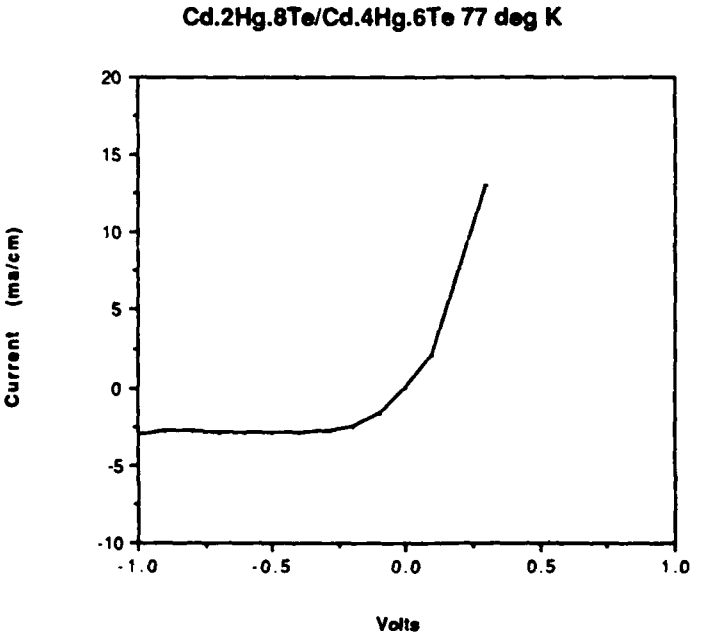
Cd.2Hg.8Te/Cd.4Hg.6Te 77 deg K
Current (ma/cm)
20
15
10
5
0
-5
-10
-1.0
-0.5
0.0
0.5
1.0
Volts

FIG. 3.

$Hg_{1-x}Cd_xTe$-BASED MULTIPLE QUANTUM WELLS FOR THE 2.5 - 3 μm WAVELENGTH RANGE

R. D. Feldman, M. N. Islam, C. Cesar, R. F. Austin,
A. E. DiGiovanni, and J. S. Shah

AT&T Bell Laboratories
Holmdel, N. J. 07733

The wavelength regime of 2.5 - 3 μm is of interest because it coincides with the anticipated minimum loss for fluoride fibers that are being developed. We have grown $Hg_{1-x}Cd_xTe$/CdTe multiple quantum well structures in this wavelength range by molecular beam epitaxy, and have measured their properties by photoluminescence, absorption, and photoacoustic spectroscopy. Sharp excitonic features, consistent with well width fluctuations on the order of one monolayer, are observed at low temperatures. These features broaden by 40 meV as the temperature is raised from 2 K to room temperature. The large value of this homogeneous broadening indicates a stronger exciton-phonon coupling than is found in III-V compounds. The temperature dependence of the exciton energy is in excellent agreement with the variation reported for the alloy composition that is in the quantum well. We have found that, with careful design of the multiple quantum well structure, we can minimize interdiffusion during growth. Films have been grown at a substrate temperature of 185 °C which show x-ray satellite peaks out to fourteenth order. Post-growth annealing experiments show that these structures are far less subject to interdiffusion than are HgTe/CdTe superlattices.

IMPURITY DOPING OF HgTe-CdTe SUPERLATTICES DURING GROWTH BY MOLECULAR BEAM EPITAXY*

M. L. Wroge, D. J. Peterman, B. J. Morris, D. J. Leopold, J. G. Broerman, and B. J. Feldman

McDonnell Douglas Research Laboratories
St. Louis, MO 63166

We report the successful doping of HgTe-CdTe superlattices with Ag and In during growth by molecular beam epitaxy (MBE). Silver and In, which have been shown to be p- and n-type dopants, respectively, in bulk-[1] and MBE-grown[2,3,4] HgCdTe alloys, are observed to be p- and n-type dopants in the superlattices as well. Hall-effect measurements on superlattices alternately doped with Ag and In reveal the existence of an electrical junction.

Figure 1 shows the carrier concentration as a function of temperature for four superlattices that were uniformly doped with Ag during MBE growth. The superlattices were (100)-oriented and were grown at substrate temperatures of 150 to 175°C on GaAs (100) substrates with CdTe buffer layers. Undoped samples grown under similar conditions are n-type with electron concentrations at 20 K of about $2\times10^{15}cm^{-3}$ and electron mobilities up to $10^5 cm^2/V\cdot s$. For all of the superlattices in Fig. 1, a transition temperature is evident below which the Hall coefficient is positive, indicating that the conduction at low temperatures is dominated by holes. We have observed hole mobilities of up to 10^4 $cm^2/V\cdot s$ in Ag-doped superlattices.

Figure 2 shows the hole concentrations at 20 K normalized to the respective superlattice growth rates, as a function of Ag-cell temperature for several p-type, uniformly Ag-doped samples. Also plotted in Fig. 2 are the normalized electron concentrations at 20 K for n-type, uniformly In-doped

*This research was supported by the Air Force Wright Aeronautical Laboratories (Contract F33615-85-C-5043).

superlattices as a function of In-cell temperature. The exponential dependences of the 20 K carrier concentrations on the respective effusion cell temperatures demonstrate that electron and hole concentrations are controllable within the range of 10^{16} to 10^{18} cm^{-3} with in-situ In and Ag doping, respectively.

We have grown several n-on-p junctions using In and Ag doping to define the n and p regions. Figure 3 is a secondary-ion mass spectroscopy (SIMS) depth profile of one of these structures grown at a substrate temperature of 160°C. The dopant profiles were fitted with a classical diffusion model, which yielded values of ~$2x10^{-13}$ and $5x10^{-15}$ cm^2/s for the Ag and In diffusion coefficients, respectively, at the superlattice growth temperature. Hall-effect measurements performed before and after removal of the In-doped layer by etching yielded results consistent with a two-layer, n-on-p structure. The ionized-In concentration (Fig. 3) was determined from the empirical relationship between SIMS count rates of uniformly In-doped samples and the corresponding electron concentrations from Hall-effect measurements. The ionized-Ag concentration was determined from the Hall-effect measurements on the etched superlattice. The net ionized-acceptor concentration is shown in Fig. 4 and was determined by subtracting the In concentration in Fig. 3 from the Ag concentration. As is evident, the profile is extremely sharp.

References

1. P. Capper, J. Crystal Growth 57, 280 (1982).
2. D. J. Peterman, M. L. Wroge, B. J. Morris, D. J. Leopold, and J. G. Broerman, J. Appl. Phys. 63, 1951 (1988).
3. M. L. Wroge, D. J. Peterman, B. J. Morris, D. J. Leopold, J. G. Broerman, and B. J. Feldman, J. Vac. Sci. Technol. A 6, 2826 (1988).
4. M. Boukerche, P. S. Wijewarnasuriya, J. Reno, I. K. Sou, and J. P. Faurie, J. Vac. Sci. Technol. A 4, 2072 (1986).

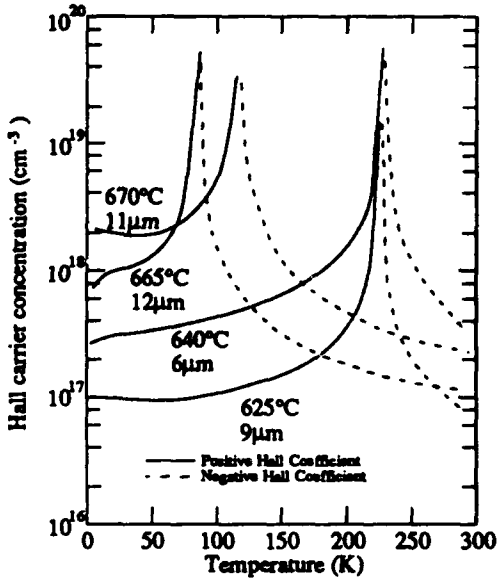

Figure 1. Hall carrier concentration as a function of temperature for four uniformly Ag-doped HgTe-CdTe superlattices. The Ag effusion-cell temperature and room temperature cutoff wavelength are listed for each curve.

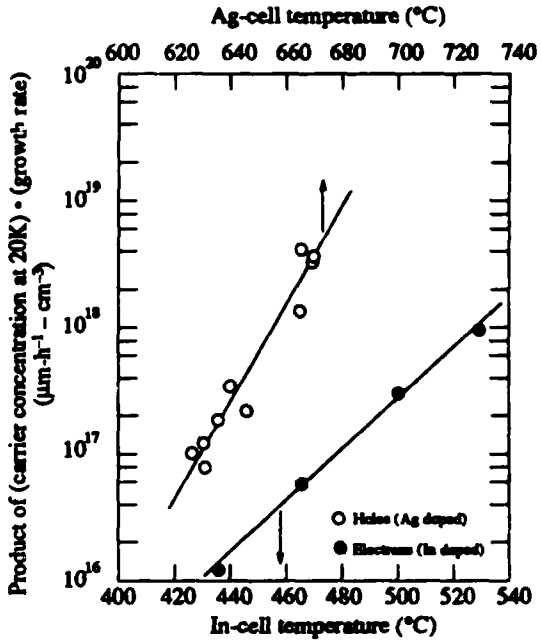

Figure 2. Charge carrier concentrations at 20K multiplied by the superlattice growth rate for superlattices that were uniformly doped with either Ag or In as functions of the Ag (top scale) or In (bottom scale) effusion-cell temperatures.

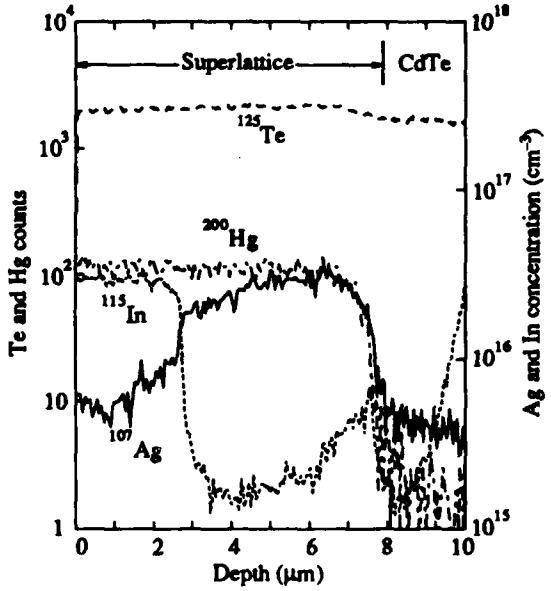

Figure 3. SIMS depth profile of a HgTe-CdTe superlattice that was alternately doped with Ag and In. The Ag and In results are plotted in terms of ionized dopant concentrations by normalizing to the results of Hall-effect measurements.

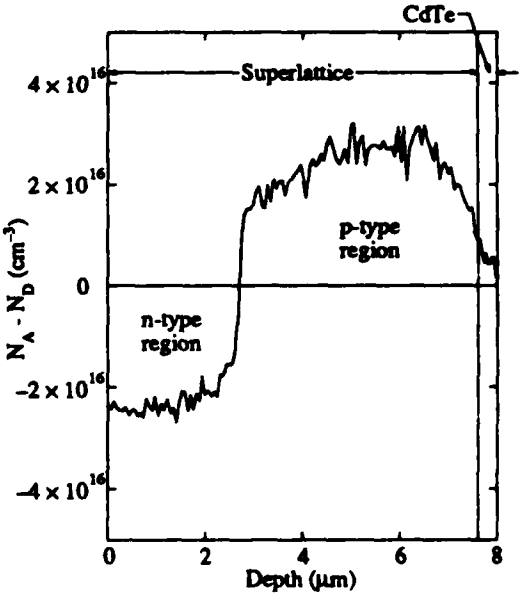

Figure 4. Net ionized acceptor concentrations as obtained from SIMS and Hall-effect measurements for the superlattice presented in Figure 3.

LOW LEVEL EXTRINSIC DOPING FOR P- AND N-TYPE MBE (100)HgCdTe

T. A. Temofonte, A. J. Noreika, M. J. Bevan,
P. R. Emtage and P. Mitra
Westinghouse R&D Center
Pittsburgh, PA 15235

Achievement of significantly advanced LWIR junction performance is expected when a low-temperature growth process, such as MBE is used to provide controlled layer and interface properties[1,2] in both P/N double layer heterojunction (DLHJ) detectors and N/N double layer isotype heterostructure (DLIHS) MIS detectors. Alternative growth approaches are expected to provide significantly reduced performance.

In PV HgCdTe homojunction devices excess recombination through generation-recombination (GR) centers in the neighborhood of the junction results in larger dark currents and therefore lower R_oA than theoretically predicted for a diffusion limited diode. GR rates can be reduced by increasing the bandgap near the junction and this is the primary motivation for the use of heterojunctions. Grading widths in such structures, eg, those resulting from high temperature growth techniques, cause barriers to the collection of photogenerated carriers. This can be avoided if the electrical junction is moved into the graded region, the base doping is reduced, and the bandgap of the cap layer is further increased. Low temperature growth, such as MBE, eliminates the need for these additional constraints.

Isotype heterostructures in MBE HgCdTe are also of interest first because they permit study of band offsets and interdiffusion at nominally abrupt composition changes and second because reduced tunneling should allow increased charge storage capability in MIS storage devices for LWIR detection.

Both devices require low absorber (base) doping levels of ~ 2-3 x 10^{15} cm^{-3}, low cap doping levels of ~ 1-1.5 x 10^{15} cm^{-3} and a compositional change (for an abrupt heterostructure) of Δx ~0.05 to 0.075. A slightly graded (~ 0.1 μm) heterointerface relaxes the cap doping requirements considerably, i.e., N_{cap} ~ 1 x $10^{16}cm^{-3}$.

It is generally believed that intrinsic doping via stoichiometric adjustment will not provide controlled uniform, stable doping. This has motivated interest in extrinsic doping with Group I (and Group V) elements as acceptors, and Group III elements as donors, with the emphasis to date mainly

on Ag and In respectively. Published data for both[3,4] indicate minimum achievable doping levels which are higher than those required for high performance LWIR detectors. We have explored Ag and In doping at levels suitable for optimized PV DLHJ and MIS DLIHS detectors. These elements were found to be relatively efficient acceptor and donor dopants respectively at lower levels than previously reported for HgCdTe.

For Ag, both continuous and modulation doping have been explored and source temperatures between 580 and 640°C have been used to provide acceptor concentrations between $8 \times 10^{14} cm^{-3}$ and $4 \times 10^{16} cm^{-3}$. Recent results for continuous Ag doping are shown in Figure 1. These characteristics were determined via Hall measurements in the temperature range 25°K to 295°K and for variable magnetic fields to 50 kG. Silver doping of (100)HgCdTe films in the range 6×10^{15} to $4 \times 10^{16} cm^{-3}$ has usually given rise to classic Hall data. Double layer MBE film structures were also grown with the last 0.25 μm of the cap layer being exposed to a Ag flux during growth. Detailed variable temperature Hall data on the underlying base layer revealed classic p-type behavior for R_H, μ and ρ. No hint of a surface or interface N layer was observed. These results also demonstrate, however, that Ag diffused rapidly at MBE growth temperatures. This facilitates excellent doping uniformity in single layers but makes preparation of as grown anisotype heterointerfaces less straightforward. Occasionally, anomalous behavior is observed for p-type films because a small number of high mobility electrons can reverse the sign of the Hall coefficient (R_H). An example of this is shown in Figure 2 for field dependence measurements taken at 40K. The true p-type character of the film is not apparent until $H \geq 20$ kG and accurate determination of N_A requires $H \geq 50$ kG! The carriers responsible for this behavior are surface electrons, not thermal electrons.

Extrinsic n-type doping has also been investigated. An InP source provides the impurity during alloy growth and source temperatures between 380°C and 445°C are required to produce donor concentrations between $1 \times 10^{15} cm^{-3}$ and $3 \times 10^{16} cm^{-3}$. The dependence of N_D on InP cell temperature for recently grown MBE films is shown in Figure 3.

Variable temperature, variable magnetic field Hall measurements have been performed on single-layer and DLIHS MBE film structures, both intrinsically and extrinsically doped. Above $N_D \sim 1 \times 10^{15} cm^{-3}$ films having $x \geq 2.0$ are usually well behaved (and confirmed with field dependence measurements) with mobilities as high as 2 to $2.5 \times 10^5 cm^2 V^{-1} s^{-1}$. This is important since films

having such properties are ideally suited to high performance LWIR PV and MIS detector absorber layers. The high electrical quality of our MBE films has been confirmed for low x material ($x < 0.20$) with mobilities as high as $6.6 \times 10^5 cm^2V^{-1}s^{-1}$. Selected Hall data for undoped and extrinsically doped MBE films are given in Table 1.

Structural evaluation (DCRC, XTEM) has been performed on films grown on both (100)CdTe and lattice matched (100)CdZnTe substrates and confirmed that films grown on near-lattice matched substrates showed lower defect densities. DCRC characterization shows FWHM values, Cu(400) reflection, in the 100-130 arc sec range. Abrupt composition change ($\leq$ 50 Å) at an isotype heterointerface was observed by the EDS/XTEM combination. Demonstration of 3-D compositional uniformity was previously reported.[2]

An all-MBE in-situ double layer isotype heterostructure (N/N) confirmed by multilevel C-V, has been grown and mesa diodes fabricated. Assuming a valence band offset given by $\Delta E_v \sim 0.35\ \Delta X$, and calculating band bending in the accumulation layer on the narrow gap side of the interface, permits a computation of the barrier height and thus R_oA. This procedure gave R_oA ~4.5 Ω-cm^2 while the value observed for the best diode was 5 Ω-cm^2. The heterointerface grading width used in this calculation was 0 Å. Even assuming the lowest base donor doping (measured previously to this run using detailed Hall characterization) implies a maximum possible grading width of ~50 Å. These initial DLIHS diode results demonstrate the control of the interface achieved in the heterostructure by low temperature MBE growth.

REFERENCES

1. A. J. Noreika, T. A. Temofonte, S. Y. Wu, and W. J. Takei, Proc. IRIS Specialty Group on IR Materials, 9 June 1987.
2. T. A. Temofonte, A. J. Noreika, P. R. Emtage, J. Greggi, M. J. Bevan, W. J. Takei, and M. H. Francombe, Proc. IRIS Specialty Group on IR Materials, 21 June 1988.
3. M. L. Wroge, D. J. Peterman, B. J. Morris, D. J. Lepold, and J. G. Broerman, U. S. Workshop on Physics and Chemistry of Mercury Cadmium Telluride, New Orleans, LA, October, 1987.
4. M. Boukerche, J. Reno, I. K. Sou, C. Hsu and J. P. Faurie, Appl. Phys. Lett. 48: 1733 (1986).

*This work was supported in part by DOD/CNVEO contract DAAB07-86-C-F069.

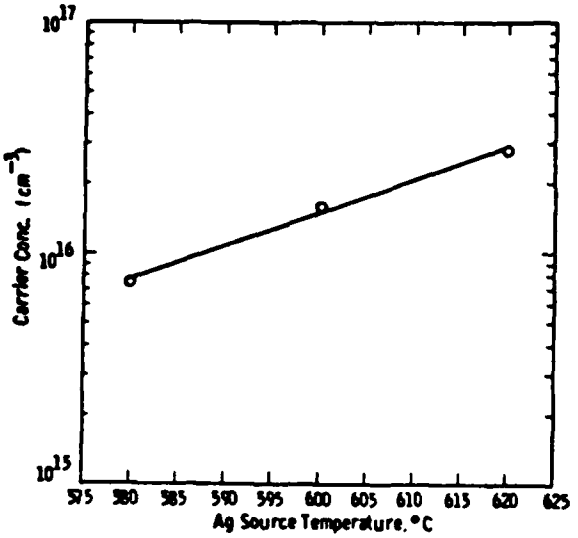

Figure 1. Carrier concentration of Ag-doped MBE HgCdTe as a function of Ag temperature

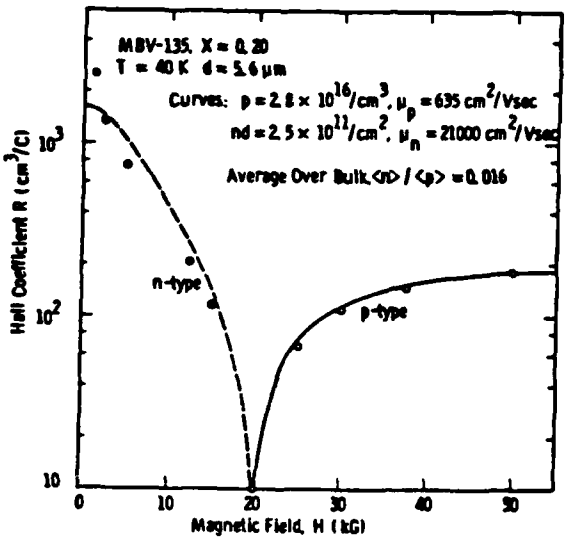

Figure 2. Observed Hall coefficient vs. field for an Ag-doped sample at 40K.

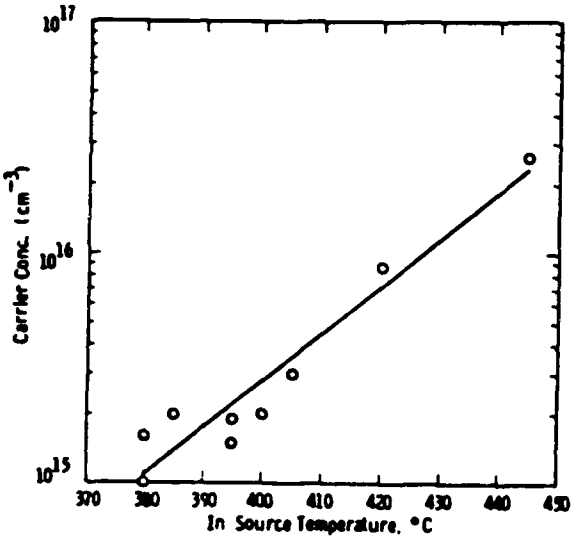

Figure 3. Carrier concentration of In-doped MBE HgCdTe as a function of In cell temperature.

Growth Run	d (μm)	X	N_D (cm^{-3})	μ ($cm^2V^{-1}s^{-1}$)	Temp (K)	Type
8**	2.9	0.26	1.4 E 15	4.3 E 4	50	N
13**	3.4	0.26	1.5 E 16	323	50	P (Ag)
571	8.4	0.26	6.5 E 15	190	77	P (Ag)
146**	3.7	0.27	6.7 E 15	132	100	P
594	5.0	0.22	4.7 E 14*	3.6 E 4	120	N
595	7.0	0.23	2.0 E 14*	3.4 E 4	115	N
599	4.0	0.235	1.5 E 16	1.1 E 5	25	N (In)
604	3.0	0.20	1.1 E 16	9.4 E 4	25	N (In)
624	4.4	0.21	1.5 E 15	1.2 E 5	25	N
625	4.5	0.26	1.2 E 45	2.1 E 5	25	N
682	5.7	0.22	1.6 E 15	6.5 E 4	25	N (In)
683	5.7	0.22	1.2 E 15	9.5 E 4	25	N (In)

* at 77K
** Raw HgI_2 System

Table 1. Hall Data (5 kG) for MBE Films Grown on (100) Substrates

VARIATION OF Hg INCORPORATION IN MBE - GROWN HgCdTe STRUCTURES DUE TO GROWTH FRONT ROUGHNESS AND MISORIENTED SUBSTRATES - ROLE OF KINK SITES

J. Singh
University of Michigan
Ann Arbor, MI 48109

J.M. Arias
Rockwell International Science Center
Thousand Oaks, CA 91360

In MBE HgCdTe growth the Hg incorporation is known to be strongly controlled by the Te_2 overpressure. In this paper we present for the first time, Monte Carlo simulations and MBE growth studies to understand the Hg incorporation on the growth front. At normally employed temperatures for MBE HgCdTe growth (175-225^{o}C), computer simulations clearly show that the Hg incorporation occurs primarily at the kink sites (sites near step edges), where the Hg sticking coefficient could be up to two orders of magnitude higher than at the free surface sites. Thus, Hg incorporation strongly depends not only the Te_2 flux, but also on the initial surface kink site density. The implication of this result is that sample preparation (polishing, chemical etching, thermal heating, buffer layer growth, etc.) plays a major role in obtaining high quality epitaxial material and good reproducibility. The kink site density can be enhanced by using off-axis substrates. We have seen such an effect when growing on the (211)B, (111)B, and (100) as shown in Table I. Computer simulations also show that starting from an atomically flat surface, the kink site density (initially zero on a flat surface) is of oscillatory nature at the beginning of the growth, because of the layer-by-layer growth mode that is controlled by Cd surface kinetics, and gradually settles down towards a steady-state value. The Hg incorporation responds to the kink site concentration, Hg incorporation is low initially, increasing as growth proceeds. This is in an important factor to consider in the technology of MBE

HgCdTe. We have carried out growth studies on different crystallographic orientations: (111)B, (111)B misoriented 8° and (211)B. From these studies we found out that on those orientations the ideal Hg/Te_2 ratio changes with time as viewed in Table II; here, ideal initial and final ratios are shown. The ideal conditions are detected and monitored by RHEED during growth. An excess Hg to Te_2 ratio at constant growth temperature gives microtwin defects which are detrimental to the growth. Such defects are avoided by continuously decreasing the Hg flux, as shown in Table II, or by increasing the growth temperature to decrease the incorporation of Hg. The effect mentioned above is especially important when thick epilayers (>10 μm) are grown. The variation of Hg incorporation is clearly seen over a long run. For instance, in Table II in order to grow HgCdTe on the (211) plane at 195°C, the ideal Hg/Te_2 ratio changes from 130.1 to 87.8 after 12 um are grown.

In conclusion, we have predicted by Monte Carlo growth simulations and then confirmed with MBE growth studies that the step density plays a major role in the growth of HgCdTe and also that such density varies with time. This is an important result for the MBE HgCdTe technology.

Work supported by the Air Force Wright Aeronautical Laboratories Contract No. F33615-87-C-5254.

TABLE I

Approximately Hg/Te Initial Flux Ratio for Different Orientations

(211)B	(111)B	(100)
90-145	159-400	600-1,062

TABLE II

Initial and Final Hg/Te Flux Ratios as a Function of Orientation, Growth Rate and Growth Time for HgCdTe grown by MBE at T ~ 195° C.

Orientation	Growth Rate µm/h	Thickness (µ)	Growth Time (h)	Initial (Hg/Te_2)	Final (Hg/Te_2)
(211)B	5.8	12.0	2.33	130.1	87.8
(211)B	6.8	25.5	3.75	90.5	47.0
(111)B-8 off	4.0	16.0	4.0	167.0	47.0
(111)B	3.0	15.0	5.0	227.0	92.0

LONG-WAVELENGTH INFRARED DETECTORS BASED ON STRAINED InAs - $Ga_{1-x}In_xSb$ TYPE II SUPERLATTICES

C. Mailhiot
Xerox Webster Research Center
Webster, NY 14580

D.L. Smith
Los Alamos National Laboratory
Los Alamos, NM 87545

Introduction

Major efforts have recently been devoted to the fabrication of two-dimensional arrays of photovoltaic detectors for the purpose of infrared imaging.[1] Such detector arrays are usually made from $Hg_{1-x}Cd_xTe$ alloys. Two major difficulties arise in the fabrication of such detector arrays: One is the large tunneling currents associated with $Hg_{1-x}Cd_xTe$-based devices. The other is the requirement of extremely precise composition control to accurately determine the cut-off wavelength (λ_c) of the device.[1] These problems are particularly severe for long-wavelength ($\lambda_c > 10\mu m$) applications. The purpose of this paper is to suggest the use of III-V materials to achieve small band-gap superlattices appropriate for infrared detector applications. We propose to take advantage of internal strains in type II InAs - $Ga_{1-x}In_xSb$ strained-layer superlattices to obtain small band-gap materials with sufficiently thin alternating layers so as to achieve large optical absorption and favorable transport properties.

Results and Discussions

The InAs - $Ga_{1-x}In_xSb$ system is a type II superlattice in which the band gap derives from electron states split up from the InAs conduction band minimum and heavy-hole states split down from the $Ga_{1-x}In_xSb$ valence band maximum by quantum confinement effects. Internal strains lower the conduction band minimum of InAs and raise the heavy-hole band in $Ga_{1-x}In_xSb$ by deformation potential effects. Consequently, *internal strains reduce the superlattice band gap (or, equivalently, increase the superlattice cut-off wavelength) at a given layer thickness.* For a type II superlattice to be a useful material for long-wavelength detection, it is extremely important that the superlattice layers remain thin at long cut-off wavelengths ($\lambda_c > 10\mu m$). This requirement is imposed because the optical matrix elements decrease very rapidly with increasing layer thickness in type II superlattices. Calculations of optical matrix elements as a function of cut-off

wavelength for [001]-oriented InAs - $Ga_{1-x}In_xSb$ strained-layer superlattices are indicated in Fig. 1. The results shown in Fig. 1 reveal that the In composition must be in the range $x \approx 0.40$ to achieve large enough optical matrix elements in the $\lambda_c \approx 10 - 12\mu m$ region. Consequently, we restrict our numerical applications to InAs - $Ga_{0.6}In_{0.4}Sb$ strained-layer superlattices.

Calculations of superlattice energy subband dispersions are indicated in Fig. 2 for an InAs - $Ga_{0.6}In_{0.4}Sb$ strained-layer superlattice consisting of 11 layers (≈ 32Å) of InAs alternating with 11 layers of $Ga_{0.6}In_{0.4}Sb$ grown along the [001] axis. The cut-off wavelength of this superlattice is $\lambda_c = 11.2\mu m$ (band gap of 110 meV). The calculations shown in Fig. 2 reveal that the electron effective mass is nearly isotropic and has a numerical value of $m^*_{super}/m \approx 0.05$. This numerical value is very convenient for the purpose of device design: it is large enough to lead to small diode tunneling currents (compared with existing $Hg_{1-x}Cd_xTe$-based diodes at the same cut-off wavelength), yet it is small enough to lead to large mobilities and diffusivities.

In Fig. 3, we compare the optical absorption coefficient for the InAs - $Ga_{0.6}In_{0.4}Sb$ strained-layer superlattice whose band structure is indicated in Fig. 2, with the absorption coefficient of a $Hg_{1-x}Cd_xTe$ alloy with $x = 0.21$. Both materials have a band gap of 110 meV ($\lambda_c = 11.2\mu m$). The calculations shown in Fig. 3 indicate that, close to threshold, the optical absorption properties of the InAs - $Ga_{0.6}In_{0.4}Sb$ strained-layer superlattice are as good as those of the $Hg_{1-x}Cd_xTe$ alloy.

Our results establish that InAs - $Ga_{1-x}In_xSb$ strained-layer superlattices are very attractive alternative materials to $Hg_{1-x}Cd_xTe$-based infrared diodes. The optical properties of InAs - $Ga_{1-x}In_xSb$ strained-layer superlattices are as good as those of the $Hg_{1-x}Cd_xTe$ alloy in the $\lambda_c \approx 10 - 12\mu m$ region. Moreover, the transport properties of InAs - $Ga_{1-x}In_xSb$ strained-layer superlattices are predicted to be far superior to those of $Hg_{1-x}Cd_xTe$ alloys. Overall, InAs - $Ga_{1-x}In_xSb$ strained-layer superlattices should have superior materials properties for long-wavelength detection than commonly used $Hg_{1-x}Cd_xTe$ alloys.

References

1. M.B. Reine, A.K. Sood, and T.J. Tredwell, in *Semiconductors and Semimetals*, ed. R.K. Willardson and A.C. Beer, **18**, 201, Academic, New York (1981).

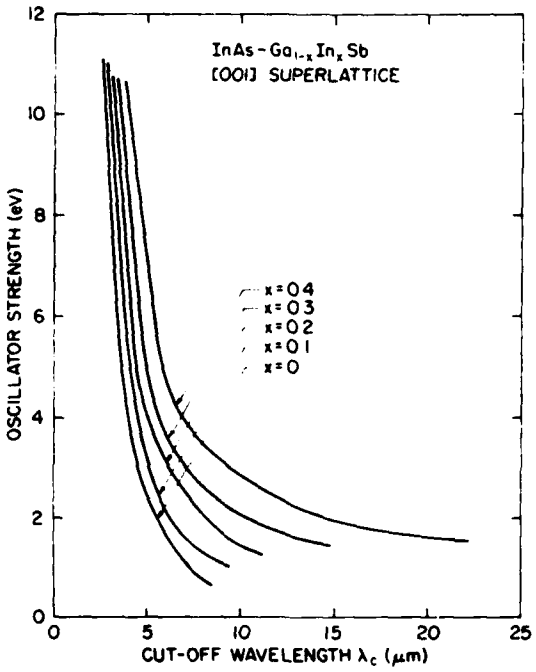

Fig. 1: Optical matrix elements calculated as a function of the InAs - $Ga_{1-x}In_xSb$ superlattice cut-off wavelength, λ_c, for various values of x. The superlattice consists of M_a layers of InAs alternating with N_b layers of $Ga_{1-x}In_xSb$ grown along the [001] axis. We consider the case of a free-standing strained-layer superlattice.

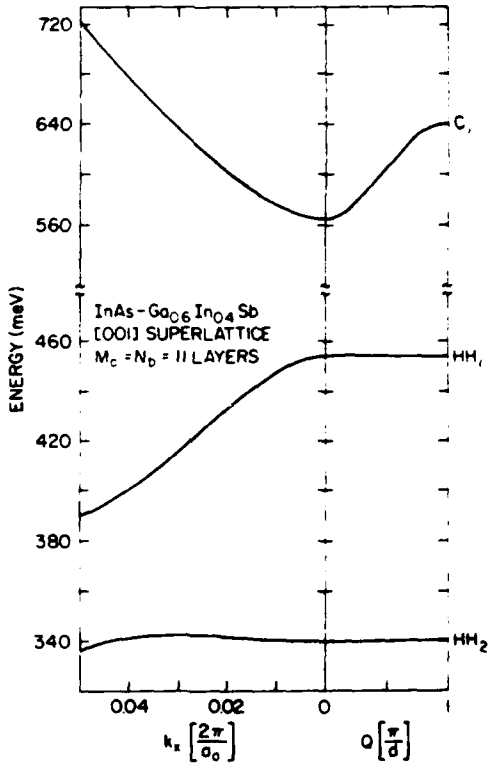

Fig. 2: Superlattice energy band structure for a free-standing strained-layer superlattice consisting of 11 layers of InAs alternating with 11 layers of $Ga_{0.6}In_{0.4}Sb$ grown along the [001] axis. The band gap of this superlattice corresponds to a cut-off wavelength of $\lambda_c = 11.2\mu m$. The large energy dispersion of the electron subband leads to favorable transport properties along the growth axis.

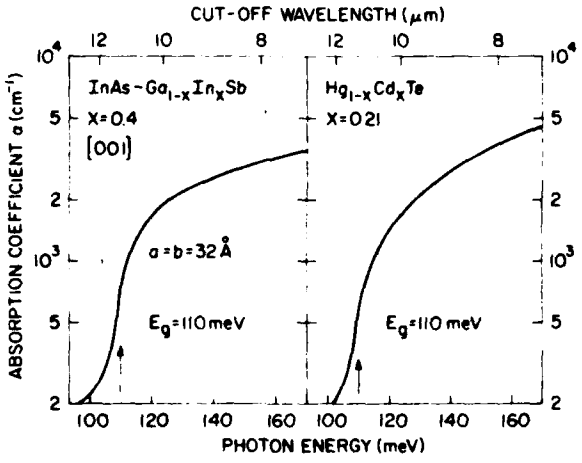

Fig. 3: Near band-edge absorption coefficient as a function of photon energy for the InAs - $Ga_{0.6}In_{0.4}Sb$ strained-layer superlattice whose band structure is indicated in Fig. 2, and for a $Hg_{1-x}Cd_xTe$ alloy with $x = 0.21$.

A Possible Resolution of the Valence Band Offset Controversy in HgTe/CdTe Superlattices*

H. Ehrenreich, P.M. Hui and N.F. Johnson

Harvard University

The valence band offset controversy in HgTe/CdTe superlattices can be simply resolved. The dilemma posed by differing values of band offset Δ obtained from photoemission ($\Delta \approx 350$meV)[1] and magneto-optical experiments ($\Delta \approx 40$meV)[2] is resolved here in favor of the larger Δ by showing that the effective mass and finite band gap obtained by Berroir *et al*[2] are consistent with the value $\Delta \approx 350$meV. Calculations based on the envelope function approximation and the Kane model show that although the 100ÅHgTe/36ÅCdTe superlattice becomes semimetallic when Δ is increased from small values, it unexpectedly reverts to semiconducting behavior as Δ is increased beyond 300meV. The band gap in this new regime occurs at the superlattice Brillouin zone face. The calculated electron cyclotron mass and band gap for $\Delta \gtrsim 350$meV and reasonable unintentional doping concentrations are found to be in better agreement with the experimental data[2] than for the smaller offset $\Delta \approx 40$meV.

The sensitivity of these semimetal/semiconductor transitions to variations in layer widths and composition is discussed and future experiments suggested.

* Supported by DARPA and the Joint Services Electronics Program.

1. S.P. Kowalczyk, J.T. Cheung, E.A. Kraut, and R.W. Grant, *Phys. Rev. Lett.* **56**, 1605 (1986); T.M. Duc, C. Hsu, and J.P. Faurie, *Phys. Rev. Lett.* **58**, 1127 (1987); C.K. Shih and W.E. Spicer, *Phys. Rev. Lett.* **58**, 2594 (1987).

2. J.M. Berroir, Y. Guldner, J.P. Vieren, M. Voos, and J.P. Faurie, *Phys. Rev. B* **34**, 891 (1986).

Temperature dependent photoemission study of the HgTe-CdTe valence-band offset

R. Sporken (a,b), S. Sivananthan (a), D. Ehlers (c), J.J. Pireaux (b), J. Fraxedas (c), R. Caudano (b), L. Ley (c), and J.P. Faurie (a)

a) University of Illinois at Chicago, Department of Physics

b) Laboratoire de Spectroscopie Electronique, Facultes Universitaires Notre-Dame de la Paix, Namur, Belgium

c) Max-Planck Institut fur Festk Orperforschung, Stuttgart, FDR

The valence-band offset between HgTe and CdTe has received a great deal of attention over the last several years. The large amount of experimental data can be essentially divided into two groups. Magneto-optical experiments, resonant Raman scattering, and infrared photoluminescence data agree with a small offset (< 100 meV). On the other hand, x-ray photoemission spectroscopy (XPS) yields a larger valence-band offset (300 meV).

The first class of experiments was mostly performed at low temperature and they require a fitting procedure with theory. On the other hand, the photoemission data were taken at room temperature. It has therefore been suggested several times that the relatively large discrepancy between these two values could be due to a temperature dependence of the valence-band offset.

We have studied the temperature dependence of the valence-band offset between HgTe and CdTe with XPS from room temperature down to 110 K and with ultra-violet photoemission spectroscopy (UPS, He I and He II) down to 50 K. Since only variations of the core level positions and of the valence-band maximum are relevant for this purpose, a high degree of accuracy can be achieved for this kind of experiment.

The samples are MBE-grown layers of HgTe and CdTe and MBE-grown HgTe-CdTe heterojunctions. All the layers are grown on CdTe(111)B substrates. They are kept under argon atmosphere and introduced into the spectrometer as fast as possible. With XPS, the samples could be measured as introduced, whereas gentle argon ion sputtering was used for in-situ cleaning prior to the UPS measurements.

At room temperature, we measure a valence-band offset of 400 meV +/ - 100 meV with both XPS and UPS. The good agreement of this result with XPS measurement performed[1] in a chamber directly connected to the MBE system proves the validity of our approach. The valence-band offset measured at low temperature (down to 50 K) is found to be equal to the room temperature value in both the XPS and UPS experiments. We therefore estimate an upper limit of about 50 meV for the temperature dependence of the HgTe-CdTe valence-band offset. As a consequence, the large discrepancy between the two classes of experimental results mentioned before cannot be attributed to a temperature dependence of the valence-band offset in this particular system.

1. T.M. Duc, C. Hsu and J.P. Faurie, Phys. Rev. Lett. 58, 1127 (1987)

EVIDENCE OF ANOMALOUS BEHAVIOR IN LOW N-TYPE MCT INDUCED BY EXTENDED DEFECTS*

B. Pelliciari - G.L. Destefanis - L. Di Cioccio

Commissariat à l'Energie Atomique, CENG - D.LETI/LIR -

85 X - 38041 Grenoble Cédex - France

Introduction

Suitable improvements of our LPE growth process unable us to obtain excellent quality p-type as-grown MCT epilayers, well adapted to high performance PV detector technology (1) (2).

Although our technology only needs undoped p-type MCT as starting material, we also convert a lot of these epilayers to n-type to check their electrical properties in view of two fondamental problems : anomalies of electrical behavior and residual doping level (3) (4).

Results and comments

After n-type annealing, most of our LPE layers have a classical behavior versus temperature even under a high magnetic field value of 10000 gauss : at 77K, values of $n_d^{77} = 2 \times 10^{14}$ cm^{-3} and $\mu^{77} = 10^5$ cm^2 v^{-1} sec^{-1} and at 27K $n_d^{27} = 2 \times 10^{14}$ cm^{-3} and $\mu^{27} = 2$ to 3×10^5 cm^2 v^{-1} sec^{-1}. TEM observations show that these layers are defect-free and this is confirmed by X-ray topography which show only the misfit dislocation pattern (figures 1a, 1b, 1c).

However, some samples have an anomalous behavior featured by a "kink" on the mobility curve between 100 and 77K, the n_d value being in the low 10^{14} range. TEM observations show in this case the presence of dislocations, the density of which is directly correlated to a more or less significant "kink" on the mobility curve ; besides the aspect of the

X-ray topography changes from a sharp misfit structure (low density of loops) to a mixte structure (higher density of loops).

If this density of loops is still increased, the X-ray topography becomes hazy and the Hall effect measurement indicates the epilayer to be p-type even after an n-type annealing (figures 2a, 2b, 2c). These loops are assumed to generate doping microinhomogeneities responsible for anomalous Hall effect behavior.

So, extended defects have to be avoided to achieve high quality MCT material ; a way to reach this goal is to grow buffered structures, the electrical properties of which are presented together with TEM observations.

References

* Work sponsored by DRET (Ministry of Defence)

(1) B. PELLICIARI J. Cryst. Growth 86 (1986) 146 - 160

(2) G.L. DESTEFANIS, G. GUERNET, B. PELLICIARI, G. TARTAVEL, J.L. TISSOT, J.L. TESZNER Proc. 3rd Intern. Conf. on Advanced Infrared Detectors and Systems, London, 1986

(3) L.F. LOU and W.H. FRYE J. Appl. Phys. 56 p 2253 (1984)

(4) M.C. CHEN, S.G. PARKER and D.F. WEIRAUCH J. Appl. Phys. 58 p 3150 (1985)

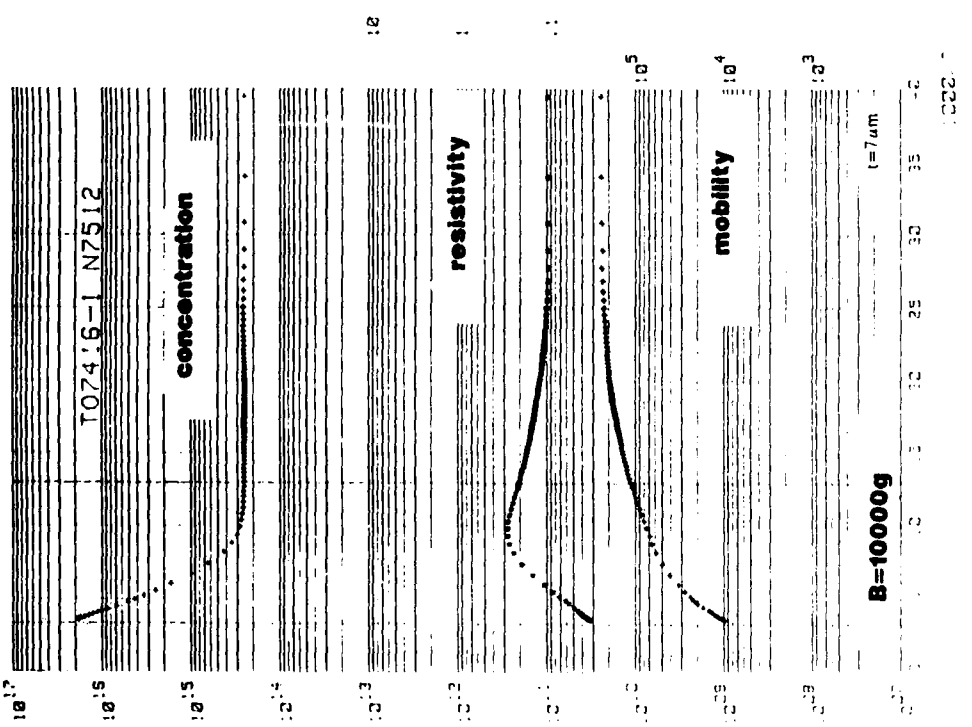

Fig. 1a = Hall effect measurement

Fig. 1b = TEM observation

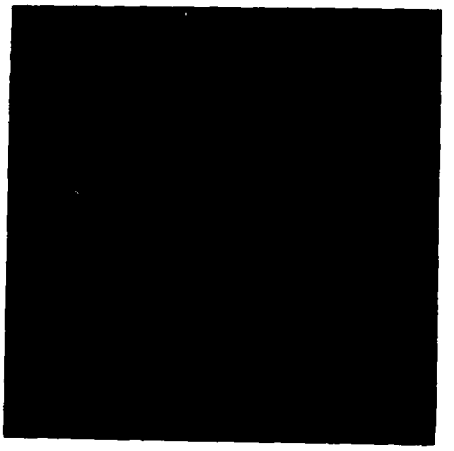

Fig. 1c = x-ray topography

Fig. 2b = TEM observation

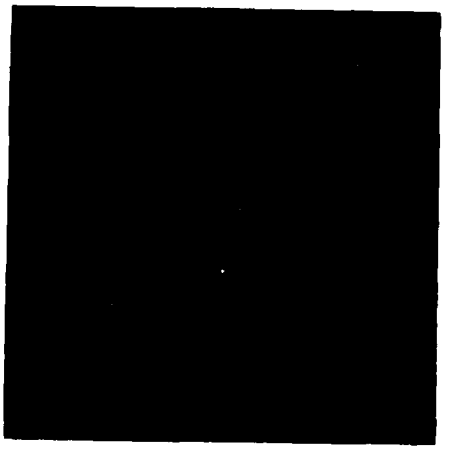

Fig. 2c = x-ray topography

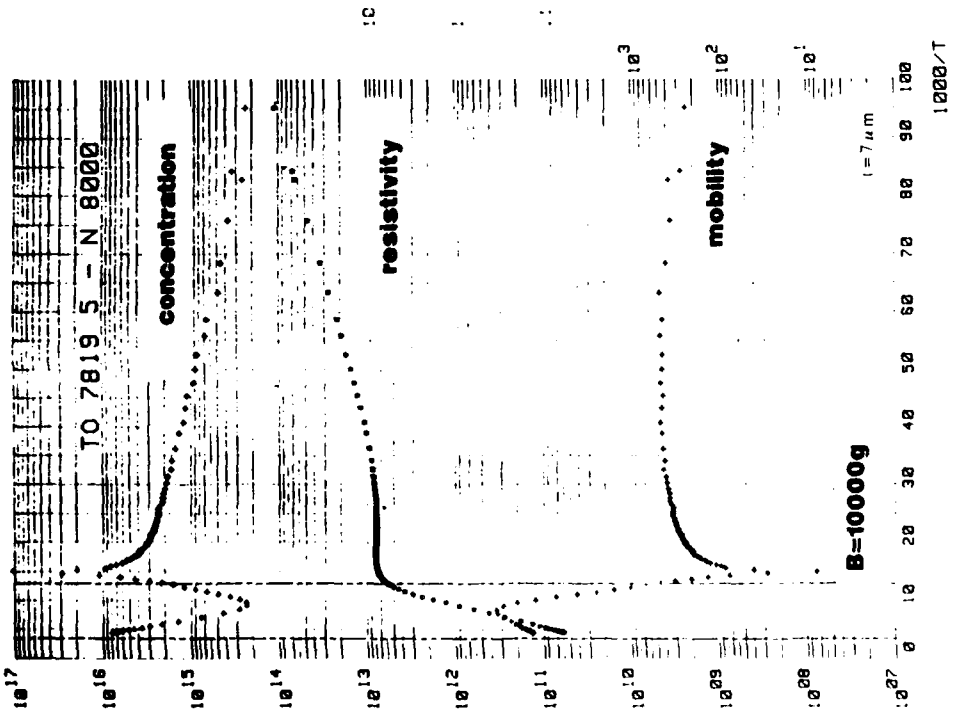

Fig. 2a = Hall effect measurement

GROWTH OF $Cd_{1-y}Zn_yTe$ CRYSTALS FOR LARGE-AREA LATTICE-MATCHED SUBSTRATES FOR $Hg_{1-x}Zn_xTe$ EPITAXY*

S. Sen, E.J. Smith, J.A. Kiele, S.M. Johnson and W.H. Konkel
Santa Barbara Research Center
Goleta, CA 93117

An alternative infrared (IR) dectector material, viz, $Hg_{1-x}Zn_xTe$, is receiving considerable current interest due to several recent theoretical and experimental investigations.[1-3] Although some effort has been directed at bulk growth of HgZnTe from the pseudo-binary melt, either by zone-leveling or solid-state recrystallization (mainly to study materials properties such as alloy hardness, defects, etc.), most work on rich melts by liquid-phase epitaxy (LPE)[3] or by the traveling heater method (THM)[4]. It was demonstrated recently that the growth of high-quality $Hg_{1-x}Zn_xTe$ epitaxial layers is critically dependent on the use of closely lattice-matched high-quality $Cd_{1-y}Zn_yTe$ substrates.[5] Motivated by this need, we have grown 2-in.-diameter $Cd_{0.80}Zn_{0.20}Te$ boules by a computer-controlled vertical modified-Bridgman (VMB) process.[6] We report here the results of this work, including assesment of the crystal quality in terms of the properties of the substrates as well as epitaxial long-wavelength IR $Hg_{0.84}Zn_{0.16}Te$ layers grown by LPE on those substrates.

(111)-oriented single-crystal substrates (free of grain boundaries and twins) up to 25 cm^2 in area have been obtained from 2-in. diameter $Cd_{0.80}Zn_{0.20}Te$ boules. Etch-pit densities in the boule ranged from 5.0×10^3 to 1.0×10^5 cm^{-2}. The higher densities are generally found in regions near the ampoule wall or near a grain boundary. X-ray double-crystal rocking-curve (DCRC) analysis has shown values of full width at half-maximum (FWHM) for (333) reflections of less than 20 arc-sec, comparable to values for the best available substrates from $Cd_{0.96}Zn_{0.04}$ boules used for $Hg_{0.80}Cd_{0.20}Te$ epitaxy. Energy-dispersive x-ray (EDX) analysis length-wise along the growth axis of one of the 2-in.-diameter boules showed that, despite the higher Zn content, the central region (5 cm in length) was of uniform composition ($y=0.20 \pm 0.01$). The crystal quality of these

improved substrates was further evaluated by growing long-wavelength $Hg_{0.84}Zn_{0.16}Te$ ($\lambda_{co} \approx 10$ μm) layers from Te-rich melts by the horizontal liquid-phase eptaxy (HLPE) technique. The structural quality of these epitaxial $Hg_{0.84}Zn_{0.16}Te$ layers on lattice-matched $Cd_{0.80}Zn_{0.2.}Te$ substrates was evaluated by x-ray DCRC analysis and x-ray topography; it compared favorably with the best $Hg_{0.80}Cd_{0.20}Te$ layers grown by LPE from Hg-rich melts on lattice-matched $Cd_{0.96}Zn_{0.04}$ substrates.

---

[1] A. Sher, A.-B Chen, and M. van Schlifgaarde, J. Vac. Sci. Technol. A. 4, 1965 (1986).

[2] J.P. Faurie, J. Reno, S. Sivananthan, I.K. Sou. X. Chu, M. Boukerche, and P.S. Wijewarnasuriya, J. Vac Sci. Technol. A. 4, 2067 (1986).

[3] A. Sher, D. Eger, A. Zemel, H. Feldstein, and A. Raizman, J. Vac. Sci. Technol. A. 4, 2024 (1986).

[4] R. Triboulet, A. Lasbley, B. Toulouse and R. Granger, J. Crystal Growth 79, 695 (1986).

[5] E.J. Smith, T. Tung, S. Sen, W.H. Konkel, J.B. James, V.B. Harper, B. F. Zuck, and R.A. Cole, J. Vac Sci. Technol. A 5, 3043 (1987).

[6] S. Sen, W.H. Konkel, S. J. Tighe, L.G. Bland, S.R. Sharma and R.E. Taylor, J. Crystal Growth 86, 111 (1988).

*This work supported in part by NASA Contract NAS1-18232 (A. Fripp, Contract Monitor).

ELECTRONIC PROPERTIES OF $Hg_{1-x-y}Cd_xZn_yTe$*

Sylvester N. Ekpenuma and Charles W. Myles
Department of Physics and Engineering Physics
Texas Tech University, Lubbock, Texas 79409-1051

INTRODUCTION

Recently, there has been interest in the development of IR detector materials with superior structural properties to those of $Hg_{1-x}Cd_xTe$. One candidate is the quaternary alloy $Hg_{1-x-y}Cd_xZn_yTe$. In particular, Colombo[1] has shown that the addition of a few per cent Zn to $Hg_{1-x}Cd_xTe$ hardens the lattice and reduces the dislocation density. In addition, Qadri et al.[2] have observed an increase in the bulk modulus of $Hg_{1-x}Cd_xTe$ on the addition of Zn. These effects apparently result from an increase in bond strength due to the presence of Zn in the lattice, as predicted by Sher et al.[3] While $Hg_{1-x-y}Cd_xZn_yTe$ thus holds promise for improved device material, its electronic properties are not well konwn. In this paper, we theoretically investigate these properties and estimate the effects of Zn on the bandgap, the effective mass, and other properties.

THEORETICAL APPROACH

Our theory treats ZnTe as an additional alloy constituent in $Hg_{1-x}Cd_xTe$ and models the resulting alloy $Hg_{1-x-y}Cd_xZn_yTe$ using both the virtual crystal approximation (VCA) and a version of the coherent potential approximation (CPA) developed for quaternary alloys.[4] Numerical results are obtained by utilizing tightbinding bandstructures for the alloy constituents. For CdTe and HgTe, we employ the sp^3s^* model of Kobayashi et al.[5] For ZnTe, we use an extension of that model to this material which was developed by us.[6] These bandstructures include the effects of spin-orbit coupling and compare well with those obtained

by other techniques[7]. Effects of the band offsets between the alloy constituents are accounted for in our theory by appropriately shifting the valence band maxima of the input bandstructures. By treating the band offsets as parameters, results for various properties can be obtained as a function of these quantities, if desired.

RESULTS AND DISCUSSION

Typical results of our calculations are shown in Figs. 1 and 2, where we have taken the band offset to be 0.35eV between CdTe and HgTe and 0.1eV between CdTe and ZnTe.

In the upper set of curves of Fig. 1, we display the predicted bandgap variation of $Hg_{0.8-y}Cd_{0.2}Zn_yTe$ with y. Three curves are displayed for this case; the dotted line is a composition weighted average of the bandgaps of the three compound constituents, the bandgap calculated in the VCA is represented by squares connected by dashes, and the dotted curve connecting the circles is the CPA bandgap. For comparison, in the lower set of curves we display similar information for the predicted x dependence of the bandgap of $Hg_{1-x}Cd_xTe$. In that case, the dotted curve, the dashed curve connecting the crosses, and the dotted curve connecting the diamond symbols are respectively the bandgaps calculated by a composition weighted average, by the VCA, and by the CPA. It is clear from the upper curves that the addition of Zn has two effects on the bandgap of $Hg_{0.8}Cd_{0.2}Te$. The first is the obvious effect of a shift with Zn composition y. The second is to introduce a downward bowing from the straight-line average. In the VCA, which includes no alloy disorder effects, the bowing is very small and is almost constant over the range of y considered. In the CPA, the bowing is larger, ranging from about 0.1eV at y=0 to a maximum of about 0.25eV for y near 0.5. This indicates that the alloy disorder effects included in the CPA should be a dominant contribution to the bandgap bowing at all Zn compositions. Furthermore, comparison of the upper curves with the lower curves

shows that the disorder induced bowing is similar for the two alloys but that the CPA bowing is expected to be larger for the quaternary alloy.

Since the primary interest in $Hg_{1-x-y}Cd_xZn_yTe$ is for possible use as an IR detector material, it is interesting to consider the dependence of various properties on the Zn compositon y when the Cd composition x is simultaneously varied so that the bandgap remains constant in the infrared regime. We have done this for a bandgap of 0.12eV and our results for the dependence of the electron effective mass on y in this case are illustrated in Fig. 2. In that figure, we plot both the VCA and CPA effective masses (dotted curve and squares connected by dashes, respectively) in units of the free electron mass. Two different types of information can be extracted from the figure. First, in both VCA and the CPA, the effective mass is almost independent of y. This is an indication that the presence of Zn in $Hg_{1-x}Cd_xTe$ should not appreciably affect the mobility. Second, the difference between the VCA and the CPA effective masses shows that alloy disorder introduces only a small shift in the effective mass.

REFERENCES

* Supported by a grant from Texas Instruments, Inc.

1. L. Colombo, Proc. IRIS Detector Spec. group meeting, Seattle, 1984.
2. S.B. Qadri, E.F. Skelton, A.W. Webb, and J. Kennedy, Appl. Phys. Lett. 46, 257 (1985).
3. A. Sher, A.-B. Chen, W.B. Spicer, and C.-K. Shih, J. Vac. Sci. Tech. A 3, 105 (1985).
4. J.R. Gregg, C.W. Myles, and Y.-T. Shen, Phys. Rev. B 35, 2532 (1987).
5. A. Kobayashi, O.F. Sankey, and J.D. Dow, Phys. Rev. B 25, 6367 (1982).
6. S.N. Ekpenuma and C.W. Myles, unpublished.
7. M.A. Berding, S. Krishnamurthy A. Sher, and A.-B. Chen, J. Vac. Sci. Tech, A 5, 3014 (1987); K.C. Hass and H.Ehrenreich, Phys. Rev. B 27, 1088 (1983).

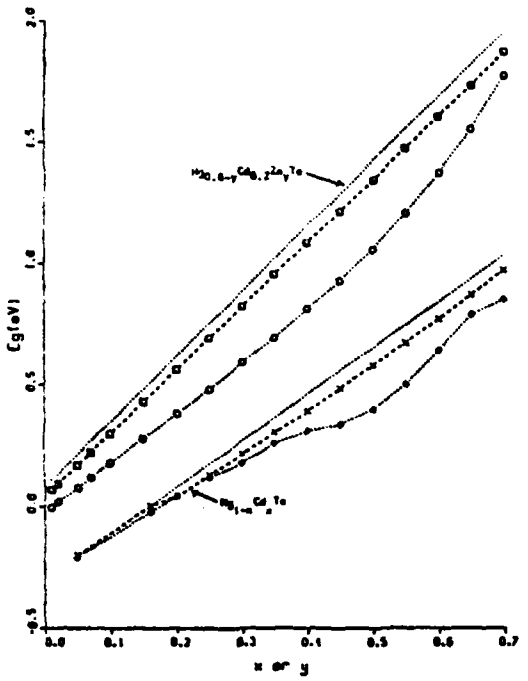

Figure 1: The upper three curves show the bandgap as a function of y in $Hg_{0.8-y}Cd_{0.2}Zn_yTe$ in three approximations: composition weighted average bandgap (dotted), VCA bandgap (squares connected by dashes), and CPA bandgap (circles connected by dots). The lower set of curves shows similar information for the dependence of the bandgap of $Hg_{1-x}Cd_xTe$ on x. The composition weighted average, VCA, and CPA bandgaps for this case are shown respectively as dotted, crosses connected by dashes, and diamonds connected by dots.

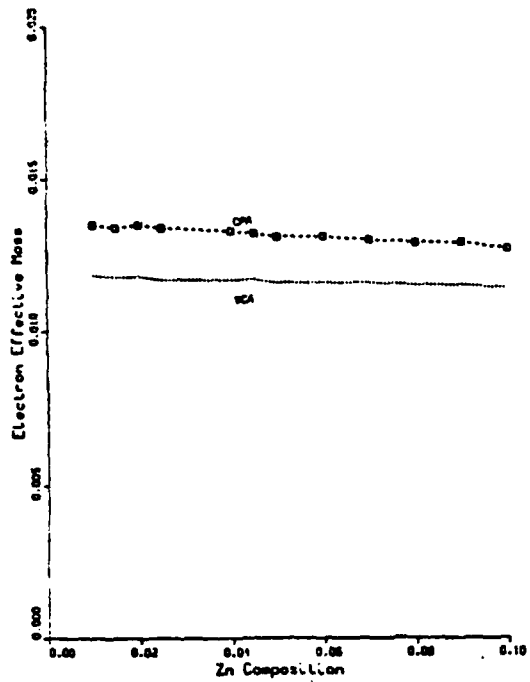

Figure 2: The dependence of the electron effective mass (in units of the free electron mass) in $Hg_{1-x-y}Cd_xZn_yTe$ on y for a constant bandgap of 0.12eV. The VCA results are shown dotted, while the CPA effective mass is shown by squares connected by dashes.

Study of CdTe Layers Grown on (111)B CdTe Surfaces by Molecular Beam Epitaxy

G. Monfroy*, S. Sivananthan, S. Burns, and J.P. Faurie
University of Illinois at Chicago, Dept. of Physics

The growth by molecular beam epitaxy (MBE) of CdTe on foreign substrates has been widely studied, which is not the case for the homoepitaxy of CdTe. Recently, Oron et al.[1], studied the homoepitaxy of CdTe grown by metalorganic chemical vapor deposition (MOCVD). X-ray double crystal rocking curves (DCRC) recorded on (111)B faces exhibited the superimposition of the substrate and the epilayer peak, with full widths at half-maximum (FWHM) for the epilayer peaks between 400 and 800 arcsec.

The growth of CdTe (111)B by MBE leads to very different results, which amazingly have not been reported before: CdTe does not grow coherently on the substrate. Two peaks are seen, the first one attributed to the substrate, the second one, broader, corresponding to the epilayer (Fig. 1). The epilayer has a higher d-spacing than the substrate.

The FWHM of the epilayer and the angular separation, $\Delta\theta$, between the substrate and the epilayer peak have been studied as a function of the growth conditions. The growth was performed on CdTe (111)B substrates, using a single effusion cell for the CdTe. The thicknesses of most of the epilayers were kept around 3μm, which corresponds to enough matter to observe a well-shaped diffraction peak for the epilayer, and still allows for the substrate reflection to be seen.

The results indicate that when the substrate temperature (Ts) is varied from 200°C to 335°C, the FWHM of the epilayer decreases, as well as $\Delta\theta$. The influence of the growth rate (GR) has been investigated at constant Ts, indicating that FWHM and $\Delta\theta$ increase with GR. The effect of the layer thickness has also been studied. FWHM in the 50 arcsec range have been recorded on 7.5 μm thick layers.

Photoluminescence experiments have also been performed on some of the samples, corroborating the x-ray diffraction results.

Based on the present results, the highest crystalline quality CdTe (111)B layers are obtained for Ts=335°C and GR=1.5Å/s.

The reason for the non-coherent growth of CdTe (111)B is not yet known. The assumption of an eventual misorientation between the substrate and the epilayer has been ruled out by measuring DCRC after rotating the sample around the

normal to its surface. Stoichiometry deviations in the epilayer and/or the substrate are likely to be responsible for the $\Delta\theta$. Indeed, $\Delta\theta$ decreases when Ts increases, i.e., when Ts gets closer to the growth temperature of bulk CdTe. This is confirmed by MOCVD results, where $\Delta\theta=0$ because MOCVD layers are grown at higher temperature than MBE layers.

1. M. Oron, A. Raizman, Hadas Shtrikman, and G. Cinader, Appl. Phys. Lett. 52, 1059 (1988).

* We are requesting a student financial assistance for Mr. Gerard Monfroy who is a full time university student and who will present this paper if accepted by the program committee.

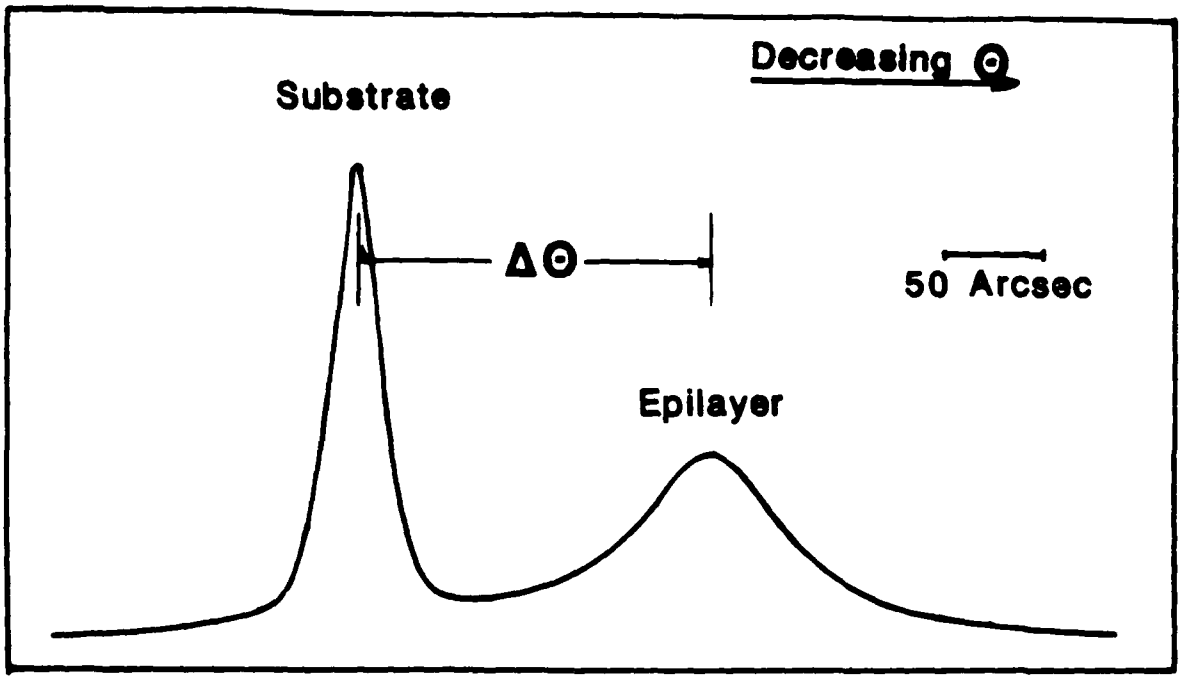

Fig.1: CdTe(111)B epilayer grown on CdTe (111)B substrate. CdTe (333) reflection measured using Cu K_{α_1} (λ = 1.540Å) and a Si (331) monochromator. Substrate temperature = 335 °C. Growth rate = 0.8 Å/s. Layer thickness = 1.1 μm.

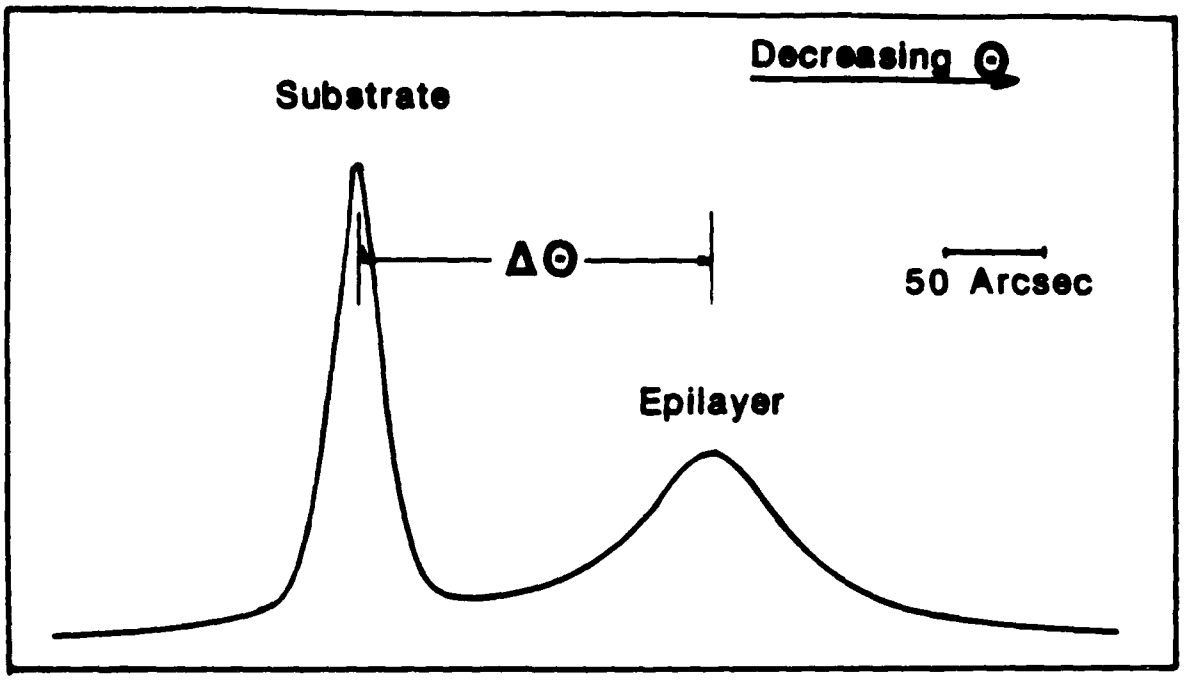

Fig.1: CdTe(111)B epilayer grown on CdTe (111)B substrate. CdTe (333) reflection measured using Cu $K\alpha_1$ (λ = 1.540Å) and a Si (331) monochromator. Substrate temperature = 335 °C. Growth rate = 0.8 Å/s. Layer thickness = 1.1 μm.

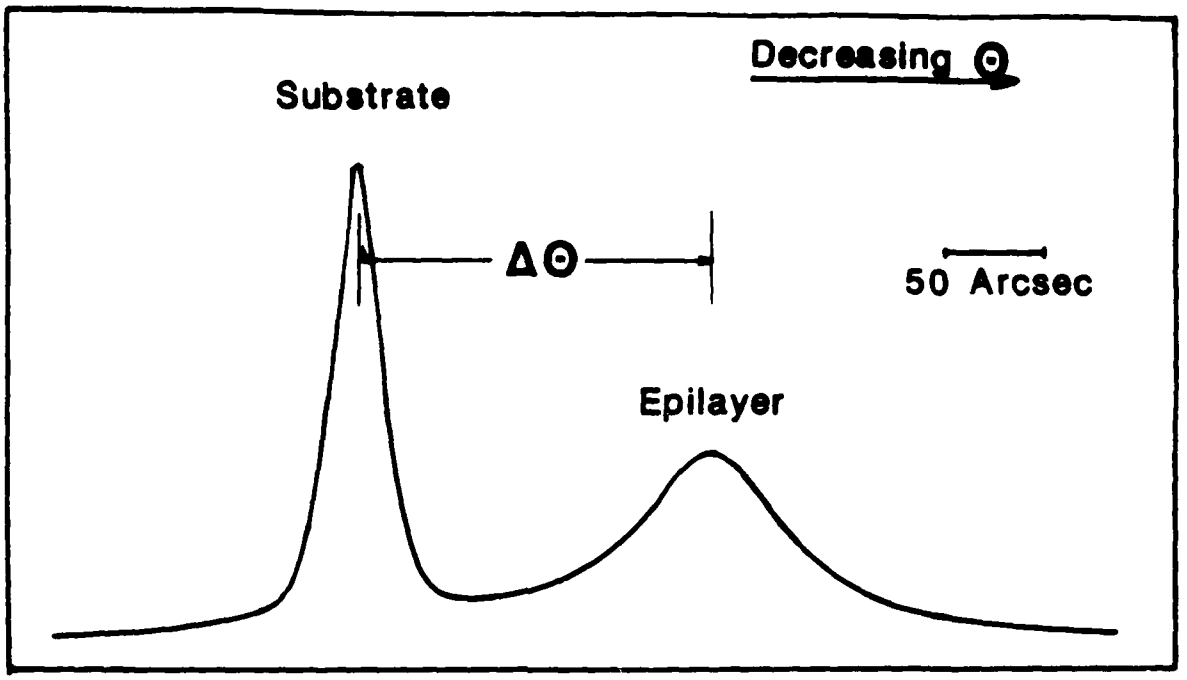

Fig.1: CdTe(111)B epilayer grown on CdTe (111)B substrate. CdTe (333) reflection measured using Cu $K\alpha_1$ (λ = 1.540Å) and a Si (331) monochromator. Substrate temperature = 335 °C. Growth rate = 0.8 Å/s. Layer thickness = 1.1 μm.

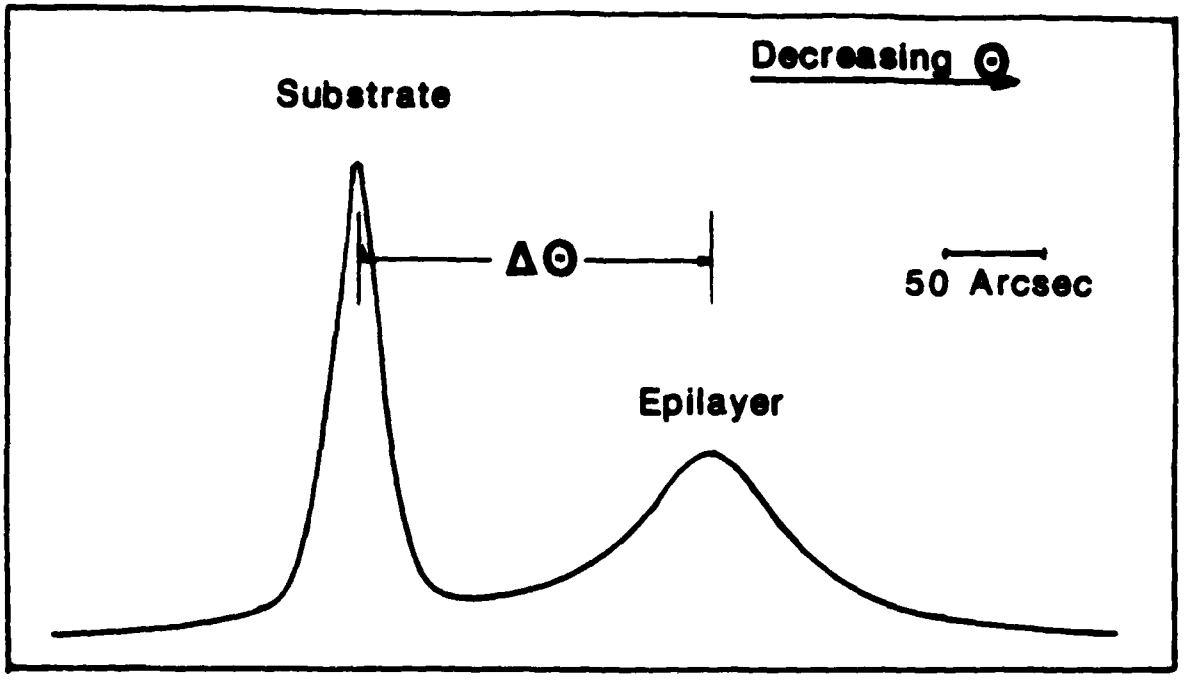

Fig.1: CdTe(111)B epilayer grown on CdTe (111)B substrate. CdTe (333) reflection measured using Cu K_{α_1} (λ = 1.540Å) and a Si (331) monochromator. Substrate temperature = 335 °C. Growth rate = 0.8 Å/s. Layer thickness = 1.1 μm.

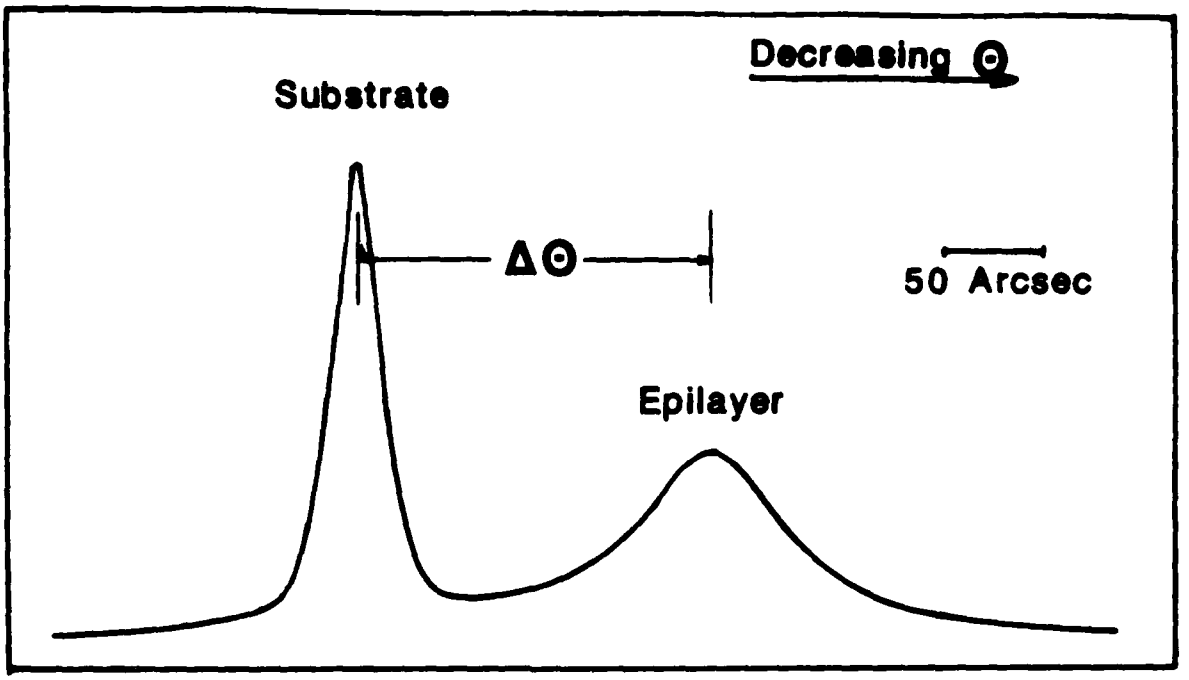

Fig.1: CdTe(111)B epilayer grown on CdTe (111)B substrate. CdTe (333) reflection measured using Cu $K\alpha_1$ (λ = 1.540Å) and a Si (331) monochromator. Substrate temperature = 335 °C. Growth rate = 0.8 Å/s. Layer thickness = 1.1 μm.

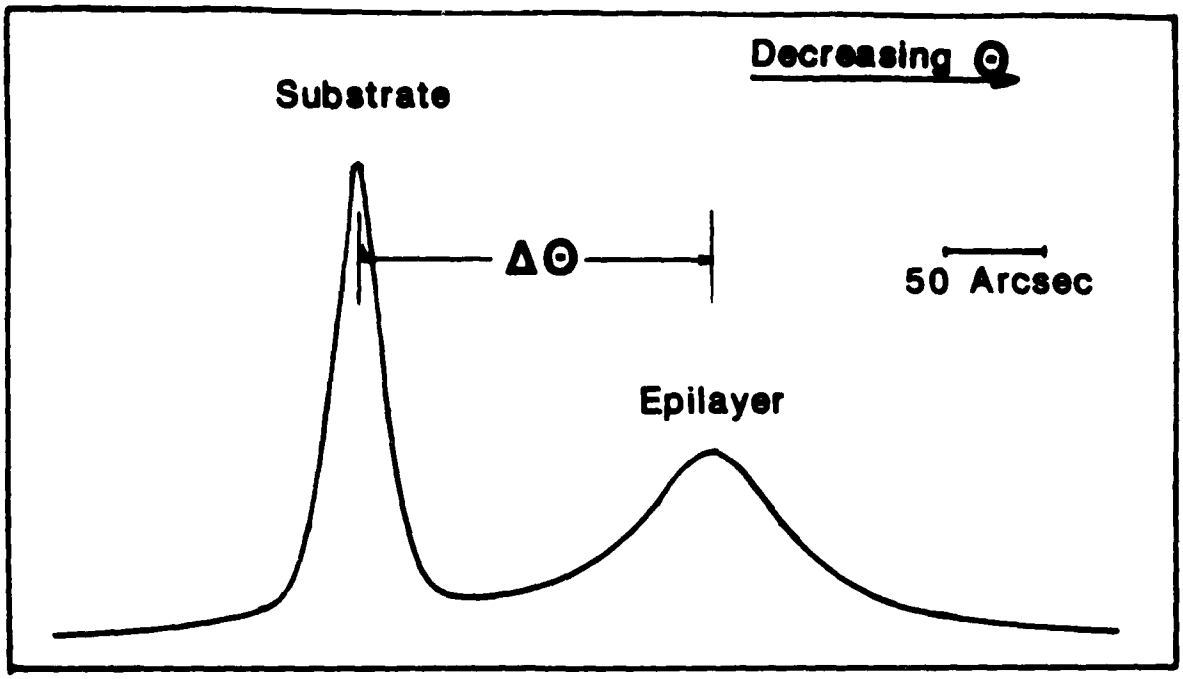

Fig.1: CdTe(111)B epilayer grown on CdTe (111)B substrate. CdTe (333) reflection measured using Cu $K\alpha_1$ (λ = 1.540Å) and a Si (331) monochromator.
Substrate temperature = 335 °C. Growth rate = 0.8 Å/s.
Layer thickness = 1.1 μm.

MOCVD GROWTH OF $Cd_{1-x}Zn_xTe$ EPITAXIAL LAYERS ON GaAs SUBSTRATES*

W.L. Ahlgren, S.M. Johnson, E.J. Smith, R.P. Ruth,
B.C. Johnston, T.W. James,** and D.L. Arney**
Santa Barbara Research Center
Goleta, CA 93117

and

K.M. James
Hughes Research Laboratories
Malibu, CA 90265

Epitaxial growth of $Cd_{1-x}Zn_xTe$ on GaAs substrates has been achieved for all alloy compositions, $0 \leq x \leq 1$. A conventional (pyrolytic) MOCVD process was employed, using dimethyl cadmium (DMC), diethyl zinc (DEZ), and diethyl tellurium (DET) as reactants. The relation between soild-phase composition x and the gas-phase DEZ/(DMC + DEZ) concentration ratio was determined experimentally, for a specific set of process parameters. GaAs substrate orientations used were {001} 2° toward <110> , {012}, {123}, and {111}. CdTe grew with the best surface morphology on GaAs {012}; ZnTe grew with the best surface morphology on GaAs {123}. Alloy layers with composition near x=0.04 were grown on GaAs {012} substrates. The x-ray rocking curve on the (115) reflection from this material had a full width at half-maximum (FWHM) of 23 arc-sec, indicating very good crystal structure. Additional characterization of these materials by x-ray diffraction and topography, electron channeling pattern analysis, cathodoluminescene, and photoluminescence will be presented.

---

*This work supported in part by NRL Contract N00014-86-C-2548 (H. Lessoff, Contract Monitor).

**Present address: Superconductor Technologies Inc., Santa Barbara, CA 93111.

PHOTOLUMINESCENCE OF GALLIUM IMPURITY IN CdTe

J.M. Wrobel, J.J. Dubowski
National Research Council of Canada
Ottawa, Ontario K1A 0R6
and
P. Becla
MIT Francis Bitter National Magnet Laboratory
Cambridge, Massachusetts 02139

INTRODUCTION

Several techniques have been utilized to prepare CdTe epitaxial layers on materials other than CdTe. The main reason for this interest is to obtain large area single crystal CdTe wafers suitable for the production of hybrid structure CdTe based devices. We used Pulsed Laser Evaporation and Epitaxy[1] (PLEE) to grow CdTe on GaAs. However, at this point we encountered a barrier which is also evident in several authors' papers.[2-5] Secondary Ion Mass Spectroscopy indicates the presence of Ga in CdTe epilayers.

Because of its sensitivity to residual impurities we implemented photoluminescence for Ga detection.

EXPERIMENTAL PROCEDURE

As a reference for our CdTe/GaAs wafers we examined several bulk CdTe samples with deliberately introduced Ga. One set of such samples was prepared by implantation with Ga. The other set was doped during synthesis using the Bridgman technique. Both sets were annealed in a Cd atmosphere at various temperatures. For reference purposes, test samples of pure CdTe were prepared under the same conditions.

Thin layers of CdTe were grown on (001) GaAs substrates by PLEE. Depending on the conditions during the deposition (001) or (111) oriented films were produced.

The photoluminescence spectra were taken with a Spex double monochromator with a resolution of about 0.7 meV. The 5114 Å argon laser line was used for excitation and we varied the power of the incident light from 1 mW to 80 mW in extreme cases. The size of the sampled area was 0.2 mm^2. All measure-

ments presented were taken at 6 K and laser power of 20 mW.

RESULTS AND DISCUSSION

Figures 1 - 3 show photoluminescence spectra of bulk CdTe with deliberately introduced Ga. Each plot is associated with a sample which has undergone the specific treatment described in the captions. Figures 1 a and b contain photoluminescence plots for Bridgman grown CdTe which was doped with Ga to the level of $<10^{17}$ cm^{-3}, and annealed at 600 °C for 3 days and at 950 °C for one day, respectively. CdTe, with a Ga concentration of $\sim 10^{17}$ cm^{-3} (obtained from SIMS and Hall measurements), annealed at 600 °C and at 800 °C for 24 hours gave the luminescence shown in Figure 2.

All these spectra have features similar to those frequently observed in CdTe. They have excitonic lines between 1.58 eV and 1.596, eV and a defect related band around 1.42 eV. There are no systematic differences observed in the defect band region which could be related to the presence of Ga other than the fact that the overall intensity of the transitions in this region is much higher in the doped samples. However, significant differences occur in the excitonic region. Besides a strong line at 1.592 eV associated with an exciton bound to a neutral donor line (D°X), two new lines are observed at 1.581 eV and 1.586 eV in Ga doped samples only. We noticed that the intensities of these two lines and the position of the defect band are both correlated with Ga concentration. Careful study of the power and temperature dependence of these two lines suggest their excitonic origin rather than free-to-bound transition. We associated these lines with donor and double acceptor complexes created by the Ga impurity and native defects.

In Figure 3 we show photoluminescence for the Ga implanted CdTe annealed for 2 hours at 500 °C in Cd vapors. When this spectrum is compared with the original unimplanted wafer, whose thermal treatment was identical, no difference in

the excitonic region can be found. On the other hand, a broad band around 1.55 eV occurred for the implanted sample only. Most likely both free-to-bound and donor acceptor pair recombination contribute to this band. However, the width of this band makes it impossible to determine the exact energy position of these transitions.

Our samples of thin epitaxial film deposited on GaAs which exhibit the best photoluminescence signal thus far, have photoluminescence spectra as presented in Figure 4. We note the presence of the two excitonic lines at 1.585 eV and 1.581 eV. As described earlier, they are present in CdTe deliberately doped with Ga. We also observe a broad band near 1.55 eV which we observed in the Ga implanted and annealed sample. Another sharp line at 1.488 eV is quite often seen in the photoluminescence spectra of our films. This line is strongly dependent on temperature suggesting a donor acceptor pair recombination mechanism. A donor level at 15 meV and an acceptor level at 100 meV explain the presence of this line as well as the presence of the donor bound exciton at 1.593 eV and the acceptor bound exciton at 1.585 eV.

The peaks at 1.585 eV, 1.581 eV and 1.488 eV, as well as the band at 1.55 eV in the luminescence spectra of our films appear to be associated with unintentional doping of the layers with Ga. The obvious source of this element must be the substrate. Currently, we are investigating the mechanism of Ga migration in this system.

1. J.J. Dubowski, Chemtronics, 3, 66 (1988).
2. S.J.C. Irvine, J. Giess, J.S. Gough, G.W. Blackmore, A. Royle, J.B. Mulin, N.G. Chew, and A.G. Cullis, Journal of Crystal Growth 77, 437 (1986).
3. R. Kay, R. Bean, K. Zanio, C. Ito, and D. McIntyre, Applied Physics Letters 51, 2211 (1987).
4. B.K. Wagner, J.D. Oak, and C.J. Summers, Journal of Crystal Growth 86, 296 (1988).
5. R. Korenstein and B. MacLeod, Journal of Crystal Growth 86, 382 (1988).

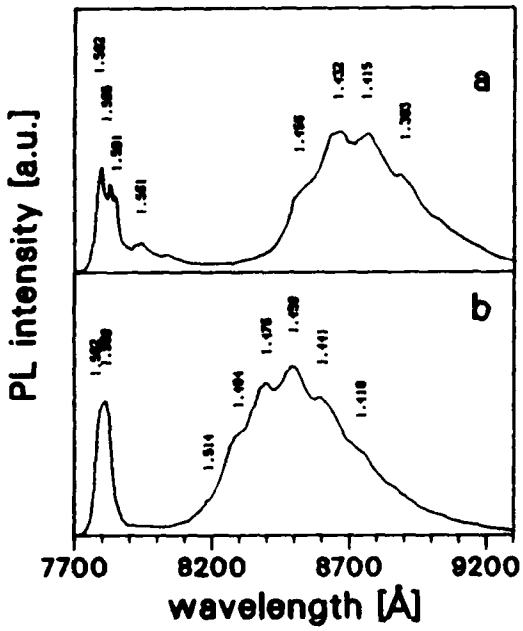

Fig. 1. PL spectra for CdTe samples doped with Ga to ~10^{17} cm^{-3} and annealed at: a) 600 °C, b) 950 °C.

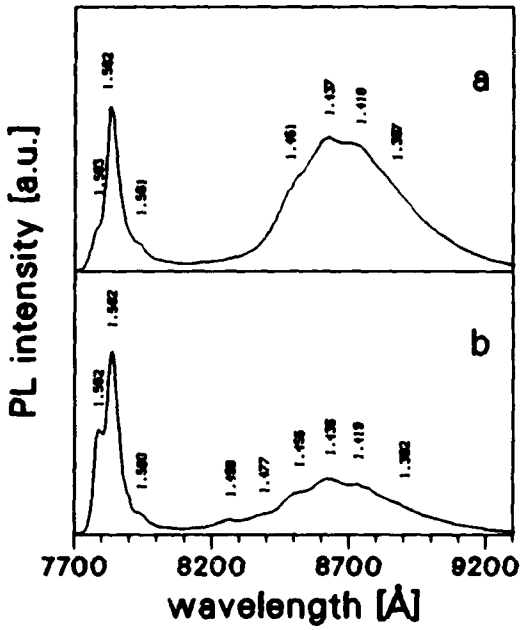

Fig. 2. Pl Spectra for samples with Ga concentration lower than in Fig. 1. annealed at: a) 600 °C, b) 800 °C.

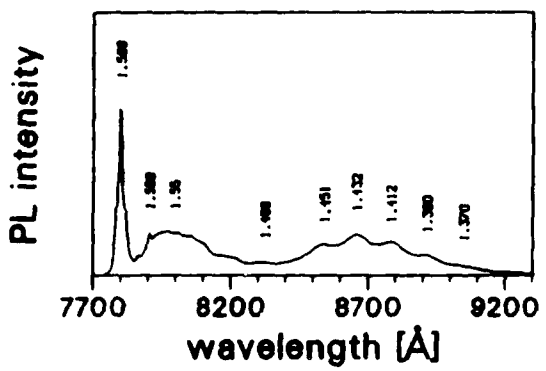

Fig. 3. Pl spectrum of high quality CdTe implanted with Ga and annealed for 2 hrs at 500 °C.

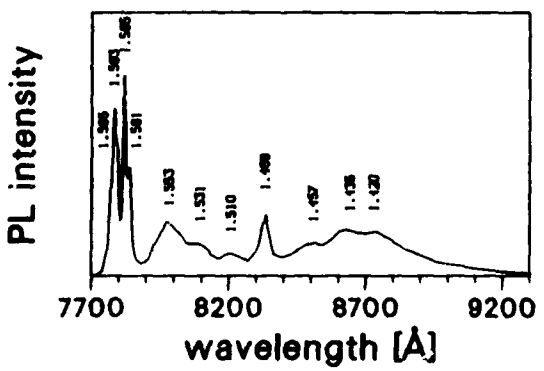

Fig. 4. Photoluminescence of a PLEE CdTe epilayer grown on GaAs substrate.

COMPARISON OF CdTeSe AND CdZnTe AS SUBSTRATES FOR HgCdTe EPITAXY*

S.Sen, J.A. Kiele, S.M. Johnson, W.H. Konkel and R.P. Ruth
Santa Barbara Research Center
Goleta, CA 93117

The use of lattice-matched substrates for growth of $Hg_{1-x}Cd_xTe$ epitaxial layers has been shown to reduce dislocation densities, reduce surface recombination velocities and improve layer morphology. Both CdZnTe and CdTeSe have been used as substrates for the growth of HgCdTe by liquid-phase epitaxy (LPE). CdZnTe succeeded the binary compound CdTe several years ago because of greater hardness, lower dislocation density and the advantages of lattice matching (resulting in fewer misfit dislocations at the substrate-layer interface). Recently, the growth of lattice-matched substrates of CdTeSe by metalorganic chemical vapor deposition (MOCVD) has been reported, supporting the importance of close lattice matching for improved HgCdTe layer quality by MOCVD growth.

Although alternative ("foreign") substrate materials, such as GaAs with an intervening CdTe buffer layer, have been used for the growth of HgCdTe by both MOCVD and molecular-beam epitaxy (MBE), the lattice mismatch between HgCdTe and CdTe generates dislocations at the interface and degrades the HgCdTe layer. Current investigation of the growth of lattice-matched CdZnTe layers grown on GaAs by MOCVD indicates promise of a possible replacement for bulk substrates of CdZnTe (and perhaps also CdTeSe) in the future. However, current development of next-generation hybrid infrared detector arrays relies upon active layers of HgCdTe grown by LPE, and the substrate materials required are in bulk-crystal form.

CdTeSe has been grown by the computer-controlled vertical modified-Bridgman (VMB) growth process at SBRC and used as substrates for epitaxial growth of $Hg_{0.80}Cd_{0.20}Te$ by LPE, MOCVD, and MBE. The results provide a good measure of the substrate quality in terms of epitaxial HgCdTe layer quality grown by these different techniques, and, in turn, give a basis

for comparison of CdTeSe and CdZnTe as substrate materials. The bulk properties of the two materials are compared (for growth under similar conditions) in terms of segregation behavior of the solutes (Zn and Se), purity of the starting Zn and Se, crystal structural quality, and yield of large-area substrate wafers per boule.

The characteristic grain structure of the VMB boule surface is similar in the two materials, indicating a similar yield of large-area substrate wafers per boule. Further characterization of the CdTeSe confirms this. Although the etch-pit density for CdSeTe has been similar to that of CdZnTe (10^4 cm^{-2} to low 10^5 cm^{-2}), the precipitate size and density were significantly reduced (by a factor of 10) in CdTeSe compared with that in CdZnTe. Clustering of etch pits around precipitates typically seen in CdTe and CdZnTe is not present in CdTeSe. X-ray topography of a longitudinal section of a CdTeSe boule shows very good crystal quality (no sub-grain features). Values of x-ray rocking curve full width at half-maximum (FWHM) for the same section range from 8 to 12 arc-sec. As expected, composition control is maintained over larger boule lengths for CdTeSe than for CdZnTe because the distribution coefficient of CdSe is about 0.97 in CdTe melt compared with 1.31 for ZnTe. The sensitivity of epitaxial $Hg_{0.80}Cd_{0.20}Te$ layer quality (grown by the three different techniques) to composition variation in the substrate, which produces variations in interfacial lattice mismatch, has also been evaluated.

---

*This work supported in part by NRL Contract N00014-87-C-2501 (H.Lessoff, Contract Monitor).

CdTe/GaAs/Si SUBSTRATES FOR HgCdTe PHOTOVOLTAIC DETECTORS

R. Bean, K. Zanio and J. Ziegler*
Ford Aerospace Corporation, Aeronutronic Division
Newport Beach, CA 92658

Introduction

Silicon as a substrate for HgCdTe detector arrays offers many potential benefits over other substrates, including possibilities for complete integration into monolithic FPAs. Improvements in the quality of the CdTe/GaAs/Si composite substrates have brought us closer to realizing those benefits. HgCdTe photovoltaic arrays have been prepared on this hetero-substrate by both close spaced and MOCVD epitaxial growth methods.[1-3] Outlined here are some of the unique problems that had to be addressed in developing processes for growth of high quality CdTe layers on the GaAs/Si.

CdTe Layer Growth Procedures

Figure 1 compares the processes for CdTe growth on GaAs/Si and bulk GaAs. In both cases, the CdTe prevents GaAs doping of the HgCdTe by diffusion through the buffer layer. No additional encapsulation to prevent vapor phase contamination of the HgCdTe is needed with GaAs/Si.

GaAs and Silicon Characteristics Affecting CdTe Growth

As substrates for CdTe growth, GaAs epilayers on Si differ from bulk GaAs in having a significant surface structure; in having high defect concentrations; in being deliberately misoriented from the nominal (100) plane; and in containing high densities of cracks, from thermal strain. The surface structure, particularly varied faceting, has a major influence on CdTe layers. Reducing such structure by polishing is complicated by the need to keep GaAs thickness under 3μm to avoid stress cracks.

A strong preference for parallel CdTe growth, (100)CdTe on (100)GaAs/Si, is one consequence of surface structure. The GaAs epilayer must be subjected to chemical polishing or special oxide dissolution steps to obtain (111)CdTe.

Another facet related factor is seen in the change of (100)CdTe layer x-ray rocking curve line widths at different measuring azimuths (Figure 2). If the beam azimuth is perpendicular to the long axis of the elongated surface pyramids on the CdTe surface, the line may be relatively narrow; at other azimuths the lines are greatly broadened or even split into double peaks. Chemical polishing to reduce GaAs layer faceting before CdTe growth eliminates this directional effect.

The (111)CdTe layers on as grown GaAs layers are plagued with rotational twins. Again, polishing appears to reduce the rotational twinning.

Substrate misorientation has a very strong influence on the specific configurations seen in the sharply faceted (100)CdTe. An abrupt change occurs at 3° misorientation from raised pyramids to elongated, sunken grooves at greater misorientations (Figure 3). Misorientation also affects (111)CdTe layers, but in a different way. On a near nominal (100) substrate, the (111)CdTe surface is nearly featureless (Figure 4A). With increasing misorientation, though, tiny streaks of (100)CdTe twins appear in increasing densities (Figure 4B). This is probably also facet related, possibly as increasing areas of a defect facet are exposed in tilting.

---

* J. Ziegler is now at Rockwell International, Anaheim, CA.

References

1. R. Kay, R. Bean, K. Zanio, C. Ito and D. McIntyre, Appl. Phys. Lett. 51, 2211 (1987)

2. K. Zanio and R. Bean, Proc. of the S.P.I.E., Symposium on Optics, Orlando, Fla., April 1988. In press.

3. K. Zanio, R. Bean, S. Taylor, C. Ito, D. McIntyre, and M. Chu, 1988 IRIS Meeting of the Specialty Group on Infrared Detectors, August 1988, Laurel, MD. Proceedings, in press.

Figures

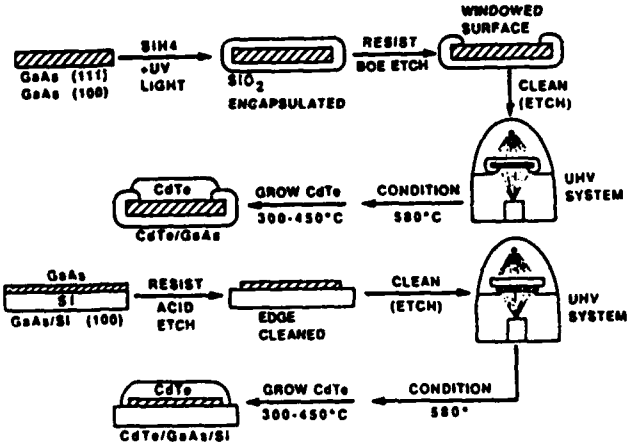

FIGURE 1. GROWTH PROCESSES FOR CdTe ON GaAs AND ON GaAs/Si.

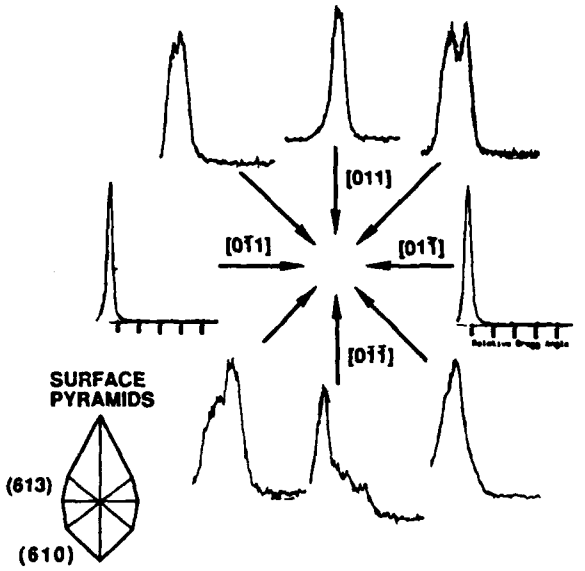

FIGURE 2. CHANGE IN ROCKING CURVE LINE WIDTHS WITH X-RAY AZIMUTH FOR (100)CdTe ON GaAs/Si.

The inset shows orientation and faceting of the typical CdTe surface pyramid.

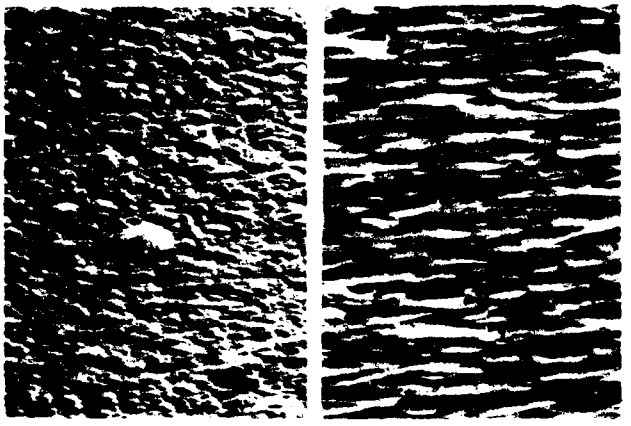

A B

FIGURE 3. CHANGE IN (100)CdTe/GaAs/Si MORPHOLOGY WITH SUBSTRATE MISORIENTATION.

A. Less than 3° misorientation.
B. More than 3° misorientation.

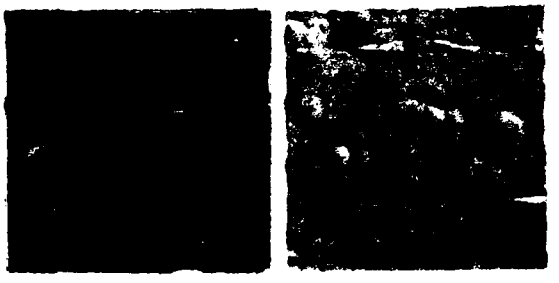

A B

FIGURE 4. (100)CdTe TWINS FORM IN (111)CdTe ON MISORIENTED GaAs/Si

A. On near nominal (100)GaAs/Si
B. On 1.5° misoriented (100) substrate

ION BEAM MILLING EFFECT ON ELECTRICAL PROPERTIES OF $Hg_{1-x}Cd_xTe$

G. Bahir and E. Finkman
Microelectronics Research Center, Department of Electrical Engineering
Technion - Israel Institute of Technology
Haifa 32000, Israel

"Dry etching" is being used increasingly in advanced Microelectronics processes in addition to the use of conventional chemical etch. The major advantages of the ion beam etching technique are related to its capabilities in fabricating fine geometry devices. Ion beam milling (IBM) is done in the low energy range of ion bombardment where it is generally agreed that only surface interaction occur. A collimated ion beam, usually in the 100 to 1000 eV range, strikes a target and "sputter off" surface atoms by breaking the forces bonding the atom to its neighbors (of the order of few eV). The sputtering process then, is one of impact and energy transfer. The technique is being implemented in various uses for small dimensions focal plane devices, it is especially suited for accurate definition of dimensions and for isolation between devices.

The electrical properties of $Hg_{1-x}Cd_xTe$ (MCT) are determined both by electrically active impurities and by native defects. The electrical properties of this material are very sensitive to processes like ion implantation, and irradiation by by electrons, neutrons, and γ rays. All can create electrically active defects. The produced material is frequently highly compensated, due to the presence of a large number of both *n* and *p*-type electrically active defects. High degree of compensation is evident by degradation in material parameters, e.g. mobility and lifetime, especially at low temperatures.

Despite the wide use of IBM in MCT technology, little had been published so far on the interaction of low energy ion beam with MCT crystal. The effect on electrical properties and creation of defects was mentioned briefly in ref. [1]. Wotherspoon [2] reported the conversion of *p*-type MCT to *n*-type by ion bombardment. Recently, this technique enabled the fabrication of novel structure photodiodes [3], and bipolar transistors [4] in MCT.

This work describes the changes induced in MCT by ion beam milling. In particular, the influence on carrier concentration, mobility, and excess carrier lifetime is studied.

The crystals under investigation were grown by solid state recrystalization. Both *n* and *p*-type materials were studied, in the composition range of $0.2<x<0.3$. *p*-type materials were annealed at 350C to achieve carrier concentration of $0.6\text{-}5\cdot10^{16}$ cm^{-3}, and mobilities of 400-800 $cm^2V^{-1}sec^{-1}$ at 77K. *n*-type materials with various degrees of compensation were used. Typical parameters for the better samples at 77K are carrier concentration of $0.5\text{-}2\cdot10^{15}$ cm^{-3}, mobilities of $1\text{-}2\cdot10^5$ $cm^2/V\cdot sec$, and lifetimes of 2-5 μsec. A Commonwealth Scientific Corp. IBM system was used. The devices were milled using a collimated, neutralized Ar ion beam, with energies of 100-150 eV, and a current density of 0.5-0.8 mA/cm^2. The sample was held on a cold stage. Sample temperature did not exceed 50 C during the process. Irradiated samples were studied by differential Hall effect, and its temperature dependence, using successive chemical etching and measurements. Steady state photoconductivity was used to derive the excess carrier lifetime. MIS capacitors were fabricated on *p* and *n* samples with x=.29 before and after irradiation, using 100-200 Å anodic sulfide and 3000 Å

evaporated ZnS passivation. C-V measurements were performed at 77K using a 1 MHz, 10 mV signal. This is most suitable to study electrical properties of the upper layer, assuming that this layer has approximately a uniform carrier concentration to a depth of 0.5-1 μm.

C-V results are shown in figures 1 and 2 for capacitors fabricated on *p* and *n* substrates, respectively. Half of the substrate was protected during irradiation for comparison. It is seen that the carrier concentration after ion bombardment, near the surface, is $2\text{-}5\cdot10^{16}$ cm $^{-3}$ for both *n* and *p*-type starting materials. Chemical etching of 1-5 μm from the irradiated surface, using 10% of Br in E.G., does not have any effect on the C-V curves. The full effect of the induced change on the top layer electrical properties was achieved within 2-3 minutes of irradiation. No further changes were detected for milling times of up to an hour. A typical C-V curve of ~100 keV ion implanted surface is also shown in figure 1 for comparison. The *n*-type carrier concentration induced in this case is about 10^{18} cm^{-3}, with a junction depth of only 0.5-1 μm. It should be noticed that IBM does not degrade the MCT surface properties. Thus, high frequency C-V curve is still observed after milling, while low frequency characteristics are found after other processes, e.g. ion implantation.

Temperature dependence of the carrier concentration and mobility are given in figures 3,4 for an *n*-type sample. The data were taken for unmilled sample, after 10 μm IBM etch at energy of 100-110 V with current density of ~0.5 mA/cm^2, and after removing few microns by chemical etch several times. The effect of low temperature annealing (75-80 C for 1 day to 1 week) was also studied. The 77 K lifetime of the device given in figs. 3,4 was 2 μsec before milling, decreased to few nsec after it, and recovered to 100-200 nsec following low temperature anneal. The effect of saturation of the electrical properties was checked using IBM on 5 μm thick Hall samples. The main conclusions are:

a. All milled surface layers are *n*-type with carrier concentration that reaches an upper limit of $2\text{-}5\cdot10^{16}$ cm^{-3} within the first 1-3 minutes of irradiation.

b. At the same time, the thickness of the induced layer extends to 5-20 μm.

c. The mobility of this layer and its temperature dependence is characteristic of that of an uncompensated *n*-type material. Milling of compensated materials, which showed originally decrease in their mobility at low temperatures due to ion scattering, improved their mobility to that of an uncompensated materials.

d. Excess carrier lifetime was reduced by a factor of 10 to 100.

e. Low temperature annealing can decrease carrier concentration again, in some samples, by up to a factor of 2; hardly affect the mobility, and the carrier profile induced by the milling; but always recovers a large part of lifetime degradation.

f. Sidewall damage in fabricating fine microstructures is very small. Can be removed by 1 μm chemical etch.

References

[1] S. Margalit, Y. Nemirovsky, and I. Rotstein, J. Appl. Phys. **50**, 6386 (1979).

[2] J. T. M. Wotherspoon, UK patent GB 2095898, 1981.

[3] I. M. Baker, M. D. Jenner, J. Parsons, R. A. Ballingall, I. D. Blenkinsop, and J. H. Firkins, IEE Conf. Publ. **228**, Conf. on advanced infrared detectors and systems, 1983.

[4] T. Ashley, G. Crimes, C. T. Elliott, and A. T. Harker, Electronics letters **22**, 611 (1986), ibid **23**, 1280 (1987).

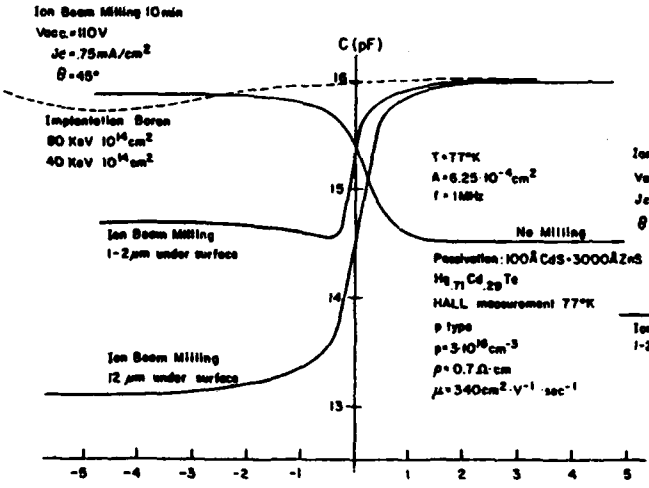

Fig. 1: C-V characteristics of p-type $Hg_{1-x}Cd_xTe$ MIS capacitor at 77 K before and after ion beam milling. A characteristics of implanted capacitor is also given for comparison.

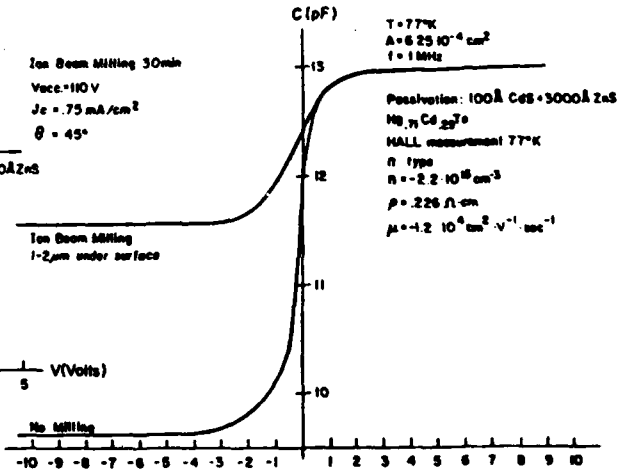

Fig. 2: C-V characteristics of n-type $Hg_{1-x}Cd_xTe$ MIS capacitor before and after IBM.

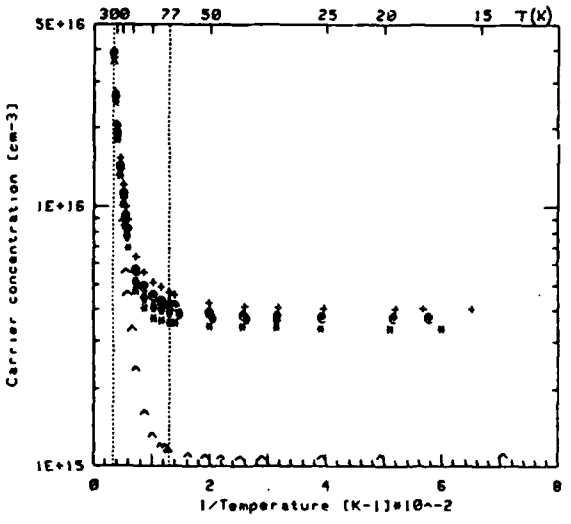

Fig. 3: Temperature dependence of the carrier concentration in x=0.215 $Hg_{1-x}Cd_xTe$ Hall sample. Λ - as prepared, + - after 60 minutes IBM, @ - after 70 C anneal for 1 week, * - after chemical etch of 12 μm, # - after additional etch of 11 μm.

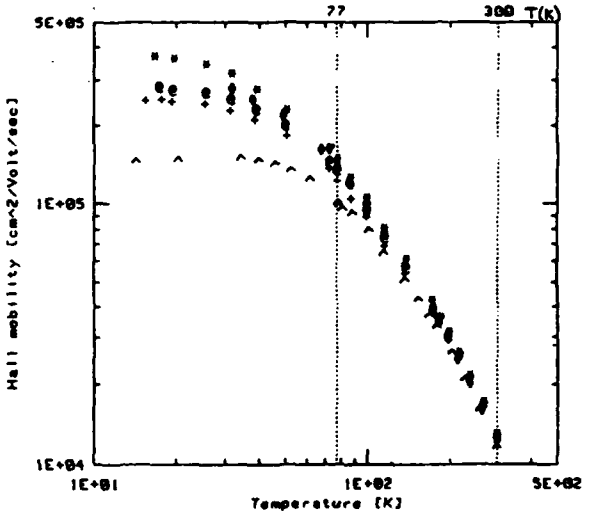

Fig. 4: Temperature dependence of electron mobility for the sample in figure 3. The processing steps are given in figure 3. Notice the increase in mobility after irradiation.

INTERSTITIAL TOTAL ENERGIES AND DIFFUSION BARRIERS IN $Hg_{1-x}Cd_xTe$*

C. G. Morgan–Pond, S. Goettig+, and J. T. Schick

Department of Physics and Astronomy, Wayne State University, Detroit, MI 48202 USA

+and Institute of Physics, Warsaw Technical University, Warsaw, Poland

Introduction

Experimental evidence indicates that interstitial defects play a major role in cation interdiffusion at CdTe/HgTe junctions,[1] and that they may be correlated with the midgap tunneling levels in Hg–rich HgCdTe.[2] Developing a more accurate picture of interstitials is important for further understanding of the diffusion mechanisms which control kinetic processes in these materials, and of the microscopic structure and properties of defects associated with the midgap levels and other observed electronic levels. The previous simple model used to study trends in the localized defect levels due to impurity and self–interstitials[3] has been extended to obtain estimates of the total energy for interstitials at different sites in the lattice. These calculations have been applied to predict the preferred tetrahedral site for Hg, Cd, In, and Te interstitials in $Hg_{1-x}Cd_xTe$, and to investigate whether the low–electron–density channel which passes alternately through tetrahedral sites between anions and tetrahedral sites between cations is likely to be an important diffusion path for these interstitials.

Theory

The simple model used in these calculations is based on the idea of describing the localized states within a minimal basis.[4] This small basis, consisting of the sp^3 bonding hybrids on the interstitial, its nearest neighbors (which are improperly coordinated due to the presence of the interstitial), and all hybrids involved in covalent bonds with nearest neighbor hybrids, is separated from the rest of the crystal by the method of "soft separation",[3] or ignoring systematically all of the weaker interactions which couple the minimal basis to the rest of the crystal. Interactions between hybrids in the minimal basis are obtained using Harrison's tight–binding parameters.[5] The results of these calculations,[3] and analogous calculations for substitutional defects, including vacancies,[6] have been compared with self–consistent Green's function and experimental results. Agreement to within 1 eV for most levels in the vicinity of the

gap, good agreement for energy trends and the general structure for hyperdeep levels, and correct deep level symmetries and occupancies were obtained.

In order to calculate total energies, the short–range repulsion arising from overlap of the electron wavefunctions centered on neighboring atoms must be included. The overlap was assumed to be proportional to the hopping matrix element divided by the average onsite energy, and to have the form assumed by Majewski and Vogl.[7] The resulting shifts in atomic orbital energies are typically the same, to within 20%, for all the orbitals in the minimal basis for a particular defect. Therefore, we have taken the effect of overlap to be a constant energy shift equal to the average energy shift for the hybrids in the minimal basis for each defect.

Preferred Interstitial Sites

The calculated total energy for neutral indium interstitials is higher in the tetrahedral position between cations (T1) than in the tetrahedral position between anions (T2) by about 3 eV in CdTe. The T2 interstitial has an even lower energy when it ionizes to In^{+}. This result supports our earlier assumption[3] that the T2 interstitial is preferred. Therefore, although T1 In interstitials have a partially filled deep level in the gap and could potentially serve as acceptors,[3] these interstitials will not be numerous enough to account for the electrical compensation which is seen in non–laser–assisted MBE–grown films of CdTe.[8]

Vydyanath has looked at the effect of Hg overpressures on the midgap tunneling centers in Hg–rich HgCdTe, and suggests these centers may be due to Hg interstitials.[2] We have previously found that the T2 Hg interstitial has an A_1 level in the gap region.[3] In this work, we find that the total energy is lower for Hg interstitials in T2 than in T1 sites. The energy difference is about 1 eV for neutral interstitials, and slightly more when the T2 interstitial ionizes to Hg^{+2}. Tetrahedral Hg interstitials therefore will tend to sit in T2 sites, and contribute A_1 electronic levels in the vicinity of the gap.

As might be expected, the T2 position (between anions) is preferred for tetrahedral Cd interstitials, while the T1 position (between cations) is preferred for tetrahedral Te interstitials.

Diffusion

Experimental studies in both CdTe and $Hg_{0.8}Cd_{0.2}Te$ suggest that interstitials play an important role in cation diffusion.[1] Our calculated total energy difference for neutral Cd

PASSIVATION OF MCT SURFACES

Y. Nemirovsky and G. Bahir

Kidron Microelectronics Research Center
Department of Electrical Engineering
Technion - Israel Institute of Technology, Haifa 32000, Israel

The characteristics of semiconductor devices, in particular narrow band-gap semiconductors, are largely governed by the properties of the semiconductor surface. The semiconductor - passivating layer interface, as well as the dielectric properties of the passivating layers, play important and very often dominant roles in determining HgCdTe device performance. This is not surprising if we bear in mind that semiconductor devices are simply materials governed by boundary conditions imposed by the interfaces at the contacts, at the surfaces, and within the device for the case of heterostructures.

The issue of surface passivation is extremely important for HgCdTe devices. So far, surface passivation has been a dominant factor in limiting device performance. This is to be expected in view of the narrow band-gap of $Hg_{1-x}Cd_xTe$ with $x \approx 0.2\text{-}0.3$, which at 77 K varies between 0.1-0.25 eV, respectively. Hence, the surface potential band bending is often of the order of the band-gap energy and can easily accumulate, deplete or invert the surface significantly, thus drastically affecting device performance. HgCdTe surface passivation is complex because of the compound nature of the semiconductor, the difference in the chemical properties of the constituents and also due to the tendency of electrically active defects to form in the interface region during the passivating process. In addition, HgCdTe surfaces cannot be exposed to temperatures above $\simeq 85°C$, thereby limiting the deposition process to low-temperature techniques.

At this point we find it appropriate to borrow a very strong statement from 'Physics Today': "It seems to me that the 1980's, and possibly the 1990's as well, will be viewed as the decade when we brought boundary regions under microscopic scrutiny". This statement relates to the wide field of the physics of semiconductor interfaces (metal-semiconductor, passivating insulators-semiconductor and semiconductor-semiconductor interfaces). HgCdTe surface passivation forms a subclass in this field of interface phenomena which is

extremely challenging, scientifically as well as technologically. The purpose of this introduction is to provide a broad perspective of this subject, as well as point out right at the beginning that improving HgCdTe surface passivation, and the study of HgCdTe interfaces, should proceed in an accelerated manner and should be the next step after the study of bulk phenomena.

This review focuses on the practical aspects of HgCdTe surfaces as related to device physics, technology and applications. For theoretical studies, clean cleaved surfaces are very interesting, since they are the closest approximation to a true crystal surface. However, for practical devices it is essential and critical to form stable and reproducible passivated surfaces, with well controlled electrical properties that can be tailored according to the device requirements. The environmental and thermal stability of the interface is of great importance for the various applications. At the same time, the passivating layers should exhibit excellent adherence and mechanical properties compatible with device bonding techniques.

We survey current surface passivation technologies and established or practical HgCdTe-interface-insulator structures, schematically shown in Fig. 1 (section 2). The unique behavior of HgCdTe surfaces and interfaces is reviewed briefly in section 3. The general theory of MOS devices as applied to the unique features of HgCdTe in metal-insulator-semiconductor (MIS) structures is outlined in section 4. The experimental structures used to study surface effects are discussed in section 5, with an emphasis on the unique features of HgCdTe surfaces that are exhibited in the above devices. Finally, the surface requirements of HgCdTe devices of current interest for present and next generation focal plane arrays are defined in section 5 and are discussed in terms of the currently used technologies surveyed in section 2.

a) low temperature (LT) deposited dielectric films, currently used.

b) a combination of a thin native layer and a thick deposited dielectric film currently used: anodic oxide or anodic sulfide with deposited ZnS.

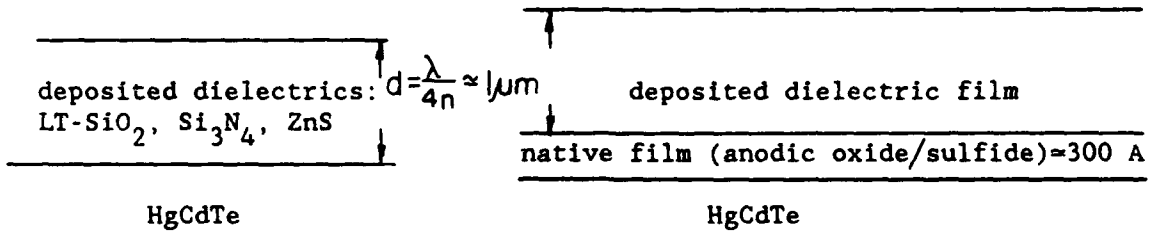

c) new possibilities that should be further considered:
additional deposited dielectrics,
additional native layers and
new combinations of native layers and deposited dielectric films.

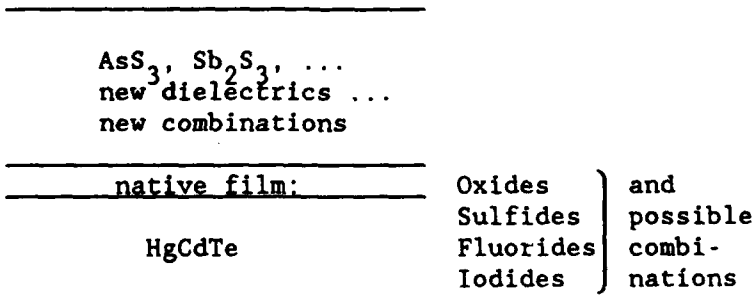

Fig. 1. Schematic representation of HgCdTe surface passivation technologies.

EFFECTS OF ANODIC FLUORO-OXIDE ON THE THERMAL STABILITY OF $Hg_{1-x}Cd_xTe$ PHOTOCONDUCTIVE ARRAYS

Nili Mainzer and Eliezer Weiss
SCD - Semi-Conductor Devices
A Tadiran-Rafael Partnership,
Misgav Mobile Post, 20179, ISRAEL

In the 1987 workshop we have reported[1] the development of a novel process for the anodic growth of native insulating films on $Hg_{1-x}Cd_xTe$ containing both oxides and fluorides. A careful selection of the hydroxyl to fluoride ion ratio in the anodization bath enabels the tuning of the band bending at the semiconductor - dielectric interface. Furthermore, the use of this anodic fluoro-oxidation yields interfaces with only low surface state densities which are stable up to aproximately 105°C.

We report here the use of anodic fluoro-oxidation in the fabrication of $Hg_{1-x}Cd_xTe$ photoconductor arrays. These arrays show an improved thermal stability relative to arrays realized with the "normal" anodic oxide.

Arrays passivated using either the anodic fluoro-oxidation or the anodic oxidation were compared in wafer form after various heat treatments (Fig. 1). The photoconductors passivated with anodic oxide show a monotonic increase of the resistance, measured at 77 K under the photon flux of a 300 K background (180° field of view. Fig 1a). The resistance of the fluoro-oxidized photoconductors, on the other hand, remains constant up to approximately 105°C. A similar trend is seen in the photoconductivity (FIG. 1b), measured as the relative change in device resistance as a result of reducing the photon flux by approximately 30%. There is a monotonic decrease of the photoconductivity of the devices passivated with the anodic oxide while in those passivated with the anodic fluoro-oxide, the photoconductivity remains constant until after annealing at temperatures ≥100°C.

Photoconductive arrays passivated by the anodic fluoro-oxidation using various solutions were packaged with 60° field of view and evaluated by measuring responsivity and detectivity. Fig. 2 shows the effect of annealing temperature on the responsivity at peak wavelength and the 1000 K blackbody detectivity at 10 kHz of arrays passivated with fluoro-oxides. Shown are averages of the results of all 100 elements in the array operated at liquid nitrogen temperature. There is little to no change in both the responsivity and the detectivity up to 105°C. The thermal stability of the arrays does not depend much on bath composition so long as it is a solution of both hydroxyl and fluoride ions.

The characterization of MIS devices[1] has shown that there is only a negligible fast surface state density in the fluoro-oxide - $Hg_{1-x}Cd_xTe$ interface. Furthermore, this low density is stable up to 105°C. This is in accordance with the results reported here.

It was suggested in Ref. 1, that the electrical behavior of devices passivated with these anodic layers may be due to fluoride ions dispersed through them, and mainly near their interface with the semiconductor. However, AES measurements have shown that anodic layers grown from such bathes are composed exclusively of
anodic oxides, sometimes having only traces of fluorine.

To confirm the above assumption we have lately analyzed the layers using a nuclear reaction having high sensitivity to fluorine atoms. It was discovered that not only does the anodic film contain fluorine, but that it is concentrated both on the surface of the film and in its interface with the semiconductor.

References

[1]E. Weiss and N. Mainzer, MCT Workshop, 1987.

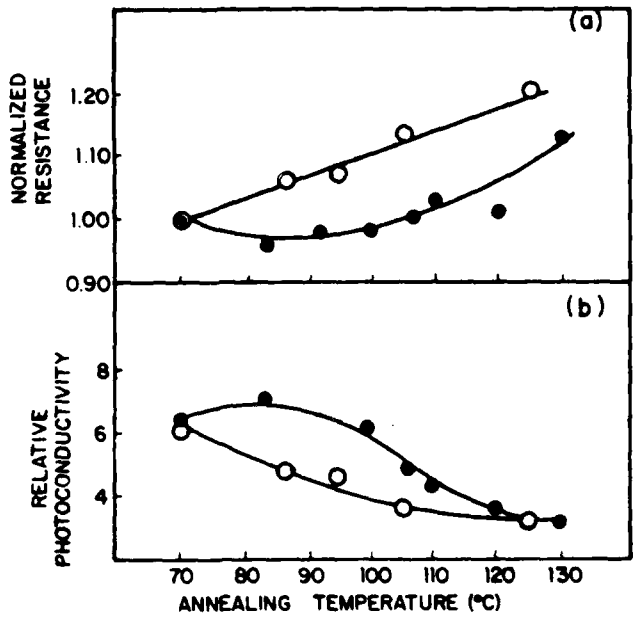

Fig. 1. Effect of annealing temperature on the average normalized resistance (a) and relative photoconductivity (b) of fifty element photoconductive arrays, still in wafer form, passivated with anodic oxide (o) and anodic fluoro-oxide (o).

Fig. 2. Effect of annealing temperature on the responsivity at peak wavelength (a) and the 1000 K blackbody detectivity at 10 kHz (b).

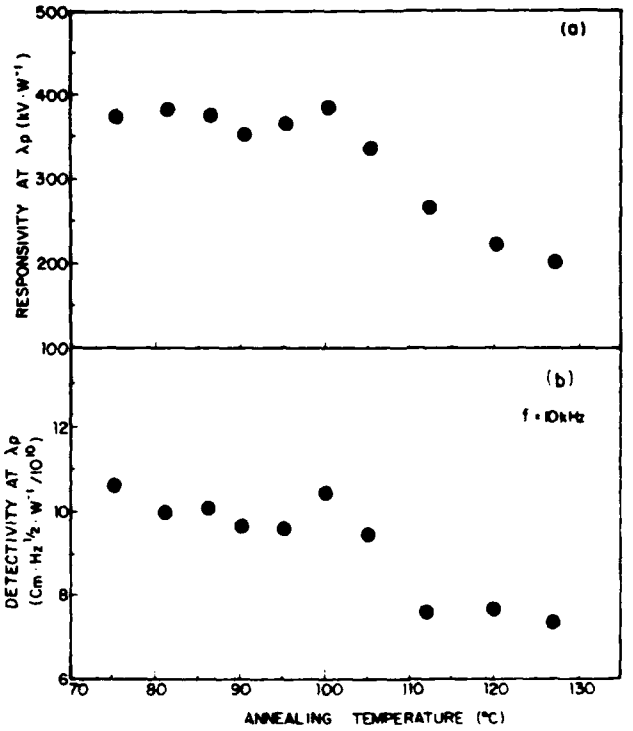

Surface Recombination Velocity of Anodic Sulfide and ZnS Coated p-HgCdTe

E. Finkman and S.E. Schacham
Microelectronics Research Center, Department of Electrical Engineering,
Technion - Israel Institute of Technology, Haifa 32000, Israel

The properties of semiconductor devices are very sensitive to their surface passivation. This is especially true for narrow gap $Hg_{1-x}Cd_xTe$, in which an ideal passivation has not been agreed upon yet. Anodic oxide, which is widely used as surface passivation for *n*-type $Hg_{1-x}Cd_xTe$, causes an inversion layer on a *p*-type material and can not be used for junction devices. Coatings of SiO_2 and ZnS, which are used for this purpose, do not have chemical reaction with the surface. Thus, interface properties like the concentration and position of interface traps, are very sensitive to process parameters, and may degrade with time. Passivation of *p*-type $Hg_{1-x}Cd_xTe$ with an anodic sulfide film has been demonstrated by Nemirovsky *et al.* to give near flatband surface, with relatively low concentration of interface traps at 77 K. A non-anodic version of native sulfide [2] was found to be very promising for device performance.

A study of the surface recombination velocity, S, can lead to a better understanding of the nature of $Hg_{1-x}Cd_xTe$ interfaces. We studied S as a function of temperature, for ZnS and anodic sulfide passivations on p-type HgCdTe samples. Various compositions were measured, with acceptor concentrations between $Na=5\times10^{15}cm^{-3}$ and $Na=2\times10^{16}cm^{-3}$ and absorption cutoff wavelength between $\lambda=10\mu m$ and $\lambda=12\mu m$ (a composition range of $0.212<x<0.225$). Samples passivated with anodic sulfide and samples coated with ZnS were implemented on the same wafer, in order to minimize variation in other parameters. Hall measurements performed on samples produced on the same wafer rendered similar results for temperature between room temperature and 25-30 K, verifying material uniformity. Surface recombination velocity was determined by measuring photoelectromagnetic (PEM) short circuit current. The excess carrier lifetime and the electron mobility as minority carrier are also extracted by fitting the PEM results. The obtained results for these parameters agree well with our previous findings, using modulated hall technique, for the same materials [3].

Figure 1 shows typical measured data, along with fitted curves, for a *p*-$Hg_{1-x}Cd_xTe$ sample ($x=0.216$; $Na=3.5\times10^{15}cm^{-3}$) following anodic sulfidization. In figure 2 we compare S for the same sample with the two different passivation studied. The main observations at the figure are characteristic to all studied pairs of samples:

a. The surface recombination velocity is similar, at high temperatures, for both surface passivations, to within a factor of 2-3, which is sometimes in favor of the ZnS passivated, and sometimes in that of the anodic sulfide interface. It should be stressed that absolute signal level and quantum efficiency of the sample are not well defined. A factor of two in S is considered to be our experimental error.

b. The value of S at 77 K is 7×10^3–3×10^4 cm/sec. There is a tendency for having lower S for higher bulk impurity concentration.

c. The surface recombination velocity increases when decreasing temperature down to ~50 K. For lower temperatures S remains constant for anodic sulfide interfaces, while continuing to rise for ZnS coated ones. The increase with temperature is almost logarithmic at high temperatures.

Spectral response curves were also used to measure S. The decrease in responsivity in the short-wavelength region is characteristic of a high S. The results agree with those quoted above.

Assuming the recombination is dominated by a single trap, using an analysis equivalent to the Shockley-Read treatment, the plateau is a result of the crossing of the trap and demarcation levels [4] and the value of S for temperatures below this point is S_o. The slope of the data at higher temperatures is governed by the relationship $S = \frac{S_o p_o}{N_v} e^{[(E_t - E_i)/kT]}$. The activation energy at high temperatures is about 20-30 meV. Typical values obtained for S_o are 1–5×10^4 cm/sec. The general expression for the surface recombination velocity contains many material parameters [5]. From the similarity of the temperature dependence for both passivations at most temperatures, it is assumed that the recombination trap is the same for both. Consequently, capture cross section for electrons and holes, as well as the trap energy position E_t are identical. The only parameter that may cause a different temperature dependence is the surface potential ϕ_s. This shows less dependence on bulk properties for the anodic sulfide interfaces, indicating a larger contribution from the surface. The dependence of the Hall coefficient on temperature also indicates a stronger inversion layer for the anodic sulfide. It is well known that early studies of the Hall effect in p-$Hg_{1-x}Cd_xTe$ showed a second sign reversal of the Hall coefficient at low temperature to a negative sign. This "anomalous" behavior was discussed in quite a few papers until it was identified as a result of a surface inversion layer which starts to dominate when the hole freezeout reduces their concentration below a certain level. The effect of sign reversal still occurs at very low temperatures in materials with low acceptor concentration (below 30 K in some of our materials). It is always shown to occur in anodic sulfide surfaces at a slightly higher temperature than in ZnS ones, indicating a higher concentration of electrons in the inversion layer of the former.

References

[1] Y. Nemirovsky, L.Burstein and I. Kidron, J. Appl. Phys. 58, 366 (1985).

[2] T. J. La Chapelle, U.S. workshop on $Hg_{1-x}Cd_xTe$ 1986, extended abstracts.

[3] S. E. Schacham and E. Finkman, J. Appl. Phys. 60, 2860 (1986).

[4] M.A. Kinch, M.J. Brau and A. Simmons, J. Appl. Phys. 44, 1649 (1973).

[5] A. Many, E. Harnik, and Y. Margoninski, Semiconductor Surface Physics (new York, 1957).

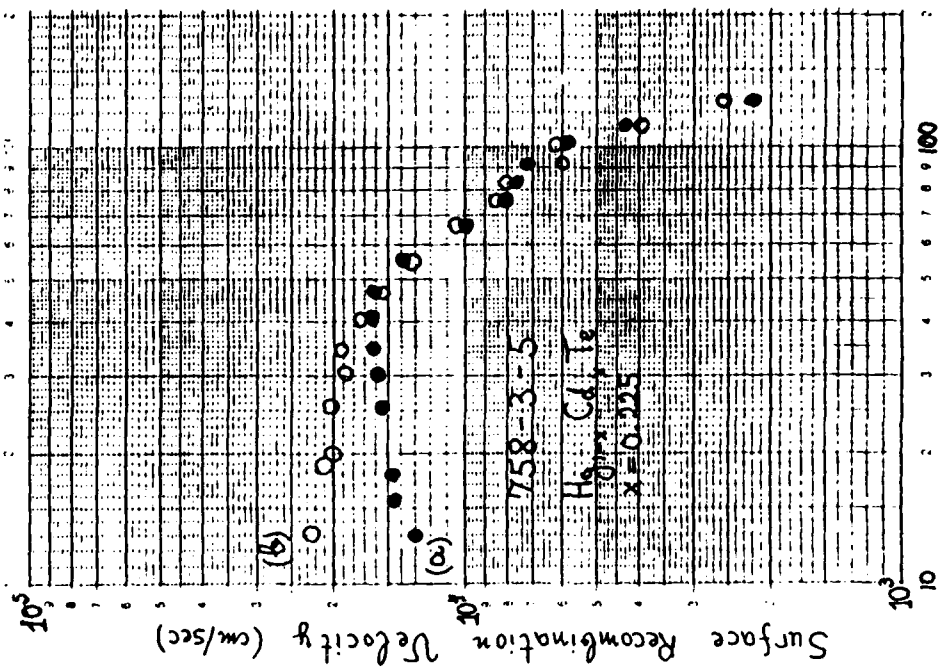

Fig. 2: Temperature dependence of surface recombination velocity for $Hg_{1-x}Cd_xTe$ with: a) - anodic sulfide, and b) - ZnS passivations.

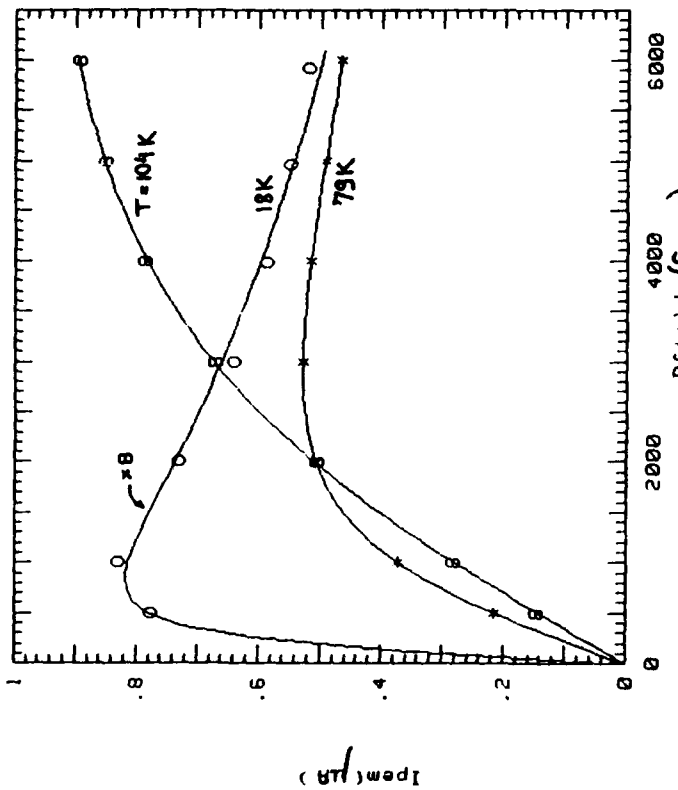

Fig. 1: Magnetic field dependence of Photo Electro Magnetic signal at different temperatures for $Hg_{1-x}Cd_xTe$ with x=0.216. The curves are drawn using a parameter fit.

THE INTERFACE CHEMISTRY OF HgCdTe PASSIVATED WITH NATIVE SULFIDE LAYERS GROWN FROM NONAQUEOUS AND AQUEOUS POLYSULFIDE SOLUTIONS*

John P. Ziegler[a]
Ford Aerospace Corporation
Newport Beach, California 92658-1440

John M. Lindquist[b] and John C. Hemminger
Department of Chemistry and
Institute for Surface and Interface Science
University of California
Irvine, California 92717

The surface passivation of HgCdTe has been intensively studied by a number of groups over the last several years and finding a reliable passivation method remains an elusive goal. The primary methods that have been used to terminate the HgCdTe lattice to date have been either oxide formation (native, plasma, or electrochemical) or deposition of dielectrics (e.g. ZnS or SiO_2). Nemirovsky and co-workers were the first to illustrate the potential merits of using anodically grown sulfide layers to passivate HgCdTe.[1,2] They grew sulfide layers from solution of Na_2S in ethylene glycol and provided Auger electron spectroscopy (AES) depth profile data indicating that the layers were composed entirely of CdS with trace amounts of Hg. Subsequent work using Rutherford backscattering spectroscopy (RBS) has shown that the anodically grown CdS layers contain a significant amount of Hg.[3,4]

In this work anodic sulfide passivation layers have been grown on HgCdTe from both aqueous and nonaqueous polysulfide solutions. The purpose was to help understand the details of CdS film growth on HgCdTe and to study the resultant interface chemistry. Accordingly, the decomposition potential of $Hg_{1-x}Cd_xTe$ in aqueous polysulfide electrolyte was calculated as a function of x-value using balanced equations like that shown in equation 1[1,2]

$$Hg_{0.7}Cd_{0.3}Te + 1.7HS^- + S_3^{2-} + 1.7OH^- \Leftrightarrow 0.3CdS + 0.7HgS_2^{2-} + TeS_3^{2-} + 1.7H_2O + 2e^- \qquad (1)$$

where the likely polysulfide solution components HS^- and S_3^{2-} are included. Figure 1 depicts the band edge positions and decomposition potentials of $Hg_{0.8}Cd_{0.2}Te$ and $Hg_{0.7}Cd_{0.3}Te$ in aqueous polysulfide electrolyte. Equation 1 is a two-electron oxidation reaction (which is expected for II-VI compounds) and has been verified experimentally using cyclic voltammetry as shown in Figure 2 for $Hg_{0.7}Cd_{0.3}Te$.

Figure 3 shows a typical capacitance-voltage curve obtained from a device passivated using nonaqueous anodic sulfide electrolyte and demonstrates 95°C bake stability. It was originally believed that nonaqueous solutions were necessary to prevent oxide formation,[1,2] but our electrochemical and initial AES depth profile data indicate that oxide formation may not occur in the aqueous polysulfide electrolyte.[7] Hence, results are reported for HgCdTe metal-insulator-semiconductor (MIS) devices passivated with both aqueous and nonaqueous anodic sulfides. Our initial MIS results suggest that devices passivated with aqueous anodic sulfides may have superior bake stability than those passivated with nonaqueous anodic sulfides. Correlations are drawn between MIS device results and depth profile data, and significant amounts of Hg and Te are found in the anodically grown CdS layers. Figure 4 shows a typical AES depth profile of a CdS film on HgCdTe.

References

* This work was supported by Ford Aerospace Corp. and the UCI Committee on Research.

a. Present address: Rockwell International, Anaheim, California.
b. Present address: Aeroject Electrosystems, Azusa, California.

1. Y. Nemirovsky and L. Burstein, Appl. Phys. Lett., 44, 443 (1984).
2. Y. Nemirovsky, L. Burstein, and I. Kidron, J. Appl. Phys. 58, 366 (1985).
3. R.L. Strong, J.D. Luttmer, D.D. Kittle, T.H. Teherani, and C.R. Helms, J. Vac. Schi. Tech. A, 5, 3207 (1987).
4. T. Ipposhi, K. Takita, K. Murakami, K. Masuda, H. Kuda, and S. Seki, J. Appl. Phys. 63, 132 (1988).
5. J.P. Ziegler and J.C. Hemminger, in "Dielectric Films on Compound Semiconductors", (V.K. Kapoor, ed.), Electrochemical Society, 1988.
6. J.P. Ziegler, J.M. Lindquist, and J.C. Hemminger, J. Appl. Phys., submitted.
7. J.P. Ziegler and J.C. Hemminger, Appl. Phys. Lett., submitted.

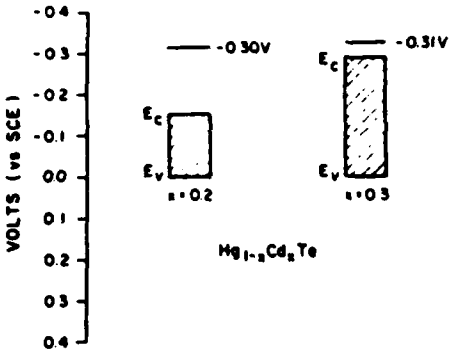

Figure 1. The band positions and calculated decomposition (CdS formation) potentials for $Hg_{0.8}Cd_{0.2}Te$ and $Hg_{0.7}Cd_{0.3}Te$ in polysulfide electrolyte. All species assumed to be at unit activity.

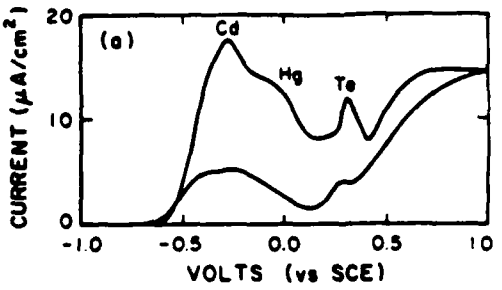

Figure 2. A cyclic voltammogram of $Hg_{0.7}Cd_{0.3}Te$ in aqueous polysulfide solution. The peaks at ca. -0.30V, -0.05V and +0.30V have been assigned to Cd, Hg, and Te sulfidization, respectively.

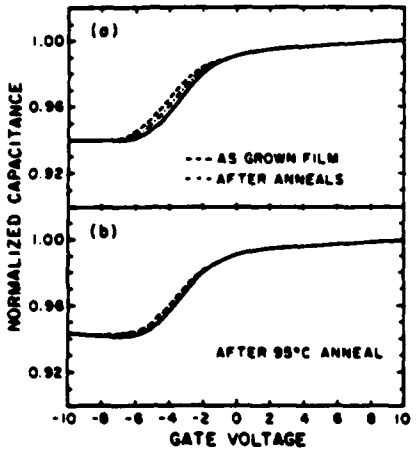

Figure 3. Capacitance-voltage curves of $Hg_{0.7}Cd_{0.3}Te$ passivated with nonaqueous anodic sulfides capped with ZnS showing ca. 0.25 volt hysteresis and positive fixed charge. (a) The as grown film, (b) after a 1 hour, 94°C vacuum bake.

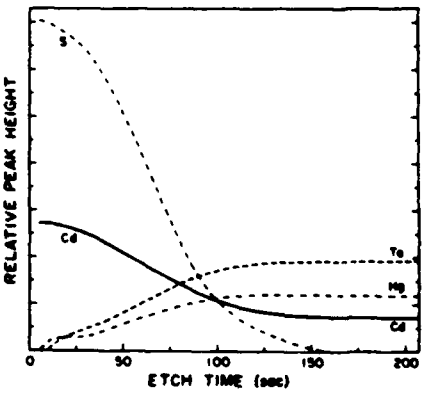

Figure 4. An Auger depth profile of a 320 angstrom CdS film on $Hg_{0.7}Cd_{0.3}Te$.

PROPERTIES OF ANODIC OXIDE PASSIVATION LAYER/$Hg_{1-x}Cd_xTe$ STRUCTURES

C. M. Stahle and C. R. Helms*
Stanford University
Stanford, CA 94305

R. L. Strong, A. Simmons, and H. F. Schaake
Texas Instruments
Dallas, Texas 72565

C. H. Becker
SRI International
Menlo Park, CA 94025

This paper presents the results[1-4] of a comprehensive study of the properties of anodic oxides grown on $Hg_{1-x}Cd_xTe$, especially as they relate to MIS devices fabricated using the anodic oxide passivation. A key property of the anodic oxide/$Hg_{1-x}Cd_xTe$ system also of interest is its thermal stability and mechanisms for thermal degredation which will also be discussed.

We will concentrate our discussion on oxides grown on $Hg_{0.8}Cd_{0.2}Te$ material passivated with ~700 Å of anodic oxide (grown in 0.1 N KOH, 90% ethylene glycol, 10% H_2O). Techniques used to characterize the structure include Auger electron spectroscopy (AES), Rutherford Backscattering Spectrometry (RBS), Secondary Ion Mass Spectrometry (SIMS), Surface Analysis by Laser Ionization (SALI), and Cross Section Transmission Microscopy (XTEM).

The results indicate that the oxide exists with a complicated structure which can be broken into 3 regions (neglecting the top surface) as shown in the upper panel of Figure 1. The bulk of the oxide has an atomic composition of approximately 61% O, 23% Te, 12% Hg, and 4% Cd which corresponds closely to a mixture of 52% $HgTeO_3$, 18% $CdTeO_3$, and 30% TeO_2, although other similarly bonded compounds cannot be ruled out. As the interface is approached (within 100-200 Å), careful comparison of the AES and SALI profiles indicates the presence of HgTe-like bonding configurations. The presence of HgTe is also confirmed by XTEM which shows actual particles of HgTe in this region.

The final region in intimate contact with the $Hg_{1-x}Cd_xTe$ is 30-50 Å thick and consists of a Cd rich oxide which is presumably $CdTeO_3$, although an exact identification cannot be made.

The electrical characteristics of MIS devices fabricated with this passivation are characterized by low interface trap densities, negligible hysterisis in CV curves, and positive fixed charge.

The low interface trap densities present are presumably due to the high quality of the $CdTeO_3/Hg_{1-x}Cd_xTe$ interface. The positive fixed charge observed in these structures may be due to the presence of the HgTe particles which would tend to be positively charged as embedded in the oxide background.

The effect of elevated temperature annealing on this structure can be understood by considering the following two reactions:

$$\begin{aligned} HgTeO_3 + CdTe &\rightarrow CdTeO_3 + HgTe \\ 3TeO_2 + 2CdTe &\rightarrow 2CdTeO_3 + 3Te \end{aligned} \qquad (1)$$

which are both exothermic.[5] The grown oxide containing ~50% $HgTeO_3$ and 30% TeO_2 reacts with the substrate via these reactions forming HgTe and elemental Te. These reactions are clearly observed as the Cd rich oxide present at the interface is seen to grow thicker with annealing, and there is evidence for Hg buildup in the substrate below the surface. An example of this process for the conversion of TeO_2 to $CdTeO_3$ and Te is shown in Figure 1. These effects are also clearly seen in MIS device electrical characteristics during anneals at 100°C, where an initial increase in fixed charge density is observed followed by conversion of the substrate from p- to n-type.

The increased fixed charge is consistent with the increased HgTe concentration expected via the mechanism mentioned above. The mechanism for conversion from p- to n-type upon subsequent annealing is not completely clear but may be due to the compensation of the acceptor by excess Hg or Te created at the interface.

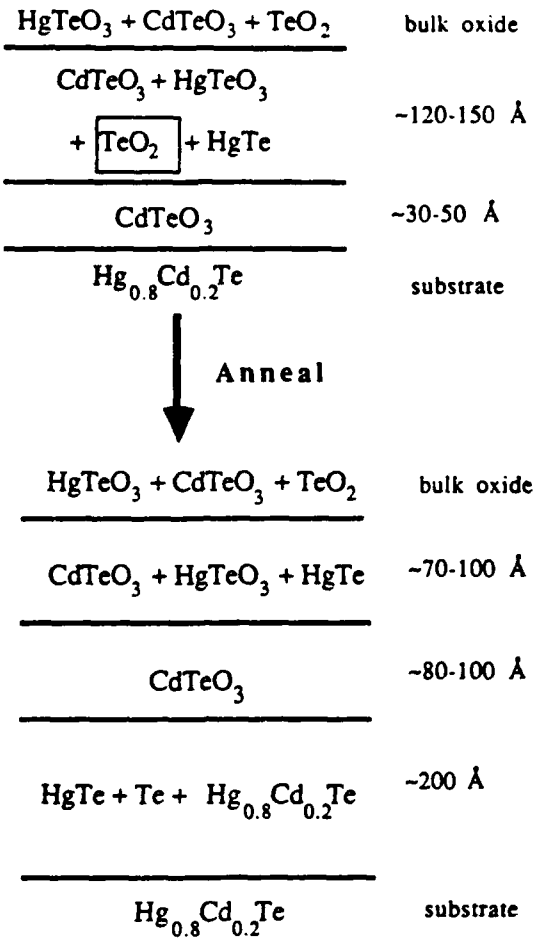

$$3TeO_2 + 10Hg_{0.8}Cd_{0.2}Te \longrightarrow 2CdTeO_3 + 8HgTe + 3Te + 25\ kcal$$

Fig. 1: The upper structure is representative of the as grown anodic oxide; the lower structure illustrates the effect of annealing on the TeO_2 present in the oxide near the interface.

References

*Work at Stanford supported by Gift Funds from Texas Instruments.

[1]C. M. Stahle, D. J. Thomson, C. R. Helms, C. H. Becker, and A. Simmons, Appl. Phys. Lett. 47, 521 (1985).

[2]R. L. Strong, J. M. Anthony, B. E. Grade, J. A. Keenan, E. Norbeck, L. W. Li, and C. R. Helms, J. Vac. Sci. Technol. A 4, 1992 (1986).

[3]C. M. Stahle, C. R. Helms, and A. Simmons, J. Vac. Sci. Technol. B 5, 1092 (1987).

[4]C. M. Stahle, Ph.D. Dissertation, Stanford University (1988).

[5]D. R. Rhiger and R. E. Kvaas, J. Vac. Sci. Technol. A 1, 1712 (1983).

Fermi Level Movement at Metal/HgCdTe Contacts Formed at Low Temperature*

G. P. Carey, A. K. Wahi, D. J. Friedman, C. E. McCants, and W. E. Spicer
Stanford Electronics Laboratories, Stanford University, Stanford, California 94305

Deposition of the metal overlayers Ag, Al, and Pd onto HgCdTe substrates held at reduced temperatures (100 K and 170 K) cause the surface Fermi level ($E_{f,s}$) to move from its initial cleaved position, typically located at or near the conduction band minimum (CBM), into the conduction band, and this movement is correlated with the absence of the movement of the overlayer metal into the semiconductor. This phenomenon is observed at the lowest coverages (submonolayer) for all three overlayer metals, and for the case of Ag grown at 100 K, is observed for higher coverages as well. The final positions of $E_{f,s}$ for the three overlayer growths match very closely to those seen for the corresponding room temperature growths.

Gaining insight into the mechanisms that induce surface Fermi level movement at metal/HgCdTe interfaces is rendered difficult since the formation of metallic contacts at room temperature (RT) on HgCdTe typically disrupts the HgCdTe lattice, leading to a complicated interface exhibiting Hg loss from the substrate and intermixing between the metal and the substrate constituents.[1] Theoretical models examined by Spicer [2] in last year's proceedings follow the predicted movement of the surface Fermi level at the metal/semiconductor interface when going from the binary to the alloy. For the case of $Hg_{1-x}Cd_xTe$, the movement of the Fermi level position at metal/CdTe interface has been extensively studied and is better understood than for the alloy since interfaces formed on CdTe tend to be much more abrupt with a less complicated morphology than for HgCdTe. All of the theoretical models[2] predict that ohmic contacts (rectifying contacts) are to be expected for metal overlayers on *n*-type (*p*-type) HgCdTe of x-value lower than approximately 0.4. In order to better understand the mechanisms behind the Fermi level movement at metal/HgCdTe ($x < 0.4$) interfaces, a simplification of the physical interface is necessary. A successful effort to reduce these effects by lowering the substrate temperature during

metal overlayer growth has been reported[2] that shows a decrease in Hg loss and reduction of intermixing for the Ag/HgCdTe and Al/HgCdTe interfaces formed at 170 K.

In an effort to further reduce semiconductor disruption during metal deposition we employ a lower HgCdTe substrate temperature (100 K) during the overlayer growth of the three metals Ag, Al, and Pd. Bulk single crystals of *p*-type HgCdTe were cleaved in ultra-high vacuum (UHV) ($p < 10^{-10}$ Torr), and metals were deposited in increments ranging from sub-monolayer at low coverages to several monolayers (ML) at higher coverages. The surfaces were monitored after each deposition with the surface sensitive techniques of photoemission spectroscopy (PES) and low energy electron diffraction (LEED).

$E_{f,s}$ is observed to move from its cleaved position, near the conduction band minimum (CBM), into the conduction band (CB) for each metal/HgCdTe overlayer. The position of $E_{f,s}$ above the VBM is shown schematically in Fig. 1. Plotted in this figure are: the position of $E_{f,s}$ at the cleave, the maximum position of $E_{f,s}$ above the VBM, and the final position of $E_{f,s}$ for each metal/HgCdTe interface studied. For example, for the LT Ag/HgCdTe interface grown at 100 K, $E_{f,s}$ moves from its initial position at the cleave to 0.55 ± 0.1 eV above the VBM at moderate Ag coverage. Upon warming the interface to RT, $E_{f,s}$ moves back 0.05 eV below its cleaved position (*i.e.*, 0.05 eV below the CBM) and is correlated with Ag diffusing in. For the Ag/HgCdTe interface formed at 170 K [Ref. 3], $E_{f,s}$ was observed at submonolayer coverages of Ag to move initially to 0.55 ± 0.1 eV, but after time move back to the initial cleave position, but at higher coverages $E_{f,s}$ remained near the initial cleave position at the CBM. Hence, the reduction in the HgCdTe substrate growth temperature to 100 K results in a more stable interface (in terms of $E_{f,s}$ position). Also at the Pd/HgCdTe interface grown at 100 K, $E_{f,s}$ moves to 0.55 ± 0.1 eV above the VBM with metal deposition, and with additional overlayer deposition moves back 0.1 ± 0.05 toward the VBM. In this case, the downward movement of $E_{f,s}$ is correlated to chemical interactions and intermixing between the Pd and the substrate. At the 100 K grown Al/HgCdTe interface, $E_{f,s}$ moves to 0.6 ± 0.1 eV above the VBM at the the initial 0.1 ML coverage, and remains at that position for all subsequent depositions.

Since Ag and Al are known to be *p*- and *n*-type, respectively, dopants in bulk HgCdTe, and the Pd doping behavior is unknown, these observations are consistent with the metal atoms, prior to their diffusing into the substrate or chemically reacting with the substrate atoms, donating electronic charge to the semiconductor, hence raising $E_{f,s}$ into the CB. When the interface becomes disrupted upon warming or increased deposition, the metal atom can diffuse into the semiconductor, doping the lattice. Both Ag and Pd have high electronegativity (EN), hence the upward movement of $E_{f,s}$ into the CB is seen even for metal overlayers of high EN. Thus, it appears that rectifying contacts are to be expected on *p*-type HgCdTe ($x < 0.4$) even for metals of high EN (workfunction) if the HgCdTe is not disrupted.

References

*Work funded by DARPA under contract # N00014-86-K-0854. Portions of this work were conducted at the Stanford Synchrotron Radiation Laboratory which is funded by the DOE under contract DE-AC03-82ER-13000, Office of Basic Energy Sciences, Division of Chemical/Material Sciences.

1 G. D. Davis, Vouto **16**, 127 (1986), and references therein.

2 W. E. Spicer, D. J. Friedman, and G. P. Carey, J. Vac. Sci. Technol. A **6**, 2746 (1988).

3 G. P. Carey, A. K. Wahi, D. J. Friedman, C. K. Shih, and W. E. Spicer, J. Vac. Sci. Technol. A **6**, 2736 (1988).

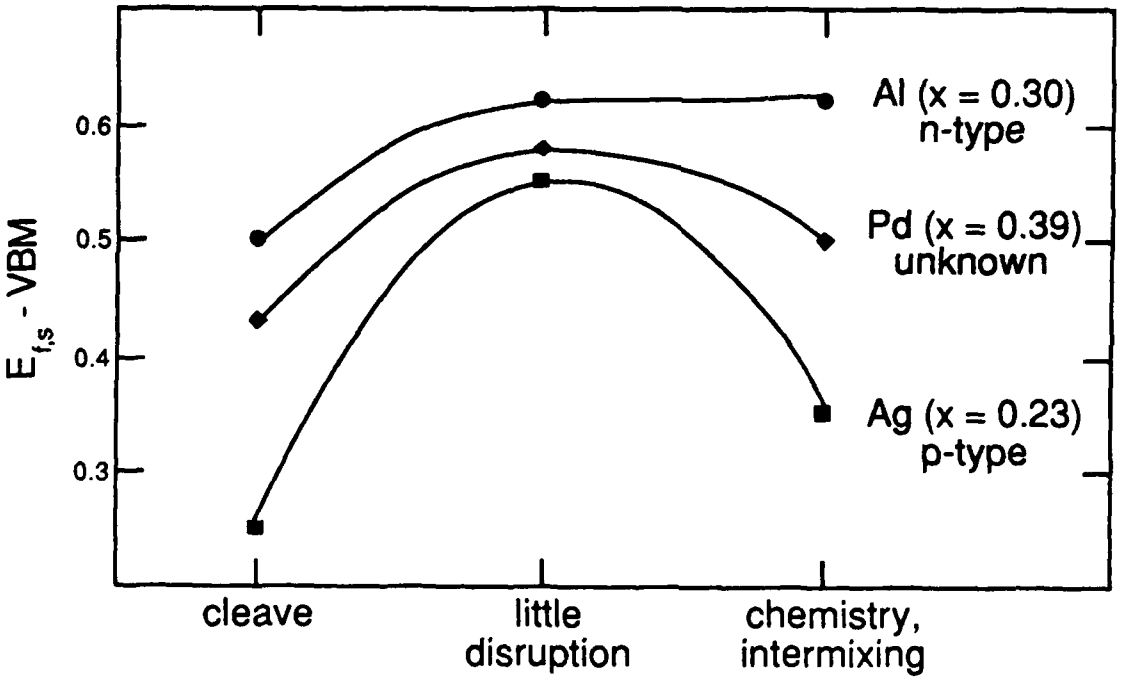

Fig 1. Position of the surface Fermi level, $E_{f,s}$, at the Ag, Pd, and Al interfaces. Plotted are the positions at each cleave, the maximum position into the CB, and the final position. The details of the movement of $E_{f,s}$ are given in the text.

THERMODYNAMIC TRENDS AND LOCAL CONTROL OF $Hg_{1-x}Cd_xTe$ / METAL JUNCTION FORMATION

A. Raisanen, A. Wall, N. Troullier, P. Philip, G. Haugstad,
X. Yu, and A. Franciosi
Department of Chemical Engineering and Materials Science
University of Minnesota, Minneapolis, MN 55455

D.J. Peterman
McDonnell Douglas Research Laboratories
St. Louis, MO 63166

The ternary semiconducting alloy Mercury-Cadmium-Telluride (MCT) has important device applications in infrared detector technology. Fabrication of devices incorporating MCT is complicated by several material-related problems stemming from the low stability of Hg-Te bonds relative to Cd-Te bonds in the semiconductor lattice. When reactive metals are deposited onto the MCT surface, as during contact fabrication, one observes atomic interdiffusion, preferential metal-Te reaction, and displacement of Hg from the near-surface region[1-3]. The resulting change in semiconductor composition at the surface may affect the Schottky barrier and induce inconsistencies in contact performance.

In previous work, our photoemission results showed that thin interlayers of Yb at MCT/Al junctions act as effective diffusion barriers, preventing metal-Te reaction and reducing the metal-induced Hg-depletion of the substrate[4,5]. In this study, we report preliminary investigations of the effect of Yb interlayers at MCT/In, MCT/Cr, and MCT/Ag junctions, together with detailed investigations of Yb interlayers at MCT/Al junctions as a function of interlayer thickness. We have demonstrated that semi-empirical calculations of bulk binary metal-cation and metal-anion thermodynamic parameters utilizing Miedema's model[6] are surprisingly useful in forecasting trends of interfacial behavior. As shown in table 1, our calculations indicate that for rare-earth metals the telluride formation enthalpy and the cation solution enthalpies in the metal overlayer are much larger than the corresponding quantities for reactive metals such as In, Al, or Cr. Pre-deposition of rare-earth overlayers should therefore stabilize the semiconductor surface against further reaction with overlayer metals and control the composition of the near-surface region during contact fabrication. We find that, as predicted, thin Yb interlayers are effective diffusion barriers at MCT/reactive metal interfaces. As an example, figure 1 illustrates the barrier effect for MCT/In junctions. Synchrotron radiation from the 1 GeV Aladdin source was used to produce angular-integrated electron distribution curves (EDC's) for the valence band and core level emission. All EDC's in Fig. 1 have been approximately normalized to the peak intensity to emphasize lineshape changes, and the binding energy scale has been referenced to the Fermi level. The metal coverage θ is given in Å (1 ML = 2.78 Å of Yb or 1.76 Å of In). In the left half of the figure we show the In 4d core emission from the MCT/In interface with no interlayer, while in the right half of Fig. 1 we show the In 4d core emission from the MCT/In interface in the presence of a pre-deposited 13 Å Yb interlayer. Without the interlayer, the broad In 4d coreemission lineshape reflects the presence of an unresolved In 4d component related to the formation of an In-Te

reacted phase[1]. With pre-deposition of a 13 Å Yb interlayer, the In 4d core lineshape retains a sharp, metallic appearance, with no visible evidence of reacted In-Te components[7].

Similar results were obtained for Yb interlayers at the Al/MCT interface[4,5,7]. Detailed studies as a function of Yb interlayer thickness have shown that the Al-Te reaction is substantially reduced at interlayer thicknesses as low as 3 Å[7]. At interlayer thicknesses greater than 10 Å, we also observe an increase in surface Hg concentration related to the formation of metallic Yb-rich phases with high solubility for Hg[4,5,7].

We also conducted preliminary studies of the MCT/Ag interface, motivated by the completely *different microscopic* reaction mechanisms that should be active for this system. Friedman *et al* [2] have indicated that defect-assisted Ag indiffusion (rather than a metal/Hg exchange reaction) is the mechanism of atomic interdiffusion at this interface. Figure 2 shows the valence band, Ag 4d, Cd 4d, and Hg 5d core emission from MCT/Ag junctions as a function of Ag coverage (1 ML = 1.16 Å of Ag). In the left half of Fig. 2 we show results with no Yb interlayer, and in the right half data obtained with a 10 Å Yb interlayer. Without the Yb interlayer, we observe a slow attenuation of the substrate features and a slow growth of the Ag 4d emission intensity, which indicates that Ag is diffusing deep into the semiconductor, in agreement with the conclusions of Friedman *et al* [2]. With pre-deposition of a 10 Å Yb interlayer, we observe a growth of the Ag 4d emission intensity one order of magnitude faster than in the no-interlayer case, as well as rapid attenuation of the substrate emission, which indicate that the Yb interlayer has in fact strongly reduced Ag indiffusion[7].

This work was supported by the Office of Naval Research under contract no. 00014-84-K-0545, and by the McDonnell Douglas Independent Research and Development Program. We thank the staff of the Synchrotron Radiation Center of the University of Wisconsin for their cheerful support.

REFERENCES

[1] G.D. Davis, N.E. Byer, R.A. Riedel, and G. Margaritondo, J. Appl. Phys. **57**, 1915 (1985)
[2] D.J. Friedman, G.P. Carey, C.K. Shih, I. Lindau, W.E. Spicer, and J.A. Wilson, J. Vac. Sci. Technol. A **4** , 1977 (1986)
[3] D.J. Peterman and A. Franciosi, Appl. Phys. Lett **45**, 1305 (1984). A. Franciosi, P. Philip, and D.J. Peterman, Phys. Rev. B **32**, 8100 (1985)
[4] A. Franciosi, A. Raisanen, A. Wall, S. Chang, P. Philip, N. Troullier, and D.J. Peterman, Appl. Phys. Lett. **52**, 1490 (1988)
[5] A. Raisanen, A. Wall, S. Chang, P. Philip, N. Troullier, A. Franciosi, and D.J. Peterman, J. Vac. Sci. Technol. A **6**, 2741 (1988)
[6] A.R. Miedema, P.F. de Chatel, and F.R. de Boer, Physica B **100**, 1 (1980)
[7] A more extensive presentation of our results will be given elsewhere: A. Raisanen, A. Wall, N. Troullier, P. Philip, G. Haugstad, X. Yu, A. Franciosi, and D.J. Peterman (to be published).
[8] K.C. Mills, *Thermodynamic Data for Inorganic Sulphides, Selenides, and Tellurides* (Butterworths, London, 1974)

Table 1. Thermodynamic parameters for Hg, Cd, representative overlayer metals Ag, In, Al, and Cr, and selected rare-earth metals. Column 1: metal; column 2: most stable metal-telluride, from [8]; column 3: enthalpy of formation for the listed metal-telluride, also from [8]; columns 4 and 5: alloying enthalpies for Cd and Hg diluted in the listed metal, expressed in kJ/mol of Cd or Hg, respectively.

metal (M)	most stable telluride	ΔH_f telluride kJ/mol	ΔH_{sol} (Cd:M) kJ/mol Cd	ΔH_{sol} (Hg:M) kJ/mol Hg
Hg	HgTe	-31.8	...	...
Cd	CdTe	-101.	...	...
Ag	Ag_2Te	-36.0	-14.5	-9.0
In	In_2Te	-79.7	+1.7	-3.3
Al	Al_2Te_3	-319.	+14.5	+17.1
Cr	n.r.	n.r.	+48.8	+67.8
Sm	SmTe	-310.	...	...
	Sm_2Te_3	-795.	-141.1	-173.2
Yb	YbTe	-301.	-74.2	-106.5
Ce	CeTe	-310.	...	...
	Ce_2Te_3	-774.	-141.5	-173.9
Eu	EuTe	-272.	-71.5	-106.4

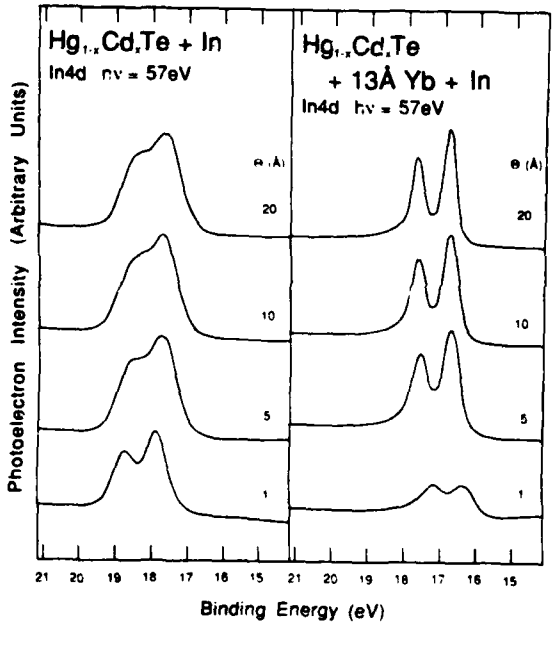

Figure 1. In4d core level emission for In/MCT interfaces. EDC's are approximately normalized to the peak intensity to emphasize lineshape changes. Left: In4d emission from the MCT/In interface. Right: In4d emission from the MCT/In interface in the presence of a pre-deposited 13 Å Yb interlayer.

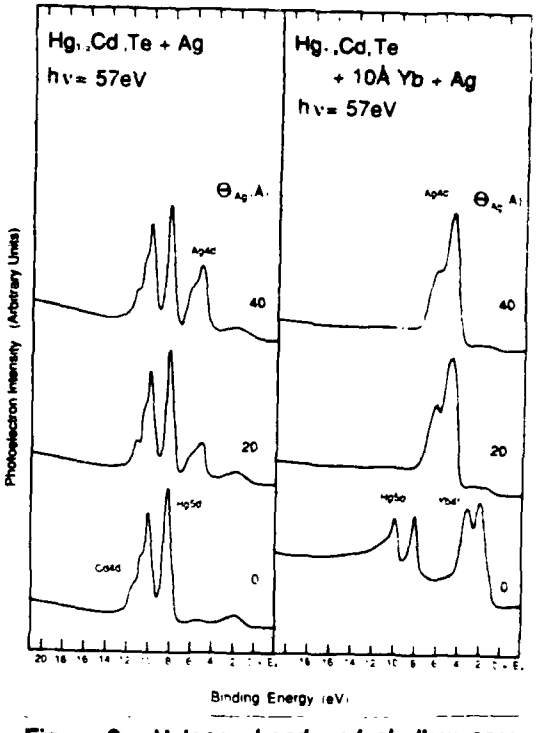

Figure 2. Valence band and shallow core emission from MCT/Ag interfaces. EDC's are approximately normalized to the peak intensity to emphasize lineshape changes. Left : Emission from the MCT/Ag interface. Right: emission from the MCT/Ag interface in the presence of a pre-deposited 10 Å Yb interlayer.

INTERDIFFUSION, INTERFACIAL STATE FORMATION, AND BAND BENDING AT METAL/CdTe INTERFACES

J.L.Shaw, R.E.Viturro, and L.J.Brillson
Xerox Webster Research Center
Webster, New York 14580

We have used a wide variety of complementary techniques to characterize the electronic and chemical structure of selected CdTe-metal interfaces. The control of Schottky barriers to CdTe and its alloys is important for several device applications but is difficult to achieve in practice. We have shown previously that interdiffusion at interfaces prepared in ultra high vacuum promotes the formation of deep states, which in turn strongly influence band bending[1,2,3]. The Fermi level consistently falls at one of several discrete energies in the middle and upper half of the energy gap, depending on the source of bulk CdTe as well as the degree of interdiffusion. These deep levels, already present in the semiconductor bulk, continue to form with time after metallization and with heat treatment. Thus fig. 1 shows an increase in luminescence intensity from a 1.1 eV deep level transition with aging and annealing. Associated with such transitions are increases in the depletion layer width up to thousands of Å. Figure 2 demonstrates this effect by the shift and curvature of the Au/CdTe interface C^{-2}-V characteristic with aging and heat treatment. These features coupled with internal photoemission measurements are consistent with a voltage-independent contribution to the depletion layer width, indicating diffusion of deep states up to 0.5 micron into the bulk.

We have reduced interdiffusion and trap formation by depositing a thin interlayer of Yb metal. The soft x-ray photoemission spectra shown in fig. 3 demonstrate reduced Te outdiffusion and the formation of new Te compounds at a Au/Yb/CdTe interface versus a Au/CdTe contact. The increased interface abruptness leads to dramatically reduced band bending as shown in fig. 4. Photoluminescence spectra (fig. 5) measured in-situ on the same SXPS-characterized interface demonstrate that the Yb interlayer inhibits the development of a 1.1eV deep level transition. Thus chemical stabilization of the interface against interdiffusion leads to more ideal

electronic behavior as well. In this case, the Fermi level position lies considerably closer to the valence band, thereby reducing the p-type contact barrier. This and similar improvements in the chemical and electronic stability of metal-CdTe interfaces may prove useful in the fabrication of both rectifying and Ohmic contacts to CdTe and its alloys.

This work supported in part by the Army Research Office.

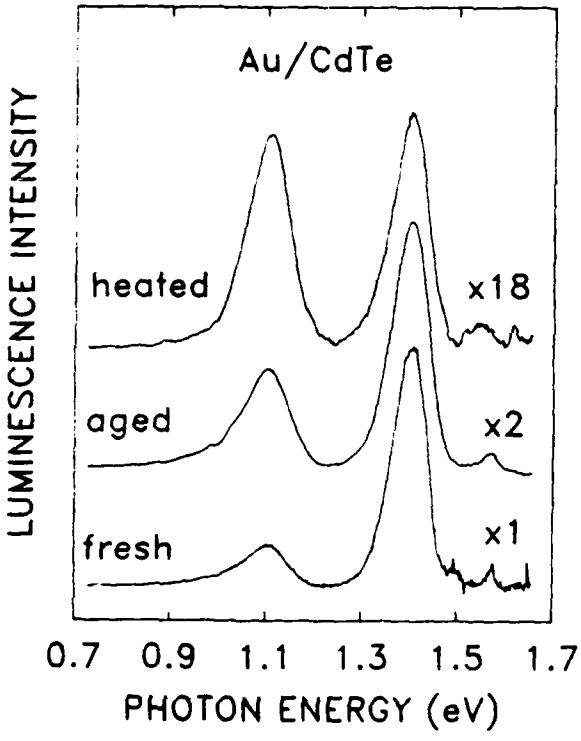

formation: 15 K in-situ photo-luminescence spectra of the same interface shown in fig. 2.

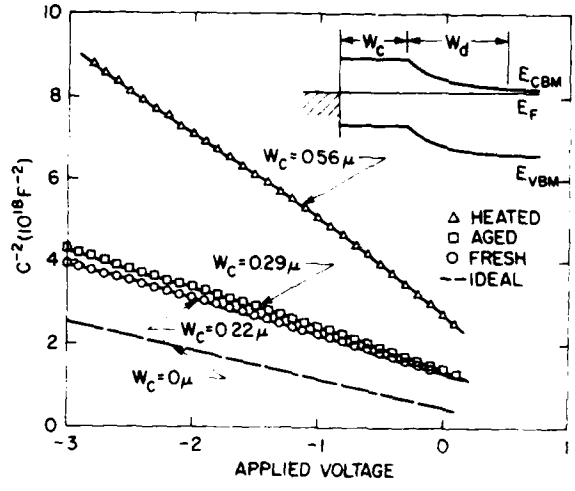

Fig. 2 Evidence of increased depletion layer width: C-2-V plots of a UHV cleaved (110) CdTe surface just after deposition of 100 Å Au, after 3 day storage in UHV, and after heating to 100 C in UHV for 1 hour. The solid lines were fitted by adding a constant, W_C, to the depletion layer width expected for an abrupt interface.

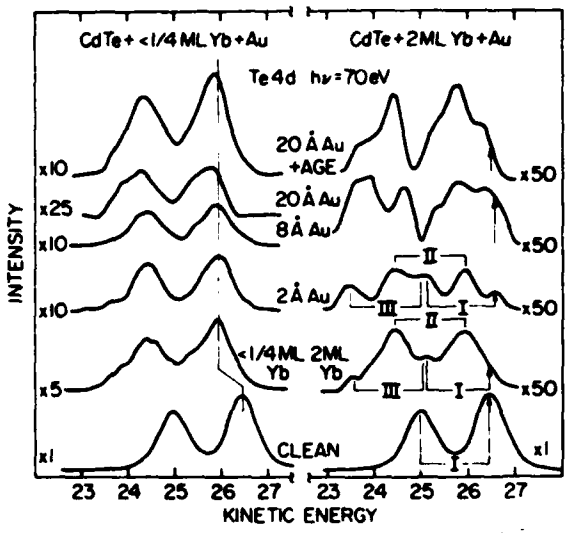

Fig 3 Reduced interdiffusion with Yb interlayer: Soft x-ray photoemission spectra of the Te 4d core level at a Au/CdTe interface containing < 1/4 ML versus 2 ML of Yb. The presence of the complete Yb layer splits the spectrum into three components. The bulk component (I) shows little or no Fermi level (E_f) movement. In contrast, spectra of the interface containing < 1/4 ML of Yb show an immediate E_f increase from E_V + 0.55 to E_V + 1.1eV.

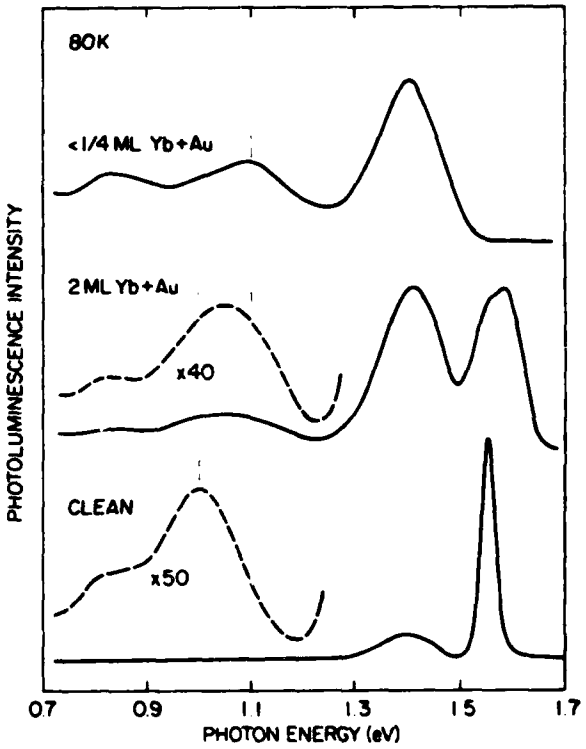

Fig. 5 Reduced deep level formation with Yb interlayer: In-situ photoluminescence spectra of a CdTe (110) surface cleaved in UHV, and after deposition of 20 Å Au on Yb metal layers < 1/4 ML thick vs. 2 ML thick.

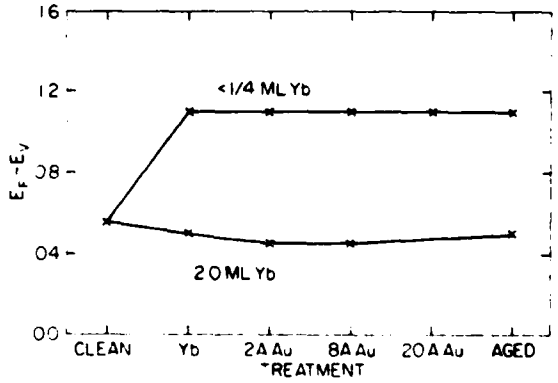

Fig. 4 Fermi level movements obtained from SXPS spectra of fig. 3. The Yb layer produces a major decrease in p-type barrier height.

References

1. J.L. Shaw, R.E. Viturro, L.J. Brillson, D. Kilday, M.K. Kelly, and G. Margaritondo, J. Electron. Mater., 17 149 (1988).

2. J.L. Shaw, R.E. Viturro, L.J. Brillson, D. Kilday, M.K. Kelly, and G. Margaritondo, J. Vac. Sci. Technol. A6, 1579 (1988).

3. J.L. Shaw, R.E. Viturro, L.J. Brillson, D. Kilday, M.K. Kelly, and G. Margaritondo, J. Vac. Sci. Technol. A6, 2752 (1988).

CdTe AND ZnTe METAL INTERFACE FORMATION AND FERMI LEVEL PINNING*

A. K. Wahi, G. P. Carey, T. T. Chiang, I. Lindau, and W. E. Spicer
Stanford Electronics Laboratory, Stanford University, Stanford, CA 94305

Metal interfaces with HgCdTe in general are highly non-abrupt, exhibiting a high degree of intermixing of metal and semiconductor components and Hg loss ranging from about 20 to 60% from the near-surface region upon metal deposition. The severity of Hg depletion from the semiconductor's top few monolayers exhibits some dependence on the reactivity of the overlayer[1]. Studies of metals on HgCdTe have pointed to the role of Hg loss as a major factor contributing to the significant semiconductor disruption that occurs with metal deposition. In this investigation of metal interfaces formed on CdTe and ZnTe, we investigate interfacial chemistry and morphology in conjunction with Fermi level pinning behavior in the absence of disruption due to Hg loss.

We focus on the three metals Al, Ag, and Pt, chosen to provide a range of reactivities with the substrate. Of these metals, Al is highly reactive with Te and Ag comparatively non-reactive with Te. For both Al and Ag, the heat of alloying for the cation (Cd or Zn) in the overlayer metal is small, whereas strong cation alloying with the Pt overlayer is expected. We emphasize Al and Ag interface formation here, but present band bending results for all three metals.

The metals Al, Ag, and Pt were deposited onto UHV-cleaved (110) surfaces of p-type bulk single crystals of CdTe and ZnTe; also Al on n-CdTe was studied. Overlayer growth and band bending were monitored with photoemission in separate experiments, using synchrotron radiation with photon energies chosen to probe the top 5 - 7 Å, and also using conventional UPS and XPS photon sources to provide both surface-sensitive (~7 Å) and bulk-sensitive (~20 Å) core level emission. Throughout the following, metal coverages are given in terms of monolayers (1 ML = 6.74×10^{14} and 7.60×10^{14} atoms/cm^2 for CdTe (110) and ZnTe (110), respectively).

Interfacial Chemistry and Morphology

For all three systems, Al/HgCdTe[2-3], Al/CdTe, and Al/ZnTe, Al exhibits a strong reaction with the substrate, with Al2p emission first emerging as a reacted species which increases in binding energy for successive coverages. In studies on HgCdTe, evidence for metallic Al first appears around 3 ML coverage; however, on CdTe only Al reacted with Te is seen up to coverages of 20 ML. Clear evidence for metallic Al on CdTe is not seen until near 40 ML, with the appearance of an Al2p component at approximately 2 eV lower binding energy than the reacted component and the simultaneous appearance of Fermi level emission. (See Figure 1.) In constrast, on ZnTe the first appearance of metallic Al occurs near 7 ML coverage, nearer the same

coverage observed for HgCdTe. Our data suggest that Hg in the alloy may act to modulate the strong Al-Te reaction. It is reasonable that the presence of Hg can account for the difference between the behavior of HgCdTe and CdTe; what is surprising, on the other hand, is the difference in behavior between ZnTe and CdTe, where simple considerations of bulk thermodynamics predict the same behavior for both. These observations point to the role of kinetics as opposed to bulk thermodynamics as a factor determining the extent of reaction and intermixing of semiconductor components with the overlayer metal.

As Figure 1 shows for CdTe and ZnTe, a strong reacted Al component is present in the surface-sensitive emission (i.e., from within the top 10 Å) at even the highest coverages. Furthermore, as shown in Figure 2, while Te attenuation in the surface region is very slow, the Cd intensity drops with coverage as one would expect due to attenuation through an overlayer. This observation suggests that a floating layer of reacted Al-Te remains on the surface. Such a surface-segregated reacted layer has been suggested in other studies of metals on HgCdTe[3] and on CdTe[4]. Comparison of the surface- and bulk-sensitive Al2p emission for the higher coverages shows the ratio of the metallic to the reacted Al intensity is greater in the bulk than in the surface region. Thus, there is a gradient in metallic Al concentration, with the outer surface rich in reacted Al and the amount of metallic Al increasing as one moves from the outer surface region towards the substrate.

The formation of the surface-segregated Al-Te layer and the decrease in the Cd/Te ratio at the surface can be explained by either a loss of Cd from the surface, which would not be expected from its heat of vaporisation, or the formation of a Cd-rich layer beneath the Te-rich reacted layer. A surprising result of this work is the lack of a signal from dissociated Cd that is clearly distinguishable from that of Cd in bulk CdTe. For example, Patterson and Williams[5] have reported the appearance of metallic Cd for thick overlayers of Al on CdTe, although they do not give quantitative values of thickness. However, in the thickness range studied here (up to 81 ML Al), it did not appear.

Ag behaves differently at interfaces with HgCdTe, CdTe, and ZnTe. On HgCdTe, no evidence for a chemical reaction has been seen, with Ag diffusing 100 to 1000 Å into the semiconductor bulk[3]. We see clear evidence for a Ag-Te reaction in ZnTe, and evidence has been seen for it in Ag/CdTe[4]. The thickness of the Al reacted layer formed on CdTe and the Ag-Te reaction which occurs in CdTe but not in HgCdTe suggest an important role for Hg loss in limiting or modulating these reactions in HgCdTe. It suggests that the kinetics at the HgCdTe interface may be dominated by the disruption due to Hg depletion, in the case of Al, perhaps by formation of a barrier to further movement of semiconductor components, and in the case of Ag, perhaps by providing a possible Ag-Hg replacement mechanism by which Ag is able to diffuse unimpeded far into the bulk.

Band Bending Results

Below we tabulate our measured values for the final surface Fermi level pinning positions relative to the valence band maximum, $E_{fi} = E_f - E_{vbm}$, for the metals Al, Ag, and Pt on vacuum cleaved surfaces of p-type CdTe and ZnTe:

	p-CdTe	p-ZnTe
Al	1.1 ± .1	0.9 ± .1 eV
Ag	0.85 ± .1	0.65 ± .1 eV
Pt	0.95 ± .1	0.7 ± .1 eV

The as-cleaved position of E_f for ZnTe was about 0.4 eV above the VBM for all three cleaves; for CdTe, E_{fi} on the cleaved surfaces was about 0.5 eV for the Al and Pt cleaves and 0.65 for the Ag cleave. In the case of Ag/ZnTe, the Fermi level moves up with coverage to 0.8 eV above the VBM and then down to the final position listed above. An interesting point is that the movement of the Fermi level in the Al/CdTe system is complete before the appearance of any metallic Al in the spectra, and therefore effects dependent upon the *metallicity* of the overlayer appear be ruled out in this case.

We find that, despite a large difference in the bandgaps for CdTe and ZnTe (E_g = 1.5 eV and 2.2 eV, respectively), for each of these metals, the Fermi level pins at roughly the same distance from the VBM in both CdTe and ZnTe, with the ZnTe value lying about 0.2 eV below that of CdTe. This result can be explained using defect models in which the defect energy levels responsible for pinning lie at nearly the same energy with respect to the VBM. The difference in pinning positions for CdTe and ZnTe is also consistent with MIGS models which predict a difference in E_{fi} for two semiconductors which depends on their band lineup[6]. The measured ZnTe - CdTe valence band offset has been determined[7] as 0.18 ± .06 eV, with the ZnTe VBM lying above that of CdTe.

The observed similarity of E_{fi} for CdTe and ZnTe (from the above results, one would expect for these metals Schottky barriers of about the same height on both p-CdTe and p-ZnTe) lead to a prediction that metal contacts on the alloy HgZnTe would have in principle the same properties as on HgCdTe[8]. However, with metal contacts to the alloys one must also consider possible mechanisms for Fermi level movement in HgCdTe not present in CdTe and ZnTe involving metal movement into the semiconductor via Hg vacancies, and the resultant doping of the substrate[1].

* Work supported by NASA under contract # NAG1-851 and by DARPA under contract # N00014-86-K0854. Work done partially at the Stanford Synchrotron Radiation Laboratory, funded by the DOE under contract # DE-AC03-82ER-13000.

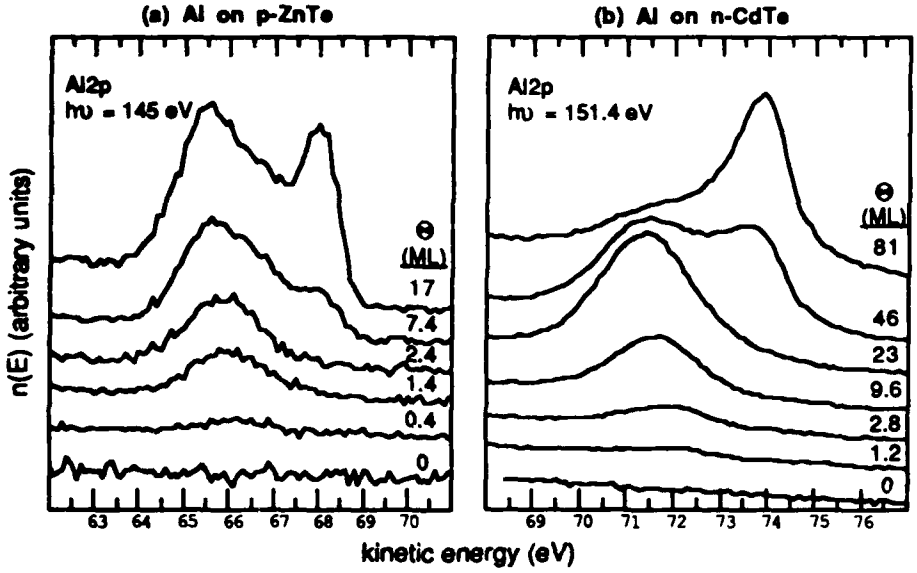

Figure 1. Surface sensitive photoemission spectra of Al2p core level as a function of Al coverage on (a) ZnTe and (b) CdTe showing emergence of metallic Al at lower binding energy for higher coverages.

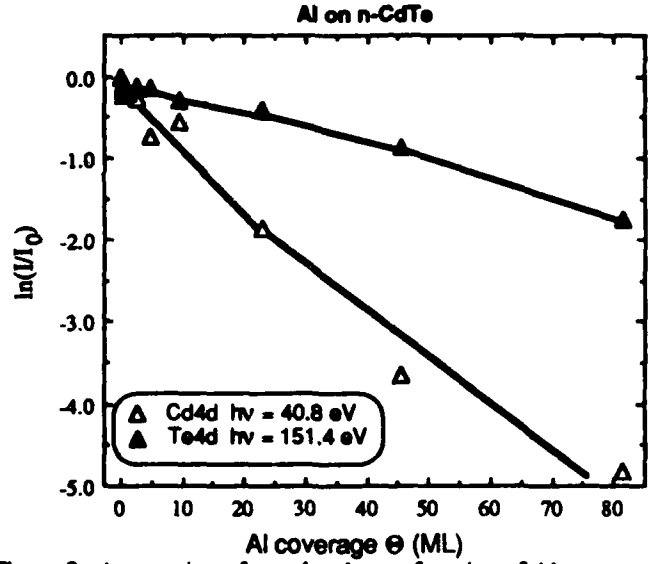

Figure 2. Attenuation of core levels as a function of Al coverage for Al on n-CdTe, showing slower Te signal attenuation from the near-surface region (within 10 Å of surface).

References

1. D. J. Friedman, G. P. Carey, I. Lindau, and W. E. Spicer, J. Vac. Sci. Technol. A 5, 3190 (1987).
2. G. D. Davis, N. E. Byer, R. A. Riedel, and G. Margaritondo, J. Appl. Phys. 57, 1915 (1985).
3. D. J. Friedman, G. P. Carey, C. K. Shih, I. Lindau, W. E. Spicer, and J. A. Wilson, J. Vac. Sci. Technol. A 4, 1977 (1986).
4. D. J. Friedman, I. Lindau, W. E. Spicer, Phys. Rev. B 37, 731 (1988).
5. M. H. Patterson and R. H. Williams, J. Cryst. Growth 59, 281 (1982).
6. J. Tersoff, Phys. Rev. Lett. 56, 2755 (1986).
7. C. K. Shih, A. K. Wahi, I. Lindau, and W. E. Spicer, J. Vac. Sci. Technol. A 6, 2640 (1988).
8. W. E. Spicer, D. J. Friedman, and G. P. Carey, J. Vac. Sci. Technol. A 6, 2746 (1988).

REACTIONS AT THE INTERFACE OF METAL/HgCdTe OXIDE

W.M. Lau[1], J.-W. He[2], K.C. Hui[1], I.R. Hill[1], P.R. Norton[2], and R. Scholes[3]

[1]Surface Science Western, University of Western Ontario, London, Ontario, Canada N6A 5B7

[2]Department of Chemistry, University of Western Ontario, London, Ontario, Canada N6A 5B7

[3]Optotek Ltd., 62 Steacie Dr., Kanata, Ontario, Canada K2K 2A9

Introduction

Surface passivation of n-type MCT is normally achieved by anodization. In the fabrication of metal-insulator-semiconductor (MIS) structures using anodic oxide as the dielectric, although direct metal depositionsof gold[1] and tin[2] have been used, a second layer dielectric such as zinc sulfide is normally applied in order to reduce the leakage current of the MIS structure. However, the reactions at the metal/MCT oxide interfaces and the integrity of MCT oxide upon metal deposition have not been studied in detail. Recently, we showed that metal deposition including indium[3], gold[4] and platinum[4] causes a rather vigorous reactions on MCT oxide. In general, oxidized tellurium of the MCT oxide at the interface is reduced and then mixed with the deposited metal. Unlike the results previously published on metal/MCT[5-7], our results on Au/MCT oxide and Pt/MCT oxide cannot be explained by bulk thermodynamic parameters. This paper reports on a comparison of the reactions of these metals on MCT oxide, and on an investigation of possible mechanisms of the observed interfacial reactions.

Experimental Procedures

The anodic oxide films were grown on $Hg_{0.8}Cd_{0.2}Te$ wafers supplied by Cominco Ltd., in 0.1M KOH in 90% ethylene glycol/10% water. The thickness of the film was about 80nm. Surface analysis was carried out using an X-ray photoelectron spectrometer (Surface Science Instrument SSX-100) housed in an ultra-high vacuum (UHV) chamber which is linked to different reaction chambers. Sputter-depositions of indium, platinum and gold, and evaporations of indium and gold were carried out in these reaction chambers. Deposition of gold was also carried out on tellurium oxide, cadmium tellurite and mercury tellurite (supported on gold foil), as well as on MCT oxide separated from the MCT substrate.

Results and Discussion

A. The metal-MCT oxide interaction

When indium, gold and platinum were deposited on MCT oxide, reduction of oxidized tellurium was observed in all of the interfacial reactions. Fig. 1 shows the tellurium $3d_{5/2}$ spectra of 1nm In/MCT oxide, 0.7nm Pt/MCT oxide, 0.9nm Au/MCT oxide, and bare MCT oxide at different polar angles of analysis. It is clear that all metal depositions induced a peak at 572.5-573.5eV which can be assigned to reduced tellurium. All depositions also caused an enrichment of tellurium in the analyzed volume.

B. Reaction mechanisms

Unlike the interfacial reactions of metal/MCT,[5-7] bulk thermodynamic parameters do not seem to pay a decisive role in determining the interfacial reactions of metal/MCT oxide. For example, although Fig. 1b shows an obvious reduction of oxidized

tellurium upon deposition of platinum on MCT oxide, the heat of reaction for $2TeO_2 + 5Pt \longrightarrow Pt_3O_4 + 2PtTe$ is about +200 kJ/mole of TeO_2. The heats of reaction for reduction of $CdTeO_3$ and $HgTeO_3$ by platinum are about +403 and +227 kJ/mole of tellurite respectively. Moreover, the spectral result shows no indication of the formation of platinum oxide. Therefore, heats of reaction alone cannot explain the observed interfacial reactions.

The deposition of gold on MCT oxide separated from the MCT substrate caused similar interfacial reactions and therefore, rules out the possibility of the involvement of the MCT substrate. One possible reaction mechanism is that deposition of metal on MCT oxide provides enough energy for the breaking of tellurium-oxygen bonds. Since direct evaporations of indium and gold gave similar results as sputter-deposition, the heat of condensation of the deposited metal is probably enough for bond breaking. The reaction between the reduced tellurium and the deposited metal will dominate over the re-oxidization of tellurium if the latter reaction has a much higher activation energy than the former one.

References

1. B.K. Janousek and R.C. Carscallen, J. Vac. Sci. Technol., 21, 442(1982).
2. Y. Nemirovsky and I. Kidron, Solid-State Elect. 22, 831(1979).
3. W.M. Lau, submitted to Appl. Phys. Lett.
4. W.M. Lau, J.-W. He, and P.R. Norton, submitted to Appl. Phys. Lett.
5. G.D. Davis, W.A. Beck, N.E. Byer, R.R. Daniels, and G. Margaritondo, J. Vac. Sci. Technol. A2, 546(1984).
6. A. Wall, A. Raisanen, S. Chang, P. Philip, N. Troullier, A. Franciosi, and D.J. Peterman, J. Vac. Sci. Technol. A5, 3193(1987).
7. D.J. Friedman, G.P. Carey, I. Lindau, and W.E. Spicer, J. Vac. Sci. Technol. A5, 3190(1987).

Te $3d_{5/2}$

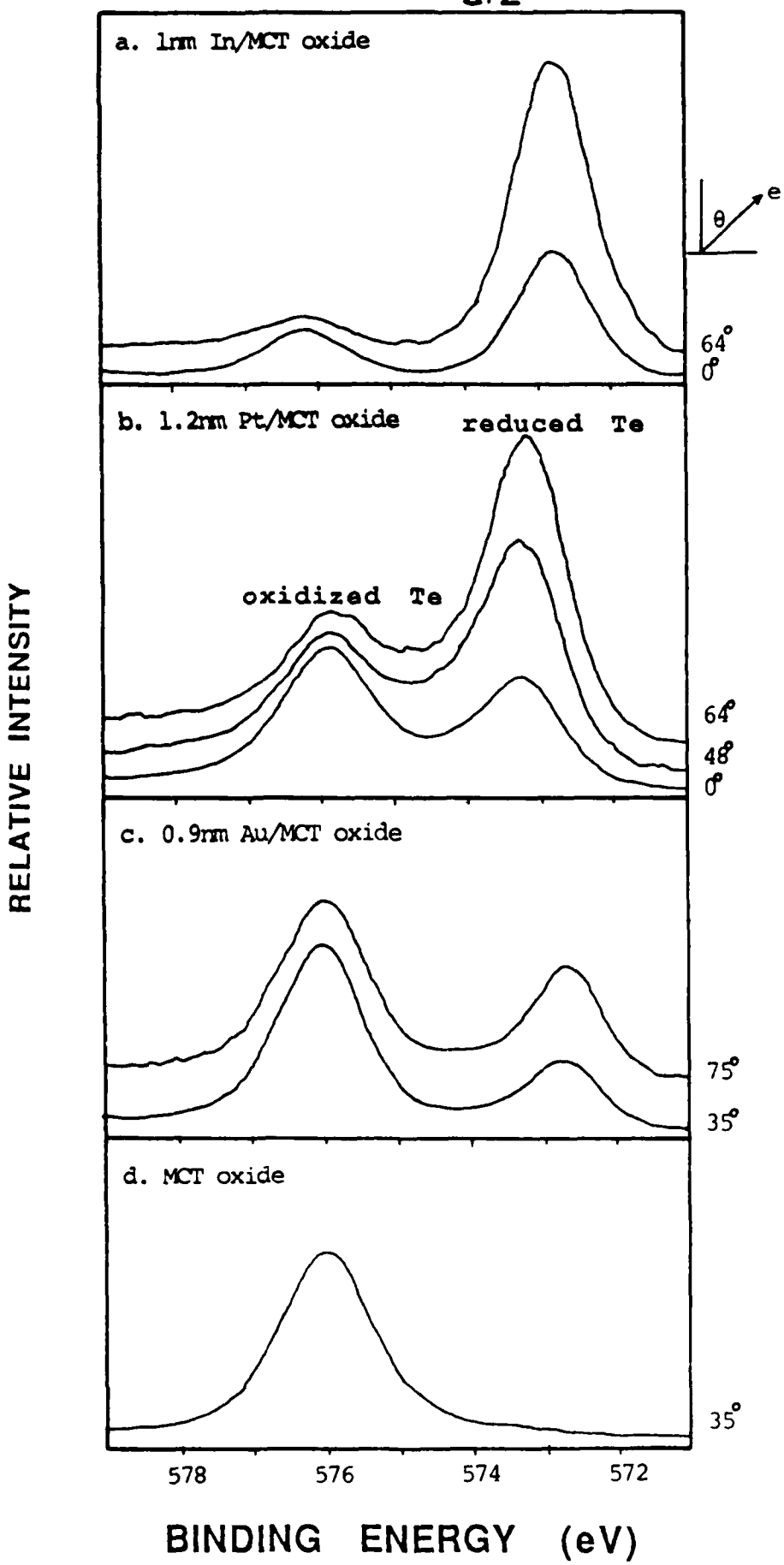
a. 1nm In/MCT oxide
θ
e
64°
0°
b. 1.2nm Pt/MCT oxide
reduced Te
oxidized Te
64°
48°
0°
c. 0.9nm Au/MCT oxide
75°
35°
d. MCT oxide
35°
578
576
574
572
RELATIVE INTENSITY
BINDING ENERGY (eV)

Defects in (Hg,Cd)Te Characterized by Etching and Transmission Electron Microscopy

H.F. Schaake, R.J. Koestner, and D. Chandra

Materials Science Laboratory
Texas Instruments Incorporated
P.O. Box 655936 MS 147
Dallas, Texas 75265

It has become clear that one of the causes of the degradation of the electrical performance of devices fabricated on (Hg,Cd)Te is extended defects such as dislocations, twins, stacking faults, precipitates, etc. Minimization of the density of these defects below some level will be required to achieve acceptable focal plane array performance. This goal can be accomplished only with proven techniques for the characterization of such defects, and detailed knowledge as to the formation mechanisms of the defects during growth.

The most widely used techniques to characterize extended defects in crystalline solids is etching with a solution proven to develop etch pits at these defects, and transmission electron microscopy. This paper will review the current status of the etch and transmission electron microscopy characterization of (Hg,Cd)Te and of our understanding of the mechanisms for the formation of these extended defects. The paper will be divided into 3 sections:

1. A critical review of the efficacy of defect etches used on both (Hg,Cd)Te and on CdTe-CdZnTe substrate materials.

2. A review of the types of defects found in material prepared by solid state recrystallization (SSR), the travelling heater method (THM), LPE, MOCVD, and MBE, and the mechanisms by which they are formed during growth.

3. A summary of where the industry stands as to the density of these defects in material produced by each of the growth techniques listed above.

Etch pit study of dislocation formation in $Hg_{1-x}Cd_xTe$ during fabrication and its effect on device performance.

Peter W. Norton, Anthony P. Erwin

Honeywell Electro-Optics Division
2 Forbes Road
Lexington, MA 02173
(617) 863-3096

William Schmidt

Naval Research Laboratory
Washington, D.C. 20375

The relationship between hybridization force, dislocation (etch pit) density and device performance has been investigated for devices fabricated from $Hg_{1-x}Cd_xTe$ LPE material. Coldwelded indium column interconnects are the predominant method used to mechanically and electrically attach mosaic arrays to silicon multiplexers. The mismatch in thermal expansion between the $Hg_{1-x}Cd_xTe$ photodiode arrays and silicon multiplexers stresses the interconnects when the arrays are cooled to their operating temperature (typically 40 K to 120 K) which can lead to failures. Increased hybridization force improves the mechanical stability of the interconnects but can introduce dislocations in the $Hg_{1-x}Cd_xTe$. Dislocations have been reported to degrade the performance of some device structures[1-3]. The threading dislocation density in the LPE films after growth is typically $\sim 8 \times 10^5$ /cm^2 and has been reported by others[4] to be dependent upon the dislocation density in the CdTe substrate. No significant change in dislocation density is seen after test structure fabrication using standard contact photolithographic techniques or after hybridization at forces up to $\sim 4 \times 10^5$ gm/cm^2 of indium column as indicated in figure 1. At forces on the order of 6×10^5 gm/cm^2 ($\sim$ 10% of the Vickers Hardness[5]) the dislocation density in the films increased to 90×10^5 /cm^2 in the areas where the indium columns are. The diffusion limited performance of the test structures at 120 K was not degraded by the increased dislocation density. A correlation between dislocation density and test structure performance at temperatures down to 80 K is reported. The structures used in the study were fabricated from LPE $Hg_{1-x}Cd_xTe$ grown on a CdTe substrate. Implantation of boron into the p-type material through a ZnS passivation layer was used to form junctions. A zero bias junction resistance of 1000-7000 Ω-cm^2 was typical for the test structures which had a cutoff wavelength of $\sim$ 4.7 μm at 120 K as measured with a Nicolet Fourier Transform spectrometer. This work was supported under Naval Research Laboratory Contract # N00014-86-C2554.

References

1. L. Colombo and A. J. Syllaios, *Technical Digest of International Electron Devices Meeting 1983*, (Electron devices society of IEEE, Washington DC, 1983), p. 718.
2. T. Yamamoto, Y. Miyamoto, and K Tanikawa, *J. Crystal Growth* **72**, 270 (1985).
3. Y. Miyamoto, H. Sakai and K Tanikawa, *Proc. of SPIE* **572**,115 (1985)
4. M. Yoshikawa, et. al., "Dislocations in HgCdTe/CdTe and HgCdTe/CdZnTe heterojunctions," *J. Vac. Sci. Technol. A (Proc. of the 1986 U. S. MCT Workshop)*5, 5 (Sep/Oct 1987)
5. J. G. Fleming, et. al., *Proc. 3rd Int. Conf. on II-VI Compounds*, Monterey, CA (1987)

(a)

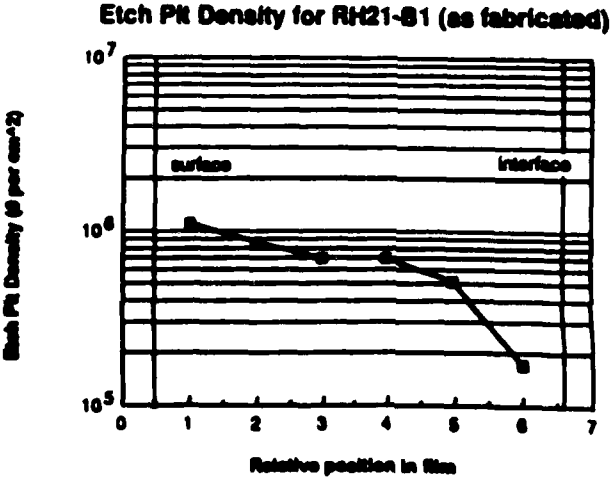

(b)

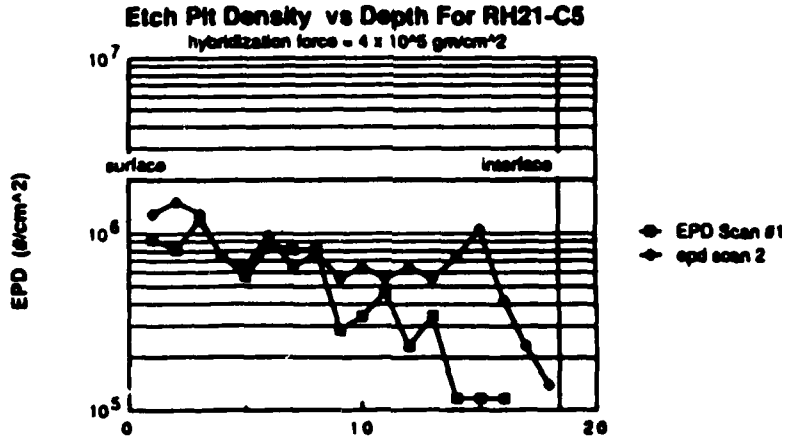

Figure 1. Typical etch pit density versus relative position through epitaxy layer for (a) samples fabricated but not bump bonded and for (b) samples hybridized with 4 x 10^5gm/cm^2 of indium column.

EVALUATION BY ELECTROREFLECTANCE OF THE LOW TEMPERATURE STORAGE TIME IN MIS DEVICES BUILT ON BULK MCT

by

Paul M. Raccah, James W. Garland and Yang De

University of Illinois at Chicago

and

Roger Strong

Texas Instruments Incorporated

The generalization[1] of the theory of electroreflectance (ER) has made possible the detailed study of defects, however the parameters determined have been related primarily to properties of the material such as the density of EL2 defects in GaAs,[2] the inhomogeneous strain at the CdTe/native oxide[3] interface, the density of stacking faults deliberately induced in MBE-grown n-type Mercury Cadmium Telluride,[4] etc... . In addition, it has been shown[3,5] that ER is very sensitive to surface phenomena, even those involving only one or two atomic layers.

Knowing these properties, we have more recently turned our attention to the behavior that could be expected of the material in devices. In particular, we have addressed the difficult problem of MIS devices built on n-type bulk MCT. In the operation of these devices the crucial parameter is the storage time, τ, at low temperatures. It can vary by about two orders of magnitude, from 1 μsec to 500 μsec, in materials which have otherwise rather similar transport and optical properties.

We have studied a set of thirty very carefully characterized samples, concentrating our efforts on the middle set of 17 with storage times covering the range from 6 to 130 μsec. All the samples were first investigated by spectroscopic ellipsometry (SE) and exhibited the expected 7Å thick native oxide. The quality of the data obtained with our SE system permits the triple derivation of the complex dielectric function, and we carried out the fitting of every one of these derivative spectra to the best Lorentzian/Gaussian combination.[6] It turned out that all of the samples were remarkably similar, and the E_1 transition energies determined were in excellent agreement with the composition x obtained from infrared transmission. Moreover, the values of Γ measured by SE varied little from sample to sample and were characteristic of samples of excellent quality. Certainly the large variations in τ were not reflected in the data obtained by SE.

On the other hand, our ER spectra were very dissimilar and, although they could

be fitted reasonably well to the generalized lineshape within the usual model, including first, second and third derivatives, the value obtained for the interband transition energies and for the linewidths Γ did not agree with the SE results. On the other hand the Γ's obtained by this fitting of the ER data correlated somewhat with the storage time. A very intriguing result indeed, were it not for the fact that the longest storage times correlated to the largest Γ's and hence the samples presumably the richest in defects. This nonphysical correlation led us through an extensive analysis, to develop a preliminary model of the surface which seems to describe reasonably well the results.

As has already been shown[3,5] in other materials, the first two or three layers at a polar semiconductor/native-oxide interface are very strongly modulated by an electric field and hence yield a large ER signal. Because of this amplification of the ER signal from the microscopic interface region, ER yields detailed information on structural and other defects present at the interface and hence important in MIS and other devices. In particular, the surface ER signal is especially sensitive to extended defects and other nucleating centers for the diffusion of cations into the oxide, which leave behind highly polarizable vacancies. Such defects, which can serve as centers for charge leakage in MIS devices, increase the linewidth Γ_s of the surface ER signal. One therefore expects the device storage time τ to be inversely proportional to the incremental surface linewidth $\delta\Gamma_s$ induced by these defects for low defect concentrations, and to vary more rapidly with $\delta\Gamma_s$ for defect concentrations high enough that regions of defect-induced diffusion begin to overlap strongly. This led us to investigate the correlation between the device parameter τ and the ER parameter Γ_s using the simple equation

$$\tau^{-1} = A\delta\Gamma_s + B(\delta\Gamma_s)^2.$$

This led to an excellent correlation, with a fractional root-mean-square error of approximately 0.15, as is shown in the attached figure.

This is the first time that a quantitative correlation has been established between a parameter measured on an unprocessed material at room temperature and the performance of a low-temperature device built on the same material. This raises the possibility of predicting, starting from a room-temperature measurement, the performance at low temperatures of a device yet to be built.

REFERENCES

1. P. M. Raccah, J. W. Garland, Z. Zhang, U. Lee, D. Z. Xue, L. L. Abels, S. Ugur and W. Wilinsky, Phys. Rev. Lett. 53, 1958 (1984).
2. P. M. Raccah, J. W. Garland, Z. Zhang, S. Mioc, Y. De, A. H. M. Chu, S. McGuigan and R. N. Thomas, SPIE Proc. No. 623, 40 (1986).
3. P. M. Raccah, J. W. Garland, Z. Zhang, L. L. Abels, S. Ugur, S. Mioc and M. Brown, Phys. Rev. Lett. 55, 1323 (1985).
4. P. M. Raccah, J. W. Garland, Z. Zhang, A. H. M. Chu, J. Reno, I. K. Sou, M. Boukerche and J. P. Faurie, J. Vac. Sci. Technol. A4, 2077 (1986).
5. P. M. Raccah, J. W. Garland, S. E. Buttrill, Jr., L. Francke and J. Jackson, Appl. Phys. Lett. 52, 1584 (1988).
6. J. W. Garland, H. Abad, M. Viccaro and P. M. Raccah, Appl. Phys. Lett. 52, 1176 (1988).

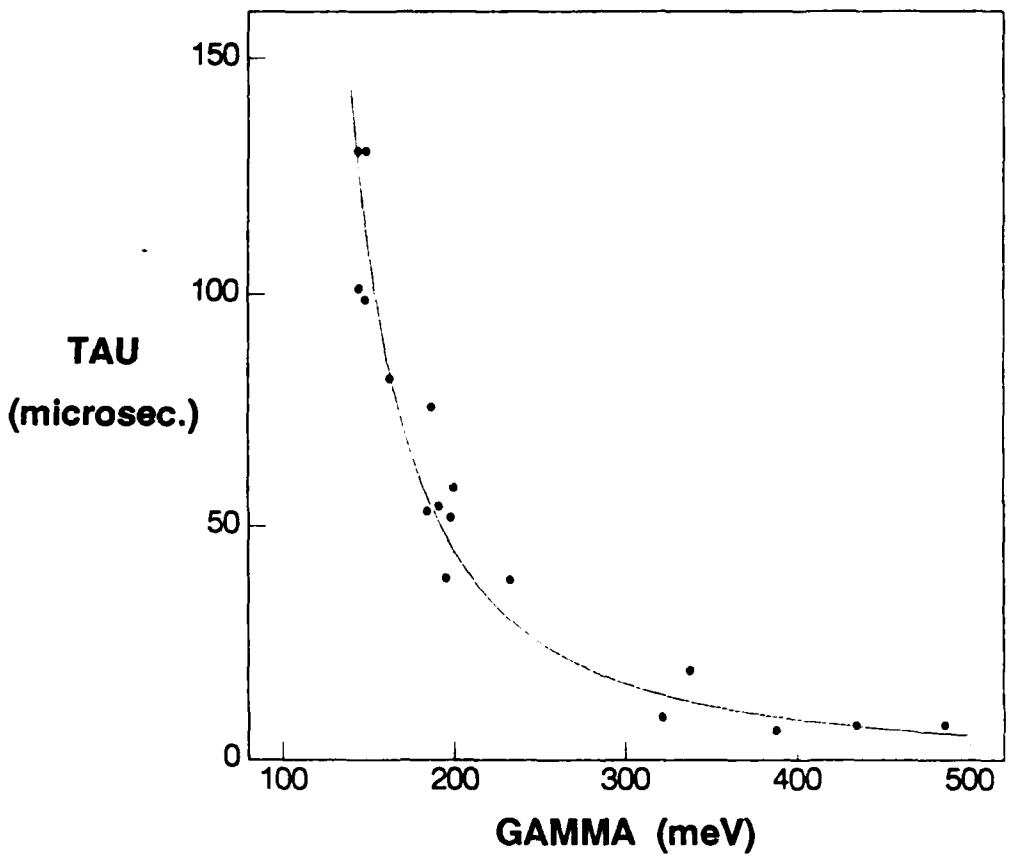

IMPROVED STRUCTURAL QUALITY OF MBE GROWN HgCdTe FILMS

Roland J.Koestner and Herbert F.Schaake
Texas Instruments, Inc.
Central Research Laboratories
Dallas Tx 75265

and

Thomas R.Hanlon
Chemistry Department
University of Texas at Dallas
Richardson Tx 75083-0688

Although Molecular Beam Epitaxial (MBE) growth of HgCdTe multilayer films (such as HgCdTe heterostructures or HgTe-CdTe superlattices) offers the promise of higher performance IR detectors, the high defect densities in these films to date has limited the technique's usefulness. We report a dramatic improvement in the structural quality of our MBE grown films; in fact, the measured defect densities in our MBE grown HgCdTe layers are now comparable to those found in HgCdTe material obtained by more mature growth technologies.

The two important structural defects encountered in MBE HgCdTe films are threading dislocations and twin faults. Threading dislocation densities as low as 5 x 10^4 cm^{-2} can routinely be obtained for (112)Te oriented HgCdTe films, while values near 2 x 10^5 cm^{-2} are generally measured for (001) oriented HgCdTe epilayers. The twin fault density for both epilayer orientations is measured to be in the low to mid 10^4 cm^{-2} range.

Figure 1 shows the defect etch micrographs for a 5.7 μm thick HgCdTe(112)Te layer (with x=0.22) in part (a) and a 7.2 μm thick HgCdTe(001)-0° layer (with x=0.25) in part (b). The threading dislocations and twin faults in the HgCdTe(112)Te film are revealed as small and large triangular etch pits, respectively. The threading dislocations for the HgCdTe(001) layer once again appear as triangular pits, while the twin faults appear as rectangular (twin lamellae) or square (pyramidal hillocks) pits. The measured defect densities for the two films equal the previously mentioned values.

Since the twin volume in the HgCdTe(112)Te layers presents a near (115)Te surface orientation, these layers can be grown with no surface hillocks present. The optimal Hg fluxes for the (112)Te and (115)Te growth directions are sufficiently close to suppress the formation of both hillocks on the epilayer surface and a

highly defective twin volume in the HgCdTe(112)Te epilayer. In contrast, HgCdTe(001) layers exhibit a high density of pyramidal hillocks since the growth orientation of the twin volume lies near a $(22\bar{1})$Te direction that requires a much lower Hg flux for optimal growth. Figure 2 illustrates the as-grown surface morphology for a 5.5 μm thick HgCdTe(112)Te film (with x=0.22) in part (a) and a 7.0 μm thick HgCdTe(001)-5° layer (with x=0.20) in part (b). Although a twin fault density of 1-2 x 10^4 cm^{-2} is measured for both films after defect etching, the twin faults only lead to surface hillocks on the HgCdTe(001)-5° layer.

As a result of the lower dislocation content present in our MBE grown HgCdTe(112)Te and (001) layers, the double crystal rocking curves (DCRC) recorded for these films show linewidths comparable to high quality III-V epitaxial layers. Figure 3(a) illustrates a (004) DCRC curve for a 5.7 μm thick HgCdTe(001)-0° film (with x=0.24) where the substrate and film linewidths are measured to be 18 and 20 arc-sec, respectively. The illuminated area is 2 x 5 mm^2 with approximately 40 percent of the epilayer removed to expose the underlying CdZnTe substrate. Figure 3(b) shows another (004) DCRC curve recorded from the same sample approximately 1cm away from the area selected in Figure 3(a). In this case, a 24 arc-sec linewidth is found.

Acknowledgments

We thank Hung-Yu Liu for all of the X-ray measurements and Don Todd for his technical assistance. This work was performed under DARPA contract No. N00014-86-C-2379.

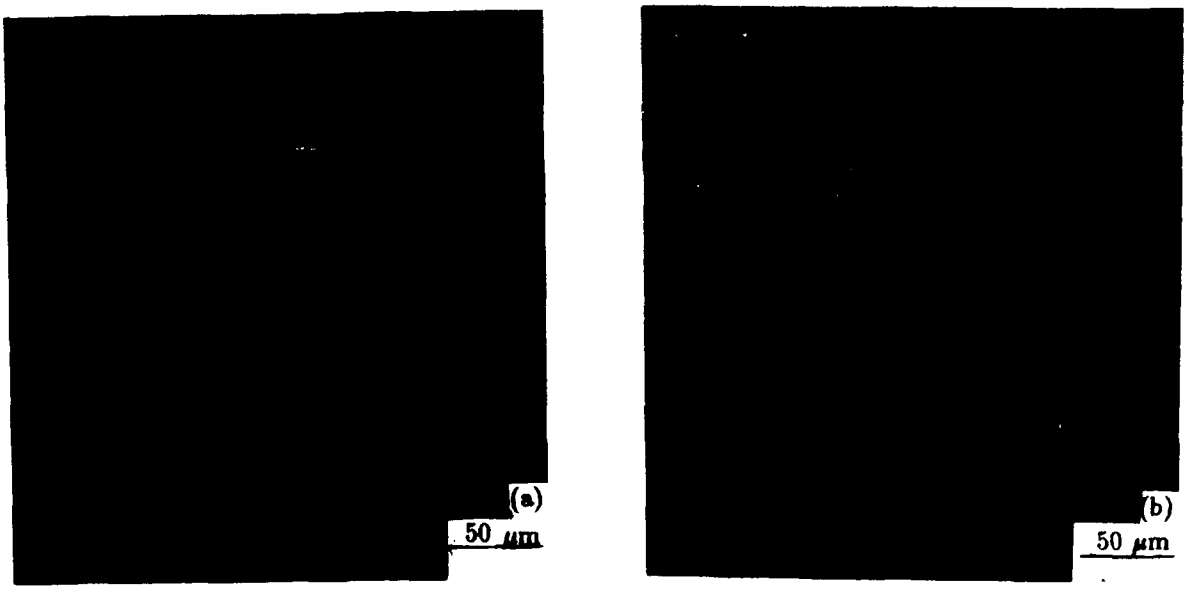

Figure 1. Defect etch micrographs for a 5.7 μm HgCdTe(112)Te (with x=0.22) in (a) and for a 7.2 μm thick HgCdTe(001)-0° layer (with x=0.25) in (b).

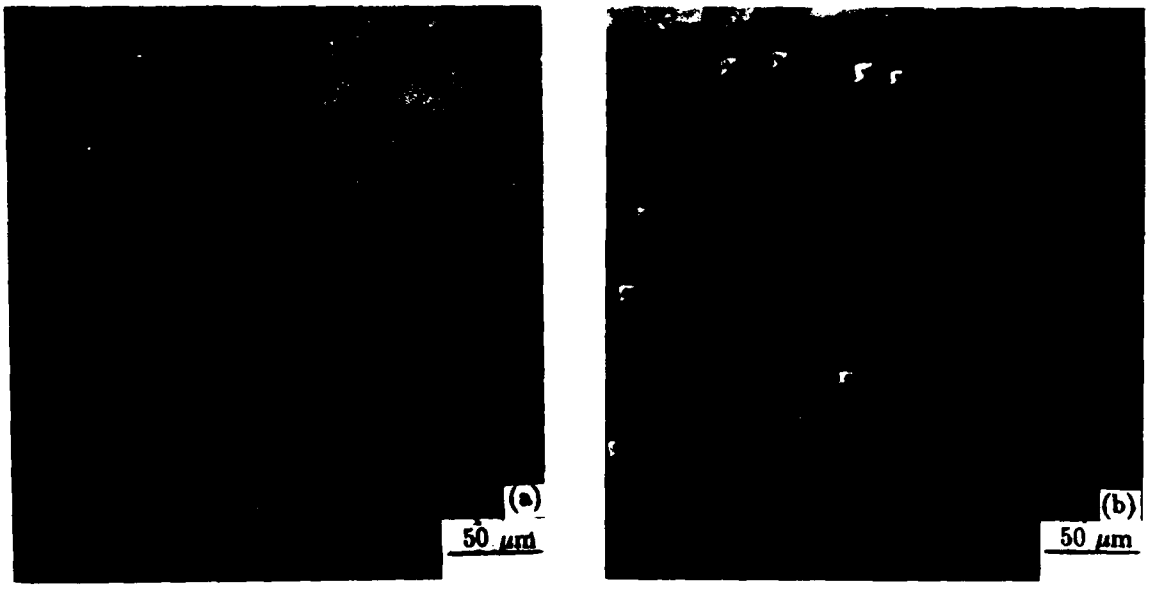

Figure 2. As-grown surface morphology for a 5.5 μm thick HgCdTe(112)Te (with x=0.22) in (a) and for a 7.0 μm thick HgCdTe(001)-5° layer (with x=0.20) in (b).

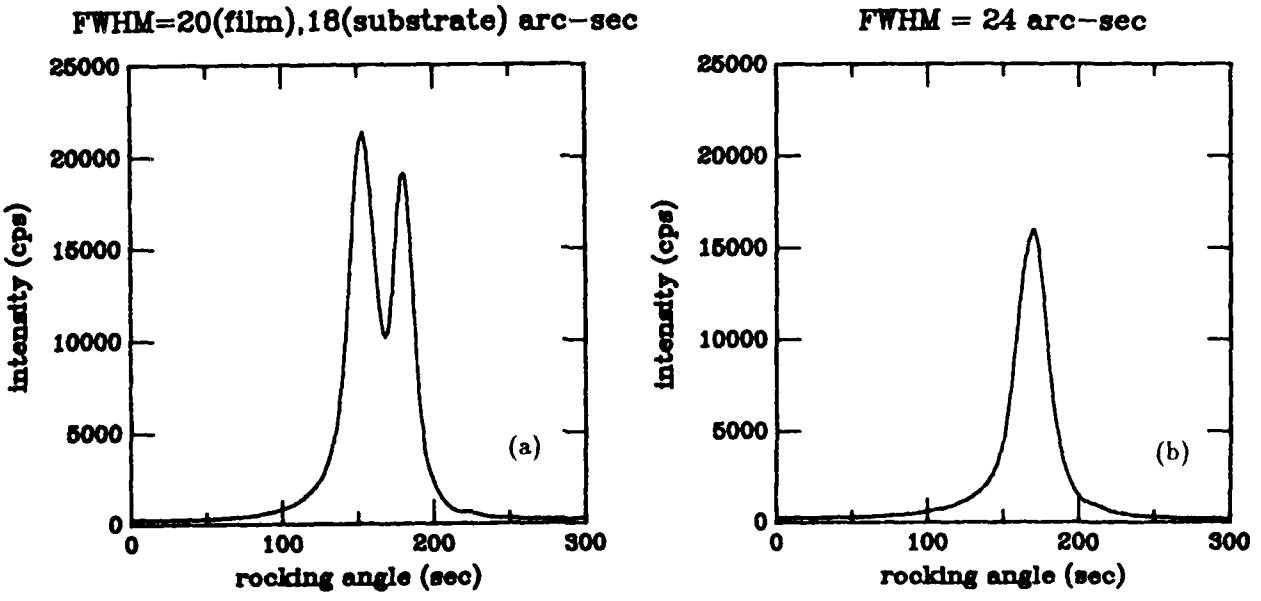

Figure 3. DCRC curves about the (004) reflection for a 5.7 μm thick HgCdTe(001)-0° film (with x=0.24). The illuminated area is 2x5 mm^2 with approximately 40 percent of the epilayer removed in (a) to expose the underlying CdZnTe substrate.

EFFECTS OF DEFECTS ON MIS PROPERTIES OF MBE FILMS

M. W. Goodwin, M. A. Kinch, and R. J. Koestner
Texas Instruments Inc.
Dallas, Tx 75265

Introduction

It has been known for a number of years[1] that physical defects in semiconductors can be very detrimental to device performance. These defects can include grain boundaries, twins, dislocations, etc. For MBE (molecular beam epitaxy) grown HgCdTe we have observed two major defects associated with film growth. These include dislocation and pryamidal hillock defects. By measuring the MIS properties of these films we have seen an improvement in device performance with lower defect densities.

Experimental

The samples reported here were grown by MBE on (001) oriented CdZnTe substrates with a CdTe buffer layer at a growth temperature of approximately 200 C in a Riber 2300 MBE machine. The pryamidal hillock density in these films ranged from $1X10^4$ to $1X10^6 cm^{-2}$. Using an etch to reveal dislocations we measured dislocation densities from the low 10^5 to the mid $10^7 cm^{-2}$.

The MIS devices were fabricated using a standard process for material evaluation. After a standard organic solvent clean-up the samples were given a light static etch in a dilute Br/Me solution. The surface of the films were then passivated by growing a standard KOH anodic oxide. After the surface passivation 2000 $\dot{A}$ of ZnS was deposited followed by deposition of 1200 $\dot{A}$ of Al to form the gate metal. The geometry of the gates are 10 X 15 mils. Contact to the gate metal was made by evaporating In onto the surface using a random dot mask. The samples were then mounted in 24 pin flatpacks and bonded with 2 mil diameter gold wire.

Testing of the MIS devices consisted of measuring the admittance of the devices for their equilibrium response and the storage time for their dynamic response. The carrier concentration of the films was determined from the capacitance vs. gate voltage curve in the high frequency limit. The equilibrium dark currents in the films were determined from the conductance vs. gate voltage curve, which was translated to an equivalent RA product.

The storage times were measured from the response of the MIS device to a voltage pulse which forces it into deep depletion. It is a measure of the dark current in a dynamic mode of operation. The spectral response of the devices were measured in an FTIR spectrometer with the device operated as a photocapacitor.

Results

The influence of defects on the MIS properties is best illustrated in Fig. 1 where results of the storage times at T=80 K for 4 MBE grown films is plotted as a function of cutoff wavelength. In a simple approximation the storage time is inversely proportional to the dark currents for the device. The dotted line represents data on typically good SSR grown material. For each sample a variation in cutoff wavelength was observed, thus results of the measurements of MIS properties could be correlated with different bandgaps as shown. All of these samples were N-type with carrier concentrations varying between 1 and $3X10^{15}cm^{-3}$. For samples 322 and 326 the dislocation density was in the low to mid $10^{7}cm^{-2}$ range and the pryamidal hillock density (hillocks) in the 10^{5} to $10^{6}cm^{-2}$ range. For samples 455 and 456 the dislocation density was reduced to the low to mid $10^{5}cm^{-2}$ range; this value of dislocation density is typical of good quality LPE (liquid-phase epitaxy) material and the substrates on which both the MBE and LPE material are grown. The hillock density for these two films was in the low $10^{4}cm^{-2}$ range.

As can be seen there is a significant improvement in the MIS properties when the density of defects is reduced. We believe that the improvement in storage times is primarily a result of the reduction of the dislocation density. Previous studies [2] have shown that dislocation densities in HgCdTe can significantly affect the MIS dark currents. Also, when the dislocation densities are comparable to those in HgCdTe grown by other methods such as SSR and LPE, the storage times are very comparable; as shown in Fig.1 samples 455 and 456 agree very well with good quality material with comparable dislocation densities.

One remaining problem with MBE films is that they have a low well capacity for minority carrier storage. That is, although the dark currents are now comparable with good quality material for low gate bias (approximately .1 V of bias beyond that necessary for minority carrier storage), applying a larger gate bias results in a significant increase in tunnel currents. This is shown in Fig.2 where the measured RA values determined from the peak of the conductance vs. gate voltage curve are plotted for the samples in Fig.1.

Although the storage times for samples 455 and 456 compare well with good quality SSR, the RA values do not except for those devices with cutoff wavelengths near 10 um. In fact the RA values show a surprising lack of dependence with bandgap in this range; for material with cutoff wavelengths near 5 um however, an increase with RA is observed. We believe this result to be indicative of large tunnel currents in the material probably due to the hillock defects since hillocks are absent in material grown by other methods discussed here.

We have also performed RA measurements as a function of temperature on samples 322 and 455 to study the dark currents in these samples. The results are shown in Figs.3 and 4. For sample 322 we observe a tunnel current limited region for $T \leq 100$ K. For $T \geq 100$ K the sample is dominated by generation-recombination dark currents due to the high defect density in this film. Generally, in good quality bulk HgCdTe with this bandgap the material is diffusion limited for $T \geq 120$ K. For sample 455 with lower defect densities we observe the tunnel current limited behavior for $T \leq 90$ K and a near-diffusion limited behavior for $T \geq 90$ K. The RA dependence for $T \geq 90$ K is dominated by a dark current process different from the tunnel current process and is probably a result of the dislocation defects in the samples.

Acknowledgements

This work was supported under DARPA contract No.N00014-86-C-2379 (OPTION).

References

1. H. F. Matare, "Defect Electronics In Semiconductors", (Wiley-Interscience, New York, 1971).

2. A. J. Syllaios and Luigi Colombo, IEDM Technical Digest, 137 (1982).

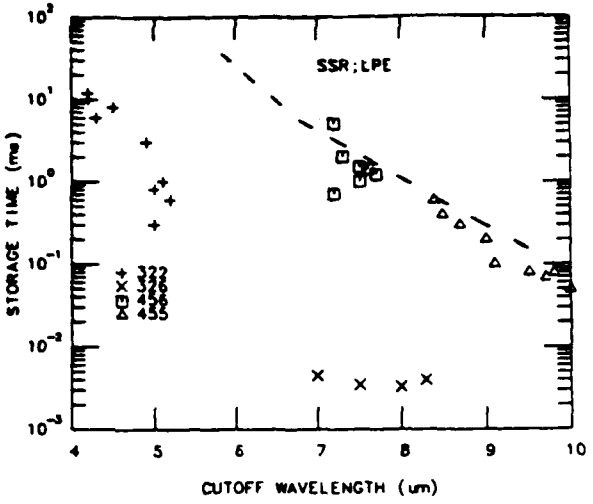

Fig. 1. Storage time vs. Cutoff wavelength for 4 MBE films showing the improvement with lower defects.

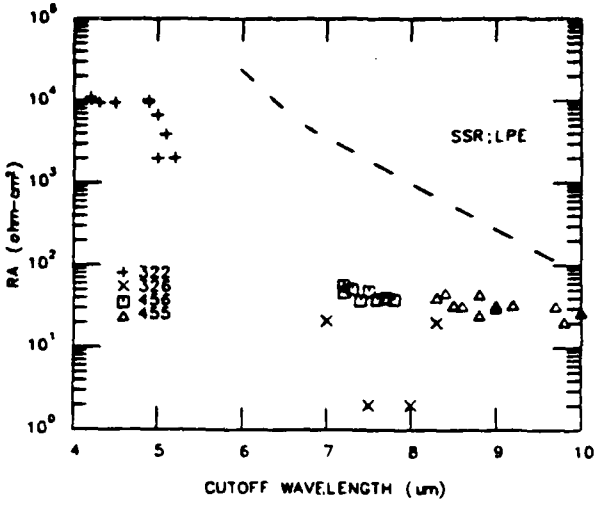

Fig. 2. RA vs. Cutoff wavelength for the 4 MBE films in Fig. 1.

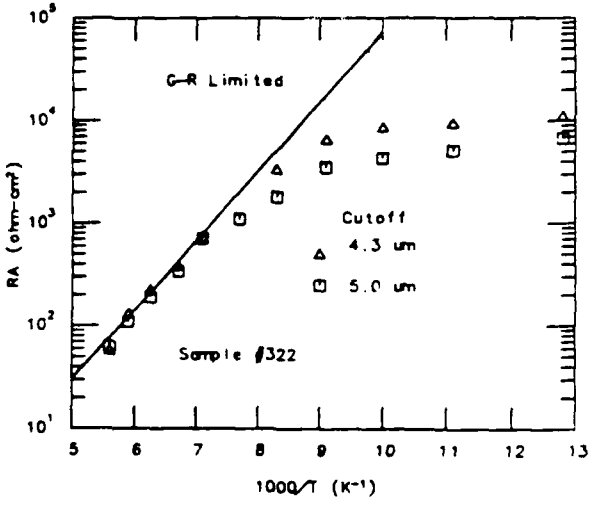

Fig. 3. RA vs. 1000/T for 2 devices on sample 322. Higher defect density causes the material to be G-R limited.

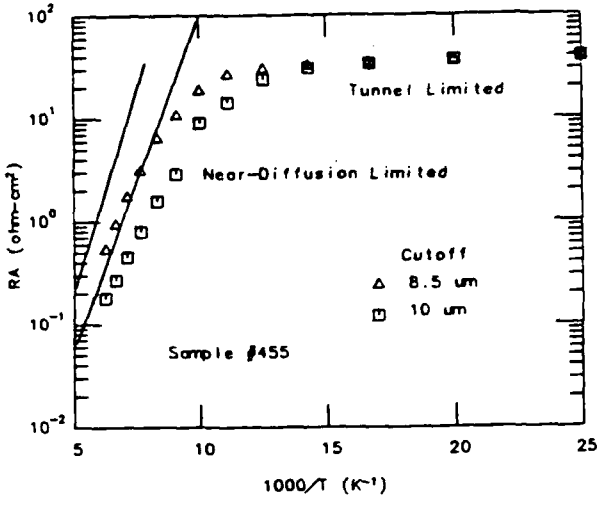

Fig. 4. RA vs. 1000/T for sample 455 with lower defect densities.

TUNNELING AND DARK CURRENTS IN HgCdTe PHOTODIODES

Y. Nemirovsky, D. Rosenfeld, R. Adar and A. Kornfeld

Kidron Microelectronics Research Center
Department of Electrical Engineering
Technion - Israel Institute of Technology, Haifa 32000, Israel

In current HgCdTe material and device technology, the performance of HgCdTe photodiodes is limited by excess dark currents and the associated noise currents. $Hg_{1-x}Cd_xTe$ ($x \approx 0.22$) photodiodes with cut-off wavelengths in the range of 8-12μm operating near 77K, exhibit DC characteristics and noise behavior that are very sensitive to material properties as well as to device processing technology. The origin and mechanism of the above currents are not yet well established. There is a considerable need for a model to correlate the dark and noise currents with the material properties such as composition, bandgap, photodiode cut-off wavelength, doping concentration, nature of the dopant, excess carrier life-time, surface potential etc.

We consider the mechanisms that produce dark currents in $Hg_{1-x}Cd_xTe$ photodiodes with $x \approx 0.22$, in various bias regions. These mechanisms also determine the differential-resistance as a function of reverse bias (Fig. 1). We model the DC behavior of the diodes and compare the measured and calculated characteristics (Fig. 2). By measuring the temperature dependence of the DC parameters in the temperature range of 65-132 K, the mechanisms are studied and the validity of the model is confirmed (Fig. 3). We correlate the mechanisms that produce the DC dark current with the measured noise phenomena in the frequency range of 1 Hz - 1 kHz. The calculated noise model and the measured data are compared in Fig. 4.

The measurements and modeling presented in this study characterize front illuminated, ion-implanted n^+-on-bulk p-$Hg_{1-x}Cd_xTe$ photodiodes with $x \approx 0.22$, operating near 77 K, used for hybrid focal plane arrays in the 8-12 μm spectral region. The major features of the photodiodes are the following:

1) The starting material is either (a) undoped crystals from Cominco Inc. in which p-type conductivity is obtained with Hg vacancies; or (b) gold doped bulk material grown by the method of solid state recrystallization.
2) The junctions are planar and the junction periphery is covered by a metallic guard ring that is connected to the n^+ region.
3) n^+ shallow junctions are formed by implanting boron with relatively low dose (3×10^{13}-3×10^{14} cm^{-2}) and low energy ($\approx$125 keV).

4) The diodes are passivated with native sulfides (≃300Å) and evaporated ZnS.
5) The junctions and photodiodes are exposed to a low-temperature post-implantation anneal (≃95°C) and temperature cycles up to 85°C.

The surfaces are characterized with MIS structures, gate-controlled diodes and variable area diodes which demonstrate that surface effects do not contribute significant dark currents in properly processed photodiodes.

The complex electrical profiles observed in implanted $Hg_{1-x}Cd_xTe$ junctions are characterized with measurements of the junction capacitance as a function of the reverse voltage. From these measurements it is apparent that the origin of the p-type conductivity (Hg vacancies or substitutional doping) plays a dominant role in determining the impurity distribution and the electrical profile of the depletion region. In the case of the undoped material from Cominco Inc., $n^+/p^-/p$ junctions are obtained with very low p-type doping near the n^+ region. The doping gradually increases, and after 1 μm is about an order of magnitude lower than the bulk doping level (≃ $1x10^{16}$ cm^{-3} at 77 K). In the case of the gold doped material, relatively abrupt n^+p junctions are formed. The electrical profile of the junction strongly affects the reverse bias current.

Three distinct mechanisms dominate the dark current; in the zero bias and low bias regions (≃±50 mV), diffusion current is the dominant current down to ≃60 K. This model is corroborated with the temperature and voltage dependence of the differential resistance. For medium reverse bias, trap assisted tunneling produces the dark current. This mechanism is examined by measuring the temperature dependence of the diode differential resistance at 80 mV reverse bias and by the fit between the calculated and measured voltage dependencies at a given temperature. For a high reverse bias, bulk band to band tunneling dominates. The bulk band to band tunneling breakdown is observed at lower reverse voltages for the n^+p junctions formed in gold doped material. For the n^+p^-p junctions formed in Cominco material, the bulk band to band tunneling breakdown is shifted to higher reverse voltages. In the higher reverse voltage region dominated by bulk band to band tunneling, the noise current spectral density is modeled in the frequency range of 1 Hz - 1 kHz with 1/f behavior that is proportional to the square root of the tunneling current.

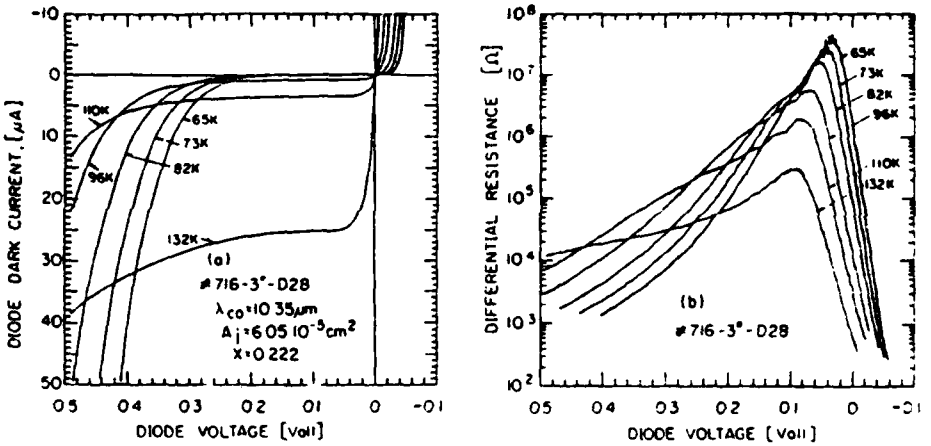

Fig. 1

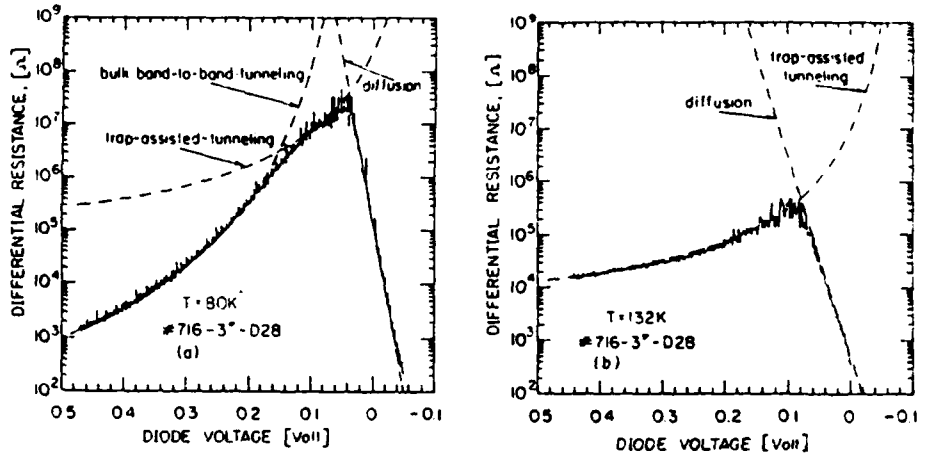

Fig. 2

Fig. 3

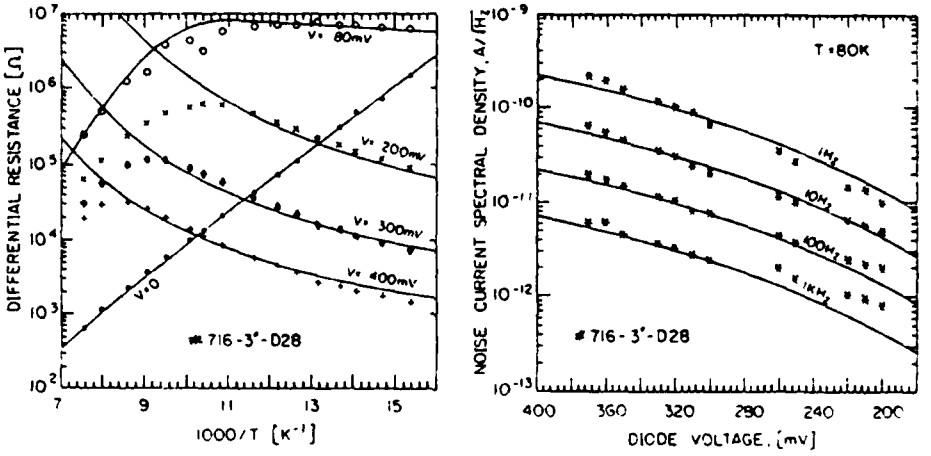

Fig. 4

Fig. 1: Measured current-voltage characteristics (a) and differential resistance-voltage characteristics (b) of $Hg_{1-x}Cd_xTe$ photodiode with x=0.22.

Fig. 2: The dependence of the measured (solid curve) and calculated (dashed curves) differential resistance upon reverse bias voltage of the diode of Fig. 1, at 80 K (a) and at 132 K (b). The calculated total dynamic resistance, which is the sum of three mechanisms, coincides with the measured characteristics.

Fig. 3: Dependence of measured and calculated (solid curves) differential resistance of the diode of Fig. 1 as a function of temperature, with the diode reverse bias voltage as a parameter.

Fig. 4: Measured and calculated (solid curves) noise current spectral density of the photodiode with the DC characteristics of Fig. 1 at 80 K, in the frequency range of 1 Hz-1 KHz. The reference shot noise level $(2qI)^{1/2}$

LIGHT INDUCED DEFECTS IN HgCdTe p-n JUNCTIONS

R.E. DeWames and J. Bajaj
Rockwell International Science Center
Thousand Oaks, CA 91360

Several studies have been reported' on the effect of gamma and electron irradiation on HgCdTe p-n junction photodiodes. In general, as expected, the dark currents increase following irradiation and the conductance at zero bias can be significantly degraded. Defects induced by irradiation experiments can be localized in the region of the interface of the insulator-semiconductor and/or in the bulk of the material. An anomalous behavior of the dark currents in passivated planar HgCdTe n^+/p photodiodes, when irradiated with high energy electrons or gammas, has recently been reported.[1] With increasing total dose, the dark current increases as expected but shows a dramatic recovery at higher doses to almost the pre-radiation values. On the basis of several empirical studies made on samples with different material interfaces, the authors suggested that the induced inventory of defects and the dominant electrical effects are likely to be associated with the properties of the insulator/semiconductor interface region.

In a high energy irradiation experiment, however, the energy deposited in the sample is uniform and both ionization and displacement processes occur. To understand the role of ionization processes and gain insight on spatial effects we have performed preliminary experiments utilizing pulsed laser sources at wavelengths of 3340Å (nitrogen laser), 1.06 μm (YAG laser) and 10.6 μm (CO_2 laser). The repetition rate, energy/pulse and the size of the laser beam were 5 pulses/sec, 3.5 mJ/pulse, 3 cm × 1.5 cm and 10 pulses/sec, 0.5 mJ/pulse, 1 cm × 1 cm for nitrogen and YAG laser respectively. The CO_2 laser operated in the cw mode. The samples used were HgCdTe p-n junctions coated with 2500Å of ZnS subsequently overcoated with SiO_2. Diodes with cutoff wavelengths in the range of 4.8 μm and 9.3 μm at 77K were used in this study.

Figure 1 shows the change in current at 50 mV reverse bias as a function of the total time in seconds the sample is exposed to the nitrogen laser. A cold shield held at 77K allows measurements of small current changes which would otherwise be masked by ambient background photocurrent. In the experiments we observe a monotonic increase in the induced persistent current and no notable recovery at 77K up to irradiation times as long as 1 hour. No permanent damage resulted which could be traced to the use of these large laser pulses; the results of isochronal annealing are shown in Fig. 2. The magnitude of increase in currents and the annealing behavior is similar to what is observed with high energy electrons and gammas. In the nitrogen laser experiment we observe no transients at 77K, whereas with YAG laser exposure a transient is observed with time constants of the order of minutes plus a persistent current. Degradation in the dark currents is observed on both 4.8 μm and 9.3 μm devices. No effects could be detected with 10.6 μm laser irradiation, even in the 9.3 μm devices after cooling down to 10K. At this temperature the cutoff wavelength is 11 μm which is longer than 10.6 μm laser wavelength. A photocurrent is observed with the CO_2 laser even at 77K where the cutoff wavelength is 9.0 μm. This response is likely to be associated with states lying close to the edge of the valence band.

In the above experiments the diodes were frontside illuminated. Similar experiments were performed with illumination through the substrate (backside) and no effects were observed. This indicates the electrical effects are mostly related to the interface region. An experiment was performed on a sample on which the junction on the surface was covered with gold that prevented the light to reach the junction. No degradation was observed with laser irradiation even though a photocurrent was observed. This experiment suggests that the dominant source of degradation is at the junction interface.

The types of current observed are tunneling related. The currents in the forward bias are exponentials in voltage and the slope decreases with increasing dose.

These types of signatures are observed on diodes of inferior performance in the pre-radiation experiments at low temperatures. We will present detailed analysis of the I-V characteristics. All the features induced by light anneal and the performance of the device completely recovered after warming to room temperatures.

The nature and type of defects which cause the observed deleterious effects are unknown but it is reasonable to assume that the degree of degradation is likely to depend on the material properties of the insulator used to passivate the p-n junctions. The observations we made suggest that some of the defects we induced with light are of the same origin as those induced by electrons and gammas. More experimental studies are required to unify the observations of persistent currents and associated carrier generation processes induced by light, high energy electrons and gammas.

The observation that the electrical effects depend on the wavelength of light suggests the possibility of being able to design experiments which could spatially resolve, by virtue of wavelength dependent absorption depth, the type of electrically active defects which cause deleterious effects.

The use of laser irradiation offers the possibility of getting some insight into the nature and type of defects located at the insulator/semiconductor interface and in conjunction I-V measurements assess the role of these defects on the electrical behavior since both the nature of defects and the concentration can be modified in a reversible manner. The material system is inhomogeneous in both the lateral and vertical direction and the utilization of focussed beam will provide a 3-dimensional diagnostic capability.

Reference

1. R.S. Stapp, D.G. Feller, L.R. Johnson, C.I. Westmark, J. Bajaj, K. Vural, P.R. Newman, and E.R. Blazejewski, Appl. Phys. Lett. 52(19), 1614 (1988).

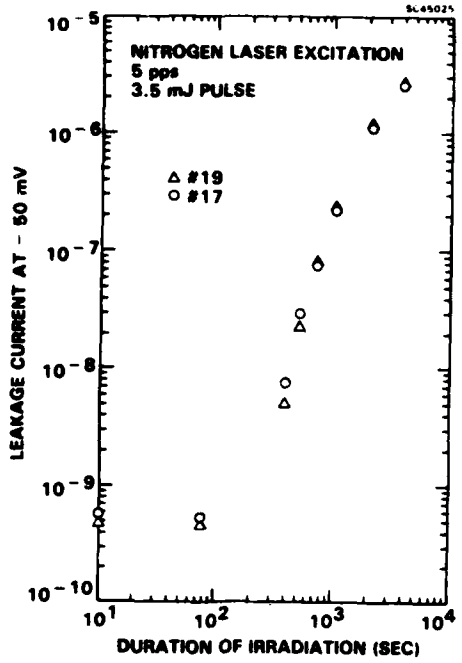

Fig. 1 Effect of nitrogen layer irradiation on leakage current of HgCdTe p-n junction.

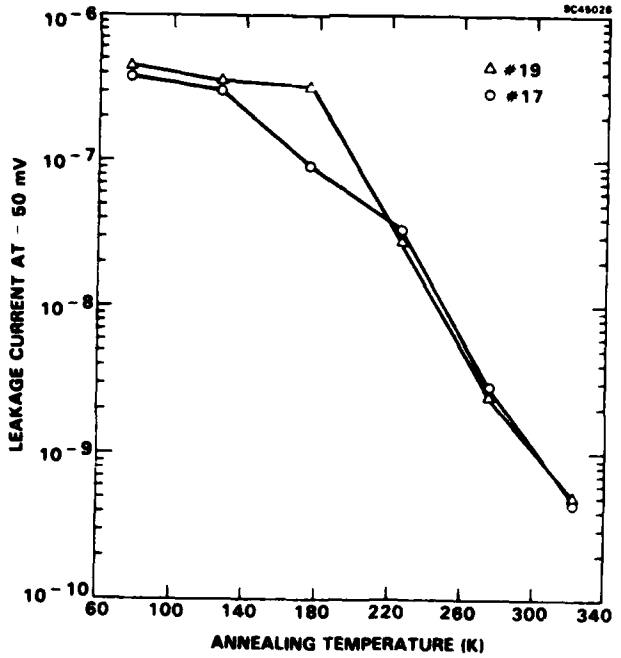

Fig. 2 Effects of annealing at various temperatures.

Component Diffusion in the $Hg_{0.8}Cd_{0.2}$ Te Pseudobinary System

Mei-Fan Sung Tang and David A. Stevenson

Department of Materials Science and Engineering

Stanford University, Stanford, Ca 94305

Introduction

Radioactive tracers are used to obtain the component diffusion coefficients for the $Hg_{0.8}Cd_{0.2}Te$ (MCT) system. Multiple branches are observed in the tracer diffusion profiles which are attributed to fast and slowly diffusing components . A diffusion model for each component is proposed that is based on the defect chemistry, a thermodynamic factor calculation, and the relationship between the component diffusion coefficients and the interdiffusion coefficients for pseudobinary systems. The model provides insight into the thermodynamic properties of the system, the mechanism for diffusion, and the practical application of tracer diffusion data to interdiffusion and to p-n junction conversion by Hg annealing.

Experimental

To provide meaningful and reproducible results, the tracer diffusion is performed under a well defined ambient using a two zone method employing a pure Hg reservoir. The component tracer diffusion is characterized as a function of temperature (from 350°C to 500°C) and the Hg partial pressure. The diffusion samples are preannealed with an appropriate reservoir so that the stoichiometry and the defect structure are established prior to the diffusion measurements. After the preanneal, the samples are quenched to room temperatures and encapsulated with radioactive isotopes. The tracers are introduced by different methods for different components: a liquid reservoir containing Hg^{203} is used for the mercury source and a nonplenished (constant amount of diffusant) electroplated source is used for both Cd^{109} and Te^{123m}. The diffusion experiments are performed under the same conditions as the preanneal. Parallel sectioning of the crystals is accomplished with a specially designed grinding device, with the section thickness evaluated from the weight loss. The activity of the isotope is determined by a γ-ray counter, and the values of tracer diffusion coefficient (D^*_i) for the three components (Hg, Cd, Te) are determined by analyzing the concentration profiles developed for specific boundary conditions.

Results

There are two branches in the diffusion profiles for each of the metal tracers and these profiles are not affected by the preannealing, indicating that the diffusion is ocurring under equilibrium conditions. The diffusion mechanisms are summarized as follows: the fast and slow components for the Hg diffusion correspond to a vacancy-interstitial mechanism proceeding in parallel and in series, respectvely. Neither of the components of the Cd diffusion profiles depends on the Hg overpressure and the proposed mechanisms involve vacancies and interstitials proceeding in series. The Te tracer diffusion profiles show two branches, but the fast one disappears for the preannealed sample; therefore, the fast component is assumed to be related to the chemical diffusion. Te diffuses much more slowly than either of metal species, and the diffusion mechanism is an interstitial mechanism.

Discussion

We previously proposed that two self-diffusion coefficients exist for each metal species on two independent diffusion networks[1], based on speculation concerning clustering effects in this system[2,3]. This model involves two lattice diffusion paths for each of the metal species, with two self-diffusion components proceeding on two independent networks. The relationship between the component diffusion coefficients (D^*_i and D_i) and the interdiffusion coefficient (D) that was derived for pseudobinary systems is used to verify the proposed models. MCT is assumed to be an ideal solution and $D^*_{Hg,f}$ and $D^*_{Cd,s}$ are related to D by a Nernst-Planck type of equation. This model, however, cannot expain why the fast component of Cd ($D^*_{Cd,f}$) does not contribute to the interdiffusion process. An alternate model is proposed based on the thermodynamic factor ([T.F.]) calculation from the available thermodynamic data provided by Brebrick et al[4,5]. At 500°C, we obtain [T.F.]=0.33 for MCT X=0.2. If we treat MCT as a quasi-regular solution, we can show that with [T.F.] <1, the mixing enthalpy of the two binaries (HgTe and CdTe) is positive.

In the present model, we consider only one self-diffusion coefficient for each metal species and only one diffusion matrix. We propose that the fast components of Hg and Cd are the true self-diffusion coefficients. The slow components of the two metal " tracer" diffusion coefficients arise from the interdiffusion between the tracer Hg* and Cd in the diffusion host for Hg and vice

versa for Cd, and they can be related to D by the Darken equation. In contrast ,the two fast diffusion components, $D^*_{Hg,f}$ and $D^*_{Cd,f}$ are true self-diffusion coefficients and can be related to D by a Nernst-Planck type of equation with the calculated thermodynamic factor value for the system.

In the present model, the mechanism for each component is the same as in the previous model, but their roles are different. The relatively slow diffusion rate of Te constrains the faster diffusing metal atom (Hg) from keeping pace with the more slowly diffusing metal atom (Cd) in order to maintain stoichiometry, and the intrinsic diffusion coefficient of Hg ($D^*_{Hg,s}$) behaves differently from the self-diffusion coefficient ($D^*_{Hg,f}$), since the former involves the slower diffusion of Cd which diffuses only by the V-I in-series mechanism. Since the Cd-Te bond is stronger than the Hg-Te bond, if Cd diffuses by either a V or I mechanism (as it would for the V-I in parallel mechanism), Cd would have to surmount a higher energy barrier since Cd would be closer to Te, in contrast to a series process in which a close approach does not take place to the same extent. This makes the V-I in series process a preferrable one for Cd diffusion.

As one applies to p-n junction conversion by Hg annealing experiment, one considers Hg diffusion under a certain initial stoichiometric condition, normally Te-rich, and the stoichiometry changes as the process proceeds. One can estimate the diffusion profile by applying the diffusion coefficient for the fast component of Hg under the P_{Hg} conditions of the annealing experiments .

Conclusions

The diffusion coefficients for the three components of MCT (X=0.2) system are studied by tracer techniques. The thermodynamic conditions of the diffusion experiments are addressed. There are fast and slow components in the tracer diffusion profiles for each of the components. We propose diffusion models based on: the experimental diffusion isotherms; the defect chemistry of the MCT system; the themodynamic properties of the MCTsystem; and the derived relationship between the different diffusion coefficients for pseudobinary systems. The results and our analysis can be summarized as follows: Te diffuses much more slowly than either of the metal species, and the fast component of Te is related to the chemical diffusion which is not seen for the preannealed samples. The two components for the self-diffusion for each metal - a fast and a slow - both appear after preannealing and are related to the lattice diffusion. In contrast to our previous model,

we propose that there is only one diffusion matrix, and the fast components for Cd and Hg are true self-diffusion coefficients. These fast components are related to the interdiffusion coefficient by a Nernst-Planck type of equation, with the thermodynamic factor calculated from available thermodynamic data. The slow components of the metal species in the tracer diffusion profile are the intrinsic diffusion coefficients and they are related to the interdiffusion coefficient by the Darken equation. MCT is close to an ideal solution, with the calculated thermodynamic factor less than one, indicating a positive mixing enthalpy of HgTe and CdTe. This is consistent with the observed results that the intrinsic diffusion coefficient of the metal species is smaller than the self-diffusion coefficient. The following mechanisms are proposed for the three components: Te diffuses by interstitials; Hg diffuses by vacancies and interstitals proceeding in parallel; and Cd diffuses by vacancies and interstials proceeding in series because of the higher bonding energy of Cd-Te. When Hg interdiffuses with Cd, the diffusion is slowed to conserve lattice sites, and the mechanism is changed to be identical with that of Cd : the V-I in series. The Hg diffusion coefficient used to estimate the p-n junction conversion by Hg annealing is the fast component of Hg - a sum of $D^*_{Hg,V}$ and $D^*_{Hg,I}$ - under the experimental Hg pressure conditions.

Acknowledgements

We thank Professor H. Schmalzried of the University of Hannover, Professor D. Shaw of Hull University, Dr. M. Brown of Grumman Corporate Research Center, and Dr. K. Zanio of Ford Aerospace and Communications Corporation for helpful discussions. This work is supported by DARPA through ONR, Contract No. N000-14-84K-0423.

References

1. M.-F. S. Tang and D. A. Stevenson, J. Vac. Sci. Technol. A 6(4),2650 (1988)
2.K. C. Hass and D. Vanderbiltt, J. Vac. Sci. Technol. A5(5), 30119, (1987)
3. A. B. Chen and A. Sher, Phys. Rev. B32, 3695, (1985)
4. R.F. Brebrick, J. Phys. Chem. Solids 40,177, (1979)
5. T. Tung, L. Golonka and R. F. Brebrick, J. Electrochem. 128, 451, (1981)

1/f NOISE CHARACTERIZATION IN n^+-p AND n-i-p $Hg_{1-x}Cd_xTe$ DETECTORS

A. van der Ziel, P. Fang, L. He, X. L. Wu and A. D. van Rheenen

E.E. Dept., Univ. of Minnesota, Minneapolis, MN 55455

Introduction

1/f noise in semiconductor devices is described by two equations[1,2]

1. Hooge's equation:[3] $S_I(f) = \alpha_H I^2/fN$ (or its modification) (1)

2. Handel's quantum equation:[4] $\alpha_H = (4\alpha_0/3\pi)\Delta v^2/c^2$ (or its modification) for noncoherent state devices and (2)

$$\alpha_H = 2\alpha_0/\pi = 4.6 \times 10^{-3} \quad (2a)$$

for coherent state devices.[5] Here α_H is the Hooge parameter, I is the current, f the frequency, N the number of carriers in the system, $\alpha_0 = 1/(137)$ the fine structure constant and Δv the vectorial change in velocity after and before a collision; it depends on the collision process involved. The derivation of (2) has been criticized, but the experimental evidence supports it in most cases. Moreover, we have a semiclassical derivation of (2).[6] Surface 1/f noise is usually not a quantum effect.

Equation (1), if properly modified, is used to evaluate α_H experimentally. If all minority carriers contribute to the 1/f noise of n^+-p diodes (1) leads to

$$S_I(f) = \alpha_H e I f(V)/f\tau \quad (3)$$

where V is the applied bias and e is the electron charge. For long n^+-p diodes[7] $[w_p > (D_n\tau_n)^{1/2}]$, $\tau = \tau_n$ is the carrier lifetime, w_p the length of the p region and

$$f(V) = f(a) = 1/3 - 1/2a + 1/a^2 - (1/a^3)\ln(1+a);\ a = \exp(eV/kT)-1 \quad (3a)$$

For short n^+-p diodes $[w_p > (D_n\tau_n)^{1/2}]$, $\tau = \tau_{dn} = (w_p^2/2D_n)$ ($\tau_{dn} \ll \tau_n$) is the diffusion time of the carriers through the p-region and[2]

$$F(V) = 1/2 \ln \frac{(D_n/w_p) + s_{cn}}{D_n/w_p + s_{cn} \exp(-eV/kT)} \qquad (3b)$$

where s_{cn} ($\simeq 10^7$ cm/sec) is the recombination velocity of electrons at the p-contact. For n-i-p diodes f(V) has not been evaluated but can be determined from experiment.

2. n^+-p diodes (devices A)

For relatively large $Hg_{1-x}Cd_xTe$ n^+-p diodes with x = 0.30, we found $\alpha_H = (4\text{-}6) \times 10^{-3}$ and $\tau_n = (1\text{-}2) \times 10^{-7}$ at T = 193°K and at T = 113°K.[7] The lifetime τ_n could be evaluated from the device admittance

$$Y = g_0(1+j\omega\tau_n)^\gamma \qquad (4)$$

with $\gamma \simeq 1/2$ near zero bias; farther away from zero bias γ was larger than 1/2 and the τ values deviated from the Honeywell lifetime tables.[8] The value of α_H indicates coherent state 1/f noise, as expected for large devices, and the admittance function indicates current flow by diffusion, if $\gamma \simeq 1/2$. We noted that $S_I(f)/[If(V)]$ was independent of bias at back bias, indicating that α_H/τ_n was constant. Hence the values of τ_n for large γ are probably incorrect and the Honeywell tables should be used.

One unit showed $\alpha_H = 5 \times 10^{-5}$ at 273°K at $\tau = 1.2 \times 10^{-7}$ sec. This value might be interpreted as Umklapp 1/f noise. In the Umklapp process the lattice takes up a momentum h/a; in that case Eq.(2) yields[9]

$$\alpha_H = \frac{4\alpha_0}{3\pi} \left(\frac{h}{m^* ac}\right)^2 \exp(-\theta_D/2T) \qquad (5)$$

where m^* is the effective mass and θ_D is the Debye temperature. This result is expected for somewhat smaller devices. Since the region was nearly intrinsic an alternate interpretation is possible.

3. p-i-n diodes (devices B)

For smaller devices with x = 0.22 and T = 80°K, the device impedance Z could be expressed as[10]

$$Z = \frac{R}{1 + j\omega CR} + \frac{Rj\omega L}{2(R + j\omega L)} \tag{6}$$

Such a resonant expression would be expected theoretically if the device were a n-i-p diode and the current flow were by recombination; the "electronic" inductance L yields the carrier lifetime τ. Measurements showed that $\tau \simeq 10^{-7}$ sec for all backbiased devices and that $\alpha_H f(V)$ was independent of bias. Since α_H should be constant, we took f(V) = 1. With this assumption and $\tau = 10^{-7}$ sec, we found $\alpha_H = 2 \times 10^{-6}$ for the best unit.

Umklapp 1/f noise would give $\alpha_H = 1.7 \times 10^{-4}$, which is far too large. Direct hole-electron pair generation-recombination 1/f noise, expected for narrow-gap semiconductors would give[2]

$$\alpha_H = \frac{4\alpha_0}{3\pi} \frac{2eE_g + 6kT + 2e|V|}{m^* c^2} \tag{7}$$

which yields $\alpha_H \simeq 2 \times 10^{-7}$. Hence, the best device lies only a factor 10 above this limit. Table I shows α_H for a number of devices; the values all lie between 2×10^{-5} and 2×10^{-6}. This indicates g-r type 1/f noise.

Devices A were supplied by G.R. Williams, Rockwell International, and devices B by W.A. Radford, Santa Barbara Research Center. The work was supported by ARO Contract DAAG29-85-K-0235. Dr. Fang is now with the E.E. Dept., University of South Florida, Tampa, FL. Dr. Wu is with Unisys, San Diego, CA.

Table I

Diode	V(mv)	I(μA)	$S_I(5)(A^2/Hz)$	α_H
M	-0.8	-3.5	2.25×10^{-23}	2.0×10^{-5}
G	-3.0	-3.5	0.95×10^{-23}	1.5×10^{-5}
F	-20	-6.0	4.3×10^{-23}	2.25×10^{-5}
J	-25	-7.0	0.9×10^{-23}	8.0×10^{-6}
K	-30	-10.0	1.0×10^{-23}	3.0×10^{-6}
H	-40	-12.0	0.8×10^{-23}	2.0×10^{-6}

References

1. A. van der Ziel, P.H. Handel, X.L. Wu and J.B. Anderson, J. Vac. Sci. Technol., A 6, 2205, 1986 (San Diego MCT Workshop, 1985).

2. A. van der Ziel, Proc. IEEE, 76, 233(1988) Review paper.

3. F.N. Hooge, Phys. Lett, A-29, 139(1969); Physica, 83B, 9(1976)

4. P.H. Handel Phys. Lett, 34, 1992(1975). Phys. Rev., 22, 745(1980).

5. P.H. Handel, in Noise in Physical Systems and 1/f Noise, Eds. M. Savelli, C. Lecoy and J. P. Nougier, New York, Elsevier 97(1983); P.H. Handel, in Noise in Physical Systems and 1/f Noise, Eds A. D. Amico and P. Mazetti, New York, Elsevier, 456 (1986).

6. A. van der Ziel, J. Appl. Phys. 63, 2456(1988).

7. X.L. Wu, J.B. Anderson, and A. van der Ziel, IEEE Trans El Devices, Ed-34, 602(1987).

8. G. Hanson and T. Casselman, Fundamental parameters in mercury cadmium telluride, Vol. 3, Table of Lifetimes in $Hg_{1-x}Cd_xTe$, Honeywell Corp. Res. Center, Minneapolis, MN Tech. Report (1982).

9. A. van der Ziel, P.H. Handel, X.C. Zhu and K.H. Duh, IEEE Trans. El. Dev., Ed-32, 667(1985).

10. P. Fang, Ph. D. Thesis, U of Minnesota (1988).